DESIGN CONSIDERATIONS FOR INDUCTIVELY COUPLED POWER TRANSFER SYSTEMS

By

Chwei-Sen Wang



A thesis submitted in partial fulfillment of the requirements for the degree of Doctor of Philosophy in Electrical and Computer Engineering, The University of Auckland, 2004

InductEV, Inc.
Exhibit 1008
Page 001

UNIVERSITY of OAKLAND
LIBRARY
OCT 2005

ABSTRACT

Inductively coupled power transfer (ICPT) systems use electromagnetic fields to transfer electric power from a primary source (power supply) to one or more secondary loads (pickups). Because there is no physical contact between the primary and secondary, ICPT systems are intrinsically safe and reliable. This technology has been significantly commercialised for around a decade. Present applications include material handling, public transport, and battery charging.

This thesis focuses on the design of ICPT systems for high power applications where both the primary and secondary coils are compensated by capacitors. The main aim is to develop systems with smaller size, less weight, lower cost, greater power and better efficiency. Previous work in this field has concentrated on either the power supply or the pickup. This thesis instead focuses on the interactions between the power supply and the pickup. When power is transferred from the primary to the secondary, the primary is affected by the secondary loading. This can result in poor displacement power factor (DPF), reduced power transfer capability, and a loss of controllability.

First, steady state linear mathematical models are developed to represent the load seen by the power supply that includes the primary compensation capacitor, the electromagnetic structure, the secondary compensation capacitor, and the pickup load. These models quantify the system behaviour in terms of the fundamental design parameters, and are used to evaluate a design procedure for ICPT systems. This evaluation provides an insight into the system, enabling suitable design decisions as well as quantification of frequency bifurcation boundaries in variable-frequency systems.

Several new primary tuning schemes are also proposed, taking into account the secondary loading effects. In loosely coupled systems, the primary and secondary resonant circuits can be tuned independently as the secondary loading effect on the primary are negligible. In well-coupled systems, the secondary loading affects the primary resonance significantly, and the proposed new tuning schemes greatly improve the DPF and power transfer capability. Various sensitivity analyses to variations in the primary and secondary compensation capacitances as well as misalignment of the electromagnetic structure show that systems designed using the proposed new tuning schemes have similar sensitivities compared with the original tuning.

Throughout the thesis work, an LCL resonant inverter driving a contact-less electric vehicle battery charger was used to verify the proposed theory. The operation of this inverter under discontinuous

InductEV, Inc.
Exhibit 1008
Page 003

current mode is also investigated. A novel design procedure is detailed and verified that enables this inverter to deliver maximum power to the load.

InductEV, Inc.
Exhibit 1008
Page 004

ACKNOWLEDGEMENTS

The author sincerely appreciates the supervision of Dr. Grant A. Covic and Dr. Oskar H. Stielau. Because of their wisdom and patience, the research work is always in a natural process going in the right direction. Particular thanks go to Prof. John T. Boys. His experience and leadership enabled this work to be carried out smoothly within the research group of inductive power transfer technology. The author is grateful for the wise advice and encouragement from EmPr. Ray Meyer. Additional thanks go to the power electronic research group, in particular Dr. Patrick A. Hu, Mr. Howard Lu and Mr. Edward Xu. Finally, it is an honour to have financial support, as a Doctoral Fellow (Top Achiever Doctoral Scholarship), from the Foundation of Research, Science and Technology (FRST), New Zealand.

In memory of my father, Lien-Jiin.

To my loving, Yu (mother), Annie (wife), Ya-Ting and Ya-Wei (daughters).

Chwei-Sen Wang

Auckland, New Zealand

Oct. 21, 2004

InductEV, Inc.
Exhibit 1008
Page 005

CONTENTS

Abstract i

Acknowledgements iii

Contents v

Nomenclature xi

List of Figures xv

List of Tables xxv

Chapter 1 Introduction 1

1-1 Background of ICPT Systems 1

1-2 Fundamental Structure of ICPT Systems 4

1-3 Motivations of the Research 4

1-4 Contributions of the Thesis 6

1-5 Scope of the Thesis 8

References 9

Chapter 2 Overview of ICPT Systems 11

2-1 Introduction 11

2-2 Electromagnetic Structures 11

2-2.1 Material 12

2-2.1.1 Magnetic Cores 12

2-2.1.2 Conductor Windings 13

2-2.2 Geometry 13

2-2.2.1 Primary Electromagnetic Structures 13

2-2.2.2 Secondary Electromagnetic Structures 14

2-2.3 Electromagnetic Coupling Model 15

InductEV, Inc.
Exhibit 1008
Page 007

2-2.4 Capability of the Electromagnetic Structure 17
2-2.4.1 Load Voltage and Current 17
2-2.4.2 Power Transfer Capability 18
2-3 Compensation 20
2-3.1 Secondary Compensation 20
2-3.2 Secondary Resonance 21
2-3.3 Primary Compensation 22
2-3.4 Primary Resonance 23
2-3.5 Basic Compensation Topologies 24
2-4 Power Converters 25
2-4.1 Overview of Power Converters 25
2-4.2 Voltage-Sourced Power Converters 27
2-4.3 Current-Sourced Power Converters 28
2-4.4 Impedance Matching 30
2-5 Controllers 31
2-5.1 Power Flow Regulation 31
2-5.2 Frequency Control 32
2-5.3 Switching Control in Voltage-Sourced Full-Bridge Inverters 32
2-5.4 Switching Control in Current-Sourced Full-Bridge Inverters 33
2-5.5 Bifurcation Phenomenon 34
2-6 Future Trends 36
2-7 Conclusions 38
References 38

Chapter 3 Development of a General Load Model 47
3-1 Introduction 47
3-2 Overview of the Load Model 47
3-3 The Pickup Load 49
3-4 The Secondary Resonant Circuit 50
3-5 The Secondary Quality Factor 51
3-6 The Reflected Impedance 52
3-7 Pickup Behaviour and Influences on the Primary 54
3-7.1 Operation at the Secondary Resonant Frequency 54

InductEV, Inc.
Exhibit 1008
Page 008

3-7.2 Normalization of the Impedance Model 56
3-7.3 Influence of Frequency on the Pickup Behaviour 56
3-7.4 Influence of Frequency on the Reflected Impedance 59
3-7.5 Operating Conditions for Maximum Power Transfer 61
3-8 The Primary Coil 62
3-9 The Primary Quality Factor 65
3-10 The Power Supply Load Model 67
3-10.1 Modelling of the Power Supply Load Impedance 67
3-10.2 The Normalized Load Impedance 69
3-11 Verification of the Load Model 71
3-12 Conclusions 75
References 76

Chapter 4 Evaluation of a Design Methodology for ICPT Systems 77
4-1 Introduction 77
4-2 A Design Procedure 77
4-2.1 Design of Ordinary Transformers 78
4-2.2 Design of ICPT Systems 79
4-3 Design Options for the Pickup Regulator 86
4-4 Design Options for the Power Supply 88
4-5 Design Evaluations 92
4-5.1 Sensitivity of the Displacement Power Factor 92
4-5.2 System Behaviour using a Fixed-Frequency Controller 98
4-5.3 System Behaviour using a Variable-Frequency Controller 101
4-5.4 Design Considerations 104
4-6 A Practical Design Example 105
4-7 Conclusions 109
References 110

Chapter 5 Tuning to Improve Power Transfer for Variable-Frequency Systems 113
5-1 Introduction 113
5-2 Primary Tuning for Unity DPF at Rated Load 114

InductEV, Inc.
Exhibit 1008
Page 009

5-3 Power Transfer Capability and Bifurcation Phenomenon 117
5-4 Bifurcation Criteria 130
5-5 Discussion 139
5-6 Verification 143
5-7 Conclusions 145
References 146

Chapter 6 Tuning to Improve DPF for Fixed-Frequency Systems 149
6-1 Introduction 149
6-2 System Behaviour with Primary Tuning for Unity DPF at Rated Load 149
6-3 Primary Tuning for Load Independent Unity DPF 154
6-3.1 Primary Capacitance and Operating Frequency 155
6-3.2 Power Transfer Capability and Secondary VA Rating 156
6-4 Discussion 163
6-5 Design Examples 164
6-6 Verification 167
6-7 Conclusions 170

Chapter 7 A Sensitivity Analysis of Systems Using the Proposed Primary Tuning Schemes 171
7-1 Introduction 171
7-2 Fundamentals of the Sensitivity Analysis 172
7-3 Compensation Capacitor Selection 173
7-4 The Influence of Variations in Primary Capacitance 177
7-4.1 Fixed-Frequency Systems 177
7-4.2 Variable-Frequency Systems 182
7-5 The Influence of Variations in Secondary Capacitance 184
7-5.1 Fixed-Frequency Systems 184
7-5.2 Variable-Frequency Systems 188
7-6 The Influence of Misalignment in the Electromagnetic Structure 190
7-6.1 Coupling Parameter Variations in an Electric Vehicle Battery Charger ... 191
7-6.2 Fixed-Frequency Systems 192

InductEV, Inc.
Exhibit 1008
Page 010

7-6.3 Variable-Frequency Systems 199
7-7 Discussion 206
7-8 Conclusions 209
References 209

Chapter 8 Investigating an LCL Resonant Inverter for ICPT Applications ... 211
8-1 Introduction 211
8-2 Overview of the System 212
8-2.1 Operating Modes of the LCL Resonant Inverter 212
8-2.2 An Analytical Procedure for System Design 214
8-3 Capability of the Inverter 214
8-3.1 The Inverter Model 214
8-3.2 Waveform of the Inverter Current 215
8-3.3 Inverter Power Delivery Capability 218
8-3.4 Fundamental Component of the Inverter Current 219
8-4 Capability of the Resonant Tank 221
8-4.1 The Resonant Tank Model 221
8-4.2 Operating Frequency 222
8-4.3 Power Absorption Capability 223
8-5 Steady State Power Flow Analysis 225
8-5.1 An Analytical Procedure for Steady State Analysis 225
8-5.2 The Switching Instants and the Series Inductance 225
8-5.3 Behaviour at Light Load 228
8-6 Verification 229
8-7 Conclusions 230
References 231

Chapter 9 Conclusions and Future Work 233
9-1 Conclusions 233
9-1.1 Variable Frequency Systems 233
9-1.2 Fixed Frequency Systems 235
9-2 Future Work 235
References 237

InductEV, Inc.
Exhibit 1008
Page 011

Appendices 239

A. **Primary Voltage and Current Gains** 239

B. **Reactive and Real Powers of the Pickup Coil** 241

C. **Quantified Secondary Current** 242

D. **Normalized Reflected Impedance of Compensated Pickup** 243

E. **Quantified Impedance of the Primary Coil** 244

F. **Normalized Reactance of the Primary Capacitance for Systems with Compensated Pickup** 244

G. **Normalized Impedance Functions for Systems with Uncompensated Pickup** 245

H. **Primary Tuning for Unity DPF at ω_0** 246

I. **Primary Tuning for Load Independent Unity DPF** 250

J. **Maximum Allowable Alternating Voltage and Current in Capacitors** 252

InductEV, Inc.
Exhibit 1008
Page 012

NOMENCLATURE

Symbol	Description
CCL	Capacitor-capacitor-inductor.
C_1, C_2	Capacitors of inverters.
C_d	dc capacitance.
C_m	Matching capacitance in CCL inverter.
C_p	Primary compensation capacitance.
C_{pn}	Normalized primary compensation capacitance.
C_s	Secondary compensation capacitance.
D, D_1, D_2, D_3, D_4	Diodes of inverters.
DPF	Displacement power factor.
ESR	Equivalent series resistance of capacitors
f, f_0, f_1, f_2	Frequency (Hz).
I	RMS current.
i	Instant current.
$I_{ac,rated}$	Rated ac current of capacitors.
ICPT	Inductively coupled power transfer.
I_{Cs}	Secondary capacitor current.
I_d	dc source current.
I_{dc}	dc load current.
I_{GAIN}	Primary current gain.
i_i, I_i	Inverter output current.
I_{i0}	Inverter output current at ω_0.
Im Z	Imaginary component of the impedance (Z).
i_p, I_p	Primary current.
i_R, I_R	Pickup load current.
i_s, I_s	Secondary current.
$I_{s0,rated}$	Rated secondary current defined at ω_0.

InductEV, Inc.
Exhibit 1008
Page 013

I_{sc}	Short circuit current of the pickup.
I_{sn}	Normalized secondary current.
k	Magnetic coupling coefficient.
k_n	Equivalent coupling coefficient of n pickups.
LCL	Inductor-capacitor-inductor.
L_d	dc inductance.
L_m	Matching inductance in LCL inverter.
L_p	Primary self-inductance.
L_s	Secondary self-inductance.
M	Mutual inductance.
M_n	Equivalent mutual inductance of n pickups.
N_p	Turn number of the primary coil.
N_s	Turn number of the secondary coil.
PP	Parallel-compensated primary and secondary.
PS	Parallel-compensated primary and series-compensated secondary.
P	Power.
P_i	Inverter power delivery.
P_n	Normalized power.
P_{rated}	Rated power defined at ω_0.
Q	Quality factor.
Q_p	Primary quality factor.
Q_{p0}	Primary quality factor at ω_0.
Q_s	Secondary quality factor.
Q_{s0}	Secondary quality factor at ω_0.
$Q_{s0,rated}$	Rated secondary quality factor defined at ω_0.
$Q'_{s0,rated}$	Rated secondary quality factor defined at $\omega_0/\sqrt{1-k^2}$.
R	Pickup ac load (Equivalent ac resistance).
R_{dc}	Pickup dc load.
Re Z	Real component of the impedance (Z).
SP	Series-compensated primary and parallel-compensated secondary.
SS	Series-compensated primary and secondary.
S_s	Apparent power (complex power) of the secondary coil.
S, S_1, S_2, S_3, S_4	Switches of inverters.
T	Period.

InductEV, Inc.
Exhibit 1008
Page 014

t, t_1, t_2, t_3	Time.
$t_n, t_{n1}, t_{n2}, t_{n3}$	Normalized time.
u	Normalized operating frequency.
V	RMS voltage.
v	Instant voltage.
VA_{Cs}	Required VA rating of the secondary compensation capacitor.
VA_s	Required secondary VA rating.
VA_{sn}	Normalized required secondary VA rating.
VA_{s0}	Required secondary VA rating at ω_0.
$VA_{s0,rated}$	Rated secondary VA rating defined at ω_0.
$V_{ac,rated}$	Rated ac voltage of capacitors.
VAR	Reactive power.
VAR_p	Primary reactive power.
VAR_s	Secondary reactive power.
V_{Cs}	Secondary capacitor voltage.
V_d	dc source voltage.
V_{dc}	dc load voltage.
V_{GAIN}	Primary voltage gain.
v_i, V_i	Inverter output voltage.
V_{i0}	Inverter output voltage at ω_0.
V_{oc}	Open circuit voltage of the pickup.
v_p, V_p	Primary voltage (parallel resonant tank voltage).
V_{p0}	Primary voltage at ω_0.
$\hat{V}_p$	Peak primary voltage (parallel resonant tank voltage).
V_{pn}	Normalized primary voltage (parallel resonant tank voltage).
v_R, V_R	Secondary pickup load voltage.
v_s, V_s	Secondary voltage.
$V_{s0,rated}$	Rated secondary voltage defined at ω_0.
V_{sn}	Normalized secondary voltage.
Y_t	Load admittance seen by the power supply.
Y_{tn}	Normalized load admittance seen by the power supply.
Z_p	Impedance of the primary track/coil.
Z_r	Reflected impedance.
Z_{r0}	Reflected impedance at ω_0.

InductEV, Inc.
Exhibit 1008
Page 015

$Z_{r0,rated}$	Rated reflected impedance defined at ω_0.
Z_{rn}	Normalized reflected impedance.
Z_s	Secondary load impedance.
Z_t	Load impedance seen by the power supply.
Z_{t0}	Load impedance seen by the power supply at ω_0.
Z_{tn}	Normalized load impedance seen by the power supply.
ω	Frequency (rad/s).
ω_0	Nominal frequency (Secondary resonant frequency).
θ_1	Phase of the load impedance seen by the power supply.
Φ_1	Phase between the fundamental inverter current and the parallel primary voltage.
ϕ	Phase between the primary and secondary currents.
$\tan \delta$	Dissipation factor of capacitors

InductEV, Inc.
Exhibit 1008
Page 016

LIST OF FIGURES

Fig. 1-1. Application examples from Daifuku (Japan). **2**

Fig. 1-2. Public transport system (New Zealand). **2**

Fig. 1-3. Application examples from Wampfler (Germany). **3**

Fig. 1-4. The block diagram of an ICPT system. **4**

Fig. 2-1. Common configurations of the primary coil. **14**

Fig. 2-2. Common configurations of the secondary core. **15**

Fig. 2-3. Circuit of the mutual inductance transformer model. **15**

Fig. 2-4. The sinusoidal mutual inductance transformer model. **16**

Fig. 2-5. Equivalent secondary circuit supplying power to a linear and resistive load. **17**

Fig. 2-6. The normalized load voltage and current of the uncompensated pickup. **18**

Fig. 2-7. Series-compensated secondary. **20**

Fig. 2-8. Parallel-compensated secondary. **20**

Fig. 2-9. Normalized load voltage and current characteristics of uncompensated as well as series and parallel-compensated pickups. **22**

Fig. 2-10. Series-compensated primary. **23**

Fig. 2-11. Parallel-compensated primary. **23**

Fig. 2-12. Basic compensation topologies ofICPT systems. **24**

Fig. 2-13. The block diagram of a power converter in an ICPT system. **25**

Fig. 2-14. Fundamental types of power source. **26**

Fig. 2-15. Switch configurations. **27**

Fig. 2-16. The voltage-sourced full-bridge power converter. **27**

Fig. 2-17. The voltage-sourced half-bridge power converter. **28**

Fig. 2-18. Voltage-sourced single-switch power converters. **28**

Fig. 2-19. The current-sourced full-bridge power converter. **29**

Fig. 2-20. The current-sourced half-bridge power converter. **29**

Fig. 2-21. Current-sourced single-switch power converters. **29**

InductEV, Inc.
Exhibit 1008
Page 017

Fig. 2-22. The LCL resonant inverter. 30
Fig. 2-23. The CCL resonant inverter. 30
Fig. 2-24. The rectangular inverter voltage being in-phase with the current. 33
Fig. 2-25. The rectangular inverter voltage leading the current. 33
Fig. 2-26. The rectangular inverter voltage lagging the current. 33
Fig. 2-27. Pulse-width of the rectangular inverter voltage is less than a full half cycle. 33
Fig. 2-28. The rectangular inverter current being in-phase with the voltage. 34
Fig. 2-29. The rectangular inverter current leading the voltage. 34
Fig. 2-30. The rectangular inverter current lagging the voltage. 34
Fig. 2-31. Pulse-width of the rectangular inverter current is less than a full half cycle. 34
Fig. 2-32. Futuristic ICPT applications. 37

Fig. 3-1. Diagram of the load seen by the power supply. 48
Fig. 3-2. Full-bridge diode rectifier with inductor output filter. 50
Fig. 3-3. Full-bridge diode rectifier with capacitor output filter. 50
Fig. 3-4. Equivalent circuits of the secondary systems. 51
Fig. 3-5. Quantified secondary current. 57
Fig. 3-6. Normalized reflected resistance for series and parallel-compensated secondary systems. 60
Fig. 3-7. Normalized reflected reactance for series and parallel-compensated secondary systems. 61
Fig. 3-8. Equivalent circuit of the primary coil. 62
Fig. 3-9. The ratio $Z_p/(j\omega_0 L_p)$ at the secondary resonant frequency ω_0 (u=1). 64
Fig. 3-10. The ratio $Z_p/(j\omega_0 L_p)$ with k=0.2. 64
Fig. 3-11. The ratio $Z_p/(j\omega_0 L_p)$ with k=0.6. 65
Fig. 3-12. Primary resonant circuits with reflected impedance. 67
Fig. 3-13. Electromagnetic structure of the contact-less battery charger. 72
Fig. 3-14. The measured coupling parameters (L_p, L_s, M) of the battery charger. 73
Fig. 3-15. Measured and calculated load admittance (Y_t) of the battery charger. 74

Fig. 4-1. A design procedure of the ordinary transformer. 79
Fig. 4-2. A design procedure of ICPT systems. 80
Fig. 4-3. A block diagram of a pickup regulator. 87
Fig. 4-4. Examples of current-sourced power supply configurations. 89

InductEV, Inc.
Exhibit 1008
Page 018

Fig. 4-5. Examples of voltage-sourced power supply configurations. **90**
Fig. 4-6. Sensitivity of DPF to u and k in systems having both the primary and secondary uncompensated. **94**
Fig. 4-7. Sensitivity of DPF to u and k in systems having a compensated primary and an uncompensated secondary. **95**
Fig. 4-8. Sensitivity of DPF to u, k and Q_{s0} in systems having an uncompensated primary and a compensated secondary. **96**
Fig. 4-9. Sensitivity of DPF to u, k and Q_{s0} in systems having both the primary and secondary compensated. **97**
Fig. 4-10. DPF operating with fixed frequency at ω_0. ..... **99**
Fig. 4-11. Required relationship between k and Q_{s0} to achieve unity DPF at ω_0 for the PP topology. **100**
Fig. 4-12. Selection of Q_{s0} to improve DPF when operating at ω_0 over a wider range of k for the PP topology. **100**
Fig. 4-13. Operating frequency with unity DPF. **102**
Fig. 4-14. Frequency shifts for bifurcation-free operations. **104**
Fig. 4-15. DPF and power transfer capability of the contact-less electric vehicle battery charger using a fixed-frequency controller operating at ω_0. ..... **106**
Fig. 4-16. Measured waveforms of the inverter current and the resonant tank voltage for the contact-less electric vehicle battery charger (operating at ω_0=19.7kHz). **107**
Fig. 4-17. Operating frequency and power transfer capability of the contact-less electric vehicle battery charger using a variable-frequency controller operating with unity DPF. ... **108**

Fig. 5-1. Primary tuning for unity DPF at rated load. **116**
Fig. 5-2. SS topology - Operating frequency and power transfer capability under variable-frequency operation. **122**
Fig. 5-3. SP topology - Operating frequency and power transfer capability under variable-frequency operation. **123**
Fig. 5-4. PP topology with loose coupling (k=0.05) - Operating frequency and power transfer capability under variable-frequency operation. **124**
Fig. 5-5. PP topology with middle coupling (k=0.2) - Operating frequency and power transfer capability under variable-frequency operation. **125**
Fig. 5-6. PP topology with good coupling (k=0.4) - Operating frequency and power transfer capability under variable-frequency operation. **126**

InductEV, Inc.
Exhibit 1008
Page 019

Fig. 5-7. PS topology with loose coupling (k=0.05) - Operating frequency and power transfer capability under variable-frequency operation. **127**

Fig. 5-8. PS topology with middle coupling (k=0.2) - Operating frequency and power transfer capability under variable-frequency operation. **128**

Fig. 5-9. PS topology with good coupling (k=0.4) - Operating frequency and power transfer capability under variable-frequency operation. **129**

Fig. 5-10. Normalized load reactance. **132**

Fig. 5-11. Normalized load susceptance. **133**

Fig. 5-12. Normalized function $G(u,Q_{p0},Q_{s0})$. **135**

Fig. 5-13. Analytical bifurcation boundary for the SS and SP topologies. **137**

Fig. 5-14. Numerical algorithm for finding bifurcation boundary. **137**

Fig. 5-15. Numerical bifurcation boundary for the PP and PS topologies. **138**

Fig. 5-16. Bifurcation boundary defined by k and Q_{s0} for the four basic topologies. **139**

Fig. 5-17. A contact-less electric vehicle battery charger with PP topology – Operating frequency and power transfer capability under variable-frequency operation (a comparison of the original and modified tuning schemes). **144**

Fig. 6-1. SP topology - DPF under fixed-frequency operation at ω_0 assuming modified primary tuning to achieve unity DPF at rated load. **151**

Fig. 6-2. PP topology - DPF under fixed-frequency operation at ω_0 assuming modified primary tuning to achieve unity DPF at rated load. **152**

Fig. 6-3. PS topology - DPF under fixed-frequency operation at ω_0 assuming modified primary tuning to achieve unity DPF at rated load. **153**

Fig. 6-4. Influences of k to the required change in C_p to achieve load independent unity DPF. ... **156**

Fig. 6-5. Influence of k to the required change in ω to achieve load independent unity DPF (the PP and PS topologies). **156**

Fig. 6-6. PP topology – System behaviour under fixed-frequency operation ($Q_{s0,rated}$=5). **159**

Fig. 6-7. PS topology – System behaviour under fixed-frequency operation ($Q_{s0,rated}$=5). **160**

Fig. 6-8. Limit of k and $Q_{s0,rated}$ when using the modified tuning to achieve load independent unity DPF. **161**

Fig. 6-9. Changes in the secondary current, secondary voltage, and required secondary VA rating under rated power operation when using the modified tuning to achieve load independent unity DPF. **162**

Fig. 6-10. Power transfer capability under fixed-frequency operation ($Q_{s0,rated}$=2). **163**

InductEV, Inc.
Exhibit 1008
Page 020

Fig. 6-11. A contact-less electric vehicle battery charger with PP topology – DPF under fixed-frequency operation (a comparison of the original and modified tuning schemes). ... **165**

Fig. 6-12. A contact-less electric vehicle battery charger with PP topology – Power transfer capability and required secondary VA rating under fixed-frequency operation (a comparison of the original and modified tuning schemes). **166**

Fig. 6-13. A contact-less electric vehicle battery charger with PS topology – DPF under fixed-frequency operation (a comparison of the original and modified tuning schemes). ... **166**

Fig. 6-14. A contact-less electric vehicle battery charger with PS topology – Power transfer capability and required secondary VA rating under fixed-frequency operation (a comparison of the original and modified tuning schemes). **167**

Fig. 6-15. A contact-less electric vehicle battery charger with PP topology, using the modified tuning to achieve load independent unity DPF (C_{pn}=1, u=1.12) - Measured waveforms of the inverter current (i_i) and the resonant tank voltage (v_p). **168**

Fig. 6-16. A contact-less electric vehicle battery charger with PP topology, using the modified tuning to achieve load independent unity DPF (C_{pn}=1, u=1.12) - Measured and calculated power and secondary VA. **168**

Fig. 6-17. A contact-less electric vehicle battery charger with PS topology, using the modified tuning to achieve load independent unity DPF (C_{pn}=0.8, u=1.12) - Measured waveforms of the inverter current (i_i) and the resonant tank voltage (v_p). **169**

Fig. 6-18. A contact-less electric vehicle battery charger with PS topology, using the modified tuning to achieve load independent unity DPF (C_{pn}=0.8, u=1.12) - Measured and calculated power and secondary VA. **169**

Fig. 7-1. High frequency power capability of capacitors. **174**

Fig. 7-2. Typical frequency dependence of the dissipation factor (tan δ) of capacitors. **175**

Fig. 7-3. Typical temperature dependence of the capacitance. **176**

Fig. 7-4. Typical aging (time dependence of the capacitance) – Class II ceramic capacitors (Source: American Technical Ceramics). **176**

Fig. 7-5. Typical voltage dependence of the capacitance (Source: WIMA) – Polyester plastic film capacitors (PET), Class II ceramic capacitors (X7R/Z5U). **176**

Fig. 7-6. Original tuning (C_{pn}=1, u=1) – The influence of variations in C_p for an electric vehicle battery charger under fixed-frequency operation (k=0.45, $Q_{s0,rated}$=1.8, PP topology, I_p=15A). **178**

InductEV, Inc.
Exhibit 1008
Page 021

Fig. 7-7. Modified tuning for unity DPF at rated load (C_{pn}=1.04, u=1) – The influence of variations in C_p for an electric vehicle battery charger under fixed-frequency operation. **179**

Fig. 7-8. Modified tuning for load independent unity DPF (C_{pn}=1, u=1.12) – The influence of variations in C_p for an electric vehicle battery charger under fixed-frequency operation. **179**

Fig. 7-9. Electromagnetic structure of the monorail material handling system. **180**

Fig. 7-10. The influence of variations in C_p for a monorail material handling system under fixed-frequency operation (k=0.086, $Q_{s0,rated}$=4.7, PP topology, C_{pn}=1, u=1). **181**

Fig. 7-11. Original tuning (C_{pn}=1) – The influence of variations in C_p for an electric vehicle battery charger under variable-frequency operation (k=0.45, $Q_{s0,rated}$=1.8, PP topology, I_p=15A). **183**

Fig. 7-12. Modified tuning for unity DPF at rated load (C_{pn}=1.04) – The influence of variations in C_p for an electric vehicle battery charger under variable-frequency operation. ... **184**

Fig. 7-13. The influence of variations in C_p for a monorail material handling system under variable-frequency operation (k=0.086, $Q_{s0,rated}$=4.7, PP topology, C_{pn}=1, I_p=54A). ... **185**

Fig. 7-14. Original tuning (C_{pn}=1, u=1) – The influence of variations in C_s for an electric vehicle battery charger under fixed-frequency operation (k=0.45, $Q_{s0,rated}$=1.8, PP topology, I_p=15A). **186**

Fig. 7-15. Modified tuning for unity DPF at rated load (C_{pn}=1.04, u=1) – The influence of variations in C_s for an electric vehicle battery charger under fixed-frequency operation. **186**

Fig. 7-16. Modified tuning for load independent unity DPF (C_{pn}=1, u=1.12) – The influence of variations in C_s for an electric vehicle battery charger under fixed-frequency operation. **187**

Fig. 7-17. The influence of variations in C_s for a monorail material handling system under fixed-frequency operation (k=0.086, $Q_{s0,rated}$=4.7, PP topology, C_{pn}=1, u=1). **187**

Fig. 7-18. Original tuning (C_{pn}=1) – The influence of variations in C_s for an electric vehicle battery charger under variable-frequency operation (k=0.45, $Q_{s0,rated}$=1.8, PP topology, I_p=15A). **188**

Fig. 7-19. Modified tuning for unity DPF at rated load (C_{pn}=1.04) – The influence of variations in C_s for an electric vehicle battery charger under variable-frequency operation (k=0.45, $Q_{s0,rated}$=1.8, PP topology, I_p=15A). **189**

InductEV, Inc.
Exhibit 1008
Page 022

Fig. 7-20. The influence of variations in C_s for a monorail material handling system under variable-frequency operation (k=0.086, $Q_{s0,rated}$=4.7, PP topology, C_{pn}=1, I_p=54A). **190**

Fig. 7-21. Misalignment of the contact-less electric vehicle battery charging system. **191**

Fig. 7-22. Measurement of the effects of misalignment on coupling parameters for the contact-less electric vehicle battery charger. **191**

Fig. 7-23. Symmetry of the electromagnetic structure of the battery charger. **192**

Fig. 7-24. Original tuning (C_{pn}=1, u=1) – The influence of variations in L_p for an electric vehicle battery charger under fixed-frequency operation (k=0.45, $Q_{s0,rated}$=1.8, PP topology, I_p=15A). **193**

Fig. 7-25. Modified tuning for unity DPF at rated load (C_{pn}=1.04, u=1) – The influence of variations in L_p for an electric vehicle battery charger under fixed-frequency operation. **193**

Fig. 7-26. Modified tuning for load independent unity DPF (C_{pn}=1, u=1.12) – The influence of variations in L_p for an electric vehicle battery charger under fixed-frequency operation. **194**

Fig. 7-27. Original tuning (C_{pn}=1, u=1) – The influence of variations in L_s for an electric vehicle battery charger under fixed-frequency operation (k=0.45, $Q_{s0,rated}$=1.8, PP topology, I_p=15A). **194**

Fig. 7-28. Modified tuning for unity DPF at rated load (C_{pn}=1.04, u=1) – The influence of variations in L_s for an electric vehicle battery charger under fixed-frequency operation. **195**

Fig. 7-29. Modified tuning for load independent unity DPF (C_{pn}=1, u=1.12) – The influence of variations in L_s for an electric vehicle battery charger under fixed-frequency operation. **195**

Fig. 7-30. Original tuning (C_{pn}=1, u=1) – The influence of variations in M for an electric vehicle battery charger under fixed-frequency operation (k=0.45, $Q_{s0,rated}$=1.8, PP topology, I_p=15A). **196**

Fig. 7-31. Modified tuning for unity DPF at rated load (C_{pn}=1.04, u=1) – The influence of variations in M for an electric vehicle battery charger under fixed-frequency operation. **196**

Fig. 7-32. Modified tuning for load independent unity DPF (C_{pn}=1, u=1.12) – The influence of variations in M for an electric vehicle battery charger under fixed-frequency operation. **197**

InductEV, Inc.
Exhibit 1008
Page 023

Fig. 7-33. The influence of variations in L_p for a monorail material handling system under fixed-frequency operation (k=0.086, $Q_{s0,rated}$=4.7, PP topology, C_{pn}=1, u=1). **197**

Fig. 7-34. The influence of variations in L_s for a monorail material handling system under fixed-frequency operation (k=0.086, $Q_{s0,rated}$=4.7, PP topology, C_{pn}=1, u=1). **198**

Fig. 7-35. The influence of variations in M for a monorail material handling system under fixed-frequency operation (k=0.086, $Q_{s0,rated}$=4.7, PP topology, C_{pn}=1, u=1). **198**

Fig. 7-36. Original tuning (C_{pn}=1) – The influence of variations in L_p for an electric vehicle battery charger under variable-frequency operation (k=0.45, $Q_{s0,rated}$=1.8, PP topology, I_p=15A). **199**

Fig. 7-37. Modified tuning for unity DPF at rated load (C_{pn}=1.04) – The influence of variations in L_p for an electric vehicle battery charger under variable-frequency operation (k=0.45, $Q_{s0,rated}$=1.8, PP topology, I_p=15A). **200**

Fig. 7-38. Original tuning (C_{pn}=1) – The influence of variations in L_s for an electric vehicle battery charger under variable-frequency operation (k=0.45, $Q_{s0,rated}$=1.8, PP topology, I_p=15A). **201**

Fig. 7-39. Modified tuning for unity DPF at rated load (C_{pn}=1.04) – The influence of variations in L_s for an electric vehicle battery charger under variable-frequency operation (k=0.45, $Q_{s0,rated}$=1.8, PP topology, I_p=15A). **202**

Fig. 7-40. Original tuning (C_{pn}=1) – The influence of variations in M for an electric vehicle battery charger under variable-frequency operation (k=0.45, $Q_{s0,rated}$=1.8, PP topology, I_p=15A). **203**

Fig. 7-41. Modified tuning for unity DPF at rated load (C_{pn}=1.04) – The influence of variations in M for an electric vehicle battery charger under variable-frequency operation (k=0.45, $Q_{s0,rated}$=1.8, PP topology, I_p=15A). **204**

Fig. 7-42. The influence of variations in L_p for a monorail material handling system under variable-frequency operation (k=0.086, $Q_{s0,rated}$=4.7, PP topology, C_{pn}=1, I_p=54A). ... **205**

Fig. 7-43. The influence of variations in L_s for a monorail material handling system under variable-frequency operation (k=0.086, $Q_{s0,rated}$=4.7, PP topology, C_{pn}=1, I_p=54A). ... **205**

Fig. 7-44. The influence of variations in M for a monorail material handling system under variable-frequency operation (k=0.086, $Q_{s0,rated}$=4.7, PP topology, C_{pn}=1, I_p=54A). ... **206**

Fig. 8-1. Circuit diagram of an ICPT system driven by an LCL resonant inverter. **212**

Fig. 8-2. Inverter voltage and current waveforms for the LCL resonant inverter. **213**

Fig. 8-3. Switching control of the LCL resonant inverter in discontinuous current mode. **213**

InductEV, Inc.
Exhibit 1008
Page 024

Fig. 8-4. Simplified model of the LCL resonant inverter. **215**
Fig. 8-5. Influences of varying V_{pn} on the inverter current waveform assuming maximum pulse width by setting t_{1n}=0, t_{3n}=0.5. ..... **216**
Fig. 8-6. Influences of V_{pn} and t_{1n} on the inverter current waveform (t_{3n} = 0.5). **217**
Fig. 8-7. Influences of V_{pn} and t_{3n} on the inverter current waveform (t_{1n} = zero). **218**
Fig. 8-8. Influences of increasing t_{1n} on the inverter current phase relationship assuming maximum t_{3n} of 0.5. ..... **220**
Fig. 8-9. Influences of decreasing t_{3n} on the inverter current phase relationship assuming minimum t_{1n} of zero. **221**
Fig. 8-10. Phase angle of the resonant tank admittance at rated load. **222**
Fig. 8-11. Influences of increasing t_{1n} on the operating frequency assuming maximum t_{3n} of 0.5 at rated load. **223**
Fig. 8-12. Resonant tank conductance at rated load. **224**
Fig. 8-13. Effects of t_{1n} on the resonant tank conductance at rated load. **224**
Fig. 8-14. Influences of t_{1n} on resonant tank power absorption capability at rated load. **225**
Fig. 8-15. An analytical procedure for the determination of steady state operation. **226**
Fig. 8-16. Inverter and resonant tank power flow balance at rated load. **227**
Fig. 8-17. Inverter current waveforms at light loads. **229**
Fig. 8-18. Calculated and measured steady state operation. **230**

InductEV, Inc.
Exhibit 1008
Page 025

LIST OF TABLES

TABLE 2-1. PICKUP VOLTAGES, CURRENTS, POWER AND REQUIRED VA RATINGS. **22**

TABLE 3-1. QUANTIFIED PICKUP VOLTAGES, CURRENTS. **58**
TABLE 3-2. LOAD IMPEDANCE OF THE BASIC TOPOLOGIES. **68**
TABLE 3-3. FUNCTIONS OF THE NORMALIZED LOAD IMPEDANCE WITH COMPENSATED PICKUP. ... **70**
TABLE 3-4. PARAMETERS OF THE CONTACT-LESS ELECTRIC VEHICLE BATTERY CHARGER. **72**

TABLE 4-1. ASSUMPTIONS OF THE DESIGN PROCEDURE IN FIG. 4-2. ..... **81**
TABLE 4-2. SUMMARY OF SYSTEM CONFIGURATIONS OF THE DESIGN PROCEDURE. **86**
TABLE 4-3. COMPARISON OF POWER SUPPLY CONFIGURATIONS. **91**
TABLE 4-4. COMPARISON OF FIXED AND VARIABLE FREQUENCY CONTROLLER. **91**
TABLE 4-5. NORMALIZED LOAD IMPEDANCES. **93**
TABLE 4-6. FUNCTIONS OF THE NORMALIZED LOAD IMPEDANCE WITH UNCOMPENSATED PICKUP. **93**
TABLE 4-7. FUNCTIONS OF THE NORMALIZED LOAD IMPEDANCE WITH COMPENSATED PICKUP. ... **94**
TABLE 4-8. DPF OPERATING WITH FIXED FREQUENCY AT ω_0. ..... **98**
TABLE 4-9. BIFURCATION BOUNDARY FOR VARIABLE-FREQUENCY OPERATION WITH UNITY DPF. **103**

TABLE 5-1. PRIMARY TUNING FOR UNITY DPF AT RATED LOAD. **117**
TABLE 5-2. NORMALIZED LOAD IMPEDANCES WITH COMPENSATED PICKUP. **118**
TABLE 5-3. FUNCTIONS OF THE NORMALIZED LOAD IMPEDANCE WITH MODIFIED TUNING. **119**
TABLE 5-4. NORMALIZED FUNCTIONS IN (5-11). **134**
TABLE 5-5. BIFURCATION CRITERIA. **139**
TABLE 5-6. IMPROVEMENT OF THE POWER TRANSFER CAPABILITY WITH THE MODIFIED TUNING FOR A LOOSELY COUPLED SYSTEM (k=0.05)..... **141**
TABLE 5-7. IMPROVEMENT OF THE POWER TRANSFER CAPABILITY WITH THE MODIFIED TUNING FOR A MIDDLE COUPLED SYSTEM (k=0.2)..... **142**

InductEV, Inc.
Exhibit 1008
Page 027

TABLE 5-8. IMPROVEMENT OF THE POWER TRANSFER CAPABILITY WITH THE MODIFIED TUNING FOR A WELL-COUPLED SYSTEM (k=0.4). **142**

TABLE 6-1. A SUMMARY OF C_{pn} FOR THE ORIGINAL TUNING AND THE MODIFIED TUNING FOR UNITY DPF AT RATED LOAD. **151**

TABLE 6-2. NORMALIZED PRIMARY COMPENSATION CAPACITANCE AND OPERATING FREQUENCY REQUIRED TO ACHIEVE LOAD INDEPENDENT UNITY DPF. **155**

TABLE 7-1. TYPICAL CAPACITANCE TOLERANCE OF PLASTIC FILM AND CERAMIC CAPACITORS. ... **175**

TABLE 7-2. LONG TERM CAPACITANCE CHANGE OF PLASTIC FILM CAPACITORS. **176**

TABLE 7-3. TYPICAL CHARACTERISTICS OF PLASTIC FILM AND CERAMIC CAPACITORS (SOURCE: WIMA). **177**

TABLE 7-4. PARAMETERS OF THE MONORAIL MATERIAL HANDLING SYSTEM. **181**

TABLE 7-5. SENSITIVITY OF DPF TO VARIATIONS IN C_P, C_S, L_P, L_S AND M UNDER FIXED-FREQUENCY OPERATION (PP TOPOLOGY). **207**

TABLE 7-6. THE INFLUENCE OF VARIATIONS IN C_S, L_S AND M ON THE POWER TRANSFER CAPABILITY UNDER FIXED-FREQUENCY OPERATION (PP TOPOLOGY). **207**

TABLE 7-7. SENSITIVITY OF THE OPERATING FREQUENCY TO VARIATIONS IN C_P, C_S, L_P, L_S AND M UNDER VARIABLE-FREQUENCY OPERATION (PP TOPOLOGY). **208**

TABLE 7-8. THE INFLUENCE OF VARIATIONS IN C_P, C_S, L_P, L_S AND M ON THE POWER TRANSFER CAPABILITY UNDER VARIABLE-FREQUENCY OPERATION (PP TOPOLOGY). **208**

TABLE 8-1. STEADY STATE OPERATIONS FOR MAXIMUM POWER WITH SELECTIONS OF t_{1n}. **228**

TABLE 8-2. SYSTEM BEHAVIOUR AT LIGHT LOAD. **228**

TABLE 8-3. MEASURED FREQUENCY, PRIMARY CURRENT AND POWER. **230**

InductEV, Inc.
Exhibit 1008
Page 028

This material may be protected by Copyright law (Title 17 U.S. Code)

CHAPTER 1

INTRODUCTION

1-1 Background of ICPT systems
1-2 Fundamental structure of ICPT systems
1-3 Motivations of the research
1-4 Contributions of the thesis
1-5 Scope of the thesis

1-1 BACKGROUND OF ICPT SYSTEMS

Inductively coupled power transfer (ICPT) systems utilize electromagnetic fields to transfer electric power from a stationary primary source to one or more movable secondary loads without contact. Using power electronic technology, ICPT systems with very low magnetic coupling strength have recently been practically realized [1][2] with the number of commercial applications growing every year.

Potential applications of ICPT systems are unlimited. Present applications include material handling, public transport and battery charging. ICPT systems are free of sparking, wear, tear and hazard. They are immune to dirt, moisture, water, snow, ice, and can be used in potentially explosive atmospheres. They are also safe, quiet and highly reliable. This low maintenance requirement improves productivity.

More than a hundred years ago, alternating current at approximately 1-2 kHz was proposed by Hutin and Leblanc [3] to supply power from a track to a railway vehicle across an air gap. Multiple secondary coils with independent circuit breakers were used for regulation of the power transferred to the motor.

In 1974, an ICPT system was suggested by Otto [4] to supply power to a moving vehicle. The suggested operating frequency was 4-10 kHz.

In 1994, Boys and Green suggested an ICPT system operating at 10 kHz for electric vehicles [5-6]. This is probably the first design suitable for practical industrial applications. The application of this invention to material handling systems and in particular to monorail and conveyor systems has since been licensed to Diafuku (Japan), one of the largest manufacturers of conveyors and material handling systems in the world. As shown in Fig. 1-1, successful commercial systems include clean room applications for semiconductor manufacturing industry as well as assembly lines for the car manufacturing industry.

InductEV, Inc.
Exhibit 1008
Page 029



(a) Clean room inter-process transportation. (b) Monorail material handling.

Fig. 1-1. Application examples from Daifuku (Japan).

In 1997, the Electrical and Computer Engineering (ECE) Department at The University of Auckland working with Wampfler AG in Germany through Auckland UniServices developed an ICPT system to provide intervention free battery charging to a specially designed low weight vehicle for use in a public transport system (Fig. 1-2), at the Whakarewarewa thermal park, Rotorua, New Zealand [2]. The charging bay is buried under the ground and the charging process is transparent to the driver. When the driver stops at the loading platform, the charging unit automatically senses the vehicle and begins charging if required. Four charging bays are provided allowing opportunity charging throughout the day. This minimizes the necessary on-board batteries, while still allowing the vehicles to be operated continuously.



Fig. 1-2. Public transport system (New Zealand).

After the success of this public transport system, Wampfler, in cooperation with Auckland UniServices and the ECE Department at The University of Auckland, invested intensively in the commercialisation and marketing of the ICPT technology. Various examples are shown in Fig. 1-3.

InductEV, Inc.
Exhibit 1008
Page 030



(a) Test track for road surfaces, Japan Public Works Research Institute.



(b) BMW-Floor conveying system, BMW AG, Site Dingolfing, Germany.



(c) E-bus, "Porto Antico", Genoa, Italy.



(d) Elevator, "Hermes Tower", Hanover, Germany.



(e) Trolley, "The Grove", Fairfax-District, Los Angeles, U.S.A.

Fig. 1-3. Application examples from Wampfler (Germany).

A recent competitor to Wampfler and Daifuku, VAHLE (Germany), has utilized ICPT technology successfully in its contact-less power transfer systems for material handling. More than 20 systems have been sold mainly to the car manufacturing industry. Its customers include Volkswagen (Germany), Volkswagen (PR China), Ford (Brazil), Volkswagen (Czech Republik), SML/Ford (Belgium), Karmann (Germany), Deckel Maho (Germany), Volkswagen (Poland), Ford (Germany), Gampro (Germany), IHI (Japan), Los Alamos National Laboratory (USA), and Nissan (USA).

In the low power market, there is growing interest in inductive charging of portable consumer products. Inductive charging systems include an electromagnetic or radio frequency coil that generates an electromagnetic field, which is coupled to a receiver coil within the device that includes a battery [7-12]. Scientists are currently researching the possibility of re-charging the battery of the artificial heart through the skin from a coil outside the body [13].

Environmental influences of electromagnetic fields (EMF) are growing fast with advancing technology such as mobile telecommunications. Thus, the anxieties and speculations about the health hazards of EMF exposure are spreading among all populations of the world. The potential health effects of EMF exposure therefore need to be clarified scientifically.

InductEV, Inc.
Exhibit 1008
Page 031

The World Health Organization (WHO) started from 1996 to assess the scientific evidence of possible health effects of EMF exposure in the frequency range from 0 to 300GHz. All reviews conducted so far have indicated that exposures below the limits recommended in the ICNIRP (1998) EMF guidelines [14], covering the full frequency range from 0 to 300GHz, do not produce any known adverse health effect. However, there are gaps in knowledge still needing to be filled before better health risk assessments can be made.

The Medical School of The University of Auckland examined the effect of 10 kHz magnetic fields in an experiment on animals [15-16]. Likewise no health hazard was found.

1-2 FUNDAMENTAL STRUCTURE OF ICPT SYSTEMS

The block diagram of an ICPT system is shown in Fig. 1-4. The system can be separated into six subsystems that include the switching power supply, the primary compensation, the electromagnetic coupling, the secondary compensation, the secondary switching controller and the load.

The power source of an ICPT system is usually the electric utility supplying voltage and current at a line frequency of 50 or 60Hz, single or three phases. For portable applications, the power source can be a battery supplying dc voltage and current.

In order to increase the amount of power transferred via the electromagnetic structure in a practical ICPT system, the power supply is used to provide high frequency voltage and current (normally above the audible range). The reactance of both the primary and secondary windings increases in proportion to increases in the operating frequency, and as such is normally compensated by capacitors. A secondary switched mode controller may be used to control the power flow to the load.

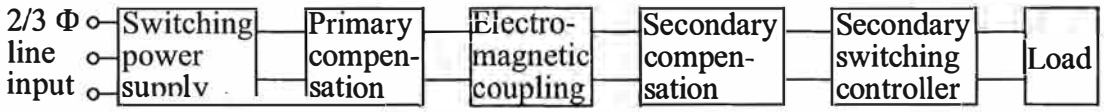


Fig. 1-4. The block diagram of an ICPT system.

1-3 MOTIVATIONS OF THE RESEARCH

This research focuses on the design of ICPT systems for high power applications, where both the primary and secondary are compensated. It is desired to enable increasing air gaps as well as increasing track length and number of pickups, while achieving greater power and better efficiency. The size, weight and cost of such systems are presently much higher than a wired connection. The challenge is to reduce the gap.

InductEV, Inc.
Exhibit 1008
Page 032

The compensated secondary pickup in an ICPT system is normally designed to ensure its tuned frequency is close to the nominal operating frequency of the system. If the operating frequency shifts away from this tuned frequency, the pickup is said to be detuned resulting in significantly lower power transfer capability.

There are two groups of ICPT systems: fixed and variable frequency systems [17]. In fixed-frequency systems, the pickup can be correctly tuned to operate at the maximum power point. In consequence, the size and cost of the pickup are minimized. However, the power supply may operate with a poor displacement power factor (DPF) and needs to be oversized to provide the additional reactive power. This results in an increase in the size and cost of the power supply.

In variable-frequency systems, the operating frequency is allowed to vary so that the power supply operates close to unity DPF. The size and cost of the power supply are therefore minimized. However, pickup frequency detuning is unavoidable and the pickup needs to be oversized to transfer the required power since it does not operate at its "ideal" maximum power point. This increases the size and cost of the pickup.

Under variable-frequency operation, the system may become "unstable" because of the onset of frequency bifurcation with load variation. Here, more than one operating mode is present in the frequency spectrum. If the system can not operate stably at the desired operating load, the required power will be unavailable. The phenomenon of bifurcation has been investigated in selected ICPT systems [1][17]. Further investigation is required to enable general design criteria to ensure system stability.

A direct approach to improve the DPF of the power supply and minimize the frequency detuning of any pickup is dynamic tuning. Here the inductance or capacitance is adjusted dynamically at either the primary or the secondary. In addition to the increased complexity of the controller, dynamically tuned systems have larger size and higher cost. Another approach proposed in [17] has additional resonant circuits consisting of inductors and capacitors at the output stage of the power converter, which significantly maximize the DPF, minimize the pickup frequency detuning, and reduce the influence of bifurcation. Again, the size and cost and complexity of the total system are increased due to additional inductors and capacitors required.

Previous work concentrates on either the primary power supply or the secondary pickups. This research instead investigates the interactions between the power supply and the pickups in order to identify influences of such interactions on the DPF, the power transfer capability, and the operating frequency. Whenever the interactions between the primary and secondary are negligible in comparison to the primary and secondary self-resonance, the primary and secondary resonance can be assumed to be independent of each other. This significantly simplifies the analysis and design of the power supply

InductEV, Inc.
Exhibit 1008
Page 033

as well as the pickups. Here, a constant primary current with a fixed frequency is usually assumed in the pickup design. For the design of the power supply, the loading effect from the pickup is normally assumed to be a variable resistor in series with the primary winding [17]. However, interactions between the primary and secondary resonant circuits become significant when the magnetic coupling strength of the system is improved, the pickup load increases, or more pickups are added [1]. A precise analysis of such systems requires the primary and secondary resonant circuits to be solved simultaneously. This approach is used here.

1-4 CONTRIBUTIONS OF THE THESIS

The contributions of this thesis have emanated mainly from investigations into the interactions between the power supply and the pickup, as well as from exploring suitable design approaches to take into account such interactions.

Quantification of System's Behaviour: Steady state linear high order mathematical model has been developed to represent the load seen by the power supply, which includes the primary compensation capacitor, the electromagnetic structure, the secondary compensation capacitor, and the pickup load. The electromagnetic structure and the primary and secondary compensation capacitors are assumed to be loss-less. The pickup load is assumed to be resistive. Four models have been developed for the four basic compensation topologies (a series compensated primary and secondary, a series compensated primary and parallel compensated secondary, a parallel compensated primary and secondary, a parallel compensated primary and series compensated secondary). The DPF of the power supply, the frequency detuning of the pickup, the bifurcation phenomenon and the power transfer capability are all quantified in terms of the fundamental design parameters, which include the operating frequency, the magnetic coupling coefficient, and the quality factors associated with the primary and secondary resonant circuits. This provides an insight into the system's behaviour at the design stage to assist the choice of the primary and secondary compensation topologies as well as the decision of the fundamental design parameters [18-22].

Description and Evaluation of a Design Methodology: A procedure has been described to illustrate step by step a design approach for ICPT systems. Here the primary and secondary resonances are assumed to be independent. The objective is to minimize the total cost by suitable choices of the operating frequency, the primary current, the electromagnetic structure, the primary and secondary compensation, the pickup regulator, and the high frequency switching power supply. The designed systems are evaluated to determine the degree of system deviation from the desired operating point resulting from loading effects of the pickup on the primary. This investigation shows that systems

InductEV, Inc.
Exhibit 1008
Page 034

designed using the four basic compensation topologies behave quite differently when the secondary loading effects are significant. The necessary design considerations for each topology are identified to ensure power transfer capability and controllability.

New Primary Tuning Schemes for Variable-Frequency Systems: Several new primary tuning schemes are proposed to improve the power transfer capability of variable-frequency systems. The system design approach is kept unchanged, and no additional components are added. The power transfer capability is simply improved by modifying the primary compensation capacitance to minimize frequency variation from the pickup tuned frequency. The necessary modification is determined for each of the four basic compensation topologies. Design criteria are developed for each system to ensure bifurcation is avoided. Significant improvements in power transfer capability are achieved for well-coupled systems where the primary and/or the secondary are parallel compensated, providing the design criteria are satisfied [19-21].

New Primary Tuning Schemes for Fixed-Frequency Systems: Additional primary tuning schemes are proposed to improve the DPF of fixed-frequency systems. Unity DPF is achievable independent of load with suitable choice of the primary compensation capacitance for series tuned primary systems. In the case of parallel tuned primary systems, load independent unity DPF can also be achieved but requires a shift in the ideal operating frequency that in turn affects the power transfer capability of the pickups and the required secondary VA rating. Despite the change in operating frequency, rated power can still be achieved in the majority of ICPT systems, providing (as is the case in practice) they are either loosely coupled systems with reasonable secondary quality factor or well-coupled systems with low secondary quality factor.

Sensitivity Analysis: The proposed new tuning schemes have been investigated further using several sensitivity analyses. Variations in the primary and secondary compensation capacitances as well as misalignment in the electromagnetic structure were considered and evaluated in terms of their influences on power transfer capability, DPF, and operating frequency. Systems designed using the new tuning schemes have similar sensitivities compared with the original tuning.

Investigation of an LCL Resonant Inverter: While the LCL resonant inverter is commonly operated with continuous current, operating under variable frequency control with discontinuous current is able to reduce the required inverter VA rating as well as the turn-on losses. The latter requires a complex design process. To deal with this complexity, a feasible design procedure was detailed to enable the inverter to deliver maximum power to the load [22].

InductEV, Inc.
Exhibit 1008
Page 035

1-5 SCOPE OF THE THESIS

Chapter 2 gives an overview of ICPT systems including the electromagnetic structure, the primary and secondary compensations, the power converters, and control options. The main objective is to clarify the current status of this technology at the on-set of this thesis work and its connections to the work of the thesis.

Chapter 3 develops a general load model as seen by the power supply. This impedance model combines the primary and secondary resonant circuits into a single high order mathematical model allowing the interactions between the primary power supply and the secondary pickups to be well described. The new load model is then normalized to characterise system behaviour in terms of the fundamental design parameters.

Chapter 4 uses the normalized load model to evaluate a design methodology where the primary and secondary resonances are assumed to be independent. A design procedure is described in detail along with a brief review of the design options for pickup regulators and power supplies. Influences of the interactions between the primary and secondary on the DPF of the power supply, the frequency detuning of the pickup, and the bifurcation phenomenon of the controller are investigated.

Chapter 5 proposes new primary tuning schemes for variable-frequency systems taking into account the secondary loading effects on the primary. The objective is to minimize the size and cost of the pickup by reducing frequency detuning. In order to avoid bifurcation, design criteria are developed to identify the boundary where bifurcation occurs.

Chapter 6 proposes alternative primary tuning schemes for fixed-frequency systems. The aim here is to minimize the size and cost of the power supply with better efficiency by improving the DPF of the power supply for all loading conditions.

Chapter 7 compares the relative sensitivity of the various systems described in earlier chapters. The sensitivity analysis focuses on variations in the primary and secondary compensation capacitance as well as misalignment of the electromagnetic structure.

Chapter 8 investigates an LCL resonant inverter using a variable-frequency controller operating under discontinuous current mode. A differential equation model is developed to analyse the capability of the inverter, while the load model describes the capability of the resonant tank. A steady state analysis using power flow balance between the inverter and the resonant tank enables suitable design and control to maximize power transfer.

Chapter 9 concludes the thesis and identifies relevant future work.

InductEV, Inc.
Exhibit 1008
Page 036

REFERENCES

[1]. J. T. Boys, G. A. Covic, A. W. Green, "Stability and control of inductively coupled power transfer systems," *IEE Proc.-Electrical Power Applications*, vol. 147, pp. 37-43, Jan. 2000.

[2]. G. A. Covic, G. Elliott, O. H. Stielau, R. M. Green, J. T. Boys, "The design of a contact-less energy transfer system for a people mover system," in *Proc. International Conference on Power System Technology*, vol. 1, 2000, pp.79-84.

[3]. M. Hutin, M. Leblanc, "Transformer system for electric railways," *United States Patent*, No. 527857, Oct. 23, 1894

[4]. V. D. Otto, "Improvements in or relating to electrified transportation," *New Zealand Patent,* No. 167422, Aug. 14, 1974.

[5]. A. W. Green, J. T. Boys, "10 kHz inductively coupled power transfer-concept and control," in *Proc. Fifth International Conference on Power Electronics and Variable-Speed Drives,* 1994, pp. 694-699.

[6]. J. T. Boys, A. W. Green, "Inductive power distribution system," *United States Patent,* No. 5293308, Mar. 8, 1994.

[7]. T. Bieler, M. Perrottet, V. Nguyen, Y. Perriard, "Contactless power and information transmission," *IEEE Transactions on Industry Applications*, vol. 38, pp. 1266-1272, Sep./Oct. 2002.

[8]. H. Abe, H. Sakamoto, K. Harada, "A noncontact charger using a resonant converter with parallel capacitor of the secondary coil," *IEEE Transactions on Industry Applications*, vol. 36, pp. 444-451, Mar./Apr. 2000.

[9]. Wonseok Lim, Jaehyun Nho, Byungcho Choi, Taeyoung Ahn, "Low-profile contactless battery charger using planar printed circuit board windings as energy transfer device," in *Proc. Power Electronics Specialists Conference*, vol. 2, 2002, pp. 579-584.

[10]. Chang-Gyun Kim, Dong-Hyun Seo, Jung-Sik You, Jong-Hu Park, B. H. Cho, "Design of a contactless battery charger for cellular phone," *IEEE Transactions on Industrial Electronics*, vol. 48, pp. 1238-1247, Dec. 2001.

[11]. Byungcho Choi, Honnyong Cha, Jaehyun Noh, Sangkyu Park, "A new contactless battery charger for portable telecommunication/computing electronics," in *Proc. International Conference on Consumer Electronics*, 2001, pp. 58-59.

[12]. Yungtaek Jang, M. M. Jovanovic, "A contactless electrical energy transmission system for portable-telephone battery chargers," in *Proc. Twenty-second International Telecommunications Energy Conference*, 2000, pp. 726-732.

InductEV, Inc.
Exhibit 1008
Page 037

[13]. Gyu Bum Joun; B. H. Cho, "An energy transmission system for an artificial heart using leakage inductance compensation of transcutaneous transformer," *IEEE Transactions on Power Electronics*, vol. 13, pp. 1013-1022, Nov. 1998.

[14]. International Commission on Non-Ionising Radiation Protection (ICNIRP) "Guidelines for limiting exposure to time-varying electric, magnetic, and electromagnetic fields (up to 300GHz)," *Health Physics*, vol. 74, pp. 494-522, 1998.

[15]. I. G. C. Robertson, W. R. Wilson, B. V. Dawson, L. J. Zwi, A. W. Green, J. T. Boys, "Evaluation of potential health effects of 10 kHz magnetic fields: A short-term mouse toxicology study," *Bioelectromagnetics*, vol. 17, pp. 111-122, 1996.

[16]. B. V. Dawson, I. G. C. Robertson, W. R. Wilson, L. J. Zwi, J. T. Boys, A. W. Green, "Evaluation of potential health effects of 10 kHz magnetic fields: A rodent reproductive study," *Bioelectromagnetics*, vol. 19, pp. 162-171, Dec. 1998.

[17]. A. P. Hu, "Selected resonant converters for IPT power supplies," *PhD thesis*, Oct. 2001, The Electrical and Electronics Engineering Department, The University of Auckland, Auckland, New Zealand.

[18]. Chwei-Sen Wang; Stielau, O.H.; Covic, G.A. "Load models and their application in the design of loosely coupled inductive power transfer systems," in *Proc. International Conference on Power System Technology*, vol. 2, 2000, pp. 1053-1058.

[19]. Chwei-Sen Wang, G. A. Covic, O. H. Stielau, "General stability criterions for zero phase angle controlled loosely coupled inductive power transfer systems," in *Proc. 27th Annual Conference of the IEEE Industrial Electronics Society*, vol. 2, 2001, pp. 1049-1054.

[20]. Chwei-Sen Wang, G. A. Covic, O. H. Stielau, "Power transfer capability and bifurcation phenomenon of loosely coupled inductive power transfer systems," *IEEE Transactions on Industrial Electronics*, vol. 51, pp. 148-157, Feb. 2004.

[21]. Chwei-Sen Wang, O. H. Stielau, G. A. Covic, "Design considerations for a contact-less electric vehicle battery charger," *IEEE Transactions on Industrial Electronics*, (accepted for publication, Feb. 2004).

[22]. Chwei-Sen Wang, G. A. Covic, O. H. Stielau, "Investigating an LCL load resonant inverter for inductive power transfer applications," *IEEE Transactions on Power Electronics*, vol. 19, pp. 995-1002, July 2004.

InductEV, Inc.
Exhibit 1008
Page 038

CHAPTER 2

OVERVIEW OF ICPT SYSTEMS

2-1 Introduction
2-2 Electromagnetic structures
2-3 Compensation
2-4 Power converters
2-5 Controllers
2-6 Future trends
2-7 Conclusions

2-1 INTRODUCTION

This chapter outlines the state-of-the-art ICPT technology. The electromagnetic structure, the primary and secondary compensation, the power supply and controller are all discussed here.

The materials and geometry of the electromagnetic structure commonly used for ICPT applications are introduced first. An electromagnetic coupling model is used to clarify the necessary approaches to boost the power transfer capability of the loosely coupled electromagnetic structures.

The requirements of primary and secondary compensations are then explained, along with the fundamental theory in the analysis of both primary and secondary resonant circuits. This theory is used to characterise the primary and secondary resonances. A summary of the basic compensation topologies is also given.

The necessary capability of power converters used for ICPT applications is then discussed. Suitable voltage and current sourced power converters for both low and high power applications are briefly introduced. Impedance matching between the inverter and primary compensation topologies are also presented.

Finally, the chapter reviews controllers commonly used for both the primary power supply and the secondary pickup, before pointing out future trends of the ICPT technology.

2-2 ELECTROMAGNETIC STRUCTURES

Similar to electromagnetic components such as inductors, transformers and induction motors, the electromagnetic structure of an ICPT system is constructed using magnetic cores surrounded by conductor windings. Magnetic cores concentrate the flux, while conductor windings conduct the

InductEV, Inc.
Exhibit 1008
Page 039

electric currents. This section introduces commonly used materials and geometry, and investigates the coupling and capability of the electromagnetic structure. These are essential in the analysis and design of ICPT systems.

2-2.1 MATERIAL

The materials commonly used for the magnetic cores and the copper windings in an ICPT system are similar to those used in the transformers for high-frequency power electronic applications. A brief summary is given in this section.

2-2.1.1 MAGNETIC CORES

Materials used for magnetic cores can be separated into two groups. In the first group are alloys principally of iron and small amounts of other elements including chrome and silicon. The iron alloy core material has a high electrical conductivity and saturation flux, typically around 1.8 tesla.

Iron alloy core materials can be found in three basic types. The first type is laminated magnetic steel. The objective of introducing laminations is to reduce eddy current losses by insulation between laminated steels. Laminated steel was evaluated in [1] in search of the most suitable materials for ICPT applications. Operating at 10 kHz, it was found that its power transfer capability is substantially limited by its core losses.

The second type of iron alloy core is powdered iron where particles are electrically isolated from each other producing a core with significantly greater resistivity than that obtained by lamination. Because of lower eddy current losses, powdered cores can be used at higher frequencies than laminated cores.

The third group of iron alloy cores, such as 'METGLAS' and 'FINEMET', are manufactured from various amorphous alloys of iron and other transition metals such as cobalt and nickel in combination with boron, silicon, and other glass-forming elements. The electrical resistivity of such alloys is larger than most magnetic steels and thus can be used for higher frequencies.

Due to eddy current loss, iron alloy core materials are usually used only in low frequency applications below 2 kHz, and as such are not suitable for most ICPT applications where the operating frequency is above 10 kHz [2-5].

The other group of materials used for magnetic cores are ferrites. Ferrite materials are basically oxide mixtures of iron and other magnetic elements. They have a high electrical resistivity but rather low saturation flux densities, typically about 0.3 tesla. Because of low eddy current losses, ferrite cores are usually the material of choice for ICPT applications.

InductEV, Inc.
Exhibit 1008
Page 040

2-2.1.2 CONDUCTOR WINDINGS

Presently the common choice of material for the conductor winding is copper because of its high conductivity as well as ductility. The high ductility of the copper makes it easy to bend the conductors into tight windings around a magnetic core and thus minimizes the amount of copper and volume needed. The high conductivity of copper also results in less copper required for the windings and thus decreases the volume and the weight.

The copper conductor may be composed of a single round wire or it may be a special multistranded conductor such as Litz wire in which each strand has a diameter of the order of a few hundred microns or less. Litz wire reduces losses due to skin effect and proximity effect, both of which become significant as the frequency is increased.

2-2.2 GEOMETRY

In a traditional transformer, the primary and secondary are fixed on a common core for tight coupling. However, the secondary in many ICPT systems is allowed to move freely relative to the primary, and as such the magnetic cores of the primary and secondary need to be separated. The magnetic core may be eliminated in the primary and/or the secondary to minimize the weight and cost of the system. In a multiple pickup system, more than one secondary draws power from a common primary. The layout of the electromagnetic structure of an ICPT system is application dependent, and there is virtually no limit to possible configurations. Configuration examples are introduced in this section.

2-2.2.1 PRIMARY ELECTROMAGNETIC STRUCTURES

The primary electromagnetic structure can be classified according to the configuration of the primary coil. For single pickup applications, the primary coil is typically constructed as a lumped coil coupled to a similar lumped coil in the secondary. In multiple pickup systems, the primary coil is usually extended to enable suitable coupling to the lumped coil of each pickup. Common configurations of the primary coil are shown in Fig. 2-1. The extended primary coil is shown in the figure as having a single turn. Multiple turn coils can be set up in the same way.

The primary coil can be extended with the cable and its return constructed in parallel as shown in Fig. 2-1 (a). The cable and its return are in close proximity to concentrate the flux. The secondary is placed between the parallel cables, and is allowed to move freely. This configuration is used in many applications where the vehicles move along linear routes [2].

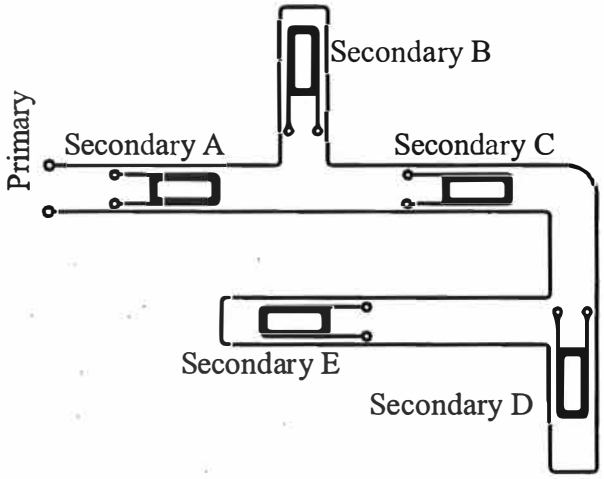
An alteration of the above configuration is to partially twist the parallel cables together as shown in

InductEV, Inc.
Exhibit 1008
Page 041

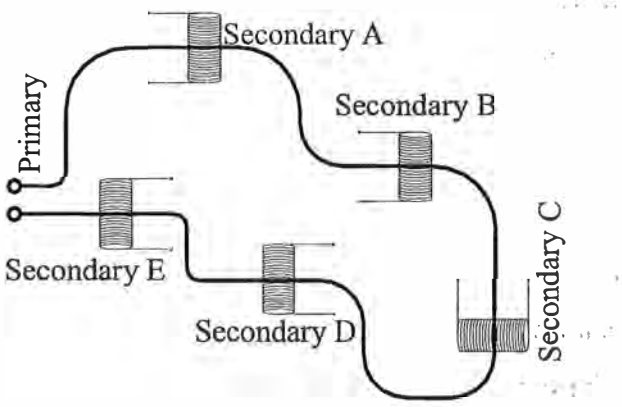
Fig. 2-1 (b). With the cable and its return partially twisted, the primary inductance is reduced. However, the secondary is allowed to draw power only at predetermined locations where the parallel cables are not twisted. A typical application of this configuration is roadway lighting [3].

Alternatively, the primary coil can be extended with the cable and its return constructed to form a loop as shown in Fig. 2-1 (c). The secondary is placed close to the cable, and is also allowed to move freely. This configuration is suitable for automatic guided vehicles.

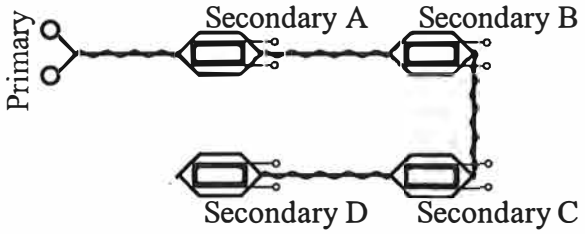
The simplest configuration of the primary coil is a lumped coil as shown in Fig. 2-1 (d). This configuration is commonly used for battery charging of electric vehicles [5-6] and portable electronic devices [7-8].



(a) Extended primary coil with the cable and its return configured in parallel.



(c) Extended primary coil with the cable and its return configured as a loop.



(b) Extended primary coil with the cable and its return configured in parallel and partially twisted.



(d) Lumped primary coil.

Fig. 2-1. Common configurations of the primary coil.

2-2.2.2 SECONDARY ELECTROMAGNETIC STRUCTURES

The secondary electromagnetic structure can be categorized according to the configuration of the secondary core. Common configurations are shown in Fig. 2-2. E-cores and H-cores are used in applications where the vehicles are running on a profile with the cable and its return fitting into each slot respectively. T-cores are used in applications where a guidance slot is given with the cable and its return positioned to the right and left of the guidance slot. Flat cores are used in applications where a

InductEV, Inc.
Exhibit 1008
Page 042

flat floor surface is demanded for full accessibility with the cables embedded in the ground.

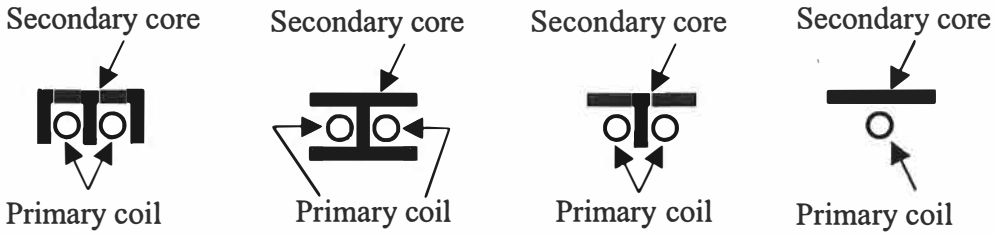


Fig. 2-2. Common configurations of the secondary core.

2-2.3 ELECTROMAGNETIC COUPLING MODEL

There are many approaches that can be used to investigate the coupling between the primary and secondary windings. The most commonly used modeling methodologies are the conventional transformer model [9-14] and the mutual inductance transformer model [15-22]. The conventional transformer model uses the concepts of transformed voltage and reflected current to describe the coupling effect. Both the transformed voltage and reflected current are expressed in terms of the turns ratio. With this model, the magnetizing and leakage inductance must be separated for circuit analysis. The conventional transformer model is therefore well suited for closely coupled systems such as transformers, because the leakage inductance is usually small. In ICPT systems, however, the leakage inductance is usually comparable or much larger than the magnetizing inductance, and the conventional transformer model becomes very complex. In order to simplify the circuit analysis for ICPT systems, the mutual inductance transformer model is used in this thesis because this model does not require the magnetizing and leakage inductance to be separated.

Using the mutual inductance transformer model, as shown in Fig. 2-3, the electromagnetic structure can be presented by three coupling parameters: the primary self-inductance L_p; the secondary self-inductance L_s; and the mutual inductance M between the primary and secondary.

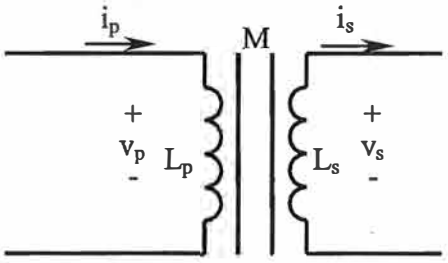


Fig. 2-3. Circuit of the mutual inductance transformer model.

The mutual inductance M is related to the magnetic coupling coefficient k by:

InductEV, Inc.
Exhibit 1008
Page 043

$$k = \frac{M}{\sqrt{L_p L_s}} \tag{2-1}$$

The primary voltage and current are represented as 'v_p' and 'i_p', while the secondary voltage and current are shown as 'v_s' and 'i_s.'

The interactions between the primary and secondary can be represented (under the assumption that no saturation occurs) by:

$$v_p = L_p \frac{di_p}{dt} - M \frac{di_s}{dt} \tag{2-2}$$

and

$$v_s = M \frac{di_p}{dt} - L_s \frac{di_s}{dt} \tag{2-3}$$

Assuming sinusoidal voltages and currents, (2-2) and (2-3) can be simplified to:

$$V_p = j\omega L_p I_p - j\omega M I_s \tag{2-4}$$

and

$$V_s = j\omega M I_p - j\omega L_s I_s \tag{2-5}$$

The equivalent circuit of the sinusoidal mutual inductance transformer model can be derived from (2-4) and (2-5), and is shown in Fig. 2-4. In this circuit, an induced voltage represents the influence of the primary current on the secondary, while the effect of the secondary current on the primary is shown as a reflected voltage. The induced and reflected voltages in this model are specified in terms of the mutual inductance M, the operational frequency ω, the primary current I_p, and the secondary current I_s.

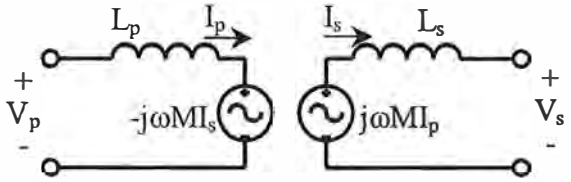


Fig. 2-4. The sinusoidal mutual inductance transformer model.

The mutual inductance M can be determined in a physical system by an open circuit test. The secondary is left open circuit and a sinusoidal primary current I_p with a known frequency ω is made to flow in the primary. The secondary voltage V_s is measured, and is called the open circuit voltage V_{oc} in this thesis. Since the secondary current I_s is zero, (2-5) leads to the open circuit voltage V_{oc} given as:

$$V_{oc} = \omega M I_p \tag{2-6}$$

The mutual inductance determined by the open circuit test is therefore:

$$M = \frac{V_{oc}}{\omega I_p} \tag{2-7}$$

InductEV, Inc.
Exhibit 1008
Page 044

Alternatively, the mutual inductance M can be determined by a short circuit test. A short circuit is placed on the secondary and a sinusoidal primary current I_p is made to flow in the primary. The secondary current I_s is measured, and is called the short circuit current I_{sc} in this thesis. In this case, the secondary voltage V_s is zero and (2-5) leads to the short circuit current I_{sc} given as:

$$I_{sc} = \frac{MI_p}{L_s} \tag{2-8}$$

The mutual inductance determined by the short circuit test is therefore:

$$M = \frac{I_{sc}L_s}{I_p} \tag{2-9}$$

2-2.4 CAPABILITY OF THE ELECTROMAGNETIC STRUCTURE

In this section, the capability of the electromagnetic structure is analyzed using the mutual inductance transformer model developed above. The load voltage and current are characterized for all load conditions. The design factors that need to be optimized to achieve maximum power transfer capability are then determined.

2-2.4.1 LOAD VOLTAGE AND CURRENT

It is assumed in the following analysis that a constant current I_p at a known frequency ω flows in the primary, while the secondary supplies power to a linear and resistive load. The equivalent secondary circuit is shown in Fig. 2-5 using the induced voltage due to the primary current.

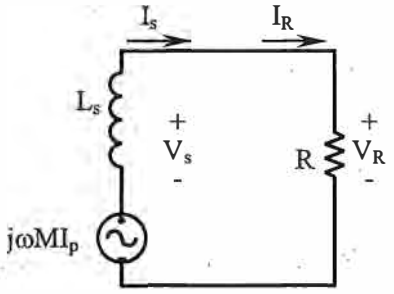


Fig. 2-5. Equivalent secondary circuit supplying power to a linear and resistive load.

The impedance of the secondary as seen by the induced voltage is:

$$Z_s = j\omega L_s + R \tag{2-10}$$

The load current (secondary current) equals the induced voltage divided by the secondary impedance, and is given by:

InductEV, Inc.
Exhibit 1008
Page 045

$$I_R = I_s = \frac{j\omega M I_p}{Z_s} = \frac{j\omega M I_p}{j\omega L_s + R} \tag{2-11}$$

The load voltage (secondary voltage) can be calculated by substituting (2-11) into (2-5) resulting in:

$$V_R = V_s = \frac{j\omega M I_p R}{j\omega L_s + R} \tag{2-12}$$

Eliminating the load resistance R from (2-11) and (2-12), the relation between the amplitudes of the load voltage and current is:

$$V_R^2 = (\omega M I_p)^2 - (\omega L_s)^2 I_R^2 \tag{2-13}$$

The above equation can be normalized using the open-circuit voltage and short-circuit current resulting in:

$$\left(\frac{V_R}{V_{oc}}\right)^2 = 1 - \left(\frac{I_R}{I_{sc}}\right)^2 \tag{2-14}$$

The normalized load voltage and current given by (2-14) are shown in Fig. 2-6 for the complete load range. As the load varies from short circuit (R=0) to open circuit (R=∞), the load current drops from I_{sc} to zero, while the load voltage increases from zero to V_{oc}.

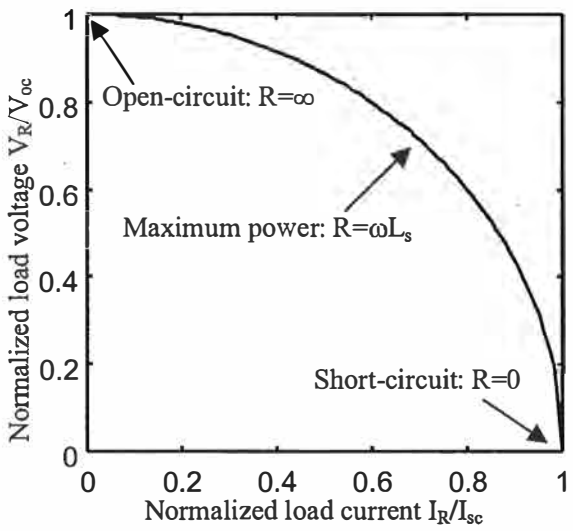


Fig. 2-6. The normalized load voltage and current of the uncompensated pickup.

2-2.4.2 POWER TRANSFER CAPABILITY

The secondary voltage is zero under short-circuit conditions, while the secondary current is zero at open-circuit. Consequently, the power transfer capability is zero under both short-circuit and open-circuit conditions. Maximum power is achieved at a particular load between these two conditions.

The power transfer is the product of the load current and voltage. Since the load current and voltage

InductEV, Inc.
Exhibit 1008
Page 046

in (2-11) and (2-12) are complex variables, the coupling power must be represented by the load current (voltage), multiplied by the conjugate of the load voltage (current) as given by:

$$P = I_R V_R^* = I_R^* V_R = I_R I_R^* R = \frac{V_R V_R^*}{R} \tag{2-15}$$

Substituting (2-10) and (2-12) into (2-15) results in:

$$P = \frac{\omega^2 M^2 R I_p^2}{\omega^2 L_s^2 + R^2} \tag{2-16}$$

The maximum power transfer can be calculated at the following load condition:

$$\frac{\partial P}{\partial R} = 0 \tag{2-17}$$

Solving (2-17) results in:

$$R = \omega L_s \tag{2-18}$$

At this load condition, both the normalized load voltage and current shown in Fig. 2-6 are equal to $1/\sqrt{2}$.

The maximum power transfer calculated using (2-16) and (2-18) is:

$$P_{\max} = \frac{\omega M^2 I_p^2}{2L_s} \tag{2-19}$$

The above equation can be rearranged as:

$$P_{\max} = \frac{V_{oc} I_{sc}}{2} \tag{2-20}$$

Substituting (2-1) into (2-19) results in:

$$P_{\max} = \left(\frac{1}{2}\right)\omega I_p^2 \left(\frac{M^2}{L_s}\right) = \left(\frac{1}{2}\right)\omega I_p^2 \left(k^2 L_p\right) \tag{2-21}$$

According to (2-21), the power transfer capability of an electromagnetic structure is proportional to the operating frequency (ω), the square primary current (I_p^2), and the coupling factor ($k^2L_p=M^2/L_s$). The nominal operating frequency should be chosen as high as possible taking into account practical considerations such as size, cost and efficiency. The limit is determined by switching losses in the semiconductors as well as high frequency losses in the passive components. To fully utilize the capability of the copper windings of an ICPT system, the primary current is normally controlled at the maximum rating to ensure maximum power transfer capability. Improving the magnetic coupling such as reducing the air gap or adding magnetic material results in increases of the three coupling parameters (M, L_p and L_s). A major aim in the design of the electromagnetic structure is to maximise the coupling factor k^2L_p ($=M^2/L_s$) in order to maximise the power transfer, while minimize the weight and cost.

InductEV, Inc.
Exhibit 1008
Page 047

2-3 COMPENSATION

Both the primary and secondary of the electromagnetic structure are often compensated by capacitors to boost the power transfer capability of the pickup, while minimizing the VA rating of the power supply. This section introduces the basic compensation topologies. The compensation level and the resonant behaviour of the primary and secondary resonant circuits are quantified for each topology.

2-3.1 SECONDARY COMPENSATION

To compensate for the secondary inductance (L_s), a capacitor (C_s) can be connected either in series [23-28] or parallel [29-34] with the secondary winding. The equivalent circuits are shown in Fig. 2-7 and 2-8 with the influence of the primary represented by the induced voltage. An equivalent resistance (R) represents the load on the secondary pickup. Under series compensation, the secondary winding, compensation capacitor and the load are all connected in series. For parallel compensation, they are all connected in parallel.

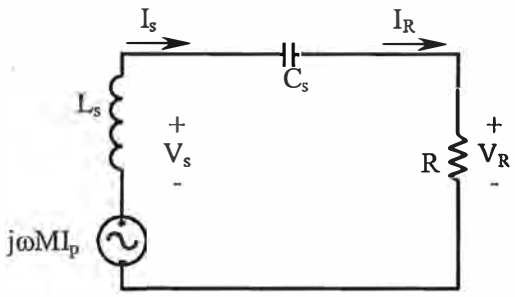


Fig. 2-7. Series-compensated secondary.

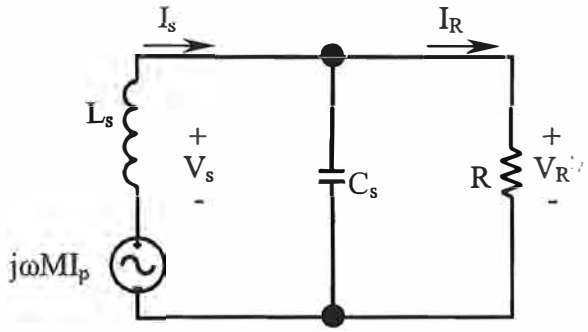


Fig. 2-8. Parallel-compensated secondary.

For maximum power transfer, the secondary resonant frequency (when C_s is in resonance with L_s) is normally designed to equal the nominal frequency (ω_0). In this case, the secondary compensation capacitance is determined as:

$$C_s = \frac{1}{\omega_0^2 L_s} \tag{2-22}$$

The secondary compensation level is quantified in terms of the secondary quality factor (Q_{s0}), defined as the ratio of reactive to real power of the secondary resonant circuit at ω_0. This secondary quality factor derived in Chapter 3 (equation 3-24) is:

$$Q_{s0} = \begin{cases} \dfrac{1}{\omega_0 C_s R} = \dfrac{\omega_0 L_s}{R} & \text{Series secondary} \\ \omega_0 C_s R = \dfrac{R}{\omega_0 L_s} & \text{Parallel secondary} \end{cases} \tag{2-23}$$

InductEV, Inc.
Exhibit 1008
Page 048

2-3.2 SECONDARY RESONANCE

Both series and parallel secondary compensation improve the power transfer capability of the pickup, but present very different characteristics to the load. The circuit equation of the series-compensated pickup (Fig. 2-7) is:

$$j\omega M I_p = \left(j\omega L_s + \frac{1}{j\omega C_s} \right) I_R + V_R \tag{2-24}$$

At ω_0, L_s is in resonance with C_s so that the load voltage V_R derived from (2-24) is identical to the open circuit voltage ($V_R=\omega M I_p=V_{oc}$). The series-compensated pickup therefore exhibits a voltage source to the load. The load current is inversely proportional to the load ($I_R=V_R/R=V_{oc}/R$), and can also be expressed in terms of I_{sc} and Q_{s0} ($I_R=I_{sc}Q_{s0}$).

With series compensation, the pickup power at ω_0 is:

$$P_{series} = V_R I_R = Q_{s0} V_{oc} I_{sc} \tag{2-25}$$

The circuit equation of a parallel-compensated pickup (Fig. 2-8) is:

$$j\omega M I_p = j\omega L_s I_s + \frac{1}{j\omega C_s}(I_s - I_R) = \left(j\omega L_s + \frac{1}{j\omega C_s} \right) I_s - \frac{1}{j\omega C_s} I_R \tag{2-26}$$

At ω_0, the pickup load current derived from (2-26) is equal to the short circuit current ($I_R=\omega^2 C_s M I_p = M I_p/L_s=I_{sc}$). The parallel-compensated pickup therefore exhibits a current source to the load. The pickup load voltage is proportional to the load ($V_R=I_R R=I_{sc}R$), and can be expressed in terms of V_{oc} and Q_{s0} ($V_R=V_{oc}Q_{s0}$).

With parallel compensation, the pickup power at ω_0 is:

$$P_{parallel} = V_R I_R = Q_{s0} V_{oc} I_{sc} \tag{2-27}$$

Comparing (2-20) with (2-25) and (2-27), it can be seen that the pickup power transfer capability is improved by a factor $2Q_{s0}$ with either series or parallel secondary compensation compared to the uncompensated case.

The normalized load voltage and current are shown in Fig. 2-9 for uncompensated as well as series and parallel compensated secondary topologies. In this figure, the load voltage is normalized using the open circuit voltage, while the load current is normalized using the short circuit current.

With series compensation, the normalized load voltage is always unity, while the normalized load current increases with increasing load. With parallel compensation, the normalized load current is always unity, whereas the normalized load voltage increases with increasing load.

InductEV, Inc.
Exhibit 1008
Page 049

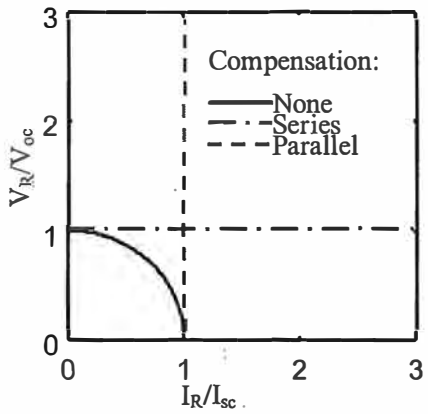


Fig. 2-9. Normalized load voltage and current characteristics of uncompensated as well as series and parallel-compensated pickups.

The pickup voltages, currents, power and required VA ratings at ω_0 are summarized in Table 2-1. In this table, the capability of the pickup at ω_0 is represented in terms of Q_{s0}, V_{oc} and I_{sc}. Although the pickup power transfer capability has been increased by the factor $2Q_{s0}$ over that of an uncompensated pickup, the disadvantage of a compensated pickup is that the required VA rating is significantly higher. The required VA rating of the secondary winding is larger than the real power by a factor of $\sqrt{1+Q_{s0}^2}$, while the required VA rating of the secondary compensation capacitor is Q_{s0} times higher than the real power. These components need to be dimensioned to handle the increased VA requirements.

TABLE 2-1
PICKUP VOLTAGES, CURRENTS, POWER AND REQUIRED VA RATINGS

Pickup topology	Series compensation	Parallel compensation
Load voltage V_R	V_{oc}	$Q_{s0}V_{oc}$
Load current I_R	$Q_{s0}I_{sc}$	I_{sc}
Pickup power P	$Q_{s0}V_{oc}I_{sc}$	$Q_{s0}V_{oc}I_{sc}$
Secondary voltage V_s	$\sqrt{1+Q_{s0}^2}V_{oc}$	$Q_{s0}V_{oc}$
Secondary current I_s	$Q_{s0}I_{sc}$	$\sqrt{1+Q_{s0}^2}I_{sc}$
Required secondary VA rating VA_s	$Q_{s0}\sqrt{1+Q_{s0}^2}V_{oc}I_{sc}$	$Q_{s0}\sqrt{1+Q_{s0}^2}V_{oc}I_{sc}$
Secondary capacitor voltage V_{Cs}	$Q_{s0}V_{oc}$	$Q_{s0}V_{oc}$
Secondary capacitor current I_{Cs}	$Q_{s0}I_{sc}$	$Q_{s0}I_{sc}$
Required secondary capacitor VA rating VA_{Cs}	$Q_{s0}^2V_{oc}I_{sc}$	$Q_{s0}^2V_{oc}I_{sc}$

2-3.3 PRIMARY COMPENSATION

Similar to the secondary compensation, a capacitor (C_p) can be connected in series [35-41] or parallel [42-46] with the primary winding. The equivalent circuits are shown in Fig. 2-10 and 2-11

InductEV, Inc.
Exhibit 1008
Page 050

with the influence of the secondary represented by the reflected voltage in series connection with the primary inductance.

The primary resonant frequency (when C_p is in resonance with L_p) is normally designed to equal the nominal frequency (ω_0). In this case, the primary compensation capacitance is determined as:

$$C_p = \frac{1}{\omega_0^2 L_p} = \frac{C_s L_s}{L_p} \tag{2-28}$$

The primary compensation level can be quantified by the primary quality factor (Q_{p0}) defined as the ratio of reactive to real power associated with the primary coil at the nominal frequency (ω_0). This primary quality factor derived in Chapter 3 (equation 3-51) as a function of the secondary quality factor (Q_{s0}) and the magnetic coupling coefficient (k) is:

$$Q_{p0} = \begin{cases} \dfrac{1}{k^2 Q_{s0}} & \text{series secondary} \\ \dfrac{1-k^2}{k^2 Q_{s0}} = \dfrac{1}{k^2 Q_{s0}} - \dfrac{1}{Q_{s0}} & \text{parallel secondary} \end{cases} \tag{2-29}$$

The primary compensation level is determined intrinsically once the secondary compensation level is selected for a given electromagnetic coupling structure.

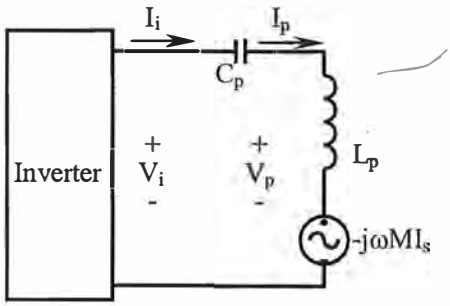


Fig. 2-10. Series-compensated primary.

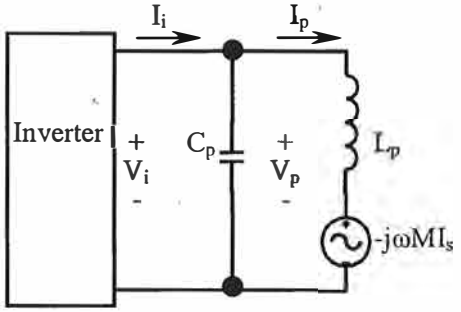


Fig. 2-11. Parallel-compensated primary.

2-3.4 PRIMARY RESONANCE

With a series-compensated primary, the voltage across the primary coil is much larger than the inverter output voltage. This voltage gain is useful for long track systems where the track voltage can be very large. The voltage gain of a series-compensated primary (derived in Appendix A as a function of the primary and secondary quality factors) is:

$$V_{GAIN} = \begin{cases} \sqrt{1+Q_{p0}^2} & \text{Series primary and series secondary} \\ \sqrt{\dfrac{Q_{s0}^2\left(1+Q_{p0}^2\right)}{1+Q_{s0}^2}} & \text{Series primary and parallel secondary} \end{cases} \tag{2-30}$$

InductEV, Inc.
Exhibit 1008
Page 051

In a parallel-compensated primary, the current flowing through the primary coil is much larger than the inverter output current. This current gain is useful when a large current is required for the primary coil. The current gain of a parallel-compensated primary (derived in Appendix A as a function of the primary and secondary quality factors) is:

$$I_{GAIN} = \begin{cases} Q_{p0} & \text{Parallel primary and series secondary} \\ \sqrt{\dfrac{\left(1+Q_{p0}Q_{s0}\right)^2}{1+Q_{s0}^2}} & \text{Parallel primary and parallel secondary} \end{cases} \quad (2\text{-}31)$$

In ICPT systems, the primary and secondary quality factors are usually larger than unity. As a result, the magnitudes of both the voltage and current gains calculated using (2-30) and (2-31) are governed by Q_p. According to (2-29), increasing Q_s or improving k results in lower Q_p, and as such less voltage or current gain.

2-3.5 BASIC COMPENSATION TOPOLOGIES

Three basic compensation choices exist for both the primary and secondary (series compensation, parallel compensation, or uncompensated). Combining the primary and secondary results in nine fundamental compensation topologies [18] as illustrated in Fig. 2-12.

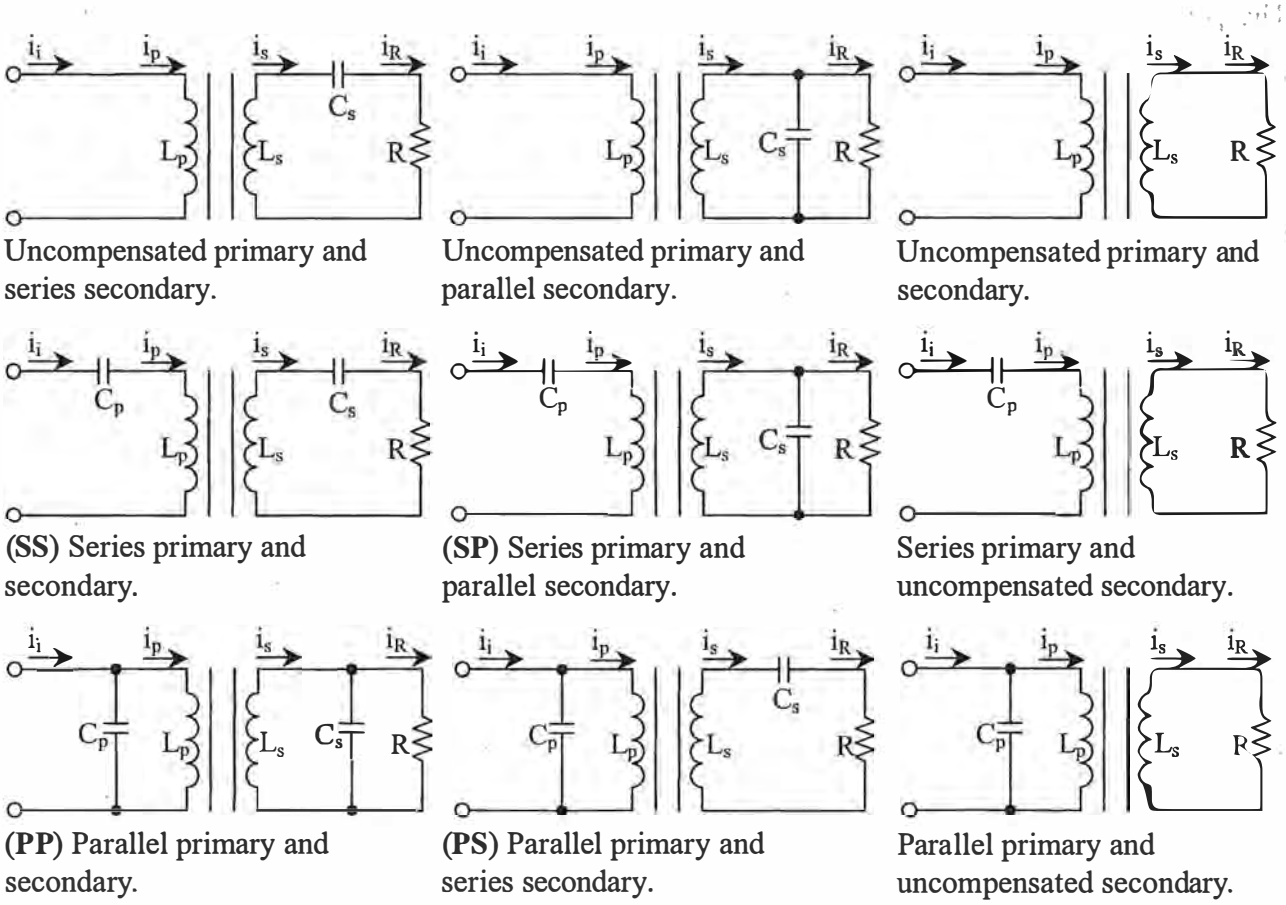


Fig. 2-12. Basic compensation topologies of ICPT systems.

InductEV, Inc.
Exhibit 1008
Page 052

This thesis focuses only on the four basic topologies with both the primary and secondary either series or parallel compensated. They are labelled as SS, SP, PP and PS as shown in Fig. 2-12, where the first S or P stands for series or parallel compensation for the primary winding and the second S or P stands for series or parallel compensation for the secondary winding. Subscripts 'p' and 's' stand for primary and secondary respectively, while the resistance R represents the load on the secondary.

2-4 POWER CONVERTERS

The selection of a suitable power converter depends strongly on the requirements of practical ICPT applications, which include size, cost and power level. Suitable power converters for ICPT applications are identified in this section.

2-4.1 OVERVIEW OF POWER CONVERTERS

ICPT power converters convert incoming utility ac power into dc by rectifiers, and then convert the dc into the required ac power by inverters. Alternatively, the dc power can be supplied from a battery. The power converter can be operated in the linear mode or switch mode. Linear mode power converters have very low efficiencies, typically between 5 and 50%. In this thesis, only switch mode power converters will be considered. The block diagram of a power converter in an ICPT system is shown in Fig. 2-13 as three subsystems: the power source, the high frequency inverter and the resonant tank.

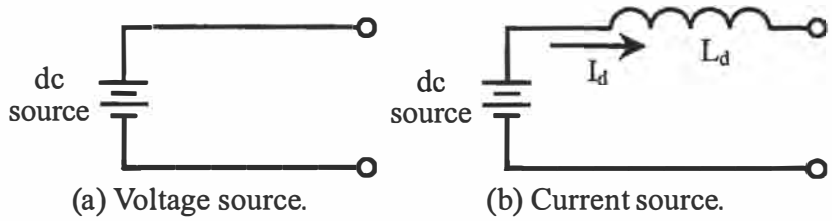


Fig. 2-13. The block diagram of a power converter in an ICPT system.

As shown in Fig. 2-14, two fundamental types of power source are available: voltage sourced and current sourced [47, 48]. The input to a voltage-sourced inverter is assumed to be a constant dc voltage. For a current-sourced inverter, a large inductor is placed in series with the dc voltage source. The input to a current-sourced inverter can thus be assumed to be a constant current. The high frequency inverter can be configured using a single switch, two switches (half-bridge), or four switches (full-bridge) as discussed in the following sections. The full-bridge topology has the highest power capability with various control options, while the single-switch topology has the lowest power capability with limited

InductEV, Inc.
Exhibit 1008
Page 053

control options. The resonant tank consists of the electromagnetic structure, the primary and secondary compensation networks, and the pickup load.



(a) Voltage source. (b) Current source.

Fig. 2-14. Fundamental types of power source.

Power switches can be categorized into three groups. In the first group are diodes with on and off states controlled by the power circuit. In the second group are naturally commutated devices, which can be turned on by a control signal but must be turned off by the power circuit. In the final group are forced commutated switches, which can be turned on and off by control signals.

Diodes can be classified into three categories. Line frequency diodes have large reverse recovery times and as such are not suitable for ICPT applications that typically operate with a frequency above a few kHz. The reverse recovery times of Schottky diodes are negligible. However, the voltage blocking capabilities limits them. Fast recovery diodes have much higher power capabilities with a small reverse recovery time.

Before the appearance of forced commutated switches, naturally commutated devices had been widely used. They still have the highest power capability. Various types of naturally commutated devices are available. The slow switching speed limits the maximum operating frequency to a few kHz.

Forced commutated switches include several device types including gate turn off thyristors (GTOs), MOS controlled thyristors (MCTs), metal-oxide-semiconductor field effect transistors (MOSFETs) and insulated gate bipolar transistors (IGBTs).

GTOs have the highest power capability but lowest switching speed. MCTs have lower power capability but faster switching speed than GTOs. However, they have been taken over by IGBTs. IGBTs with improved characteristics including increased power capability and switching speed have become readily available in recent years. MOSFETs have the lowest power capability but fastest switching speed.

In order to reduce the size and cost of ICPT systems, it is desirable to increase the operating frequency to well above the audible range. This leaves MOSFETs and IGBTs as the most suitable choices for such applications.

Switches can be configured as either reverse conducting or reverse blocking using associated

InductEV, Inc.
Exhibit 1008
Page 054

diodes. The reverse conducting switch configuration has an anti-parallel diode as shown in Fig. 2-15 (a). With this configuration, the current can flow in either direction but the voltage can be blocked in only one direction. The reverse blocking switch configuration has a series diode as shown in Fig. 2-15 (b). This configuration can block voltage in either direction, but the current can flow in one direction only.



(a) Reverse conducting switch configuration. (b) Reverse blocking switch configuration.

Fig. 2-15. Switch configurations.

2-4.2 VOLTAGE-SOURCED POWER CONVERTERS

A voltage-sourced full-bridge power converter, as shown in Fig. 2-16, uses four reverse conducting switches. With the diagonal switch pairs (S_1/S_4 and S_2/S_3) in alternating conduction, the inverter output voltage (v_i) is approximately rectangular. This configuration has been used for ICPT applications such as medical implants [49-54], electric vehicles [55-58] and material handling facilities [59-61]. In this thesis, a voltage-sourced full-bridge power converter is used in a practical example for contact-less electric vehicle battery charging.

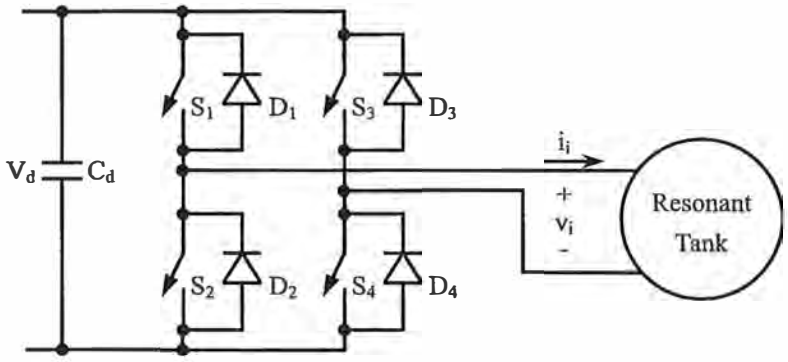


Fig. 2-16. The voltage-sourced full-bridge power converter.

In a voltage-sourced half-bridge power converter, as shown in Fig. 2-17, one leg of the full-bridge is replaced by centre-tapped capacitors. The two switches alternate their conduction resulting in an approximately rectangular inverter output voltage. This inverter utilizes only two switches and therefore is cheaper than the full-bridge topology. However, the amplitude of the rectangular output voltage is only half the dc voltage. This topology has been used for medical implants [62-65], portable

InductEV, Inc.
Exhibit 1008
Page 055

electronics devices [66], electric vehicles [67-71] and material handling facilities [72].

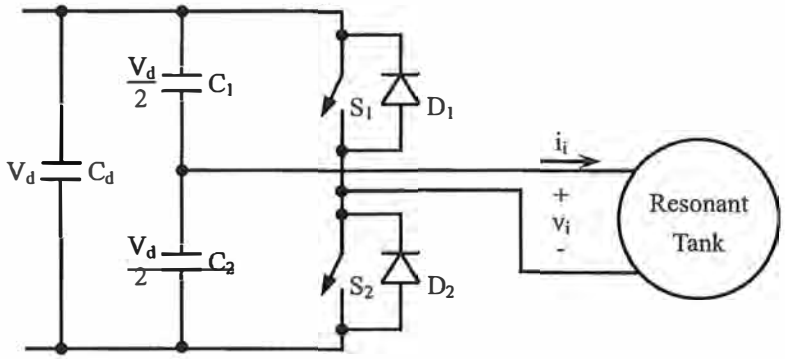
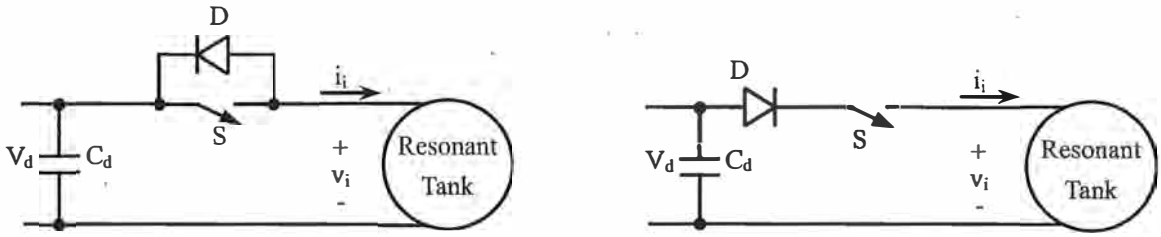


Fig. 2-17. The voltage-sourced half-bridge power converter.

Voltage-sourced single-switch topologies have been investigated in detail in [73-74] for induction heating applications. A common topology for ICPT applications is shown in Fig. 2-18 (a) using a single reverse conducting switch. Low power applications of this topology can be found in [42][75]. Alternatively, a reverse blocking switch can be used as shown in Fig. 2-18 (b).



(a) Reverse conducting switch configuration. (b) Reverse blocking switch configuration.

Fig. 2-18. Voltage-sourced single-switch power converters.

2-4.3 CURRENT-SOURCED POWER CONVERTERS

While current-sourced power converters are not as popular as the voltage-sourced power converters due to the requirement for bulky dc inductors, they have been commonly used in early ICPT systems developed over the past decade [47][76-79]. This is because the current-sourced power converter has the intrinsic ability to maintain constant track/coil current. This is essential to ICPT systems especially for the track-type high power industrial applications with multiple pickups.

A current-sourced full-bridge power converter, as shown in Fig. 2-19, consists of four reverse blocking switches. Diagonal switch pairs conduct in alternate half cycles, producing an inverter output current that is close to a square wave.

In a current-sourced half-bridge power converter as shown in Fig. 2-20, a centre-tapped transformer

InductEV, Inc.
Exhibit 1008
Page 056

replaces the top two switches of the full-bridge.

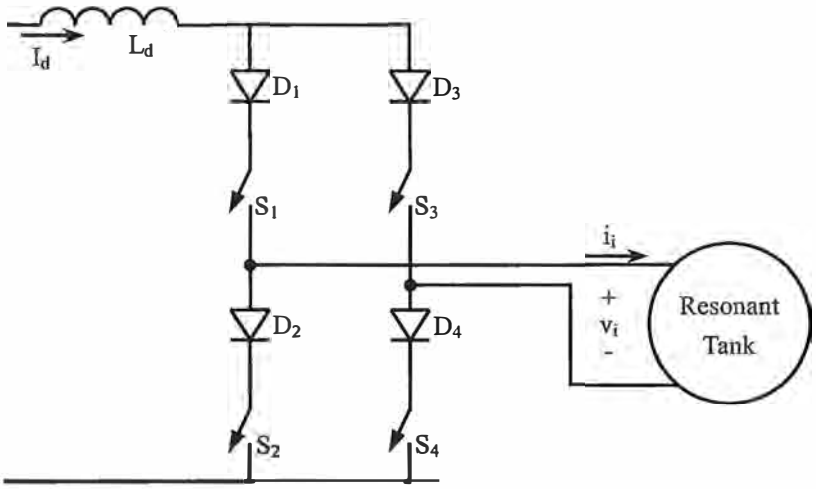


Fig. 2-19. The current-sourced full-bridge power converter.

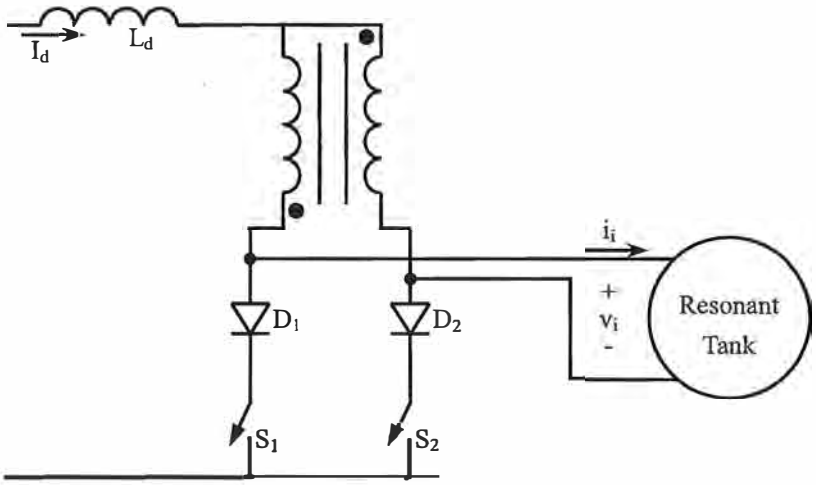
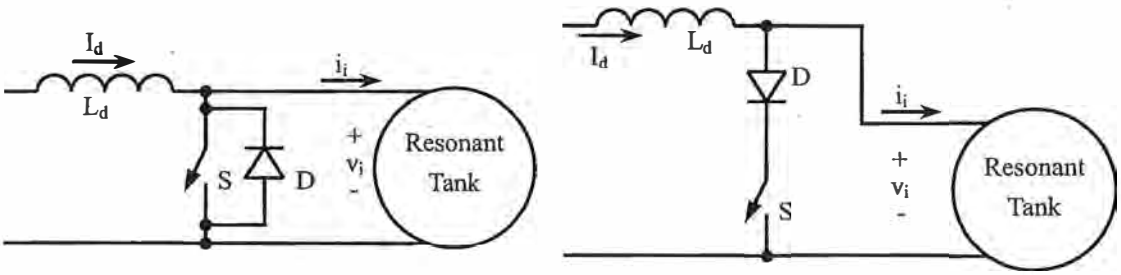


Fig. 2-20. The current-sourced half-bridge power converter.

Current-sourced single-switch topologies have been investigated in detail in [73-74] for induction heating applications. A common configuration for ICPT applications is shown in Fig. 2-21 (a) using a single reverse conducting switch. Low power applications using this topology can be found in [80-81]. Alternatively, the reverse blocking switch can be used as shown in Fig. 2-21 (b).



(a) Reverse conducting switch configuration. (b) Reverse blocking switch configuration.

Fig. 2-21. Current-sourced single-switch power converters.

InductEV, Inc.
Exhibit 1008
Page 057

2-4.4 IMPEDANCE MATCHING

For the voltage-sourced power converter with a rectangular output voltage waveform, a series inductor is required at the inverter output stage in order to avoid current spikes caused by sudden changes in voltage. With a series-compensated primary, the primary winding plays the role of such a series inductor and therefore voltage-sourced inverters can be used directly without additional impedance matching components. An additional series inductor is necessary if a voltage-sourced inverter is used to drive a parallel-compensated primary as shown in Fig. 2-22. This arrangement results in an LCL resonant inverter.

LCL resonant inverters operating with continuous current have been used for both induction heating [82-85] and ICPT applications [47]. In this thesis, an LCL resonant inverter operating in discontinuous current mode is used to supply high frequency voltage and current to a practical ICPT application for contact-less electric vehicle battery charging. Its operation is discussed in detail in Chapter 8.

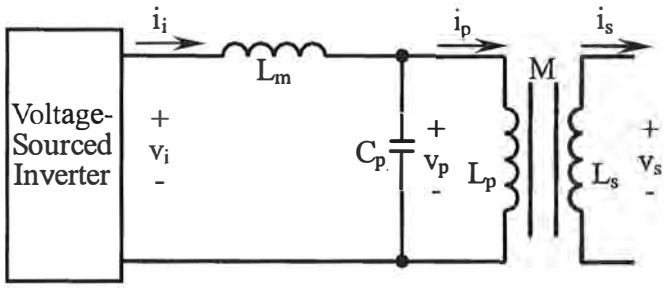


Fig. 2-22. The LCL resonant inverter.

For a current-sourced power converter with a rectangular output current waveform, a parallel capacitor is required across the inverter output stage in order to avoid voltage overshoots caused by sudden changes in the direction of current. With a parallel-compensated primary, the primary capacitor plays the role of the parallel capacitor and therefore current-sourced inverters can be used directly without impedance matching components. An additional parallel capacitor is necessary if a current-sourced inverter is used to drive a series-compensated primary as shown in Fig. 2-23. This arrangement results in a CCL resonant inverter.

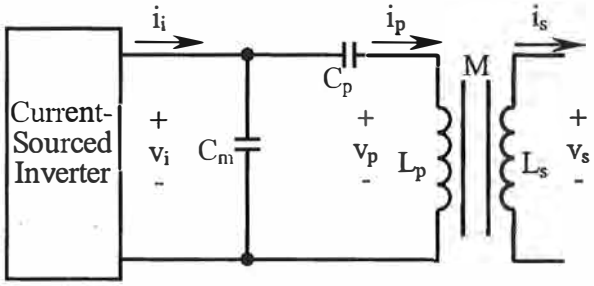


Fig. 2-23. The CCL resonant inverter.

InductEV, Inc.
Exhibit 1008
Page 058

2-5 CONTROLLERS

Various controllers may be used in the primary or the secondary. These are often necessary to accommodate varying operating conditions such as variations in the load, misalignment of the electromagnetic structure, fluctuations in the power source, as well as the tolerance, thermal effects and aging of the circuit components. In this section, control options suitable for ICPT systems are discussed. The bifurcation phenomenon (multiple operating modes in the frequency spectrum) present in variable-frequency systems is also introduced.

2-5.1 POWER FLOW REGULATION

For single pickup applications, power flow regulation can be implemented in the primary or the secondary. Most single pickup low power ICPT applications, such as battery charging for medical implants and portable consumer products, do not employ a secondary controller and as such the primary controller is responsible for providing suitable voltage, current and power to the secondary load. This approach may have the advantage of reduced size and cost of the pickup, but a feedback loop from the secondary to the primary is often necessary. The feedback loop is normally achieved using an additional wireless communication link. When a secondary controller is used to regulate pickup power flow, the feedback communication link may be eliminated. In this case, one of the control objectives of the primary controller is to achieve a constant primary current. In order to fully utilize the capability of the electromagnetic structure, the primary current is normally controlled at the maximum current rating.

In a multiple pickup system, the loading condition on each pickup is almost always different. Since power flow regulation at the primary affects all secondary pickups, it is not a good choice for multiple pickup applications and a secondary controller is required for each individual pickup [1-4][9][14-15] [20][45][47][79]. These secondary controllers normally utilize a switch mode converter to regulate power flow. The pickup regulator will be discussed further in section 4-3.

One option to control power or current in the primary is to regulate the dc voltage [31][48][67] [86]. This approach is suitable for all inverter topologies, but the disadvantage is increased size and cost of the dc-stage. Another option for single pickup applications is to shift the operating frequency around the resonant frequency (ω_0) of the pickup. This approach is applicable for both full-bridge and half-bridge inverters, but the resulting switching losses needs to be considered carefully. For the full-bridge inverter, controlling the duty-cycle of the inverter is a common choice.

InductEV, Inc.
Exhibit 1008
Page 059

2-5.2 FREQUENCY CONTROL

The primary controller can be separated into two major groups respectively with fixed or variable frequency control. A fixed-frequency controller forces the operating frequency to a predetermined value, while a variable-frequency controller allows the operating frequency to vary over a predetermined range.

With a fixed-frequency controller, the secondary resonant frequency is designed to be equal to the operating frequency in order to ensure maximum power transfer to the pickup. Fixed-frequency controllers thus have the advantage that a compensated pickup will always run at its correct tuned frequency. However, the power supplies need to be overrated since the displacement power factor (DPF) will invariably not be unity due to varying operating conditions.

Variable-frequency controllers allow the operating frequency to vary so that the inverter operates close to unity DPF. This ensures that the power supply does not have to be overrated, but frequency-detuning effects within the pickup are unavoidable resulting in reduced power transfer capability.

In this thesis, several new primary tuning approaches are proposed to reduce frequency detuning in variable-frequency systems, and to improve the DPF of fixed-frequency systems.

2-5.3 SWITCHING CONTROL IN VOLTAGE-SOURCED FULL-BRIDGE INVERTERS

In a voltage-sourced full-bridge inverter, switching exactly at the zero crossing of the output current, as shown in Fig. 2-24, results in zero switching losses. Here, the rectangular output voltage is controlled to be in-phase with the current and as such the voltage and current ratings of the inverter are minimized for a given power transfer.

When switching ahead of the zero crossing of the output current, as shown in Fig. 2-25, the switches are turned off with non zero current resulting in turn-off losses. There are, however, no turn-on losses since the switches are turned on with zero voltage as the current is flowing through the anti-parallel diodes. The current flows through the switches when it changes direction and in consequence starts another power transfer period. With this switching strategy, the rectangular output voltage is leading the output current and the voltage and current ratings of the inverter are higher than the transferred power.

When switching occurs after the zero crossing of the current, as shown in Fig. 2-26, the switches are turned off with zero voltage as the current flows through the anti-parallel diodes. This results in zero turn-off loss. When the switches are turned on, the current commutates from the anti-parallel diodes to the switches, resulting in turn-on losses as well as diode reverse recovery. With this switching strategy,

InductEV, Inc.
Exhibit 1008
Page 060

the rectangular output voltage lags the output current and the voltage and current ratings of the inverter are higher than the transferred power.

For the switching controls shown in Fig. 2-24 to 2-26, the pulse-width of the rectangular inverter voltage is identical to a full half cycle. Here, the diagonal switches are controlled at the same time. Many applications control the pulse-width of the rectangular inverter voltage to regulate power flow as shown in Fig. 2-27. With this strategy, both switches of each diagonal switch-pair are controlled with a phase shift. As the current freewheels through the top or bottom bridge legs, the inverter output voltage is zero. With this approach, it is possible that the left-leg of the full-bridge is switched after zero crossing, while the right leg is switched before the zero crossing of the current. As a result, both switches in the left leg have no turn-off loses but turn-on losses and diode reverse recovery exist. On the other hand, both switches in the right-leg have no turn-on losses but turn-off losses exist.

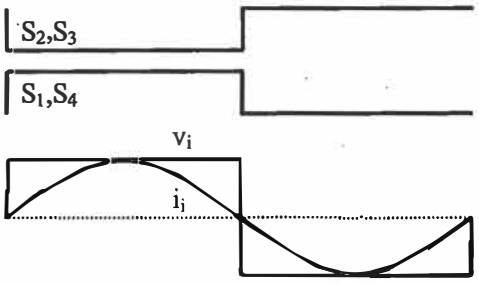


Fig. 2-24. The rectangular inverter voltage being in-phase with the current.

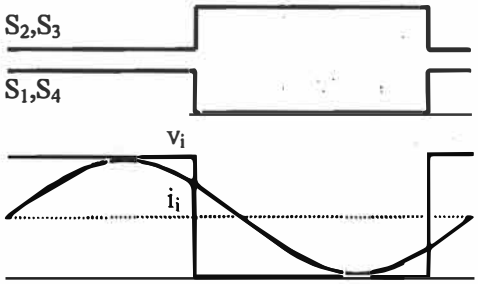


Fig. 2-25. The rectangular inverter voltage leading the current.

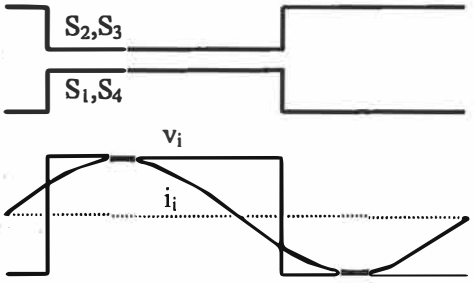


Fig. 2-26. The rectangular inverter voltage lagging the current.

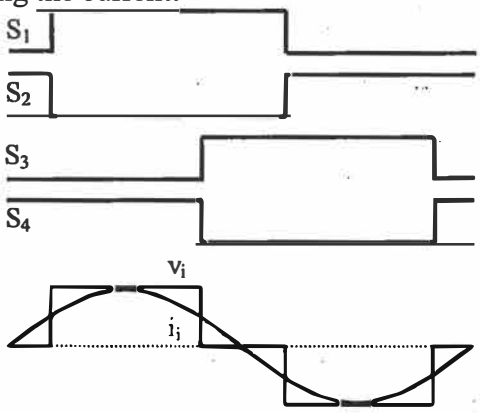


Fig. 2-27. Pulse-width of the rectangular inverter voltage is less than a full half cycle.

2-5.4 SWITCHING CONTROL IN CURRENT-SOURCED FULL-BRIDGE INVERTERS

In a current-sourced full-bridge inverter, switching exactly at the zero crossing of the inverter output voltage, as shown in Fig. 2-28, results in no switching losses since the switches are turned on and off with zero voltage. Moreover, the voltage and current ratings of the inverter are minimized

InductEV, Inc.
Exhibit 1008
Page 061

because the inverter voltage and current are in-phase, eliminating reactive power flow.

When the rectangular inverter current is leading the inverter voltage, as shown in Fig. 2-29, the switches are turned on with the inverter output voltage across them. This results in turn-on losses. But there are no turn-off losses because the switches are turned off with zero voltage and current when the inverter output voltage is blocked by the series diode. With this switching strategy, the voltage and current ratings of the inverter are higher than the transferred power.

If the rectangular inverter current is lagging the voltage, as shown in Fig. 2-30, the switches are turned on with zero voltage and current as the inverter output voltage is blocked by the series diode and therefore there is no turn-on loss. However, the switches are turned off with the inverter output voltage across them, resulting in turn-off losses. With this switching strategy, the voltage and current ratings of the inverter are higher than the transferred power.

When controlling the pulse-width of the rectangular inverter current, as shown in Fig. 2-31, the top two switches have turn-on losses but no turn-off losses, while the bottom two switches have turn-off losses but no turn-on losses.

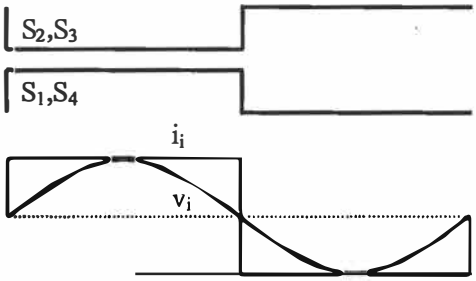


Fig. 2-28. The rectangular inverter current being in-phase with the voltage.

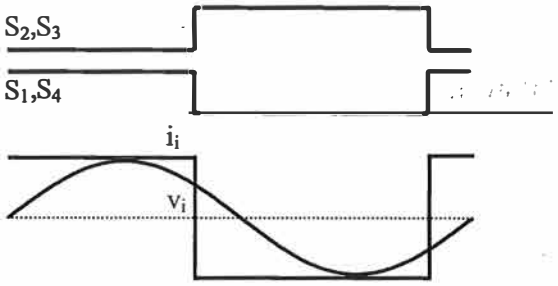


Fig. 2-29. The rectangular inverter current leading the voltage.

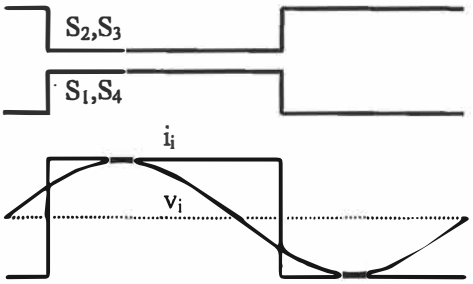


Fig. 2-30. The rectangular inverter current lagging the voltage.

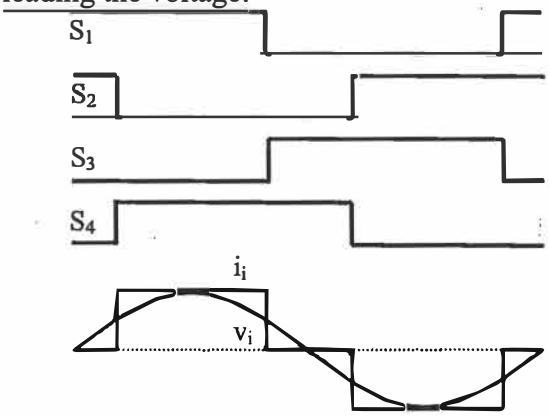


Fig. 2-31. Pulse-width of the rectangular inverter current is less than a full half cycle.

2-5.5 BIFURCATION PHENOMENON

As noted in 2-5.2, a variable-frequency controller allows the frequency to vary so that the power

InductEV, Inc.
Exhibit 1008
Page 062

supply operates with unity DPF. With full-bridge or half-bridge inverters, this is achievable with the inverters switched to track the zero crossing of the inverter output current (in a voltage-sourced power converter) or voltage (in a current-sourced power converter) [2][47][79]. Using this approach, the inverter output voltage and current can be controlled in phase, with the operating frequency varying in response to system variations.

As noted in [2][47][79], there could be more than one operating point in the frequency spectrum, and the variable-frequency controller may jump around these operating modes. Apart from this uncertainty, the operating frequency can shift significantly above or below the secondary resonant frequency resulting in substantial pickup detuning. This phenomenon is termed as a problem of 'frequency stability' in [2][47][79], and is simply labelled as 'bifurcation' in this thesis.

For the design of a variable-frequency system, it is usually required to ensure the system is designed to operate below the bifurcation boundary under all practical operating conditions. If the system needs to operate above the bifurcation boundary, the variable-frequency controller has to be forced to operate at the right operating mode to ensure power transfer capability. In practice, this is difficult.

To date only a limited analysis has been undertaken to determine the bifurcation criterion for selected ICPT systems. In the multiple pickup material handling system [2][79], it was found that bifurcation occurs if the number of pickups is increased such that:

$$n \geq \frac{L_p L_s}{Q_{s0}^2 M^2} \tag{2-32}$$

where n is the number of coupled secondary pickups.

Substituting (2-1) into (2-32) results in:

$$Q_{s0} \geq \frac{1}{\sqrt{n}k} \tag{2-33}$$

As noted in [2][79], this analysis is an approximation assuming high Q_{s0}, and both the parallel-compensated primary and secondary circuits are transformed into series compensated circuits to simplify the analysis. Consequently, the above bifurcation criterion is valid only for ICPT systems with series-compensated primaries and secondaries with high Q_{s0}.

As will be shown in Chapter 9, the equivalent coupling coefficient of a multiple pickup system is found to be proportional to the square root of the number of pickups ($k_n = \sqrt{n}k$). The bifurcation criterion (2-33) expressed in terms of the equivalent coupling coefficient is then:

$$Q_{s0} \geq \frac{1}{k_n} \tag{2-34}$$

With high Q_{s0}, it can be found from (2-23), (2-29) and (2-34) that the bifurcation criterion can be expressed in terms of Q_{p0} and Q_{s0} as:

InductEV, Inc.
Exhibit 1008
Page 063

$$Q_{p0} > Q_{s0} \tag{2-35}$$

As shown the system can achieve bifurcation-free operation when Q_{p0} is larger than Q_{s0}.

A more general bifurcation criterion was developed in [47] for ICPT systems with series-compensated primaries and secondaries. This bifurcation criterion was found to be:

$$Q_{s0} < \frac{\sqrt{1+\sqrt{1-k^2}}}{\sqrt{2}k} \tag{2-36}$$

Using (2-23) and (2-29), the above bifurcation criterion can be expressed in terms of Q_{p0} and Q_{s0} given by:

$$Q_{p0} > \frac{4Q_{s0}^3}{4Q_{s0}^2 - 1} \tag{2-37}$$

At high Q_{s0}, this bifurcation criterion again simplifies to (2-35).

The above bifurcation analysis is again only valid for ICPT systems with series compensated primaries and secondaries. In this thesis, general bifurcation criteria are developed for all basic topologies with the primary and secondary either series or parallel compensated.

2-6 FUTURE TRENDS

Present ICPT technology developments are busy meeting the commercial requirements of industrial applications as well as consumer products. Likely future developments are discussed below.

Wireless Communication Links: Wireless communication between the primary power supply and the secondary pickup is of great importance for many applications where the primary power supply intends to control and/or monitor the secondary pickup. For single pickup coil-type applications such as medical implants, the primary and secondary are very close to each other and communication links have been popularly implemented using radio frequency transceivers on both sides. However, this approach is normally not suitable for multiple pickup track-type applications such as material handling systems in manufacturing sites due to RFI and EMI considerations.

VAHLE (Germany) has been using the slotted microwave guide (SMG) to set up communication links for multiple pickup track-type applications. According to VAHLE, SMG was originally developed by MBB (Messerschmitt-Boelkow-Blohm), now DASA (Deutsche Aerospace), to transmit data to the magnetic levitation train (Transrapid) travelling at speeds of up to 250 mph. VAHLE acquired this technology at the end of 1994 and now has over 1,000 installations worldwide in successful operation.

InductEV, Inc.
Exhibit 1008
Page 064

A favourable approach for communication links in track-type applications would be to use the primary coil to carry radio frequency channels, at a frequency well above that of the power supply. The information transmission is achieved via the same electromagnetic coupling structure used for power transmission, eliminating the additional wave-guide.

New Electromagnetic Materials: Current commercial track-type applications are relatively short (around several hundred meters). The main challenge to enable longer distance is how to overcome conduction losses within the primary coil while limiting voltages. The solution would rely on new materials of conductor windings. Another challenge for long distance track-type applications is that it is economically not acceptable to use expensive magnetic materials such as ferrite along the track to improve magnetic coupling. One possible solution is to utilize cheap magnetic materials such as iron sand.

New Power Electronic Devices and Intelligent Controllers: New semiconductor switches offering better power capability and less loss will enable the operating frequency of high power ICPT industrial applications to be increased, resulting in smaller size magnetic materials. This in turn will extend potential commercial applications. New generations of microprocessors will enable intelligent controllers to be built for very complex multiple pickup applications. In such applications, power and traffic management are critical, requiring low cost high bandwidth wireless communications alongside the contact-less power transfer.

Futuristic Applications: As shown in Fig. 2-32, the aerial cab, the underwater transportation and the electric city bus are among many futuristic projects that are becoming more attractive and realizable with on-going improvements in ICPT technology as well as power electronic and telecommunication techniques.



(a) Aerial cab. (b) Underwater transportation. (c) Electric city bus.

Fig. 2-32. Futuristic ICPT applications.

InductEV, Inc.
Exhibit 1008
Page 065

2-7 CONCLUSIONS

In ICPT systems, the coupling strength of the electromagnetic structure is normally weak and cannot deliver the required power with reasonable size and cost at the line frequency of 50/60 Hz. It is often necessary to increase the frequency to between several kHz and many MHz, depending on the application requirements.

The increased reactance of the primary and secondary windings that arises from these increases in the operating frequency often must be compensated by capacitors connected in series or parallel. Secondary compensation is required for boosting power transfer capability, while primary compensation is introduced to minimize the VA rating of the power supply.

The choice of compensation topologies results in very different circuit characteristics. The series-compensated secondary resembles a voltage source, while the parallel-compensated secondary looks like a current source. The objective of series primary compensation is to achieve a voltage gain between the switching power supply and the primary coil, whereas parallel primary compensation is utilized to obtain a current gain.

Either voltage or current sourced power converters can be used to generate the necessary high frequency voltage and current for ICPT systems. According to the number of switches used, they can be separated into three groups: full-bridge, half-bridge and single switch. Impedance matching must be considered carefully between the selected inverter and primary compensation topology.

Many control strategies can be used to accommodate system variations. For single pickup applications, power control can be implemented at the primary or the secondary. In multiple pickup systems, each pickup needs an individual power regulator.

Both fixed and variable frequency operations can be used for the primary controller. Fixed-frequency operation minimizes pickup detuning, while variable-frequency operation improves the DPF of the power supply. Bifurcation (multiple operating modes) may occur in a variable-frequency system and needs to be considered carefully at the design stage to ensure power transfer capability and controllability.

REFERENCES

[1]. A. Okuno, L. Gamage, M. Nakaoka, "Performance evaluations of high-frequency inverter-linked DC/DC converter with noncontact pickup coil," *IEEE Transactions on Industrial Electronics*, vol. 48, pp. 475-477, Apr. 2001.

[2]. A. W. Green, J. T. Boys, "An inductively coupled high-frequency power system for material handling applications," in *Proc. Int. Power Electronics Conference*, vol. 2, 1993, pp. 821-826.

InductEV, Inc.
Exhibit 1008
Page 066

[3]. A. W. Green, J. T. Boys, "Intelligent Road Studs – Lighting the Paths of the Future," *IPENZ Transactions*, no. 24, pp. 33-40, 1997.

[4]. G. A. Covic, G. Elliott, O. H. Stielau, R. M.Green, J. T. Boys, "The design of a contact-less energy transfer system for a people mover system," in *Proc. International Conference on Power System Technology*, vol. 1, 2000, pp. 79-84.

[5]. Chwei-Sen Wang, G. A. Covic and O. H. Stielau, "Power transfer capability and bifurcation phenomena of loosely coupled inductive power transfer systems," *IEEE Transactions on Industrial Electronics*, vol. 51, pp. 148-157, Feb. 2004.

[6]. R. Laouamer, M. Brunello, J. P. Ferrieux, O. Normand, N. Buchheit, "A multi-resonant converter for non-contact charging with electromagnetic coupling," in *Proc. 23rd International Conference on Industrial Electronics, Control and Instrumentation*, vol. 2, 1997, pp. 792-797.

[7]. Gyu Bum Joun, B. H. Cho, "An energy transmission system for an artificial heart using leakage inductance compensation of transcutaneous transformer," *IEEE Transactions on Power Electronics*, vol. 13, pp. 1013-1022, Nov. 1998.

[8]. Chang-Gyun Kim, Dong-Hyun Seo, Jung-Sik You, Jong-Hu Park, B. H. Cho, "Design of a contactless battery charger for cellular phone," *IEEE Transactions on Industrial Electronics*, vol. 48, pp. 1238-1247, Dec. 2001.

[9]. J. T. Boys, G. A. Covic, G. A. J. Elliott, "Pick-up transformer for ICPT applications," *Electronics Letters*, vol. 38, pp. 1276-1278, Oct. 2002.

[10]. S. C. Tang, S. Y. Hui, Henry Shu-Hung Chung, "Coreless planar printed-circuit-board (PCB) transformers-a fundamental concept for signal and energy transfer," *IEEE Transactions on Power Electronics*, vol. 15, pp. 931-941, Sep. 2000.

[11]. M. Jufer, N. Macabrey, M. Perrottet, "Modeling and test of contactless inductive energy transmission," *Mathematics and computers in simulation*, vol. 46, pp. 197-211, 1998.

[12]. A. Esser, A. Nagel, "Contactless high speed signal transmission integrated in a compact rotatable power transformer," in *Proc. Fifth European Conference on Power Electronics and Applications*, vol. 4, 1993, pp. 409-414.

[13]. M. Eghtesadi, "Inductive power transfer to an electric vehicle-analytical model," in *Proc. IEEE 40th Vehicular Technology Conference*, 1990, pp. 100-104.

[14]. A. W. Kelley, W. R. Owens, "Connectorless power supply for an aircraft-passenger entertainment system," *IEEE Transactions on Power Electronics*, vol. 4, pp. 348-354, July 1989.

[15]. Yong Xiang Xu, J. T. Boys, G. A. Covic, "Modeling and controller design of ICPT pick-ups," in *Proc. International Conference on Power System Technology*, vol. 3, 2002, pp. 1602-1606.

InductEV, Inc.
Exhibit 1008
Page 067

[16]. S. Hussmann, P. A. Hu, "A micro-computer controlled ICPT power pick-up and its EMC considerations for moving sensor applications," in *Proc. International Conference on Power System Technology*, vol. 2, 2002, pp. 1011-1015.

[17]. Chwei-Sen Wang, G. A. Covic, O. H. Stielau, "General stability criterions for zero phase angle controlled loosely coupled inductive power transfer systems," in *Proc. 27th Annual Conference of the IEEE Industrial Electronics Society*, vol. 2, 2001, pp. 1049-1054.

[18]. O. H. Stielau, G. A. Covic, "Design of loosely coupled inductive power transfer systems," in *Proc. International Conference on Power System Technology*, vol. 1, 2000, pp. 85-90.

[19]. Chwei-Sen Wang, O. H. Stielau, G. A. Covic, "Load models and their application in the design of loosely coupled inductive power transfer systems," in *Proc. International Conference on Power System Technology*, vol. 2, 2000, pp. 1053-058.

[20]. G. A. J. Elliott, J. T. Boys, A. W. Green, "Magnetically coupled systems for power transfer to electric vehicles," in *Proc. International Conference on Power Electronics and Drive Systems*, vol. 2, 1995, pp. 797-801.

[21]. H. Matsuki, M. Shiiki, K. Murakami, T. Yamamoto, "Investigation of coil geometry for transcutaneous energy transmission for artificial heart," *IEEE Transactions on Magnetics*, vol. 28 pp. 2406-2408, Sept. 1992.

[22]. W. J. Heetderks, "RF powering of millimeter- and submillimeter-sized neural prosthetic implants," *IEEE Transactions on Biomedical Engineering*, vol. 35, pp. 323-327, May 1988 .

[23]. Yungtaek Jang, M. M. Jovanovic, "A contactless electrical energy transmission system for portable-telephone battery chargers," *IEEE Transactions on Industrial Electronics*, vol. 50, pp. 520-527, June 2003.

[24]. Byungcho Choi, Honnyong Cha, Jaehyun Noh, Sangkyu Park, "A new contactless battery charger for portable telecommunication/computing electronics," in *Proc. International Conference on Consumer Electronics*, 2001, pp. 58-59.

[25]. J. Hirai, Tae-Woong Kim, A. Kawamura, "Study on intelligent battery charging using inductive transmission of power and information," *IEEE Transactions on Power Electronics*, vol. 15, pp. 335-345, March 2000.

[26]. D. A. G. Pedder, A. D. Brown, J. A. Skinner, "A contactless electrical energy transmission system," *IEEE Transactions on Industrial Electronics*, vol. 46, pp. 23-30, Feb. 1999.

[27]. A. Kawamura, K. Ishioka, J. Hirai, "Wireless transmission of power and information through one high-frequency resonant AC link inverter for robot manipulator applications," *IEEE Transactions on Industry Applications*, vol. 32, pp. 503-508, May-June 1996.

InductEV, Inc.
Exhibit 1008
Page 068

[28]. A. Ghahary, B. H. Cho, "Design of transcutaneous energy transmission system using a series resonant converter," *IEEE Transactions on Power Electronics*, vol. 7, pp. 261-269, Apr. 1992.

[29]. J. T. Boys, G. A. Covic, Yongxiang Xu, "DC analysis technique for inductive power transfer pick-ups," *IEEE Power Electronics Letters*, vol. 1, pp. 51-53, June 2003.

[30]. H. Abe, H. Sakamoto, K. Harada, "Load voltage stabilization of noncontact energy transfer using three resonant circuit," in *Proc. Power Conversion Conference*, vol. 2, 2002, pp. 466-471.

[31]. A. P. Hu, Z. J. Chen, S. Hussmann, G. A. Covic, J. T. Boys, "A dynamically on-off controlled resonant converter designed for coalmining battery charging applications," in *Proc. International Conference on Power System Technology*, vol. 2, 2002, pp. 1039-1044.

[32]. D. O'Sullivan, M. Willers, M. G. Egan, J. G. Hayes, P. T. Nguyen, C. P. Henze, "Power-factor-corrected single-stage inductive charger for electric-vehicle batteries," in *Proc. Power Electronics Specialists Conference*, vol. 1, 2000, pp. 509-516.

[33]. J. G. Hayes, M. G. Egan, "A comparative study of phase-shift, frequency, and hybrid control of the series resonant converter supplying the electric vehicle inductive charging interface," in *Proc. Applied Power Electronics Conference and Exposition*, vol. 1, 1999, pp. 450-457.

[34]. L. Juby, A. Green, A. Collinson, "The design of a non-contact charging system for electric vehicles," in *Proc. 32nd Universities Power Engineering Conference*, 1997, pp. 573-576.

[35]. S. Valtchev, B. V. Borges, J. B. Klaassens, "Contactless energy transmission with optimal efficiency," in *Proc. 28th Annual Conference of the Industrial Electronics Society*, vol. 2, 2002, pp. 1330-1335.

[36]. Byeong-Mun Song, R. Kratz, S. Gurol, "Contactless inductive power pickup system for Maglev applications," in *Proc. IEEE Industry Applications Society Annual Meeting*, vol. 3, 2002, pp. 1586-1591.

[37]. Byungcho Choi, Jachyun Nho, "Contactless energy transfer using planar printed circuit board windings," *Electronics Letters*, vol. 37, pp. 1007-1009, Aug. 2001.

[38]. N. H. Kutkut, D. M. Divan, D. W. Novotny, R. H. Marion, "Design considerations and topology selection for a 120-kW IGBT converter for EV fast charging," *IEEE Transactions on Power Electronics*, vol. 13, pp. 169-178, Jan. 1998.

[39]. A. Esser, H.-C. Skudelny, "A new approach to power supplies for robots," *IEEE Transactions on Industry Applications*, vol. 27, pp. 872-875, Sept.-Oct. 1991.

[40]. K. Sylvan, J. R. Jordan, H. W. Whittington, "A shunt-excited inductive power link," *Journal of Medical Engineering and Technology*, vol. 13, pp. 215-219, July/Aug. 1989.

InductEV, Inc.
Exhibit 1008
Page 069

[41]. J. Lukacs, M. Kiss, I. Nagy, G. Gonter, R. Hadik, K. Kaszap, A. Tarsoly, "Inductive energy collection for electric vehicles," in *Proc. Fourth Power Electronics Conference*, 1981, pp. 71-81.

[42]. T. Bieler, M. Perrottet, V. Nguyen, Y. Perriard, "Contactless power and information transmission," *IEEE Transactions on Industry Applications*, vol. 38, pp. 1266-1272, Sep./Oct. 2002.

[43]. H. Abe, H. Sakamoto, K. Harada, "A noncontact charger using a resonant converter with parallel capacitor of the secondary coil," *IEEE Transactions on Industry Applications*, vol. 36, pp. 444-451, Mar.-Apr. 2000.

[44]. A. Hu, J. T. Boys, G. A. Covic, "Dynamic ZVS direct on-line start up of current fed resonant converter using initially forced DC current," in *Proc. IEEE International Symposium on Industrial Electronics*, vol. 1, 2000, pp. 312-317.

[45]. A. W. Green, J. T. Boys, "10 kHz inductively coupled power transfer-concept and control," in *Proc. Fifth International Conference on Power Electronics and Variable-Speed Drives*, 1994, pp. 694-699.

[46]. A. W. Green, "Modelling a push-pull parallel resonant convertor using generalised state-space averaging," *IEE Proc. Electric Power Applications*, vol. 140, pp. 350-356, Nov. 1993.

[47]. A. P. Hu, "Selected resonant converters for IPT power supplies," *PhD thesis*, Oct. 2001, The Electrical and Electronics Engineering Department, The University of Auckland, New Zealand.

[48]. N. H. Kutkut, K. W. Klontz, "Design considerations for power converters supplying the SAE J-1773 electric vehicle inductive coupler," in *Proc. Applied Power Electronics Conference and Exposition*, vol. 2, 1997, pp. 841-847.

[49]. L. Zhao, C. F. Foo, K. J. Tseng, "A new structure transcutaneous transformer for artificial heart system," *IEEE Transactions on Magnetics*, vol. 35, pp. 3550-3552, Sept. 1999.

[50]. G. B. Joung, B. H. Cho, "An energy transmission system for an artificial heart using leakage inductance compensation of transcutaneous transformer," in *Proc. Power Electronics Specialists Conference*, vol. 1, 1996, pp. 898-904.

[51]. H. Matsuki, Y. Yamakata, N. Chubachi, S.-I. Nitta, H. Hashimoto, "Transcutaneous DC-DC converter for totally implantable artificial heart using synchronous rectifier," *IEEE Transactions on Magnetics*, vol. 32, pp. 5118-5120, Sept. 1996.

[52]. C. G. Kim, B. H. Cho, "Transcutaneous energy transmission with double tuned duty cycle control," in *Proc. Energy Conversion Engineering Conference*, vol. 1, 1996, pp. 587-591.

InductEV, Inc.
Exhibit 1008
Page 070

[53]. T. H. Nishimura, T. Eguchi, K. Hirachi, Y. Maejima, K. Kuwana, M. Saito, "A large air gap flat transformer for a transcutaneous energy transmission system," in *Proc. Power Electronics Specialists Conference*, vol.2, 1994, pp. 1323-1329.

[54]. T. H. Nishimura, L. Ding, "Implantable artificial heart system and new actuator control by power electronic system," in *Proc. International Conference on Systems Engineering*, 1989, pp. 289-292.

[55]. Sung-Hun Lim, Seong-Ryong Lee, Byoung-Sung Han, "A novel noncontact electric energy transfer system with regulating AC voltage/frequency," in *Proc. Power Electronics Specialists Conference*, vol. 2, 2001, pp. 713-717.

[56]. H. Sakamoto, K. Harada, S. Washimiya, K. Takehara, Y. Matsuo, F. Nakao, "Large air-gap coupler for inductive charger [for electric vehicles]," *IEEE Transactions on Magnetics*, vol. 35, pp. 3526-3528, Sept. 1999.

[57]. J. G. Hayes, M. G. Egan, J. M. D. Murphy, S. E. Schulz, J. T. Hall, "Wide-load-range resonant converter supplying the SAE J-1773 electric vehicle inductive charging interface," *IEEE Transactions on Industry Applications*, vol. 35, pp. 884-895, July-Aug. 1999.

[58]. K. W. Klontz, D. M. Divan, D. W. Novotny, "An actively cooled 120 kW coaxial winding transformer for fast charging electric vehicles," *IEEE Transactions on Industry Applications*, vol. 31, pp. 1257–1263, Nov.-Dec. 1995.

[59]. J. Hirai, Tae-Woong Kim, A. Kawamura, "Wireless transmission of power and information for cableless linear motor drive," *IEEE Transactions on Power Electronics*, vol. 15, pp. 21-27, Jan. 2000.

[60]. J. M. Barnard, J. A. Ferreira, J. D. van Wyk, "Sliding transformers for linear contactless power delivery," *IEEE Transactions on Industrial Electronics*, vol. 44, pp. 774-779, Dec. 1997.

[61]. Y. Hiraga, J. Hirai, Y. Kaku, Y. Nitta, A. Kawamura, K. Ishioka, "Decentralized control of machines with the use of inductive transmission of power and signal," in *Proc. IEEE Industry Applications Society Annual Meeting*, vol. 2, 1994, pp. 875-881.

[62]. C.-C. Tsai, B.-S. Chen, C.-M. Tsai, "Design of wireless transcutaneous energy transmission system for totally artificial hearts," in *Proc. IEEE Asia-Pacific Conference on Circuits and Systems*, 2000, pp. 646-649.

[63]. T. Inoue, T. H. Nishimura, M. Saito, M. Nakaoka, "A transcutaneous energy transmission system for an artificial organ by using a novel resonant converter," in *Proc. IEEE International Conference on Systems Engineering*, 1992, pp. 294-297.

InductEV, Inc.
Exhibit 1008
Page 071

[64]. A. Djemouai, M. Sawan, M. Slamani, "An efficient RF power transfer and bidirectional data transmission to implantable electronic devices," in *Proc. International Symposium on Circuits and Systems*, vol. 2, 1999, pp. 259-262.

[65]. J. S. Mueller, R. S. Gyurcsik, "Two novel techniques for enhancing powering and control of multiple inductively-powered biomedical implants," in *Proc. International Symposium on Circuits and Systems*, vol. 1, 1997, pp. 289-292.

[66]. Wonseok Lim, Jaehyun Nho, Byungcho Choi, Taeyoung Ahn, "Low-profile contactless battery charger using planar printed circuit board windings as energy transfer device," in *Proc. Power Electronics Specialists Conference*, vol. 2, 2002, pp. 579-584.

[67]. A. Esser, "Contactless charging and communication for electric vehicles," *IEEE Industry Applications Magazine*, vol. 1, pp. 4-11, Nov.-Dec. 1995.

[68]. H. Sakamoto, K. Harada, K. Yamasaki, "A novel high power converter for non-contact charging with magnetic coupling," in *Proc. International Conference on Power Electronics and Drive Systems*, vol. 1, 1995, pp. 461-464.

[69]. K. W. Klontz, A. Esser, P. J. Wolfs, D. M. Divan, "Converter selection for electric vehicle charger systems with a high-frequency high-power link," in *Proc. Power Electronics Specialists Conference*, 1993, pp. 855-861.

[70]. A. Esser, "Contactless charging and communication system for electric vehicles," in *Proc. IEEE Industry Applications Society Annual Meeting*, vol. 2, 1993, pp. 1021-1028.

[71]. K. W. Klontz, A. Esser, R. R. Bacon, D. M. Divan, D. W. Novotny, R. D. Lorenz, "An electric vehicle charging system with 'universal' inductive interface," in *Proc. Power Conversion Conference*, 1993, pp. 227-232.

[72]. J. I. Rodriguez, D. K. Jackson, S. B. Leeb, "Capability analysis for an inductively coupled power transfer system," in *Proc. 7th Workshop on Computers in Power Electronics*, 2000, pp. 59-63.

[73]. O. H. Stielau, "High frequency, high power resonant electronic converters for induction heating," *PhD thesis*, Jan. 1991, The Electrical and Electronics Engineering Department, Rand Afrikaans University, South Africa

[74]. H. W. E. Koertzen, "Varying load induction heating by medium frequency power electronic converters," *PhD thesis*, Nov. 1994, The Electrical and Electronics Engineering Department, Rand Afrikaans University, South Africa

[75]. Y. Kanai, M. Mino, T. Sakai, T. Yachi, "A non-contact power-supply card powered by solar cells for mobile communications," in *Proc. Applied Power Electronics Conference and Exposition*, vol. 2, 2000, pp. 1157-1162.

InductEV, Inc.
Exhibit 1008
Page 072

[76]. A. P. Hu, J. T. Boys, G. A. Covic, "ZVS frequency analysis of a current-fed resonant converter," in *Proc. IEEE International Power Electronics Congress*, 2000, pp. 217-221.

[77]. A. P. Hu, J. T. Boys, G. A. Covic, "Frequency analysis and computation of a current-fed resonant converter for ICPT power supplies," in *Proc. International Conference on Power System Technology*, vol. 1, 2000, pp. 327-332.

[78]. J. T. Boys, A. P. Hu, G. A. Covic, "Critical Q analysis of a current-fed resonant converter for ICPT applications," *Electronics Letters*, vo. 36, pp. 1440-1442, Aug. 2000.

[79]. J. T. Boys, G. A. Covic, A. W. Green, "Stability and control of inductively coupled power transfer systems," *IEE Proc. Electric Power Applications*, vol. 147, pp. 37-43, Jan. 2000.

[80]. P. R. Troyk, M. A. K. Schwan, "Closed-loop class E transcutaneous power and data link for MicroImplants," *IEEE Transactions on Biomedical Engineering*, vol. 39, pp. 589-599, June 1992.

[81]. C. M. Zierhofer, E. S. Hochmair, "The Class-E Concept For Efficient Wide-Band Coupling-Insensitive Transdermal Power And Data Transfer," in *Proc. Annual International Conference of the IEEE Engineering in Medicine and Biology Society*, vol.2, 1992, pp. 382-383.

[82]. S. Dieckerhoff, M. J. Ruan, R. W. De Doncker, "Design of an IGBT-based LCL-resonant inverter for high-frequency induction heating," in *Proc. IEEE Industry Applications Society Annual Meeting*, vol. 3, 1999, pp. 2039-2045.

[83]. J. M. Espi, E. J. Dede, E. Navarro, E. Sanchis, A. Ferreres, "Features and design of the voltage-fed L-LC resonant inverter for induction heating," in *Proc. Power Electronics Specialists Conference*, vol. 2, 1999, pp. 1126-1131.

[84]. G. L. Fischer, H. Doht, "An inverter system for inductive tube welding utilizing resonance transformation," in *Proc. IEEE Industry Applications Society Annual Meeting*, vol. 2, 1994, pp. 833-840.

[85]. J. M. Espi, A. E. Navarro, J. Maicas, J. Ejea, S. Casans, "Control circuit design of the L-LC resonant inverter for induction heating," in *Proc. Power Electronics Specialists Conference*, vol. 3, 2000, pp. 1430-1435.

[86]. K. W. Klontz, D. M. Divan, D. W. Novotny, R. D. Lorenz, "Contactless power delivery system for mining applications," *IEEE Transactions on Industry Applications*, vol. 31, pp. 27-35, Jan.-Feb. 1995.

InductEV, Inc.
Exhibit 1008
Page 073

InductEV, Inc.
Exhibit 1008
Page 074

CHAPTER 3

DEVELOPMENT OF A GENERAL LOAD MODEL

3-1 Introduction
3-2 Overview of the load model
3-3 The pickup load
3-4 The secondary resonant circuit
3-5 The secondary quality factor
3-6 The reflected impedance
3-7 Pickup behaviour and influences on the primary
3-8 The primary coil
3-9 The primary quality factor
3-10 The power supply load model
3-11 Verification of the load model
3-12 Conclusions

3-1 INTRODUCTION

ICPT systems are normally designed to deliver power from a stationary primary source to one or more movable secondary loads (pickups) over large air gaps via magnetic coupling. Both the primary and pickup secondary are often compensated using capacitors connected in series or parallel to boost the power transfer capability while minimizing the VA rating of the power supply. In such a system, the primary resonant circuit is magnetically coupled with one or more secondary resonant circuits that supply power to a load. Consequently, the load seen by the power supply is a high order load resonant tank consisting of both the primary and secondary resonant circuits. The behaviour of this load resonant tank is mathematically complex and highly sensitive to variations in system parameters such as the operating frequency, the load, as well as misalignment in the electromagnetic structure.

To better facilitate the design of an ICPT system, this chapter develops a model to generally quantify the characteristics of the load resonant tank. The behaviour of the pickup and its influences on the primary are investigated to identify the influences of the operating frequency, the load, and the electromagnetic coupling structure. This chapter focuses on single pickup applications. Multiple pickup systems are discussed later in this thesis. The developed power supply load model is verified by a practical example.

3-2 OVERVIEW OF THE LOAD MODEL

In an ICPT system, the primary and secondary can be either series or parallel compensated or remain un-compensated. This results in nine basic topologies. To simplify the discussion, this thesis

InductEV, Inc.
Exhibit 1008
Page 075

only focuses on the analysis and design of the four topologies with both primary and secondary compensations as this reflects the majority of such systems in the medium-high power range. In practice, topologies without primary and/or secondary compensations can be analysed using a similar approach.

Sinusoidal steady state analysis is used for modelling the load resonant tank. The electromagnetic structure and the primary and secondary compensation capacitors (C_p and C_s) are assumed to be loss-less. The pickup load is assumed to be linear and resistive. The electromagnetic structure is modelled using the transformer mutual inductance coupling model (as noted in section 2.2.3). Here the coupling parameters include the primary self-inductance L_p, the mutual inductance M between the primary and secondary, and the secondary self-inductance L_s. Linear and frequency dependent impedances are used to represent the reactive elements (C_p, L_p, M, L_s and C_s) within the load resonant tank.

The load seen by the power supply, as shown in Fig. 3-1, consists of the primary compensation, an electromagnetic structure, the secondary compensation and a load. In this figure, the electromagnetic coupling between the primary and secondary is represented by an induced voltage and a reflected voltage (as has been noted in section 2-2.3). The load seen by the power supply can be separated into two interrelated resonant circuits: the primary and secondary. The primary resonant circuit includes the primary compensation, the primary inductance (L_p) and the reflected voltage ($-j\omega MI_s$). The secondary resonant circuit is formed by the induced voltage ($j\omega MI_p$), the secondary inductance (L_s), the secondary compensation and the load.

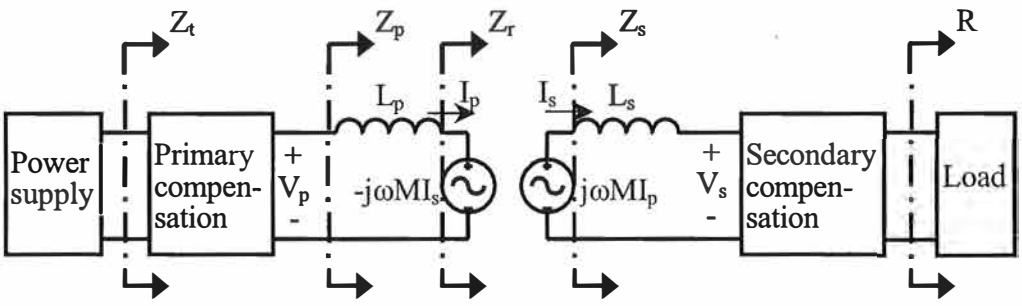


Fig. 3-1. Diagram of the load seen by the power supply.

The voltages and currents of a resonant circuit with a high quality factor are close to sinusoidal. As such, a sinusoidal ac analysis is suitable. With this approach, the circuit model of the load seen by the power supply can be transformed into an impedance model as shown in Fig. 3-1. The pickup load normally consists of a rectifier and a filter supplying power to a dc load with or without a switched-mode controller. To facilitate the linear sinusoidal ac analysis, this controlled dc load is

InductEV, Inc.
Exhibit 1008
Page 076

represented as an equivalent variable ac load (R). A secondary load impedance (Z_s) is used to represent the impedance seen by the induced voltage. The secondary load impedance is formed by the secondary inductance, the secondary compensation and an equivalent ac load. A reflected impedance (Z_r) is also used to represent the loading effect of the secondary resonant circuit on the primary. The reflected impedance is defined as the reflected voltage divided by the primary current. The impedance of the primary coil (Z_p) is a combination of the reactance of the self-inductance of the primary coil and the reflected impedance. Combining the impedance of the primary coil with the primary compensation results in the total load impedance (Z_t) seen by the power supply.

3-3 THE PICKUP LOAD

The high frequency ac voltage and current of the pickup may be used to supply power to a simple resistive load, a low frequency ac load such as an ac motor, or a dc load such as a dc motor or battery charger. When supplying power to a low frequency ac load, a frequency conversion device such as an ac-ac converter is required. To power up a dc load, a rectifier is commonly used to transform the ac voltage and current into a dc voltage and current, the harmonics of which can then be reduced by employing an output filter.

To simplify the resonant circuit analysis of the pickup, an equivalent resistive load can be developed to represent the pickup loading system. Two common examples are discussed in this section. Other pickup loading systems can be analysed using a similar approach.

For a diode bridge rectifier with an inductor output filter as shown in Fig. 3-2, the average current of the dc load capacitor at steady state is zero. As such the average of the inductor current equals the dc load current. Assuming a significantly large inductor output filter, the variation of the inductor current is negligible. In consequence, the input current (i_R) to the rectifier is approximately rectangular with a magnitude of the dc load current (I_{dc}) [1]. The fundamental component of this rectangular current is:

$$I_R = \frac{2\sqrt{2}I_{dc}}{\pi} \tag{3-1}$$

Assuming the input voltage (v_R) to the rectifier is sinusoidal in a resonant circuit, at steady state, the average voltage across the inductor is zero and as such the average of the rectified input voltage equals the dc load voltage (V_{dc}) [1]. As a result, the RMS value of v_R is:

$$V_R = \frac{\pi V_{dc}}{2\sqrt{2}} \tag{3-2}$$

The equivalent ac load found from (3-1)&(3-2) is therefore:

$$R = \frac{V_R}{I_R} = \frac{\pi^2 V_{dc}}{8I_{dc}} = \frac{\pi^2 R_{dc}}{8} \tag{3-3}$$

InductEV, Inc.
Exhibit 1008
Page 077

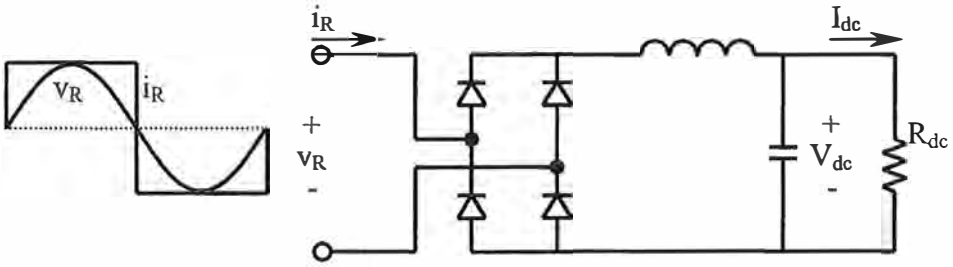


Fig. 3-2. Full-bridge diode rectifier with inductor output filter.

For a diode bridge rectifier with a capacitor output filter as shown in Fig. 3-3, the variation of the load voltage is negligible, assuming a substantially large capacitor. In consequence, the input voltage (v_R) to the rectifier is approximately rectangular with a magnitude of the dc load voltage (V_{dc}) [1]. The fundamental component of this rectangular voltage is:

$$V_R = \frac{2\sqrt{2}V_{dc}}{\pi} \tag{3-4}$$

Assuming the input current (i_R) to the rectifier is sinusoidal in a resonant circuit, at steady state, the average capacitor current is zero and as such the average of the rectified input current equals the dc load current (I_{dc}) [1]. As a result, the RMS value of i_R is:

$$I_R = \frac{\pi I_{dc}}{2\sqrt{2}} \tag{3-5}$$

The equivalent ac load found from (3-4)&(3-5) is thus:

$$R = \frac{V_R}{I_R} = \frac{8V_{dc}}{\pi^2 I_{dc}} = \frac{8R_{dc}}{\pi^2} \tag{3-6}$$

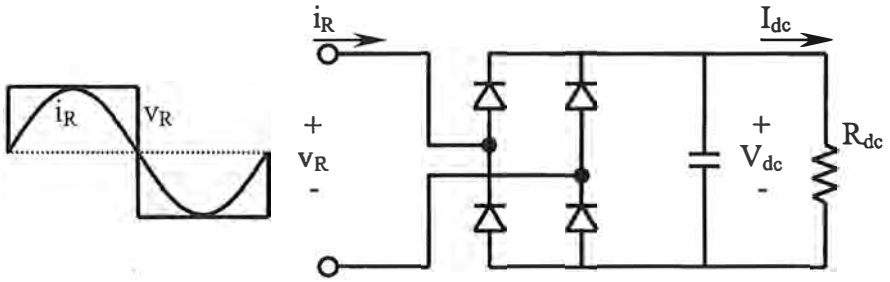


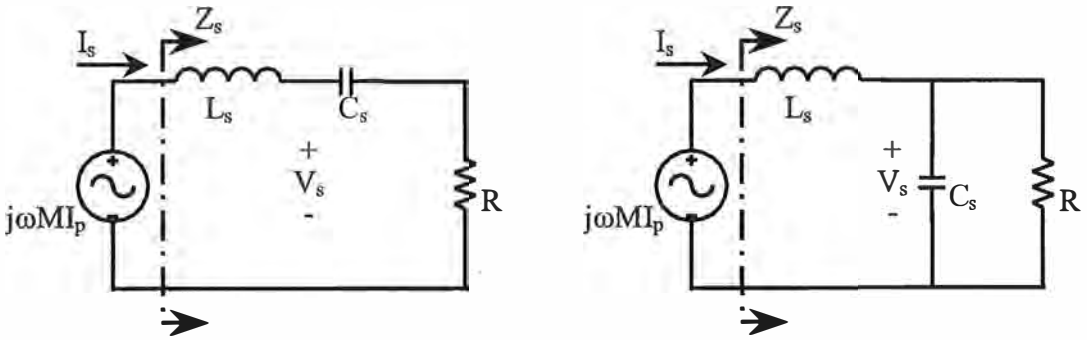
Fig. 3-3. Full-bridge diode rectifier with capacitor output filter.

3-4 THE SECONDARY RESONANT CIRCUIT

With the pickup loading system represented as an equivalent resistor, the equivalent circuits of series and parallel compensated secondary systems are shown respectively in Fig. 3-4 (a) and (b). In these circuits, the induced voltage ($j\omega MI_p$) in the secondary coil is represented as a voltage source in

InductEV, Inc.
Exhibit 1008
Page 078

series connection with the secondary inductance. The induced voltage arises from the magnetic coupling (M) between the primary and secondary and is dependent on the operating frequency of the primary power supply as well as the primary current flowing through the primary coil.



(a) Series compensated secondary. (b) Parallel compensated secondary.

Fig. 3-4. Equivalent circuits of the secondary systems.

To simplify the analysis, the secondary resonant circuit can be represented as a lumped impedance (Z_s) driven by the induced voltage. As shown in Fig. 3-4, the lumped secondary impedance depends on the compensation topology. With a series compensated secondary system, the secondary impedance consists of an inductor, a capacitor and a load in series connection. For a parallel-compensated secondary, the secondary impedance is formed by an inductor in series connection with the parallel-connected capacitor and load. The secondary impedances derived respectively from the circuits of series and parallel compensated secondary systems in Fig. 3-4 (a) and (b) are:

$$Z_s = \begin{cases} j\omega L_s + \dfrac{1}{j\omega C_s} + R & \text{series secondary} \\ j\omega L_s + \dfrac{1}{j\omega C_s + \dfrac{1}{R}} & \text{parallel secondary} \end{cases} \tag{3-7}$$

3-5 THE SECONDARY QUALITY FACTOR

The secondary resonance can be quantified by the quality factor (Q_s) associated with the secondary resonant circuit. The quality factor of a resonant circuit is defined as the ratio of reactive to real power as:

$$Q = \frac{VAR}{P} \tag{3-8}$$

In either series or parallel-compensated pickups, the reactive power of the pickup coil equals the reactive power of the secondary compensation capacitor (C_s), while the real power transferred by the pickup coil equals the power going to the load (R) as noted in Appendix B. They are calculated below

InductEV, Inc.
Exhibit 1008
Page 079

to determine the secondary quality factor.

Series compensated secondary: When the secondary is series compensated, the secondary current (I_s) flows through the pickup coil, the secondary compensation capacitor (C_s) and the load (R). The following analysis of series compensated secondary resonant circuit refers to the secondary current.

The reactive power of the secondary compensation capacitor is:

$$VAR_s = \frac{I_s^2}{\omega C_s} \tag{3-9}$$

The real power of the load is:

$$P = I_s^2 R \tag{3-10}$$

The secondary quality factor of a series-compensated pickup is then:

$$Q_s = \frac{VAR_s}{P} = \frac{1}{\omega C_s R} \tag{3-11}$$

Parallel-compensated secondary: When the secondary is parallel compensated, the secondary voltage (V_s) appears across the pickup coil, the secondary compensation capacitor and the load. The following analysis of parallel-compensated secondary resonant circuit refers to the secondary voltage.

The real power of the load R is:

$$P = \frac{V_s^2}{R} \tag{3-12}$$

The reactive power of the secondary capacitor is:

$$VAR_s = V_s^2 \omega C_s \tag{3-13}$$

The secondary quality factor of a parallel-compensated pickup is then:

$$Q_s = \frac{VAR_s}{P} = \omega C_s R \tag{3-14}$$

3-6 THE REFLECTED IMPEDANCE

Using the mutual inductance coupling model, as noted in section 2-2.3, a reflected voltage ($-j\omega MI_s$) can be used to represent the loading effects of the secondary resonant circuit on the primary coil. This reflected voltage in the primary coil arises from the magnetic coupling between the primary and secondary and is dependent on the operating frequency of the primary power supply as well as the secondary current flowing through the secondary coil. Equivalently, this can be regarded as a voltage source in series connection with the primary inductance.

With the secondary impedance given in (3-7), the secondary current is then:

InductEV, Inc.
Exhibit 1008
Page 080

$$I_s = \frac{j\omega M I_p}{Z_s} \tag{3-15}$$

The reflected voltage from the secondary to the primary calculated using (3-15) is:

$$-j\omega M I_s = -j\omega M\left(\frac{j\omega M I_p}{Z_s}\right) = \frac{\omega^2 M^2 I_p}{Z_s} \tag{3-16}$$

In order to simplify the analysis of the loading effects of the secondary resonant circuit, a reflected impedance can be calculated by dividing the reflected voltage given in (3-16) by the primary current as:

$$Z_r = \frac{-j\omega M I_s}{I_p} = \frac{\omega^2 M^2}{Z_s} \tag{3-17}$$

As shown above, the reflected impedance is dependent on the operating frequency, the mutual inductance, and the secondary impedance.

Substituting (3-7) into (3-17), the reflected resistance and reactance can be derived for the specified secondary compensation as:

$$\mathrm{Re}\,Z_r = \begin{cases} \dfrac{\omega^4 C_s^2 M^2 R}{\left(\omega^2 C_s L_s - 1\right)^2 + \omega^2 C_s^2 R^2} & \text{series secondary} \\ \dfrac{\omega^2 M^2 R}{R^2\left(\omega^2 C_s L_s - 1\right)^2 + \omega^2 L_s^2} & \text{parallel secondary} \end{cases} \tag{3-18}$$

and

$$\mathrm{Im}\,Z_r = \begin{cases} \dfrac{-\omega^3 C_s M^2\left(\omega^2 C_s L_s - 1\right)}{\left(\omega^2 C_s L_s - 1\right)^2 + \omega^2 C_s^2 R^2} & \text{series secondary} \\ \dfrac{-\omega^3 M^2\left[C_s R^2\left(\omega^2 C_s L_s - 1\right) + L_s\right]}{R^2\left(\omega^2 C_s L_s - 1\right)^2 + \omega^2 L_s^2} & \text{parallel secondary} \end{cases} \tag{3-19}$$

where the operators 'Re' and 'Im' represent the real and imaginary components of the corresponding complex variable respectively.

The power transferred from the primary to the secondary is the reflected resistance multiplied by the square of the primary current as given by:

$$P = (\mathrm{Re}\,Z_r) I_p^2 \tag{3-20}$$

The primary current I_p is normally controlled constant in ICPT systems especially for high power applications [2-3]. With such systems, the power transfer capability is proportional to the reflected resistance according to (3-20).

The required VA rating of the secondary compensation capacitor is:

$$VA_{Cs} = VAR_s = Q_s P \tag{3-21}$$

InductEV, Inc.
Exhibit 1008
Page 081

The secondary VA rating required for the pickup coil is then:

$$VA_s = \sqrt{P^2 + (VAR_s)^2} = \left(\sqrt{1+Q_s^2}\right)P \tag{3-22}$$

3-7 PICKUP BEHAVIOUR AND INFLUENCES ON THE PRIMARY

In this section, the steady state behaviour of both series and parallel-compensated pickups are quantified, which in turn enables their influences on the primary circuit to be determined. The pickups in the system are normally designed to operate at or near their resonant frequency. Consequently, this section initially focuses on the influence of the pickup when operating at this frequency. However, under variable-frequency control, the operating frequency may shift from the secondary resonant frequency. Alternatively, in some applications the operating frequency may be deliberately changed to regulate power flow. In either case, this frequency shift dramatically influences the system operation. As such a general analysis is undertaken across the frequency spectrum to quantify this effect.

3-7.1 OPERATION AT THE SECONDARY RESONANT FREQUENCY

The secondary resonant frequency ω_0 (the frequency where L_s is in resonance with C_s) is given by:

$$\omega_0 = \frac{1}{\sqrt{L_s C_s}} \tag{3-23}$$

The voltages, currents, power and VAs of the secondary resonant circuit when operated at the secondary resonant frequency have been investigated in section 2-3.2, with a summary of these results given in Table 2-1.

The quality factor of the pickup at ω_0 can be derived from (3-11), (3-14) and (3-23) as:

$$Q_{s0} = Q_s(\omega = \omega_0) = \begin{cases} \dfrac{1}{\omega_0 C_s R} = \dfrac{\omega_0 L_s}{R} & \text{series secondary} \\ \omega_0 C_s R = \dfrac{R}{\omega_0 L_s} & \text{parallel secondary} \end{cases} \tag{3-24}$$

Since Q_{s0} is a function of the load, this dimensionless parameter is used in the thesis as a fundamental design parameter representing the pickup load. It equals the secondary quality factor when operating at ω_0. At other operating frequencies (ω), it relates to the operating secondary quality factor (Q_s) as:

$$Q_s = \begin{cases} \dfrac{Q_{s0}}{\omega/\omega_0} & \text{series secondary} \\ (\omega/\omega_0)Q_{s0} & \text{parallel secondary} \end{cases} \tag{3-25}$$

InductEV, Inc.
Exhibit 1008
Page 082

To investigate the loading effects of the secondary resonant circuit on the primary coil when operated at ω_0, the reflected resistance and reactance at ω_0 can be calculated from (3-18) and (3-19) for the specified secondary compensation as:

$$\mathrm{Re}Z_{r0} = \mathrm{Re}Z_r(\omega=\omega_0) = \begin{cases} \dfrac{\omega_0^2 M^2}{R} = \left(\dfrac{\omega_0 M^2}{L_s}\right) Q_{s0} & \text{series secondary} \\ \dfrac{M^2 R}{L_s^2} = \left(\dfrac{\omega_0 M^2}{L_s}\right) Q_{s0} & \text{parallel secondary} \end{cases} \tag{3-26}$$

and

$$\mathrm{Im}Z_{r0} = \mathrm{Im}Z_r(\omega=\omega_0) = \begin{cases} 0 & \text{series secondary} \\ -\dfrac{\omega_0 M^2}{L_s} & \text{parallel secondary} \end{cases} \tag{3-27}$$

As shown in (3-26), if the system operates at ω_0, both the reflected resistance and the power transfer capability (assuming a constant primary current) in a series compensated secondary increase to infinity when the load R is reduced to zero ($Q_{s0}=\infty$). A similar result arises for a parallel-compensated secondary as the load R increases to infinity ($Q_{s0}=\infty$). When expressed in terms of the secondary quality factor (Q_{s0}), the reflected resistance at ω_0 for series compensation becomes identical to that determined with parallel compensation.

As can be seen in (3-27), a series compensated secondary has zero reflected reactance, whereas a parallel-compensated system reflects a capacitive load that is independent of the loading conditions on the pickup. This is one of the major differences between series and parallel-compensated secondary systems.

The power transfer capability at ω_0 can be calculated by substituting the reflected resistance given in (3-26) into (3-20). The result is identical to (2-25) and (2-27) respectively for series and parallel-compensated secondary systems.

Equating (3-20) with (2-25) and (2-27), the reflected resistance at ω_0 can be expressed in terms of the open circuit voltage and the short circuit current as:

$$\mathrm{Re}Z_{r0} = \frac{P}{I_p^2} = \frac{Q_{s0} V_{oc} I_{sc}}{I_p^2} \tag{3-28}$$

According to the above equation, this reflected resistance is strongly related to the capability of the electromagnetic structure (the open circuit voltage and the short circuit current) as well as the secondary compensation level (the secondary quality factor).

InductEV, Inc.
Exhibit 1008
Page 083

3-7.2 NORMALIZATION OF THE IMPEDANCE MODEL

The loading effect of the secondary pickup on the primary coil is represented as a reflected impedance (Z_r) in section 3-6. Similarly (as discussed later in section 3-10.1) the loading effect of the load resonant tank, consisting of both the primary and secondary resonant circuits, on the power supply is represented as a load impedance (Z_t). Analysis of these impedance models is complex. The pickup reflected impedance is a function of the operating frequency (ω), the mutual inductance (M), the secondary self-inductance (L_s), the secondary compensation capacitance (C_s), and the pickup load (R). In addition to these parameters (ω, M, L_s, C_s and R), the power supply load impedance also depends on the primary self-inductance (L_p) and the primary compensation capacitance (C_p).

For a general analysis across the frequency spectrum, both the pickup reflected impedance and the power supply load impedance models can be simplified using normalization methods. Since the pickup is generally designed to operate at ω_0, this frequency is therefore selected as a base parameter in the normalization process. The normalized frequency (u) is defined as:

$$u = \frac{\omega}{\omega_0} \tag{3-29}$$

When operating above or below ω_0, u varies from unity indicating the percentage of frequency detuning within the pickup. To ensure power transfer capability of the pickup, it is normally desirable to minimize this frequency detuning.

For a general analysis of the load, another useful base parameter for normalization is Re Z_{r0} (as noted in section 3-7.1) as this represents the designed power transfer capability of the system operating with constant primary current. Using this parameter, the normalized pickup reflected impedance (Z_{rn}) and power supply load impedance (Z_{tn}) are defined as:

$$Z_{rn,tn} = \frac{Z_{r,t}}{\mathrm{Re}\, Z_{r0}} \tag{3-30}$$

With this approach, Z_{rn} represents the pickup loading effects on the primary coil relative to the designed power transfer capability of the pickup, while Z_{tn} indicates the loading effects seen by the power supply scaled to the designed power transfer capability of the pickup.

3-7.3 INFLUENCE OF FREQUENCY ON THE PICKUP BEHAVIOUR

The ratio of the secondary current (I_s) given in (3-15) to the short circuit current (I_{sc}) given in (2-8) is:

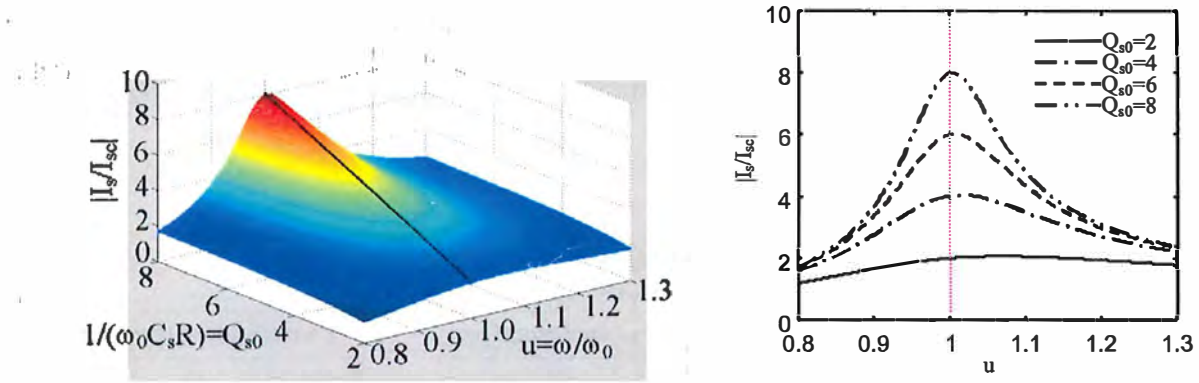
$$\frac{I_s}{I_{sc}} = \frac{j\omega L_s}{Z_s} \tag{3-31}$$

InductEV, Inc.
Exhibit 1008
Page 084

This ratio (as derived in Appendix C) is a function of the normalized frequency (u) and the secondary quality factor at ω_0 (Q_{s0}) for the specified secondary compensation as:

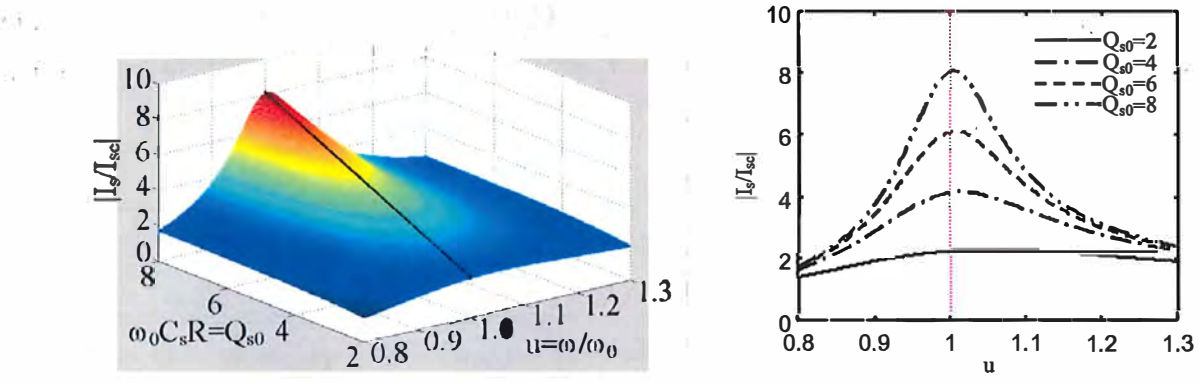
$$\left|\frac{I_s}{I_{sc}}\right| = \begin{cases} \dfrac{\sqrt{Q_{s0}^4 u^4 \left(u^2-1\right)^2 + Q_{s0}^2 u^6}}{u^2 + Q_{s0}^2\left(u^2-1\right)^2} & \text{series secondary} \\ \dfrac{\sqrt{\left[Q_{s0}^2 u^2\left(u^2-1\right)+u^2\right]^2 + Q_{s0}^2 u^2}}{u^2 + Q_{s0}^2\left(u^2-1\right)^2} & \text{parallel secondary} \end{cases} \tag{3-32}$$

Equation (3-32) can be used to investigate variations in the secondary current as the pickup is detuned from the design frequency ω_0, or when the secondary quality factor changes with the load. They are compared in Fig. 3-5 for series and parallel-compensated secondary systems. In this figure, the selected range of Q_{s0} is from 2 to 8 and u is chosen to be around unity (the secondary resonant frequency ω_0), since typical ICPT systems are normally designed to operate close to ω_0 (u close to unity) with Q_{s0} below 10 [1-2]. The cross-sections of these surfaces are also drawn at selected Q_{s0} of 2, 4, 6 and 8 to clarify corresponding features.



(i) Surface function. (ii) Cross sections of the surface.

(a) Series compensated secondary.



(i) Surface function. (ii) Cross sections of the surface.

(b) Parallel compensated secondary.

Fig. 3-5. Quantified secondary current.

InductEV, Inc.
Exhibit 1008
Page 085

Both series and parallel-compensated secondary systems have similar features. The maximum secondary current occurs close to ω_0, and drops quickly when the operating frequency shifts away. This sensitivity increases as the secondary quality factor becomes larger with increasing load.

Using a similar approach, the ratio of the load current (I_R) and the secondary capacitor current (I_{Cs}) to the short circuit current (I_{sc}) can be derived as functions of only the normalized operating frequency (u) and the secondary quality factor (Q_{s0}). Similarly, the ratio of the secondary voltage (V_s), the load voltage (V_R) and the secondary capacitor voltage (V_{Cs}) to the open circuit voltage (V_{oc}) can also be derived as functions of only u and Q_{s0}. The open circuit voltage is calculated using (2-6) with the frequency (ω) set equal to the secondary resonant frequency (ω_0). A summary of these functions is given in Table 3-1. The ratio of the power transfer, the required VA rating of the secondary coil and the required VA rating of the secondary capacitor to the product of open circuit voltage and short circuit current can be derived using functions of relevant voltages and currents. The results are once again functions of only u and Q_{s0}.

An analysis of these functions in Table 3-1 across the frequency spectrum for selected Q_{s0} shows they are similar to the results shown in Fig. 3-5 for the secondary current. In consequence, maximum voltages, currents, power and VAs of both series and parallel compensated pickups all occur when the system operates at or close to the secondary resonant frequency, and becomes substantially lower with large frequency detuning.

TABLE 3-1
QUANTIFIED PICKUP VOLTAGES, CURRENTS

Pickup topology	Series compensation	Parallel compensation
Secondary current $\lvert I_s / I_{sc}\rvert$	$\frac{\sqrt{Q_{s0}^4 u^4 (u^2-1)^2 + Q_{s0}^2 u^6}}{u^2 + Q_{s0}^2 (u^2-1)^2}$	$\frac{\sqrt{\left[Q_{s0}^2 u^2 (u^2-1) + u^2\right]^2 + Q_{s0}^2 u^2}}{u^2 + Q_{s0}^2 (u^2-1)^2}$
Secondary voltage $\lvert V_s / V_{oc}\rvert$	$\frac{\sqrt{Q_{s0}^2 u^8 + u^2\left[u^2 - Q_{s0}^2 (u^2-1)\right]^2}}{u^2 + Q_{s0}^2 (u^2-1)^2}$	$\frac{\sqrt{Q_{s0}^2 u^4 + Q_{s0}^4 u^2 (u^2-1)^2}}{u^2 + Q_{s0}^2 (u^2-1)^2}$
Load current $\lvert I_R / I_{sc}\rvert$	$\frac{\sqrt{Q_{s0}^4 u^4 (u^2-1)^2 + Q_{s0}^2 u^6}}{u^2 + Q_{s0}^2 (u^2-1)^2}$	$\frac{\sqrt{u^4 + Q_{s0}^2 u^2 (u^2-1)^2}}{u^2 + Q_{s0}^2 (u^2-1)^2}$
Load voltage $\lvert V_R / V_{oc}\rvert$	$\frac{\sqrt{Q_{s0}^2 u^4 (u^2-1)^2 + u^6}}{u^2 + Q_{s0}^2 (u^2-1)^2}$	$\frac{\sqrt{Q_{s0}^2 u^4 + Q_{s0}^4 u^2 (u^2-1)^2}}{u^2 + Q_{s0}^2 (u^2-1)^2}$
Secondary capacitor current $\lvert I_{Cs} / I_{sc}\rvert$	$\frac{\sqrt{Q_{s0}^4 u^4 (u^2-1)^2 + Q_{s0}^2 u^6}}{u^2 + Q_{s0}^2 (u^2-1)^2}$	$\frac{\sqrt{Q_{s0}^4 u^4 (u^2-1)^2 + Q_{s0}^2 u^6}}{u^2 + Q_{s0}^2 (u^2-1)^2}$
Secondary capacitor voltage $\lvert V_{Cs} / V_{oc}\rvert$	$\frac{\sqrt{Q_{s0}^2 u^4 + Q_{s0}^4 u^2 (u^2-1)^2}}{u^2 + Q_{s0}^2 (u^2-1)^2}$	$\frac{\sqrt{Q_{s0}^2 u^4 + Q_{s0}^4 u^2 (u^2-1)^2}}{u^2 + Q_{s0}^2 (u^2-1)^2}$

InductEV, Inc.
Exhibit 1008
Page 086

3-7.4 INFLUENCE OF FREQUENCY ON THE REFLECTED IMPEDANCE

According to the above investigation, the electric characteristics of the secondary resonant circuit are sensitive to variations in the operating frequency and the load. In consequence, the loading effects of the second resonant circuit on the primary will exhibit a similar sensitivity. To enable a general analysis of the pickup loading effects, a normalized reflected impedance is calculated using (3-30) as:

$$Z_{rn} = \frac{Z_r}{\mathrm{Re}\, Z_{r0}} = \frac{\mathrm{Re}\, Z_r}{\mathrm{Re}\, Z_{r0}} + j\frac{\mathrm{Im}\, Z_r}{\mathrm{Re}\, Z_{r0}} = \mathrm{Re}\, Z_{rn} + j\,\mathrm{Im}\, Z_{rn} \tag{3-33}$$

The resistive and reactive components of Z_m (as derived in Appendix D) are both functions of the secondary quality factor (Q_{s0}) and the normalized operating frequency (u) as stated below for the specified secondary compensation:

$$\mathrm{Re}\, Z_{rn} = \frac{\mathrm{Re}\, Z_r}{\mathrm{Re}\, Z_{r0}} = \begin{cases} \dfrac{u^4}{\left(u^2-1\right)^2 Q_{s0}^2 + u^2} & \text{series secondary} \\ \dfrac{u^2}{\left(u^2-1\right)^2 Q_{s0}^2 + u^2} & \text{parallel secondary} \end{cases} \tag{3-34}$$

and

$$\mathrm{Im}\, Z_{rn} = \frac{\mathrm{Im}\, Z_r}{\mathrm{Re}\, Z_{r0}} = \begin{cases} \dfrac{-u^3\left(u^2-1\right)Q_{s0}}{\left(u^2-1\right)^2 Q_{s0}^2 + u^2} & \text{series secondary} \\ \dfrac{-u^3\left[\left(u^2-1\right)Q_{s0} + \dfrac{1}{Q_{s0}}\right]}{\left(u^2-1\right)^2 Q_{s0}^2 + u^2} & \text{parallel secondary} \end{cases} \tag{3-35}$$

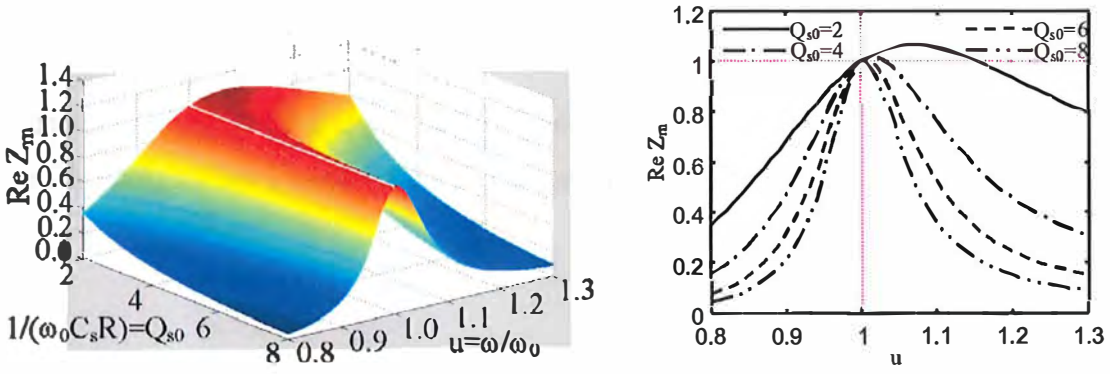
The normalized reflected resistance and reactance are compared in Fig. 3-6 and Fig. 3-7 for series and parallel compensated secondary systems respectively. They are shown as functions of the secondary quality factors (Q_{s0}) and the normalized operating frequency (u). Cross-sections of the surfaces at selected Q_s of 2, 4, 6 and 8 are drawn to show the influences of u and Q_{s0}.

The normalized reflected resistance at ω_0 is shown as white lines on the surfaces in Fig. 3-6 (a-i)&(b-i). The normalized reflected reactance at ω_0 is shown as black lines on the surfaces in Fig. 3-7 (a-i)&(b-i). The reflected resistance and reactance of the series and parallel-compensated secondary systems once again have similar features. As with the electric characteristic of the pickup, both the reflected resistance and reactance are highly sensitive to variations in the operating frequency. This sensitivity increases as the secondary quality factor increases.

For both series and parallel compensated secondary systems, maximum reflected resistance and

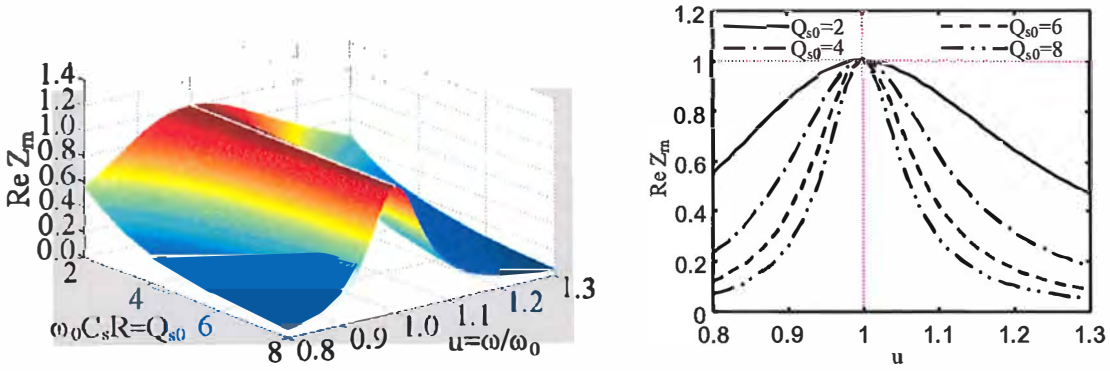
InductEV, Inc.
Exhibit 1008
Page 087

power transfer capability under constant primary current control, is achieved when operated close to ω_0. As the operating frequency shifts away, both the reflected resistance and power transfer capability quickly drop. Assuming a secondary quality factor of 5, if u is 0.9 (representing a 10% drop below ω_0), the power transfer capability decreases by 62% for series compensated pickups, and 53% for parallel-compensated pickups. Whereas a 10% frequency increase (u=1.1) results in decreases in power of 37% and 48% for series and parallel-compensated pickups respectively.



(i) Surface function. (ii) Cross sections of the surface.

(a) Series compensated secondary.



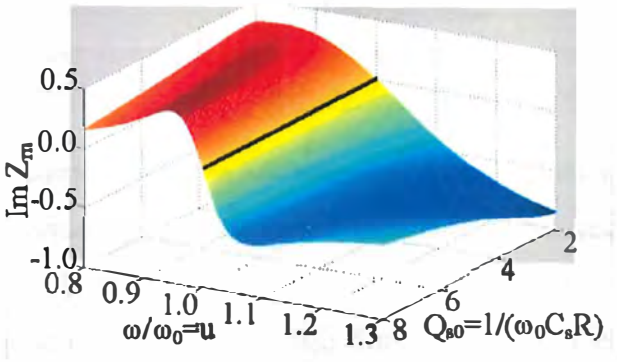
(i) Surface function. (ii) Cross sections of the surface.

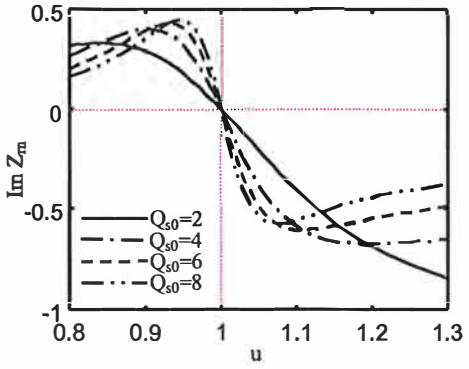
(b) Parallel compensated secondary.

Fig. 3-6. Normalized reflected resistance for series and parallel-compensated secondary systems.

The reflected reactance from a series compensated secondary is always zero at ω_0. This reflected reactance is inductive (positive) below ω_0, and capacitive (negative) above ω_0. The parallel-compensated secondary system, however, reflects a capacitive reactance at ω_0. This reflected reactance becomes less capacitive and eventually inductive as the operating frequency moves below ω_0. It becomes more capacitive as the operating frequency shifts above ω_0.

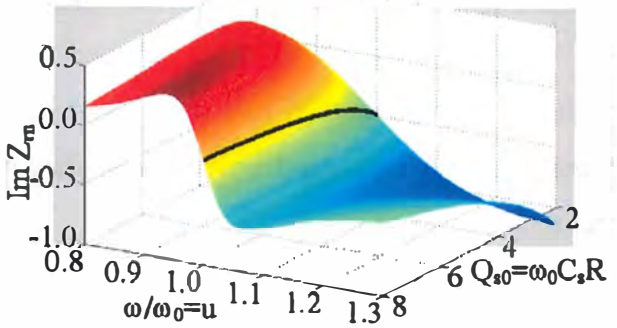
InductEV, Inc.
Exhibit 1008
Page 088

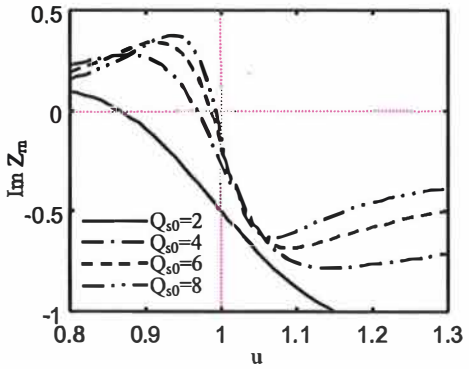




(i) Surface function. (ii) Cross sections of the surface.

(a) Series compensated secondary.





(i) Surface function. (ii) Cross sections of the surface.

(b) Parallel compensated secondary.

Fig. 3-7. Normalized reflected reactance for series and parallel-compensated secondary systems.

3-7.5 OPERATING CONDITIONS FOR MAXIMUM POWER TRANSFER

According to (3-20), the power transfer from the primary to the secondary depends on the reflected resistance and the primary current. Assuming constant primary current, the power transfer is then proportional to the reflected resistance. In this case, the operating frequency for maximum power transfer can be determined by:

$$\frac{\partial\left(\frac{\mathrm{Re}\,Z_r}{\mathrm{Re}\,Z_{r0}}\right)}{\partial u}=0 \tag{3-36}$$

The result is found to be:

$$u=\begin{cases}\sqrt{\dfrac{2Q_{s0}^2}{2Q_{s0}^2-1}} & \text{series secondary}\\ 1 & \text{parallel secondary}\end{cases} \tag{3-37}$$

Substituting (3-37) into (3-34) results in:

InductEV, Inc.
Exhibit 1008
Page 089

$$\frac{\mathrm{Re}\,Z_r}{\mathrm{Re}\,Z_{r0}} = \begin{cases} \dfrac{4Q_{s0}^2}{4Q_{s0}^2 - 1} & \text{series secondary} \\ 1 & \text{parallel secondary} \end{cases} \tag{3-38}$$

With a series compensated secondary system, the operating frequency for maximum power transfer is higher than the secondary resonant frequency. This maximum power transfer, however, is only slightly higher than the available power at the secondary resonant frequency. With Q_{s0} of 2, the difference in both frequency and power transfer is about 7%. Such differences become negligible as the secondary quality factor increases (with Q_{s0} of 5, the difference in both frequency and power transfer is only 1%). Consequently, the usual approach is to design the pickup to operate at the secondary resonant frequency rather than the maximum power frequency, which is load dependent and as such difficult for a pickup design to follow.

For a parallel-compensated secondary system, the operating frequency for maximum power transfer is identical to the secondary resonant frequency under all loading conditions. The secondary resonant frequency is therefore a logical choice for the pickup design.

3-8 THE PRIMARY COIL

With the loading effects of the secondary resonant circuit represented by the reflected impedance, the equivalent circuit of the primary coil consists of its self-inductance (L_p) in series with the secondary pickup reflected impedance (Z_r) as shown in Fig. 3-8.

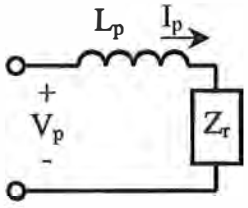


Fig. 3-8. Equivalent circuit of the primary coil.

The impedance of the primary coil calculated from the circuit in Fig. 3-8 is:

$$Z_p = j\omega L_p + Z_r \tag{3-39}$$

The first term in (3-39) is inductive, corresponding to the self-inductance of the primary coil. It is proportional to the operating frequency and independent of the load. The second term in (3-39) is the reflected impedance. As noted in section 3-7.4, it can be either capacitive or inductive as the frequency varies across the frequency spectrum, and is a non-proportional function of the operating frequency and the load.

InductEV, Inc.
Exhibit 1008
Page 090

The impedance of the primary coil is analysed relative to the reactance of its self-inductance at the secondary resonant frequency thereby enabling the influence of Z_r (representing the secondary loading effect) to be easily seen. This ratio is determined to be:

$$\frac{Z_p}{j\omega_0 L_p} = \frac{\omega}{\omega_0}\left(1 - \frac{jk^2\omega L_s}{Z_s}\right) \tag{3-40}$$

Substituting (3-29)&(3-31) into (3-40) results in:

$$\frac{Z_p}{j\omega_0 L_p} = u\left(1 - \frac{k^2 I_s}{I_{sc}}\right) \tag{3-41}$$

This ratio (as derived in Appendix E) is a function of the secondary quality factor (Q_{s0}), the normalized operating frequency (u), as well as the magnetic coupling coefficient (k), and is given for the specified secondary compensation as:

$$\left|\frac{Z_p}{j\omega_0 L_p}\right| = \begin{cases} \dfrac{\sqrt{k^4 Q_{s0}^2 u^8 + u^2\left\{u^2 + Q_{s0}^2\left(u^2-1\right)\left[u^2\left(1-k^2\right)-1\right]\right\}^2}}{u^2 + Q_{s0}^2\left(u^2-1\right)^2} & \text{series secondary} \\ \dfrac{\sqrt{k^4 Q_{s0}^2 u^4 + u^2\left\{u^2\left(1-k^2\right) + Q_{s0}^2\left(u^2-1\right)\left[u^2\left(1-k^2\right)-1\right]\right\}^2}}{u^2 + Q_{s0}^2\left(u^2-1\right)^2} & \text{parallel secondary} \end{cases} \tag{3-42}$$

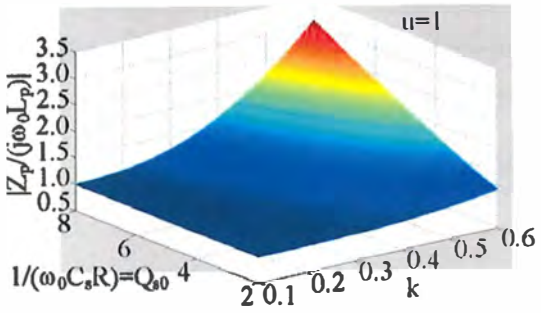
To further clarify the effects of the magnetic coupling strength and the secondary quality factor, the ratio $Z_p/(j\omega_0 L_p)$ at the secondary resonant frequency (u=1) can be derived from (3-42) as:

$$\left|\frac{Z_p(u=1)}{j\omega_0 L_p}\right| = \begin{cases} \sqrt{k^4 Q_{s0}^2 + 1} & \text{series secondary} \\ \sqrt{k^4 Q_{s0}^2 + \left(1-k^2\right)^2} & \text{parallel secondary} \end{cases} \tag{3-43}$$

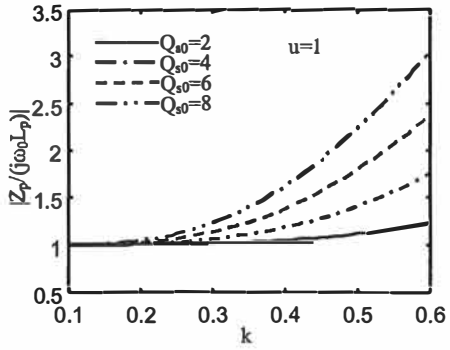
The result is a function of Q_{s0} and k, and is shown in Fig. 3-9. As can be seen, the ratio $Z_p/(j\omega_0 L_p)$ at the secondary resonant frequency is close to unity at low secondary quality factor or magnetic coupling, but increases with increasing secondary quality factor or magnetic coupling due to loading effects of the secondary. As shown, the effects due to the secondary quality factor are nearly linear, while the effects due to the magnetic coupling are close to following a square law. These characteristics can be verified from (3-43).

In order to investigate the effects of frequency variations, the ratio $Z_p/(j\omega_0 L_p)$ is compared in Fig. 3-10 and Fig. 3-11 for series and parallel compensated secondary systems. It is shown as a function of Q_{s0} and u at selected k. The values at selected Q_{s0} of 2, 4, 6 and 8 are also drawn to clarify the features in each case. Once again, series and parallel compensations exhibit similar features.

InductEV, Inc.
Exhibit 1008
Page 091

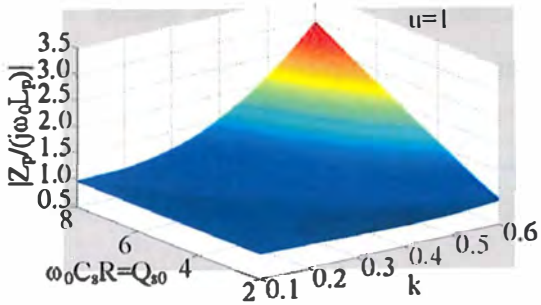


(i) Surface function.

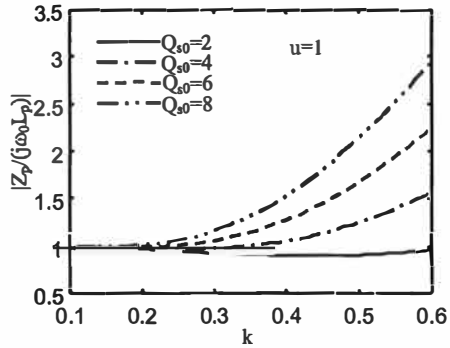


(ii) Cross sections of the surface.

(a) Series compensated secondary.



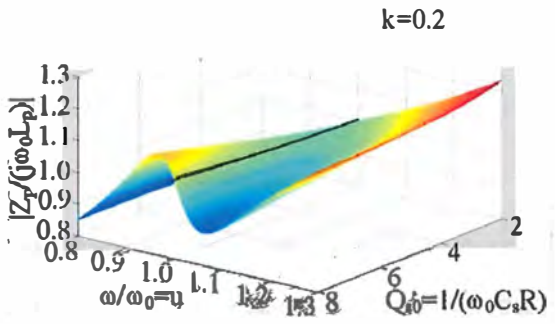
(i) Surface function.



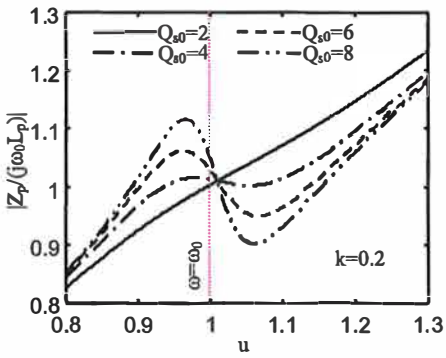
(ii) Cross sections of the surface.

(b) Parallel compensated secondary.

Fig. 3-9. The ratio $Z_p/(j\omega_0 L_p)$ at the secondary resonant frequency ω_0 (u=1).

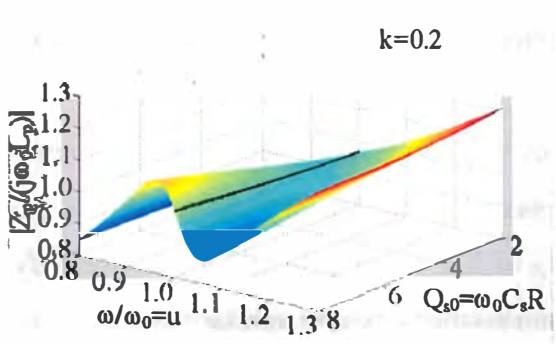


(i) Surface function.

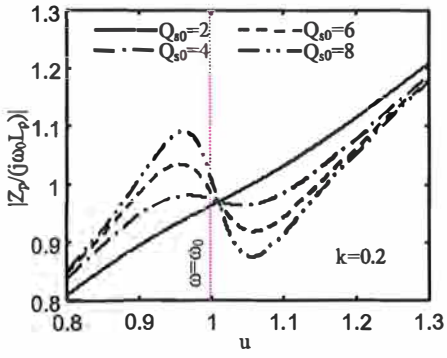


(ii) Cross sections of the surface.

(a) Series compensated secondary.



(i) Surface function.

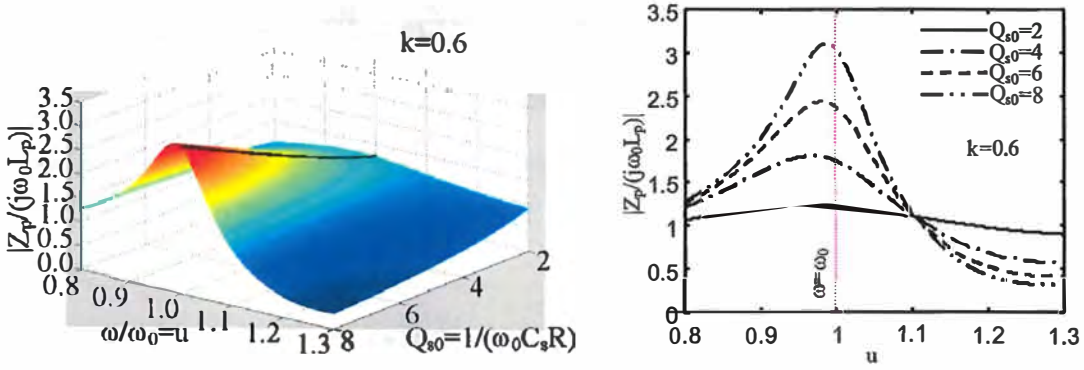


(ii) Cross sections of the surface.

(b) Parallel compensated secondary.

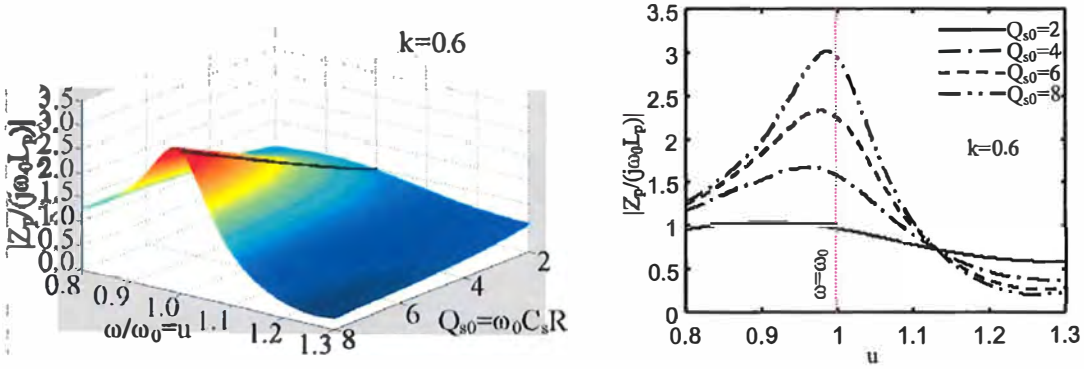
Fig. 3-10. The ratio $Z_p/(j\omega_0 L_p)$ with k=0.2.

InductEV, Inc.
Exhibit 1008
Page 092



(i) Surface function. (ii) Cross sections of the surface.

(a) Series compensated secondary.



(i) Surface function. (ii) Cross sections of the surface.

(b) Parallel compensated secondary.

Fig. 3-11. The ratio $Z_p/(j\omega_0 L_p)$ with k=0.6.

As can be seen, in loosely coupled systems (low k) with low compensation levels (low Q_s) the impedance of the primary coil increases with the frequency. The relationship is closely linear because the loading effects of the secondary on the primary are negligible. With improved magnetic coupling and increased compensation level, the secondary loading effects gradually dominate the impedance of the primary coil.

3-9 THE PRIMARY QUALITY FACTOR

The primary quality factor (Q_p) associated with the primary coil is calculated in this section. The reactive power of the primary coil is:

$$VAR_p = (\omega L_p + \mathrm{Im}\, Z_r) I_p^2 \tag{3-44}$$

The real power transferred by the primary coil was calculated in (3-20). The primary quality factor defined as the ratio of reactive to real power is then:

InductEV, Inc.
Exhibit 1008
Page 093

$$Q_p = \frac{VAR_p}{P} = \frac{(\omega L_p + \mathrm{Im}Z_r)I_p^2}{(\mathrm{Re}Z_r)I_p^2} = \frac{\frac{\omega L_p}{\mathrm{Re}Z_{r0}} + \frac{\mathrm{Im}Z_r}{\mathrm{Re}Z_{r0}}}{\frac{\mathrm{Re}Z_r}{\mathrm{Re}Z_{r0}}} = \frac{\frac{\omega L_p}{\mathrm{Re}Z_{r0}} + \mathrm{Im}Z_{rn}}{\mathrm{Re}Z_{rn}} \tag{3-45}$$

The normalized reactance of the self-inductance (L_p) of the primary coil can be derived from (3-26) and (3-29):

$$\frac{\omega L_p}{\mathrm{Re}Z_{r0}} = \frac{\omega L_p}{\left(\frac{\omega_0 M^2}{L_s}\right)Q_{s0}} = \frac{uL_pL_s}{M^2Q_{s0}} \tag{3-46}$$

The relation of the mutual inductance (M) and the coupling coefficient (k) derived from (2-1) is:

$$M^2 = k^2 L_p L_s \tag{3-47}$$

Substituting (3-47) into (3-46) results in:

$$\frac{\omega L_p}{\mathrm{Re}Z_{r0}} = \frac{u}{k^2 Q_{s0}} \tag{3-48}$$

Substituting (3-48) into (3-45) results in:

$$Q_p = \frac{\frac{u}{k^2 Q_{s0}} + \mathrm{Im}Z_{rn}}{\mathrm{Re}Z_{rn}} \tag{3-49}$$

Substituting (3-34) and (3-35) into (3-49), the primary quality factor is determined to be functions of k, u and Q_{s0} for the specified secondary compensation as:

$$Q_p = \begin{cases} \dfrac{u^2 + Q_{s0}^2(u^2-1)\left[(1-k^2)u^2-1\right]}{k^2u^3Q_{s0}} & \text{series secondary} \\ \dfrac{(1-k^2)u^2 + Q_{s0}^2(u^2-1)\left[(1-k^2)u^2-1\right]}{k^2uQ_{s0}} & \text{parallel secondary} \end{cases} \tag{3-50}$$

The primary quality factor at ω_0 derived from (3-50) is then:

$$Q_{p0} = Q_p(\omega=\omega_0) = Q_p(u=1) = \begin{cases} \dfrac{1}{k^2Q_{s0}} & \text{series secondary} \\ \dfrac{1-k^2}{k^2Q_{s0}} = \dfrac{1}{k^2Q_{s0}} - \dfrac{1}{Q_{s0}} & \text{parallel secondary} \end{cases} \tag{3-51}$$

Normally, ICPT systems are designed to operate close to ω_0. In such systems, the fundamental design parameters k, Q_{p0} and Q_{s0} are related. The primary quality factor reduces when the secondary quality factor increases or the electromagnetic structure improves.

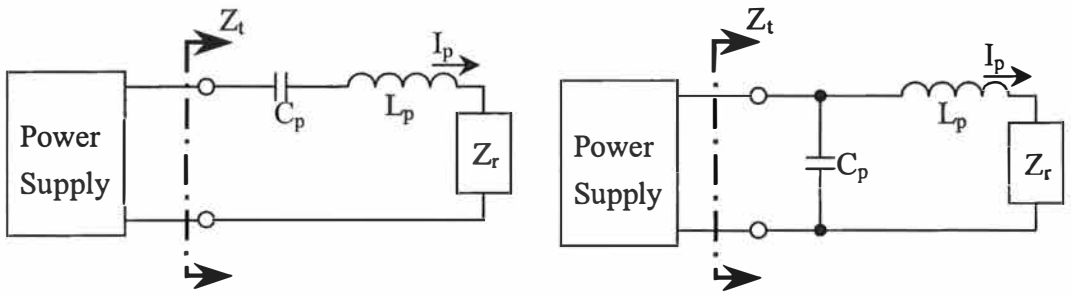
InductEV, Inc.
Exhibit 1008
Page 094

3-10 THE POWER SUPPLY LOAD MODEL

According to above analysis, when the magnetic coupling is weak and the secondary quality factor is low, the loading effect of the secondary on the primary is negligible comparing to the self-inductance of the primary coil. In this case, the primary and secondary resonance can be assumed to be independent and as such significantly simplifies the design process. For such systems, a constant primary current at the secondary resonant frequency can be assumed in the design of the secondary pickup, and the secondary loading effect can be assumed to be a resistance in the design of the primary power supply [2-4]. However, a common trend in the design of ICPT systems is to improve magnetic coupling and increase secondary quality factor in order to transfer more power. The primary and secondary resonances thus become strongly interlinked. For optimal design of these systems, the simplified design approach is not accurate enough. It is necessary to consider all of the interactions between the primary and secondary. This section develops a mathematical model to represent the complete load resonant tank consisting of both the primary and secondary resonant circuits. The resulting power supply load models of commonly used compensation topologies are compared. They are then normalized to simplify the analysis and used as a design tool in following chapters.

3-10.1 MODELLING OF THE POWER SUPPLY LOAD IMPEDANCE

Both series and parallel-compensated primary resonant circuits are shown in Fig. 3-12 with the loading effects of the secondary represented by the reflected impedance (Z_r) in series connection with the primary self-inductance. To simplify the analysis of the load seen by the power supply, the primary resonant circuits can be represented as a lumped impedance (Z_t). As noted in Fig. 3-12, this lumped load impedance seen by the power supply depends on the primary compensation topologies. With a series compensated primary, it consists of the primary capacitance in series connection to the primary coil (formed by the self-inductance and the reflected impedance). For a parallel-compensated primary, it is formed by the primary capacitance in parallel connection with the primary coil.



(a) Series compensated primary. (b) Parallel compensated primary.

Fig. 3-12. Primary resonant circuits with reflected impedance.

InductEV, Inc.
Exhibit 1008
Page 095

The power supply load impedance (Z_t) is derived for the specified primary compensation as:

$$Z_t = \begin{cases} \dfrac{1}{j\omega C_p} + Z_p = \dfrac{1}{j\omega C_p} + j\omega L_p + Z_r & \text{series primary} \\ \dfrac{1}{j\omega C_p + \dfrac{1}{Z_p}} = \dfrac{1}{j\omega C_p + \dfrac{1}{j\omega L_p + Z_r}} & \text{parallel primary} \end{cases} \tag{3-52}$$

The real part of the load impedance (Re Z_t) is the load resistance and represents real power transfer. The imaginary part (Im Z_t) is the load reactance and dictates reactive power flow.

As noted above, the load impedance seen by the supply is a function of the reflected impedance (Z_r), which in turn depends on the secondary compensation topology. In consequence, the load impedance seen by the power supply depends on not only the primary but also the secondary compensation topology. Since both the primary and secondary can be either series or parallel compensated, there are four basic topologies labelled as SS, SP, PP and PS (as noted in section 2-3.5). A summary of the load impedance is given in Table 3-2 for each topology.

TABLE 3-2
LOAD IMPEDANCE OF THE BASIC TOPOLOGIES

Topology	Load impedance
SS	$Z_t = \dfrac{1}{j\omega C_p} + j\omega L_p + \dfrac{\omega^2 M^2}{j\omega L_s + \dfrac{1}{j\omega C_s} + R}$
SP	$Z_t = \dfrac{1}{j\omega C_p} + j\omega L_p + \dfrac{\omega^2 M^2}{j\omega L_s + \dfrac{1}{j\omega C_s + \dfrac{1}{R}}}$
PP	$Z_t = \dfrac{1}{j\omega C_p + \dfrac{1}{j\omega L_p + \dfrac{\omega^2 M^2}{j\omega L_s + \dfrac{1}{j\omega C_s + \dfrac{1}{R}}}}}$
PS	$Z_t = \dfrac{1}{j\omega C_p + \dfrac{1}{j\omega L_p + \dfrac{\omega^2 M^2}{j\omega L_s + \dfrac{1}{j\omega C_s} + R}}}$

InductEV, Inc.
Exhibit 1008
Page 096

3-10.2 THE NORMALIZED LOAD IMPEDANCE

Similar to the normalization process of the reflected impedance (Z_r) in section 3-7.4, the load impedance (Z_t) is normalized in this section with respect to the reflected resistance at the secondary resonant frequency ($\mathrm{Re}\, Z_{r0}$) using (3-30), while the operating frequency (ω) is normalized with respect to the secondary resonant frequency (ω_0) using (3-29). The normalised load impedance is calculated as:

$$Z_{tn} = \frac{Z_t}{\mathrm{Re}\, Z_{r0}} = \frac{\mathrm{Re}\, Z_t}{\mathrm{Re}\, Z_{r0}} + j\frac{\mathrm{Im}\, Z_t}{\mathrm{Re}\, Z_{r0}} = \mathrm{Re}\, Z_{tn} + j\,\mathrm{Im} Z_{tn} \tag{3-53}$$

This definition is suitable for series compensated primary systems, however it is often much easier to describe the load impedance in terms of its admittance value (conductance and susceptance) when dealing with parallel compensated primary systems, so that:

$$Z_{tn} = \frac{1}{Y_t(\mathrm{Re}\, Z_{r0})} = \frac{1}{(\mathrm{Re}\, Y_t)(\mathrm{Re}\, Z_{r0}) + j(\mathrm{Im}\, Y_t)(\mathrm{Re}\, Z_{r0})} = \frac{1}{\mathrm{Re}\, Y_{tn} + j\,\mathrm{Im} Y_{tn}} = \frac{1}{Y_{tn}} \tag{3-54}$$

Substituting (3-52) into (3-53), the normalized load resistance and reactance for series compensated primary systems are given by:

$$\mathrm{Re}\, Z_{tn} = \mathrm{Re}\, Z_{rn} \tag{3-55}$$

and

$$\mathrm{Im} Z_{tn} = -\frac{1}{\omega C_p(\mathrm{Re}\, Z_{r0})} + \frac{\omega L_p}{\mathrm{Re}\, Z_{r0}} + \mathrm{Im} Z_{rn} \tag{3-56}$$

Substituting (3-52) into (3-54), the normalized load conductance and susceptance for parallel compensated primary systems are derived as:

$$\mathrm{Re}\, Y_{tn} = \frac{\mathrm{Re}\, Z_{rn}}{(\mathrm{Re}\, Z_{rn})^2 + \left(\frac{\omega L_p}{\mathrm{Re}\, Z_{r0}} + \mathrm{Im} Z_{rn}\right)^2} \tag{3-57}$$

and

$$\mathrm{Im}\, Y_{tn} = \omega C_p(\mathrm{Re}\, Z_{r0}) - \frac{\frac{\omega L_p}{\mathrm{Re}\, Z_{r0}} + \mathrm{Im} Z_{rn}}{(\mathrm{Re}\, Z_{rn})^2 + \left(\frac{\omega L_p}{\mathrm{Re}\, Z_{r0}} + \mathrm{Im} Z_{rn}\right)^2} \tag{3-58}$$

As shown above, for a series compensated primary the load resistance is identical to the reflected resistance. The load reactance, however, depends on the primary capacitance and inductance, and also the reflected reactance. For a parallel-compensated primary the load conductance depends on the primary inductance, and also the reflected resistance and reactance, while the load susceptance depends on the primary capacitance and inductance as well as the reflected resistance and reactance.

InductEV, Inc.
Exhibit 1008
Page 097

Equations (3-55) to (3-58) can be simplified if they are written in terms of the normalized operating frequency ($u=\omega/\omega_0$), and the quality factors (Q_{p0} and Q_{s0}) associated to the primary and secondary resonant circuits at ω_0. These equations consist of the normalized reactance of the self-inductance of the primary coil, the normalized reactance of the primary compensation capacitance, and the normalized reflected resistance and reactance as summarized in Table 3-3. This simplification process of the normalized load impedance is discussed following.

TABLE 3-3
FUNCTIONS OF THE NORMALIZED LOAD IMPEDANCE WITH COMPENSATED PICKUP

$\dfrac{1}{\omega C_p(\mathrm{Re}Z_{r0})}$	$\begin{cases} \dfrac{Q_{p0}}{u}=\dfrac{1}{uk^2Q_{s0}} \\ \left(\dfrac{1}{u}\right)\left(Q_{p0}+\dfrac{1}{Q_{s0}}\right)=\dfrac{1}{uk^2Q_{s0}} \end{cases}$	Series secondary. Parallel secondary.
$\dfrac{\omega L_p}{\mathrm{Re}Z_{r0}}$	$\begin{cases} uQ_{p0}=\dfrac{u}{k^2Q_{s0}} \\ u\left(Q_{p0}+\dfrac{1}{Q_{s0}}\right)=\dfrac{u}{k^2Q_{s0}} \end{cases}$	Series secondary. Parallel secondary.
$\mathrm{Re}Z_{rn}=\dfrac{\mathrm{Re}Z_r}{\mathrm{Re}Z_{r0}}$	$\begin{cases} \dfrac{u^4}{(u^2-1)^2Q_{s0}^2+u^2} \\ \dfrac{u^2}{(u^2-1)^2Q_{s0}^2+u^2} \end{cases}$	Series secondary. Parallel secondary.
$\mathrm{Im}Z_{rn}=\dfrac{\mathrm{Im}Z_r}{\mathrm{Re}Z_{r0}}$	$\begin{cases} \dfrac{-u^3(u^2-1)Q_{s0}}{(u^2-1)^2Q_{s0}^2+u^2} \\ \dfrac{-u^3[(u^2-1)Q_{s0}+1/Q_{s0}]}{(u^2-1)^2Q_{s0}^2+u^2} \end{cases}$	Series secondary. Parallel secondary.

The normalized reflected resistance and reactance depend on the secondary compensation topology (either series or parallel) and are derived in section 3-7.4 with the results given in (3-34) and (3-35). They are functions of u and Q_{s0} only.

The normalized reactance of the self-inductance of the primary coil given in (3-48) can be rearranged using (3-51) as a function of u, Q_{p0} and Q_{s0} given by:

$$\frac{\omega L_p}{\mathrm{Re}Z_{r0}}=\begin{cases} uQ_{p0} & \text{series secondary} \\ u\left(Q_{p0}+\dfrac{1}{Q_{s0}}\right) & \text{parallel secondary} \end{cases} \tag{3-59}$$

The primary compensation capacitance is normally selected using (2-28). With this conventional choice, the normalized reactance of the primary compensation capacitance as derived in Appendix F is

InductEV, Inc.
Exhibit 1008
Page 098

also a function of u, Q_{p0} and Q_{s0} given by:

$$\frac{1}{\omega C_p(\mathrm{Re}Z_{r0})} = \begin{cases} \dfrac{Q_{p0}}{u} & \text{series secondary} \\ \left(\dfrac{1}{u}\right)\left(Q_{p0} + \dfrac{1}{Q_{s0}}\right) & \text{parallel secondary} \end{cases} \quad (3\text{-}60)$$

As noted in section 3-9, the primary quality factor depends on the magnetic coupling coefficient and the secondary quality factor. Consequently, these functions can be expressed alternatively in terms of the normalized frequency (u), the magnetic coupling coefficient (k), and the secondary quality factor (Q_{s0}) as given also in Table 3-3. This enables the identification of the influence of the magnetic coupling structure and the pickup compensation level on the load seen by the power supply.

3-11 VERIFICATION OF THE LOAD MODEL

In order to validate the theoretical load model, a contact-less electric vehicle battery charging system was designed using the design methodology proposed in the following chapter. This system delivers 30kW across a 45mm air gap at a nominal frequency of 20 kHz with a primary current I_p of 150A. The loading system (load resonant tank) on the power supply consists of the electromagnetic structure, the primary and secondary compensation capacitances, and the pickup load that is formed by a rectifier, a filter and a dc regulator. In this test system, the pickup load is replaced by a linear resistor to simplify the verification process. With the power supply disconnected, the load impedance seen by the power supply was measured at the input to the load resonant tank. This measured impedance was then compared with the theoretical calculation using the load model developed in section 3-10.1.

The electromagnetic structure of this system is given in Fig. 3-13. Here the primary and secondary windings are identical, each having concentrated coils with distributed ferrites. It is assumed that the secondary winding is attached to the underside of an electric vehicle, while the primary winding is buried in the ground. Once an electric vehicle has stopped over the charging station, electric power is transferred to the vehicle across an air gap via magnetic coupling between the primary coil in the ground and secondary coil on the vehicle.

For compensation, a PP topology was chosen since it is commonly used for high power industrial applications [2]. The current source characteristic of the parallel-compensated secondary is well suited for battery charging, whereas the parallel-compensated primary is used to generate a large primary current.

The measured coupling and compensation parameters, along with other key system parameters used for the above design, are given in Table 3-4. A variable-frequency Fluke PM 6306 RLC meter was used to measure the coupling parameters of the electromagnetic structure. The primary self-inductance

InductEV, Inc.
Exhibit 1008
Page 099

(L_p) was measured with the secondary left open circuit, while the secondary self-inductance (L_s) was measured with the primary left open circuit. The mutual inductance (M) was determined by measuring the change of the primary inductance (ΔL_p) with a short-circuited secondary. This change occurs due to the reflected impedance from the secondary, and the relationship is given by:

$$Z_r = j\omega(\Delta L_p) \tag{3-61}$$

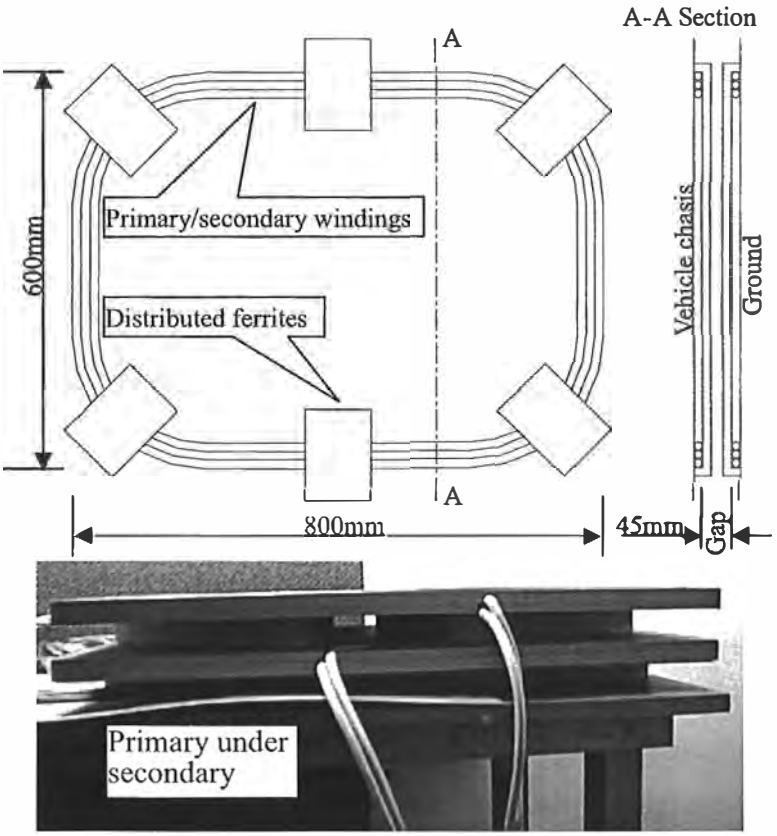


Fig. 3-13. Electromagnetic structure of the contact-less battery charger.

TABLE 3-4
PARAMETERS OF THE CONTACT-LESS ELECTRIC VEHICLE BATTERY CHARGER

Nominal resonant frequency (f)	20kHz
Rated power (P)	30kW
Primary rated current (I_p)	150A
Rated load (R)	6Ω
Primary inductance (L_p)	29.6μH
Primary capacitance (C_p)	2.21μF
Mutual inductance (M)	12.7μH
Secondary inductance (L_s)	26.9μH
Magnetic coupling coefficient (k)	0.45
Secondary capacitance (C_s)	2.42μF

With the secondary placed under short circuit (R=0, uncompensated secondary), the secondary impedance derived from (3-7) is:

InductEV, Inc.
Exhibit 1008
Page 100

$$Z_s = j\omega L_s \tag{3-62}$$

Substituting (3-62) into (3-17), the reflected impedance calculated using the mutual inductance (M) is:

$$Z_r = -j\frac{\omega M^2}{L_s} \tag{3-63}$$

From (3-61) and (3-63), the mutual inductance is determined as:

$$M = \sqrt{-(\Delta L_p)L_s} \tag{3-64}$$

Substituting (3-64) into (2-1), the magnetic coupling coefficient is determined as:

$$k = \sqrt{-\frac{\Delta L_p}{L_p}} \tag{3-65}$$

As shown, the magnetic coupling strength of an electromagnetic coupling structure can be determined by simply measuring the rate of change in the primary inductance when the secondary is placed in a short circuit.

The measured coupling parameters (L_p, M, L_s) of the electromagnetic structure are shown in Fig. 3-14 for selected frequency range from 15kHz to 25kHz around the nominal frequency of 20kHz. As shown, variations with frequency are negligible.

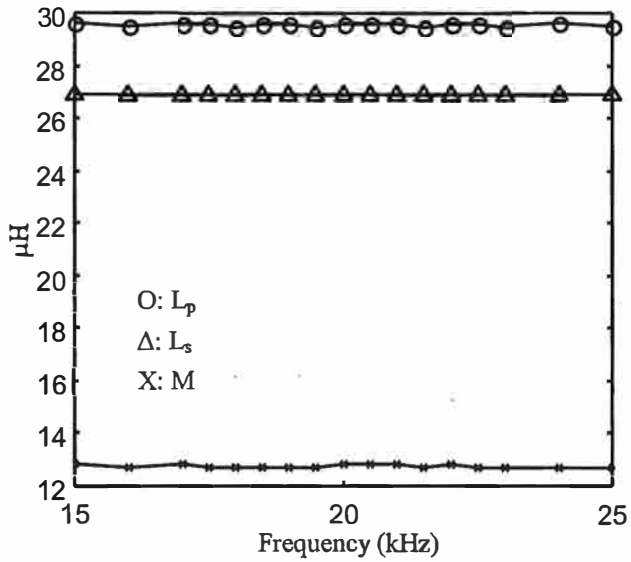


Fig. 3-14. The measured coupling parameters (L_p, L_s, M) of the battery charger.

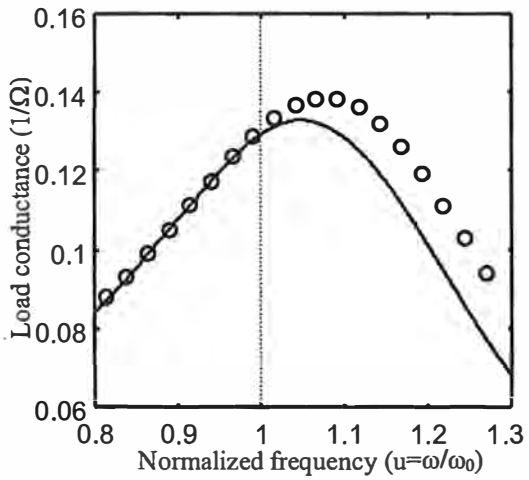
Both the primary and secondary compensation capacitances in Table 3-4 are designed for the nominal frequency using (2-22) and (2-28). With the selected secondary compensation capacitance (C_s=2.42 μF), the secondary resonant frequency (f_0) calculated by (2-22) is 19.7 kHz, which is slightly lower than the nominal resonant frequency (20 kHz). The primary compensation capacitance (C_p) calculated by (2-28) is 2.20 μF. The measured value of C_p as shown in Table 3-4 is 2.21 μF, which is

InductEV, Inc.
Exhibit 1008
Page 101

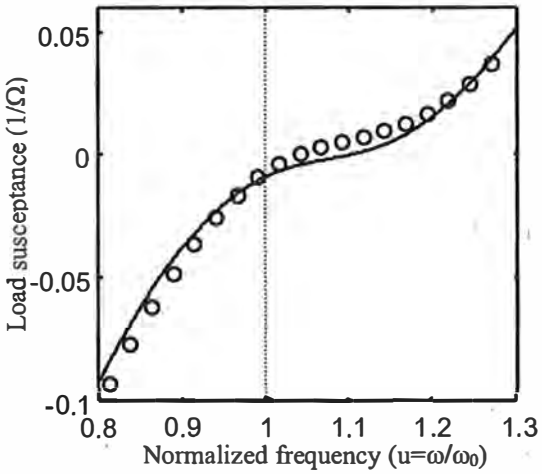
slightly higher than the theoretical value. In order to compare the experimental measurements with the analytical load model, the measured values of both the primary and secondary capacitances are used in the theoretical calculations.

The variable-frequency Fluke PM 6306 RLC meter was also used to measure the power supply load impedance (Z_t). The coupling parameters (L_p, M, L_s) of the electromagnetic structure and the primary and secondary compensation capacitances (C_p, C_s) were kept unchanged at the values given in Table 3-4. Firstly, Z_t was measured at rated load (6Ω) and various frequencies around f_0. Secondly, Z_t was measured by fixing the frequency at the secondary resonant frequency (f_0=19.7 kHz), while varying the load about its rated value.

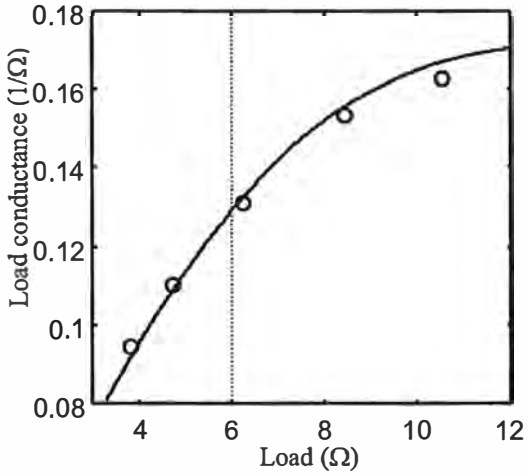
The measured load impedance was recalculated in terms of a load admittance (Y_t=1/Z_t), and compared with the theoretical values as shown in Fig. 3-15. Here, the measured values are shown as circles, whereas solid lines are used to indicate the theoretical values.



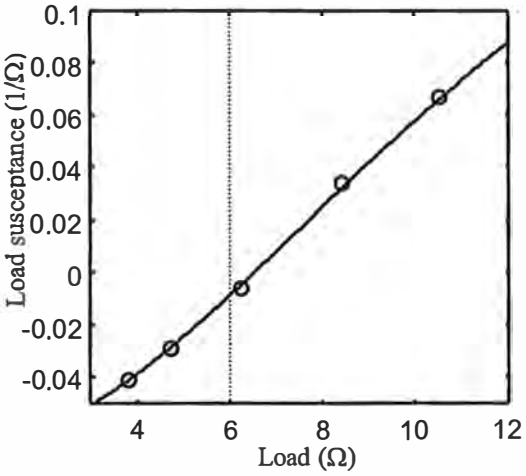
(a) Load conductance (Re Y_t) with R=6Ω.



(b) Load susceptance (Im Y_t) with R=6Ω.



(c) Load conductance (Re Y_t) with u=ω/ω0=1.



(d) Load susceptance (Im Y_t) with u=ω/ω0=1.

Fig. 3-15. Measured and calculated load admittance (Y_t) of the battery charger.

InductEV, Inc.
Exhibit 1008
Page 102

As previously discussed, Fig. 3-15 (a) and (b) show comparisons with the load (R) fixed at its rated value of 6Ω while varying the frequency about f_0, whereas Fig. 3-15 (c) and (d) show comparisons at f_0 while varying R about its rated value. As can be seen, the measured values follow the theoretical predictions closely despite simplifications in the model that assumes sinusoidal voltages and currents, and ignores losses in the inductors and capacitors. The differences are most notable in Fig. 3-15 (a) but are still within 10% across the selected range of frequencies, and mainly arise because the rated load used in the test system is slightly larger than 6Ω and has a stray inductance of about 2.4μH. The influence of the stray inductance increases with increasing frequency.

3-12 CONCLUSIONS

A general load impedance model as seen by the power supply is developed in this chapter to investigate steady state operation of an ICPT system. The developed load model was verified by comparing measured and calculated values in a practical contact-less electric vehicle battery charging system. The measured values follow theoretical calculations within practical limitations. The models therefore can be used confidently in the analyses and designs of ICPT systems.

A major assumption in developing the load model is that the pickup load is linear and resistive. In practice, the pickup load is often a non-linear system, and an equivalent linear resistive load needs to be developed when applying the load model. The electromagnetic structure and the primary and secondary compensation capacitors (C_p and C_s) are assumed to be loss-less. The electromagnetic structure is modelled using the transformer mutual inductance coupling model. The coupling parameters include the primary self-inductance L_p, the mutual inductance M between the primary and secondary, and the secondary self-inductance L_s. The reactive elements (C_p, L_p, M, L_s and C_s) are modelled as impedances that are assumed to be linear functions of the frequency.

The load model is then used to investigate the system behaviour of each topology. The resonant frequency of the pickup (the frequency when L_s is in resonance with C_s) is a key parameter called the secondary resonant frequency (ω_0). To generally quantify system characteristics, the developed impedance models can be expressed in terms of the normalized frequency ($u=\omega/\omega_0$), the quality factors (Q_{p0} and Q_{s0}) associated with the primary and secondary resonant circuits at ω_0, and the magnetic coefficient (k) of the electromagnetic structure. These dimensionless parameters (u, k, Q_{p0} and Q_{s0}) have major influences on system performance, and need to be chosen carefully when designing and optimising the systems.

The frequency for maximum power transfer capability is found to be exactly at ω_0 when the pickup is parallel compensated. However, if the pickup uses series compensation, this frequency is

InductEV, Inc.
Exhibit 1008
Page 103

unexpectedly higher (although the variation from ω_0 becomes negligible as Q_s gets large). The secondary quality factor can be increased to improve the power transfer, however, it also increases its sensitivity to frequency variations. In such systems, the power transfer capability of the pickup drops substantially as the frequency shifts away from the secondary resonant frequency. This pickup frequency detuning has to be minimized in a practical system. The loading effects of the secondary pickup on the primary are also found to increase with increases in Q_s and k, and consequently need to be carefully considered in the design of ICPT systems.

REFERENCES

[1]. N. Mohan, T. M. Undeland, W. P. Robbins, *Power electronics: converters, applications, and design.* New York: John Wiley & Sons, second edition, 1995.

[2]. O. H. Stielau, G. A. Covic, "Design of loosely coupled inductive power transfer systems," in *Proc. 2000 Int. Conf. Power System Technology*, vol. 1, Dec. 2000, pp. 85-90.

[3]. J. T. Boys, G. A. Covic, A. W. Green, "Stability and control of inductively coupled power transfer systems," *Proc. IEE -Elect. Power Applicat.*, vol. 147, no. 1, pp. 37-43, Jan. 2000.

[4]. A. P. Hu, *Selected resonant converters for IPT power supplies*. PhD thesis. The Electrical and Electronics Engineering Department, The University of Auckland, New Zealand, 2001.

InductEV, Inc.
Exhibit 1008
Page 104

CHAPTER 4

EVALUATION OF A DESIGN METHODOLOGY FOR ICPT SYSTEMS

4-1 Introduction
4-2 A design procedure
4-3 Design options for the pickup regulator
4-4 Design options for the power supply
4-5 Design evaluations
4-6 A practical design example
4-7 Conclusions

4-1 INTRODUCTION

Many design examples of ICPT systems have been described in the literature [1-12], but each is dependent on its particular application. Currently, the optimisation and design of an ICPT system relies strongly on experience and experimental verification. This requires suitable design choices for the operating frequency, the primary current, the electromagnetic structure, the primary and secondary compensation, the pickup regulator, and the high frequency switching power supply. This chapter briefly reviews design options used in these areas in terms of their advantages and disadvantages. Since the design choices are inter-related, a design procedure is described with the aim of achieving a controllable power transfer capability over a specified operating range with minimum total cost. As an integrated tool with the design procedure, the normalized load model (developed in chapter 3) is used to evaluate the system behaviour under fixed and variable frequency control in order to determine its sensitivity to the fundamental design parameters u (the normalized frequency), k (the magnetic coupling coefficient) and Q_s (the secondary quality factor).

4-2 A DESIGN PROCEDURE

The power transfer capability of a compensated pickup in an ICPT system (developed in section 2-3.2) was determined as:

$$P = V_{oc} I_{sc} Q_{s0} = \omega_0 I_p^2 \left(k^2 L_p\right) Q_{s0} = \omega_0 I_p^2 \left(\frac{M^2}{L_s}\right) Q_{s0} \tag{4-1}$$

with the required secondary VA rating given by:

InductEV, Inc.
Exhibit 1008
Page 105

$$VA_{s0} = V_{oc} I_{sc} Q_{s0} \sqrt{1+Q_{s0}^2} = P\sqrt{1+Q_{s0}^2} \tag{4-2}$$

As shown to achieve the desired power there are four major design factors: the operating frequency (ω_0), the primary current (I_p), the magnetic design factor ($k^2L_p=M^2/L_s$) and the secondary quality factor (Q_{s0}). The operating frequency and the primary current are restricted by the primary power supply as well as the primary track/coil. The magnetic design factor is restricted by the application layout as well as the geometry and material of the electromagnetic structure. The pickup VA rating as well as stability considerations of the controller restrict the secondary quality factor. Since these design factors are interrelated, an iterative design procedure is introduced in this section to optimise the cost distribution of the total system.

It is assumed in this design procedure that if compensated both the primary and secondary resonance are designed by:

$$\omega_0 = \frac{1}{\sqrt{C_p L_p}} = \frac{1}{\sqrt{C_s L_s}} \tag{4-3}$$

The secondary quality factor at ω_0 (developed in section 3-5) is given by:

$$Q_{s0} = Q_s(\omega=\omega_0) = \begin{cases} \dfrac{1}{\omega_0 C_s R} = \dfrac{\omega_0 L_s}{R} & \text{series secondary} \\ \omega_0 C_s R = \dfrac{R}{\omega_0 L_s} & \text{parallel secondary} \end{cases} \tag{4-4}$$

System stability under variable-frequency control is considered in the design procedure in terms of the magnetic coupling coefficient (k) and the quality factors (Q_{p0} and Q_{s0}) associated with the primary and secondary resonant circuits at ω_0. These three parameters (as noted in section 3-9) are related by:

$$Q_{p0} = \begin{cases} \dfrac{1}{k^2 Q_{s0}} & \text{series secondary} \\ \dfrac{1-k^2}{k^2 Q_{s0}} = \dfrac{1}{k^2 Q_{s0}} - \dfrac{1}{Q_{s0}} & \text{parallel secondary} \end{cases} \tag{4-5}$$

An ICPT system is essentially a transformer with the additional flexibility of relative movement between the primary and secondary. The design procedure of an ICPT system therefore is more complex than an ordinary transformer. This section describes a design procedure to deal with the additional complexities.

4-2.1 DESIGN OF ORDINARY TRANSFORMERS

The design of the ordinary transformer is a well-known procedure. A simplified design methodology for ordinary transformers is shown in Fig. 4-1. The main consideration is a suitable

InductEV, Inc.
Exhibit 1008
Page 106

choice of the geometries and sizes of the magnetic cores. Normally an iterative process is followed that results in the optimum core size. For a given core geometry, the winding parameters are calculated. If the primary and secondary windings do not fit into the chosen common magnetic core, a larger core is necessary. If the window area is not fully utilised, a smaller core should be used.

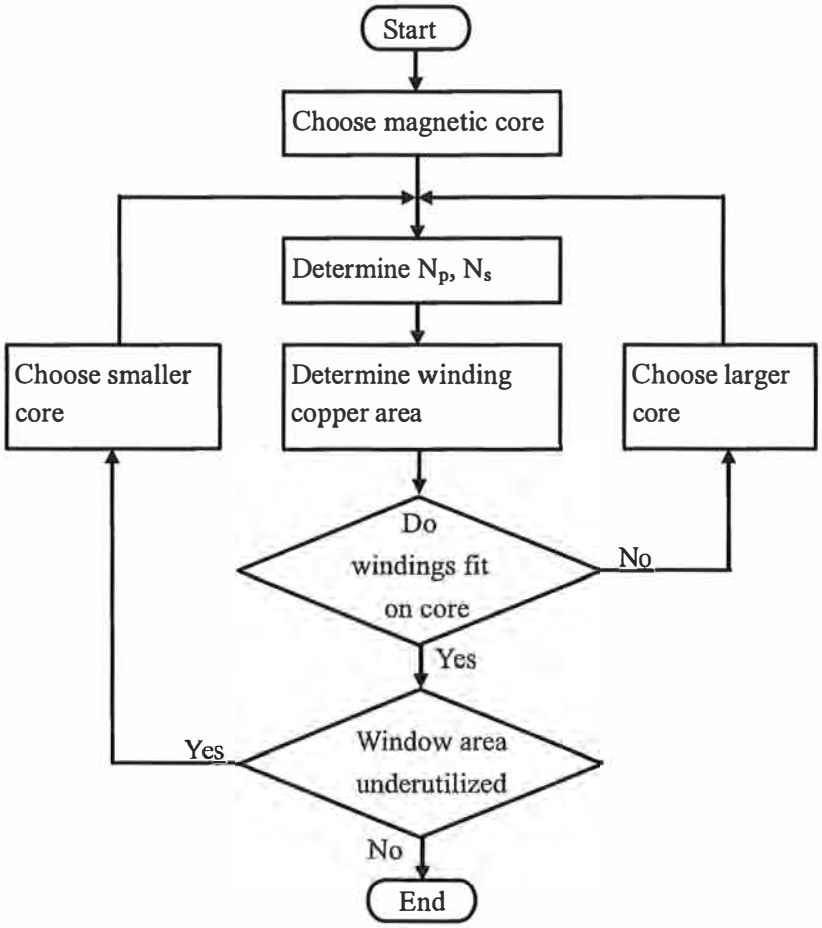


Fig. 4-1. A design procedure of the ordinary transformer.

4-2.2 DESIGN OF ICPT SYSTEMS

To deal with the additional complexities of ICPT systems, a design methodology has been proposed in [12]. This design methodology is extended here to include primary compensation considerations as well as control options (either fixed or variable frequency control). System behaviour under fixed and variable frequency control is quantified in terms of u, k, Q_{p0} and Q_{s0} using the normalized load model seen by the power supply (as developed in chapter 3). This design procedure is shown in Fig. 4-2, and is discussed step by step below. Many choices need to be made throughout the design process, influenced mainly by the cost distribution of the various components in the system.

InductEV, Inc.
Exhibit 1008
Page 107

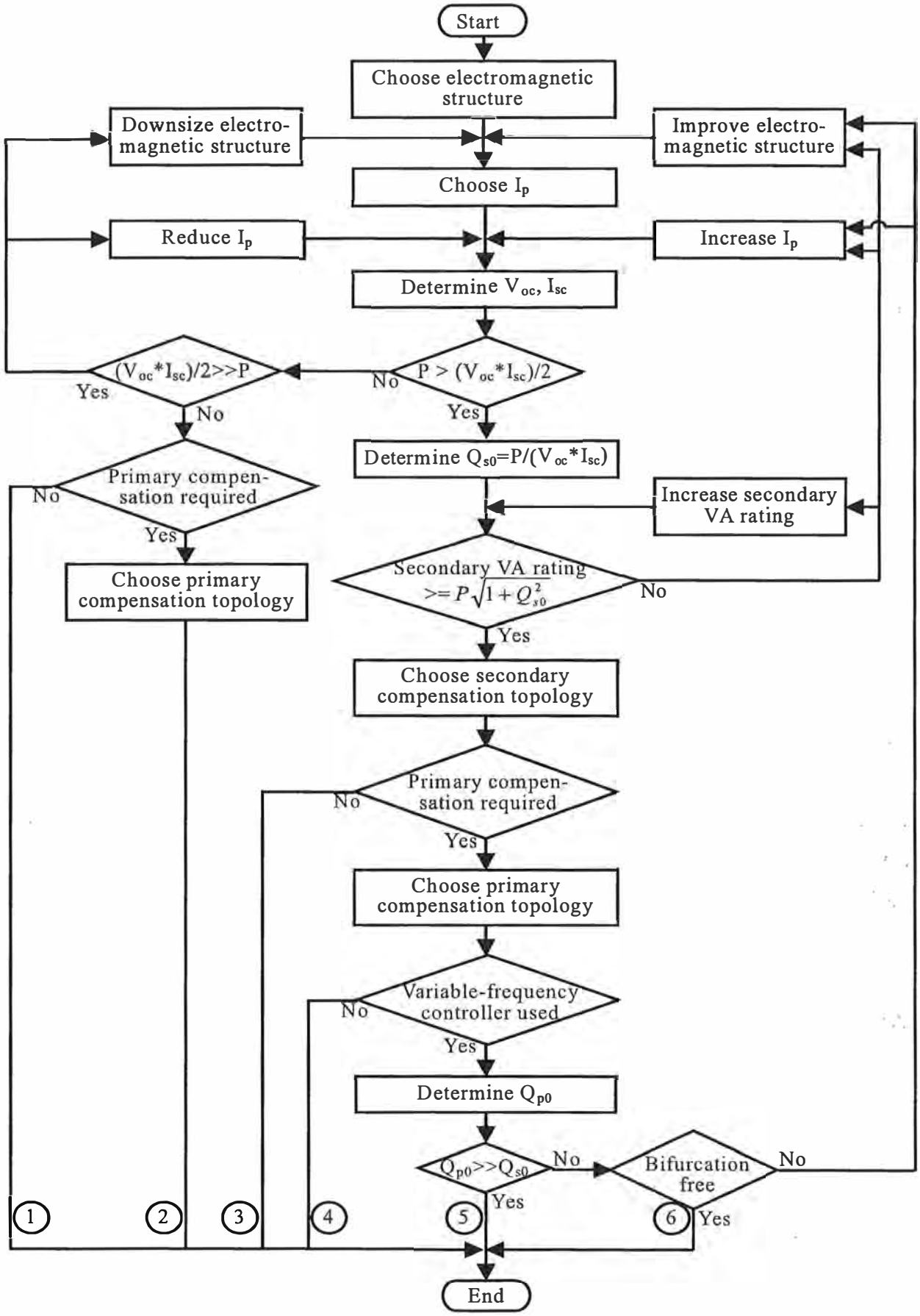


Fig. 4-2. A design procedure of ICPT systems.

InductEV, Inc.
Exhibit 1008
Page 108

Due to the complexity involved in the design procedure, it is necessary to make some assumptions. A summary of the assumptions is given in Table 4-1 and is discussed following. One important assumption is that the desired operating frequency (nominal frequency) ω_0 is known. The power transfer capability of any ICPT system is a strong function of ω_0. In theory increasing ω_0 reduces the size, weight and cost of the total system for the same power transfer capability. However, the choice of ω_0 is limited by practical restrictions in the system components that include the choice of the power switch and the electromagnetic structure.

TABLE 4-1
ASSUMPTIONS OF THE DESIGN PROCEDURE IN FIG. 4-2

1.	Known operating frequency (nominal frequency): ω_0.
2.	Primary and secondary resonant design: $\omega_0 = \frac{1}{\sqrt{C_p L_p}} = \frac{1}{\sqrt{C_s L_s}}$.
3.	Linear and resistive pickup load.
4.	Constant primary current.
5.	Known power supply VA rating.

The capability of commercially available power switches plays a crucial role in the determination of ω_0. Two major considerations are the switching speed and power handling capability. Suitable power switches for ICPT applications are MOSFETs and IGBTs. The switching speeds of MOSFETs are much faster than IGBTs, while the power handling capabilities of IGBTs are much higher than MOSFETs. In consequence, MOSFETs are usually used for low power applications with an operating frequency of up to tens of MHz, while IGBTs are normally selected for high power applications with an operating frequency of up to tens of kHz.

As shown in section 2-2.4, the power transfer capability of an electromagnetic structure increases linearly with frequency. Practically, the core and copper losses also increase with frequency due to hysteresis as well as skin and proximity effects. As a result, the power does not increase linearly with frequency. Increasing core and copper losses result in increasing temperatures, which may exceed the thermal limits of the materials used. The maximum operating frequency of an ICPT system is therefore also limited by the thermal capability of the electromagnetic components, which can be improved by using better materials or additional heat dissipation devices.

The choice of ω_0 thus involves a trade-off between the complexity of the power supply and the power transfer capability of the electromagnetic structure. The power transfer capability of an

InductEV, Inc.
Exhibit 1008
Page 109

electromagnetic structure increases with frequency. However, the complexity of the power supply also increases with increasing frequency. An iterative process is necessary to determine the most cost effective operating frequency.

In compensated systems, it is assumed that the primary and secondary compensation capacitances are calculated by (4-3). The primary compensation minimizes the power supply VA rating, while the secondary compensation boosts the power transfer capability to the pickup. In applications where frequency is adjusted to regulate power flow, operation above or below ω_0 (the secondary resonant frequency) may be preferred in order to improve the controllability [1] because in such applications the relationship between frequency and power has been found to be approximately linear over the operating frequency range. For most applications, however, operation at or near ω_0 is a logical choice because maximum power transfer capability can be achieved at this point.

The primary and secondary compensation capacitors need to work with significant amount of apparent power. A major consideration when choosing these capacitors is their high frequency power handling capability as well as temperature and lifetime stability. The capacitance stability is particularly necessary in high Q systems where the resonant circuit and power transfer capability are highly sensitive to small variations. Such design considerations are discussed later in chapter 7, whereas here it is assumed that accurate tuning can be achieved for normal Q_s from 1 to 10.

In this design procedure, the secondary load is assumed to be linear which simplifies the determination of the power transfer capability and the secondary VA rating. Practical design options for the pickup regulator are discussed in section 4-3.

On the primary side, it is assumed that the primary current is controlled constant at the rated value to fully utilize the electromagnetic structure. The electromagnetic structure of an ICPT system is again dependent on the practical applications for which the ICPT system is being designed as discussed in section 2-2. The design considerations are thus very different to a traditional high frequency transformer. Those aspects that are similar include the material of the electromagnetic structure and its ratings, which are dominated by the core and copper losses. The voltage rating is normally determined by core losses, while the current rating is usually determined by copper losses. Where they differ is that both the primary and secondary windings of a conventional transformer surround a common magnetic core. To utilize the magnetic core fully, the primary is usually operated at rated voltage corresponding to rated flux density while the current is allowed to change with the load. However, the primary and secondary magnetic cores in an ICPT system are separate allowing the pickup to move relative to the primary. As such a major portion of the magnetomotive force will be situated across a substantial air gap. Consequently, it is advantageous to fully utilize the primary by operating at rated current, while allowing the voltage to change with the load.

InductEV, Inc.
Exhibit 1008
Page 110

Finally the power supply configuration is assumed to have been chosen with a specified VA rating. Design options for the power supply are discussed in section 4-4.

The design process starts with a choice of the electromagnetic structure, which is application-oriented. The structure for an ordinary transformer is limited to available magnetic cores, but the possibilities for ICPT systems are virtually unlimited. Systems of all shapes and sizes have been built, and a good first choice relies strongly on experience. As noted in section 2-2.2, typical configurations of the primary coil (Fig. 2-1) are: (a) an extended primary coil with the cable and its return configured in parallel; (b) an extended primary coil with the cable and its return configured in parallel and partially twisted; (c) an extended primary coil with the cable and its return configured as a loop; (d) a lumped primary coil. Typical configurations of the secondary core (Fig. 2-2) are: (a) an E-core; (b) a T-core; (c) a Flat-core. A major design consideration of the electromagnetic structure is to maximize the magnetic design factor k^2L_p ($=M^2/L_s$) for power transfer capability. This is normally done using magnetic design methods often by modelling the system taking into account practical constraints as well as the cost and weight. Simulation techniques such as finite element analysis can be used.

Under normal operating conditions, the coupling parameters (L_p, L_s and M) can be assumed to be constant for ordinary transformers due to fixed relative position between the primary and secondary. In ICPT systems, however, the relative position between the primary and secondary can vary resulting in variations in the coupling parameters. The power transfer capability in an ICPT system is a strong function of these coupling parameters. In practice, the misalignment in the electromagnetic structure is constrained mechanically or controlled electrically to a reasonable range such that system operations in the worst case are acceptable. Influences of this misalignment can be determined using the load model developed in chapter 3 and are investigated later in chapter 7. Here, it is assumed that the electromagnetic structure is properly aligned.

The next step is to choose a primary current. Since the cost of the primary is a strong function of this current, the first choice should be to choose a low current. If the system cannot transfer the required power, the current can be progressively increased. With the given electromagnetic structure and primary current, the voltage across the primary winding can be calculated and the primary VA rating is determined.

With a selected primary current, the measured or predicted (by simulation) values of open circuit voltage (V_{oc}) and short circuit current (I_{sc}) can be used to determine the power transfer capability of the electromagnetic structure. The maximum power transfer capability without secondary compensation is equal to half the value of the product of the open circuit voltage and short circuit current ($V_{oc}*I_{sc}/2$) as noted in section 2-2.

If the power to be transferred is less than $V_{oc}*I_{sc}/2$, the selected electromagnetic structure and

InductEV, Inc.
Exhibit 1008
Page 111

primary current is able to deliver the required power so that the secondary can be left uncompensated. However, it is necessary to ensure the primary current is not much larger than necessary and the electromagnetic structure is not oversized. In this case, the primary current and the electromagnetic structure needs to be reduced to make the required power transfer only slightly lower than $V_{oc}*I_{sc}/2$.

The design process then considers the primary compensation. If the primary VA rating does not exceed the VA rating of the selected power supply, the primary can be left uncompensated. This resulting system configuration is noted as design '1' in Fig. 4-2 and Table 4-1, with both the primary and secondary uncompensated. When the VA rating of the power supply is exceeded, either series or parallel compensation can be used to reduce the necessary power supply VA rating, resulting in a system configuration noted as design '2' with a compensated primary and an uncompensated secondary.

The series compensated primary provides voltage amplification between the power supply and the primary coil, and is suitable for long track applications. A parallel-compensated primary provides current amplification between the power supply and the primary coil, and is attractive for applications where a large primary current is required. The choice is also related to the configuration of the selected high frequency switching power supply as discussed in section 4-4.

If the power to be transferred to the pickup exceeds $V_{oc}*I_{sc}/2$ (assuming the electromagnetic structure is sufficiently well designed), then the secondary needs to be compensated by a capacitor connected either in series or parallel. Here a series compensated secondary has a voltage source characteristic. A parallel-compensated secondary has a current source characteristic. The choice is related to the configurations of the pickup regulator as well as the requirements of the applications as discussed in section 4-3.

Once compensated, the power transfer capability of the secondary is increased by the factor $2Q_{s0}$. As such, the magnitude of Q_{s0} required to provide the necessary power (P) is determined by the ratio: $P/(V_{oc}*I_{sc})$. However, secondary compensation also increases the required secondary VA rating of the pickup by the factor $\sqrt{1+Q_{s0}^2}$. If the actual VA rating of the secondary, given by the selected material and components, is more than this value, the system will be able to transfer the power. If not, the chosen configuration will need to be modified to increase the power transfer capability in one of the following three ways.

(a) Increasing the secondary VA rating by adding more copper or magnetic material.

(b) Increasing the primary current.

(c) Improving the coupling of the electromagnetic structure.

The first option increases the cost of the secondary, the second option increases the cost of the primary, and the third option increases the cost of the coupling structure. To optimise the system

InductEV, Inc.
Exhibit 1008
Page 112

design, a few iterations might be necessary to achieve the highest benefit to cost distribution.

It is also necessary to consider whether primary compensation is required by comparing the primary VA rating with the VA rating of the selected power supply using a similar approach discussed above. If primary compensation is not necessary, the design is complete, resulting in a system configuration noted as design '3' having an uncompensated primary and a compensated secondary.

If primary compensation is required, the resulting design is more complex with the primary and secondary either series or parallel compensated. In this case, the choice of either a fixed-frequency controller or variable-frequency controller needs to be considered. When a fixed-frequency controller is used, the design is complete resulting in a system configuration noted as design '4'. In this case, the operating frequency can be fixed at ω_0, but the power supply may operate with a displacement power factor less than unity. Consequently, the required VA rating of the power supply becomes higher. This can be evaluated in terms of k and Q_s using the normalized load model as shown later in this chapter.

If a variable-frequency controller is used, the frequency can be controlled to ensure the displacement power factor of the power supply is close to unity. In this case, the necessary VA rating of the power supply is minimized, but the pickup does not operate at the maximum power point due to frequency detuning. Such influences on power transfer capability once again can be evaluated in terms of k and Q_s using the normalized load model as shown later in this chapter.

When operation with variable-frequency control, it is also necessary to ensure that the system is stable and controllable under all reasonable loading conditions. This depends on the relationship between the primary and secondary quality factors (Q_p and Q_s). Stable and controllable operation can be assured if Q_p is much larger than Q_s ($Q_p >> Q_s$, where the primary reactive energy is much larger than the secondary reactive energy) as has been noted in section 2-5.5. The resulting system configuration is noted as design '5'.

With the given electromagnetic structure and secondary quality factor, the primary quality factor can be calculated using (4-5). Typical values of Q_s in practical circuits range from about 2 to 10, while typical values of Q_p lie between 2 and 30. Using (4-5), the stability requirement $Q_p >> Q_s$ can be expressed alternatively as $Q_s << 1/k$. To ensure $Q_p > Q_s$ in a loosely coupled system with a k of 0.1, the maximum Q_s is about 10. In a well-coupled system with a k of 0.5, this maximum Q_s drops to about 2.

If Q_p is close to Q_s, it is necessary to identify the bifurcation boundary. This can be done using the normalized load model developed in chapter 3, and will be explained later in this chapter. If the system design falls within the bifurcation boundary, stable and controllable operation is available. The design is thus complete, resulting in a system configuration noted as design '6'. If the system design is outside the bifurcation boundary, the design has to be modified to increase the power transfer capability by the following two ways.

InductEV, Inc.
Exhibit 1008
Page 113

(a) Increasing the primary current.

(b) Improving the coupling of the electromagnetic structure.

Table 4-2 summarizes system configurations resulting from the design procedure. The sensitivity of the system behaviour is compared in each case. Such sensitivities may result in a poor power supply displacement power factor when using a fixed-frequency controller operating at the secondary resonant frequency, or significant pickup frequency detuning when using a variable-frequency controller operating with unity displacement power factor. In each case, the system may be unable to deliver the required power. For system configurations '1', '2' and '3' within Table 4-2, the power supply is less sensitive to system variations as part of the system is left uncompensated. The remaining system configurations have both the primary and secondary either series or parallel compensated and therefore are more sensitive to system variations. The sensitivity in this case depends on k and Q_s and will be investigated later in this chapter.

TABLE 4-2
SUMMARY OF SYSTEM CONFIGURATIONS OF THE DESIGN PROCEDURE

System configurations*	Secondary compensation	Primary compensation	Fixed/variable-frequency controller	System sensitivity
1.	None	None	Fixed/variable	Small
2.	None	Series/parallel	Fixed/variable	Small
3.	Series/parallel	None	Fixed/variable	Small
4.	Series/parallel	Series/parallel	Fixed	Medium/High
5.	Series/parallel	Series/parallel	Variable	Medium
6.	Series/parallel	Series/parallel	Variable	High

*: these numbers represent system configurations as shown in Fig. 4-2.

4-3 DESIGN OPTIONS FOR THE PICKUP REGULATOR

A pickup may be used to supply power directly to a linear resistive load, however when it is used to supply power to a dc load such as a dc motor or a battery charger, a rectifier and a filter are necessary. If the load requires a low frequency ac supply such as an ac motor, frequency conversion is required. Although an ac-ac converter may be used, it is often necessary to use a two-stage process with an intermediate dc-bus to ensure stable output voltage and current.

Power flow regulation is often necessary to accommodate system variations such as misalignment of the electromagnetic structure and variations in the load. For single pickup applications, this could be controlled at either the primary or the secondary. With multiple pickup systems, the required power of

InductEV, Inc.
Exhibit 1008
Page 114

each pickup is often different. Since primary regulation affects all secondary pickups, it is not a good choice for multiple pickup applications. For these systems, power flow regulation needs to be implemented on the secondary pickup.

A block diagram of a pickup regulator that utilizes switching controllers to regulate power flow to a dc load is shown in Fig. 4-3. The switching control can be configured on either the ac or dc side (before or after the rectifier). Various configurations are possible [13-19]. The topology of the switching controller depends on the secondary compensation. Parallel compensation has current source characteristics requiring a controller that can work with a current source input. Series compensation requires a controller operating off a voltage source input.

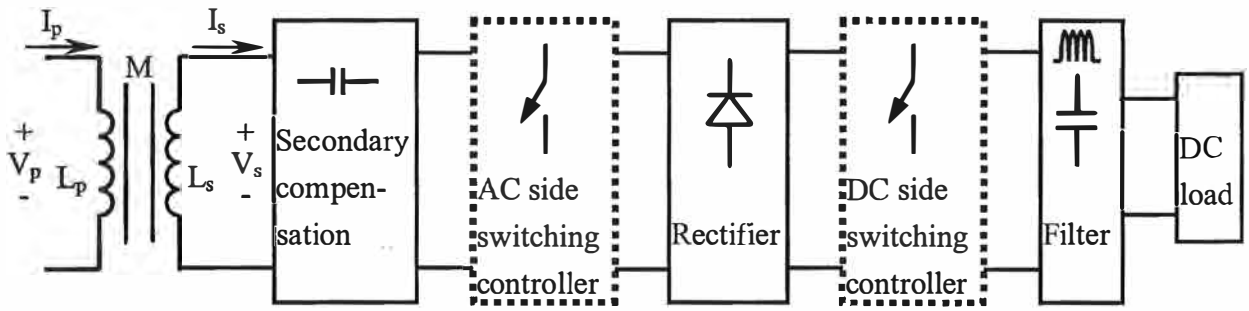


Fig. 4-3. A block diagram of a pickup regulator.

The real and reactive power transferred to the pickup can be calculated using the induced voltage ($j\omega MI_p$) and the secondary current (I_s) as:

$$\text{Real power} = P = \omega M I_p I_s \sin\phi \tag{4-6}$$

and

$$\text{Reactive power} = \omega M I_p I_s \cos\phi \tag{4-7}$$

where ϕ is the phase angle between the primary and secondary currents.

According to (4-6), the parameters that are controllable by the pickup regulator are the magnitude of the secondary current (I_s) and the phase relationship (ϕ) between the primary and secondary currents. In practice, this may be achieved indirectly via controlling other parameters such as V_s. Consequently, there are two fundamental strategies for the pickup regulator to control power. One strategy is to control the magnitude of I_s and the other strategy is to control ϕ. These two strategies can also be combined.

When controlling ϕ, it is desirable that the magnitude of I_s is kept at the maximum value to ensure maximum power transfer. The phase angle ϕ is controlled close to 90° for rated load, and reduced for light load operations. With this strategy, the reactive power flow is negligible at rated load condition,

InductEV, Inc.
Exhibit 1008
Page 115

but increases as ϕ is reduced with decreasing load. Because of this reactive power flow, the power loss in the secondary winding and the influence of the pickup on the primary are larger in comparison to the strategy of controlling the magnitude of I_s as discussed below. An example of this strategy can be found in [13].

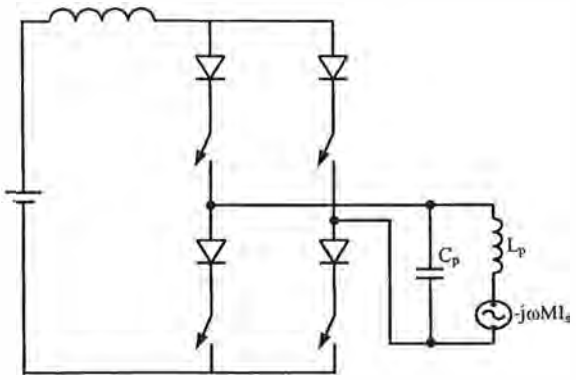
When controlling the magnitude of I_s, it is desirable that ϕ is kept close to the maximum value of 90° as this assures maximum power transfer with negligible reactive power flow as can be seen in (4-6) and (4-7). The secondary current is controlled at the maximum value for rated load, and reduced for light load operations. In consequence, the power loss in the secondary winding is minimized as I_s drops with decreasing load. This strategy has been applied to many industrial applications [15-19].

The actual switching frequency that can be used in a pickup regulator is restricted [18]. A low frequency (slow switching) option allows better transient response but a high frequency (fast switching) option gives lower output ripple. With slow switching, the switch is either closed or open for a relatively long period of time so that the switching transient actually dies out completely before the switch changes state again. In this case, the regulator essentially switches between two states, one at full power and the other at zero power. When the switching speed is much lower than the operating frequency of an ICPT system, the transition times are negligible. The average power output is the maximum possible power output moderated by the duty cycle of the switch. With fast switching, the averaging process happens so quickly that the power flow is quasi stable and the resonant voltage and current of the pickup are stable at the same average value as for slow switching under steady state conditions. Both slow and fast switching systems are therefore mathematically identical in terms of output power and average Q_s versus switch duty cycle. In this thesis, an equivalent resistance represents this average load.

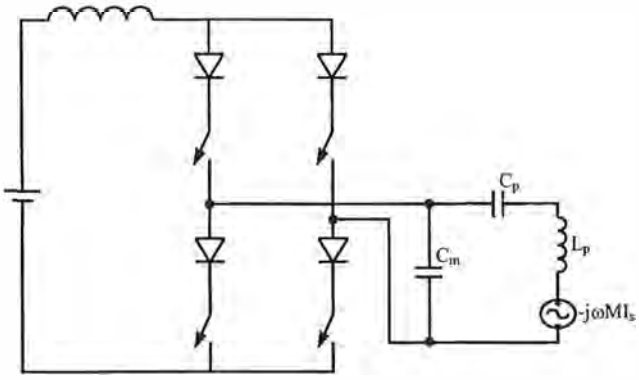
4-4 DESIGN OPTIONS FOR THE POWER SUPPLY

The configuration of the power supply is normally classified according to the input source as well as the inverter and resonant tank topologies. The input can be either voltage or current-sourced. The topology of the inverter can be single-switch, half-bridge, or full-bridge. The fundamental resonant tank topologies use either series or parallel-resonance. One or more reactive elements may be added to the resonant tank. The common configurations for ICPT applications are summarized in Fig. 4-4 and Fig. 4-5 respectively when using either a current or voltage source. In these figures, a reflected voltage ($-j\omega MI_s$) in series with the primary inductance is used to represent the loading effects of all the secondary pickups on the primary track/coil. The strength and weakness of these configurations are compared in Table 4-3.

InductEV, Inc.
Exhibit 1008
Page 116

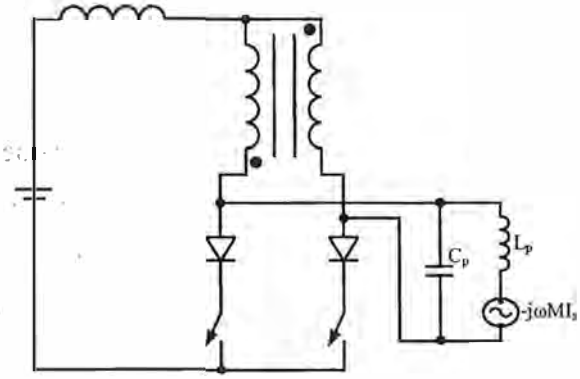


Current-sourced, full-bridge, parallel-resonant

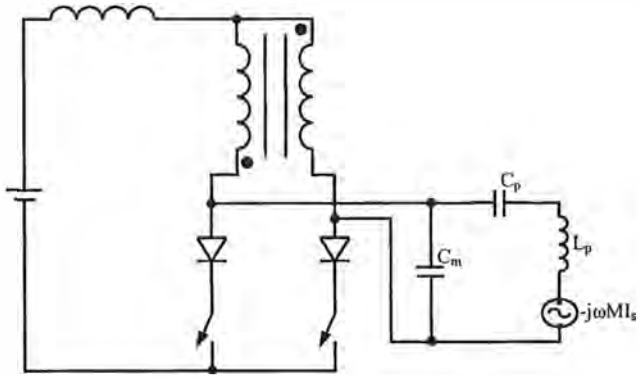


Current-sourced, full-bridge, CCL-resonant

(a) Full-bridge.

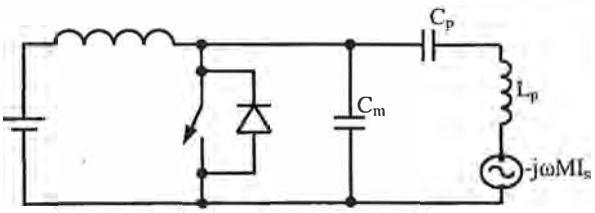


Current-sourced, half-bridge, parallel-resonant

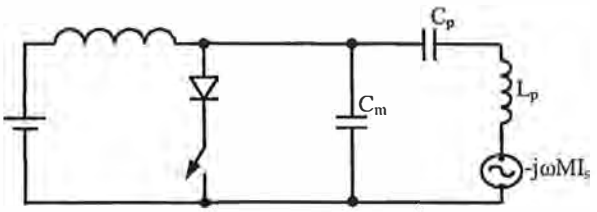


Current-sourced, half-bridge, CCL-resonant

(b) Half-bridge.



Current-sourced, single-reverse-conducting-switch, CCL-resonant



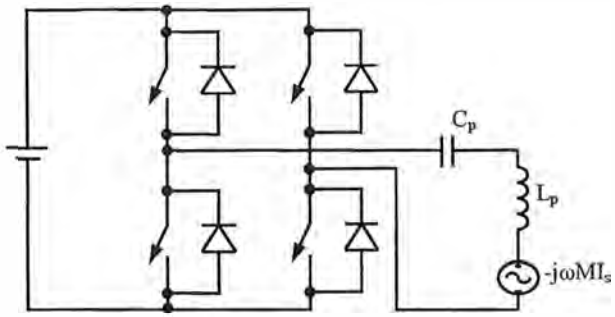
Current-sourced, single-reverse-blocking-switch, CCL-resonant

(c) Single-switch.

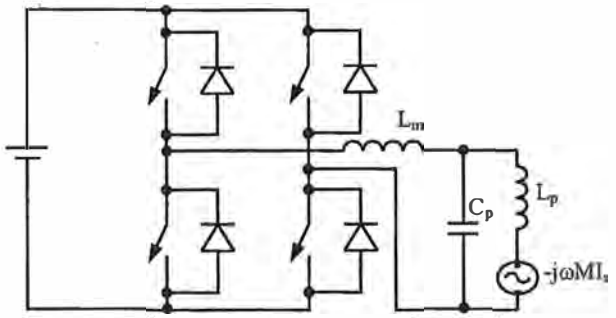
Fig. 4-4. Examples of current-sourced power supply configurations.

For both the voltage-sourced and current-sourced configurations, the power capability as well as the cost and size are mainly determined by the inverter topologies. The full-bridge inverter has the largest power capability with the highest cost and size, while the single-switch inverter has the least power capability with the lowest cost and size. The primary current (track current) and the track length are dependent on the resonant tank topologies. Parallel resonance enables a large primary current, while series resonance allows a long track length. In practice, many series capacitors may be distributed along the track.

InductEV, Inc.
Exhibit 1008
Page 117

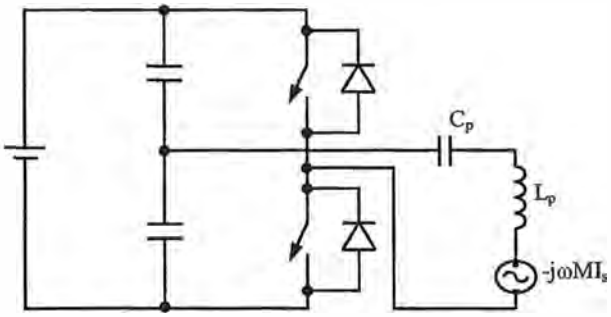


Voltage-sourced, full-bridge, series-resonant

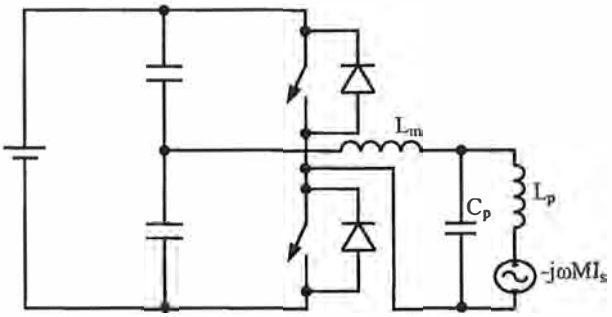


Voltage-sourced, full-bridge, LCL-resonant

(a) Full-bridge.

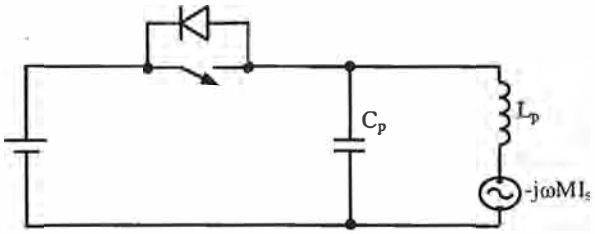


Voltage-sourced, half-bridge, series-resonant

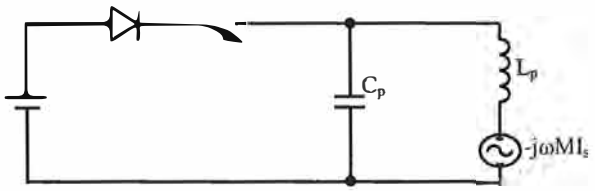


Voltage-sourced, half-bridge, LCL-resonant

(b) Half-bridge.



Voltage-sourced,
single-reverse-conducting-switch,
parallel-resonant



Voltage-sourced, single-reverse-blocking-switch,
parallel-resonant

(c) Single-switch.

Fig. 4-5. Examples of voltage-sourced power supply configurations.

As noted in section 2-5, both fixed and variable-frequency controllers can be used to control the power supply in ICPT systems. The advantages and disadvantages are compared in Table 4-4. Fixed-frequency controllers normally operate at the tuned frequency of the pickup for maximum power transfer. Since the operating frequency is fixed, there are no bifurcation problems in the frequency domain. However, it is unavoidable that the power supply will operate with a displacement power factor less than unity. Consequently, the power supply needs to be oversized and the efficiency is reduced.

Variable-frequency controllers usually operate with unity displacement power factor to minimize the VA rating of the power supply and to improve the efficiency. However, the power transfer

InductEV, Inc.
Exhibit 1008
Page 118

capability of the system is reduced due to frequency detuning effects in the pickup. Moreover, operation may become unstable or uncontrollable if frequency bifurcation occurs.

TABLE 4-3
COMPARISON OF POWER SUPPLY CONFIGURATIONS

Power supply configurations			Power capability	Track length	Primary current	System sensitivity	Cost	Size
Voltage-sourced	Full-bridge	Series-resonant	H	H	L	M	H	H
		LCL-resonant	H	L	H	H	H	H
	Half-bridge	Series- resonant	M	H	L	M	M	M
		LCL- resonant	M	L	H	H	M	M
	Single-switch	Reverse-conducting, parallel-resonant	L	L	L	M	L	L
		Reverse-blocking, parallel-resonant	L	L	L	M	L	L
Current-sourced	Full-bridge	Parallel-resonant	H	L	H	M	H	H
		CCL-resonant	H	H	H	H	H	H
	Half-bridge	Parallel-resonant	M	L	H	M	M	M
		CCL-resonant	M	H	H	H	M	M
	Single-switch	Reverse-conducting, CCL-resonant	L	L	L	H	L	L
		Reverse-blocking, CCL-resonant	L	L	L	H	L	L

H=High, M=Medium, L=Low

TABLE 4-4
COMPARISON OF FIXED AND VARIABLE FREQUENCY CONTROLLER

Controller	Advantages	Disadvantages
Fixed-frequency controller	1. Operation at the tuned frequency of the pickup for maximum power transfer. 2. No bifurcation problems.	1. Reduced displacement power factor. 2. Oversized power supply. 3. Reduced efficiency.
Variable-frequency controller	1. Operation with unity displacement power factor. 2. Minimized VA rating of the power supply. 3. Improved efficiency.	1. Pickup frequency detuning. 2. Reduced power transfer. 3. Unstable or uncontrollable operation due to bifurcation.

InductEV, Inc.
Exhibit 1008
Page 119

4-5 DESIGN EVALUATIONS

In this section the normalized load model developed in chapter 3 is used to evaluate system designs resulting from the design procedure described in section 4-2. The sensitivity of the displacement power factor to the fundamental design parameters u, k and Q_s are evaluated generally for all possible configurations where the primary and secondary can be either series, parallel or uncompensated. Here u varies across the operating frequency spectrum, while Q_s changes over the operating load range.

The thesis then focuses on systems with compensated primary and secondary because this is the usual case for high power applications. The system behaviour under fixed and variable frequency control is investigated. Such analysis is essential when the fundamental design parameters are determined. As noted in chapter 3, the loading effects of the secondary pickup on the primary may have significant influences on the behaviour of the load resonant tank (seen by the power supply) when the secondary quality factor or the magnetic coupling coefficient is increased. When designing ICPT systems, it is necessary to identify such influences on the displacement power factor of the power supply, the power transfer capability to the pickup, and the stability and controllability of the controller.

4-5.1 SENSITIVITY OF THE DISPLACEMENT POWER FACTOR

As the cost of the power supply depends on its VA rating, it is desirable that the power supply operates with unity displacement power factor to minimize this. The phase angle between the fundamental components of the output voltage and current of the power supply can be calculated using the normalized load impedance as:

$$\tan\theta_1 = \frac{\mathrm{Im}\,Z_{in}}{\mathrm{Re}\,Z_{in}} = \frac{-\mathrm{Im}\,Y_{in}}{\mathrm{Re}\,Y_{in}} \tag{4-8}$$

The displacement power factor (DPF) of the power supply can then be determined from this phase angle as:

$$\text{Displacement Power Factor (DPF)} = \cos\theta_1 \tag{4-9}$$

The normalized load impedance (defined in section 3-10.2) depends on the primary compensation topology and is summarized in Table 4-5.

When the secondary is left uncompensated, maximum power transfer to the pickup is achieved when '$\omega_0 L_s$' and R are equal (as shown in section 2-2.4.2). In this case, the normalized load impedance given in Table 4-5 is a function of u and k as derived in Appendix G. A summary of the normalized function for each term within this normalized load impedance is given in Table 4-6.

InductEV, Inc.
Exhibit 1008
Page 120

TABLE 4-5
NORMALIZED LOAD IMPEDANCES

Uncompensated primary: $Z_{tn} = \frac{Z_t}{\mathrm{Re}Z_{r0}} = \mathrm{Re}Z_{tn} + j\,\mathrm{Im}Z_{tn}$	$\mathrm{Re}Z_{tn} = \mathrm{Re}Z_{rn}$
	$\mathrm{Im}Z_{tn} = \frac{\omega L_p}{\mathrm{Re}Z_{r0}} + \mathrm{Im}Z_{rn}$
Series primary: $Z_{tn} = \frac{Z_t}{\mathrm{Re}Z_{r0}} = \mathrm{Re}Z_{tn} + j\,\mathrm{Im}Z_{tn}$	$\mathrm{Re}Z_{tn} = \mathrm{Re}Z_{rn}$
	$\mathrm{Im}Z_{tn} = -\frac{1}{\omega C_p(\mathrm{Re}Z_{r0})} + \frac{\omega L_p}{\mathrm{Re}Z_{r0}} + \mathrm{Im}Z_{rn}$
Parallel primary: $Z_{tn} = \frac{1}{Y_{tn}} = \frac{1}{\mathrm{Re}Y_{tn} + j\,\mathrm{Im}Y_{tn}}$	$\mathrm{Re}Y_{tn} = \frac{\mathrm{Re}Z_{rn}}{(\mathrm{Re}Z_{rn})^2 + \left(\frac{\omega L_p}{\mathrm{Re}Z_{r0}} + \mathrm{Im}Z_{rn}\right)^2}$
	$\mathrm{Im}Y_{tn} = \omega C_p(\mathrm{Re}Z_{r0}) - \frac{\frac{\omega L_p}{\mathrm{Re}Z_{r0}} + \mathrm{Im}Z_{rn}}{(\mathrm{Re}Z_{rn})^2 + \left(\frac{\omega L_p}{\mathrm{Re}Z_{r0}} + \mathrm{Im}Z_{rn}\right)^2}$

TABLE 4-6
FUNCTIONS OF THE NORMALIZED LOAD IMPEDANCE WITH UNCOMPENSATED PICKUP

$\frac{1}{\omega C_p(\mathrm{Re}Z_{r0})} = \frac{2}{uk^2}$	$\frac{\omega L_p}{\mathrm{Re}Z_{r0}} = \frac{2u}{k^2}$
$\mathrm{Re}Z_{rn} = \frac{\mathrm{Re}Z_r}{\mathrm{Re}Z_{r0}} = \frac{2u^2}{1+u^2}$	$\mathrm{Im}Z_{rn} = \frac{\mathrm{Im}Z_r}{\mathrm{Re}Z_{r0}} = \frac{-2u^3}{1+u^2}$

With the secondary compensated, the normalized load impedance has been developed in section 3-10.2 as a function of u, k and Q_{s0}. A summary of the normalized function for each term within the normalized load impedance has been shown in Table 3-3, and is given again in Table 4-7 for convenience.

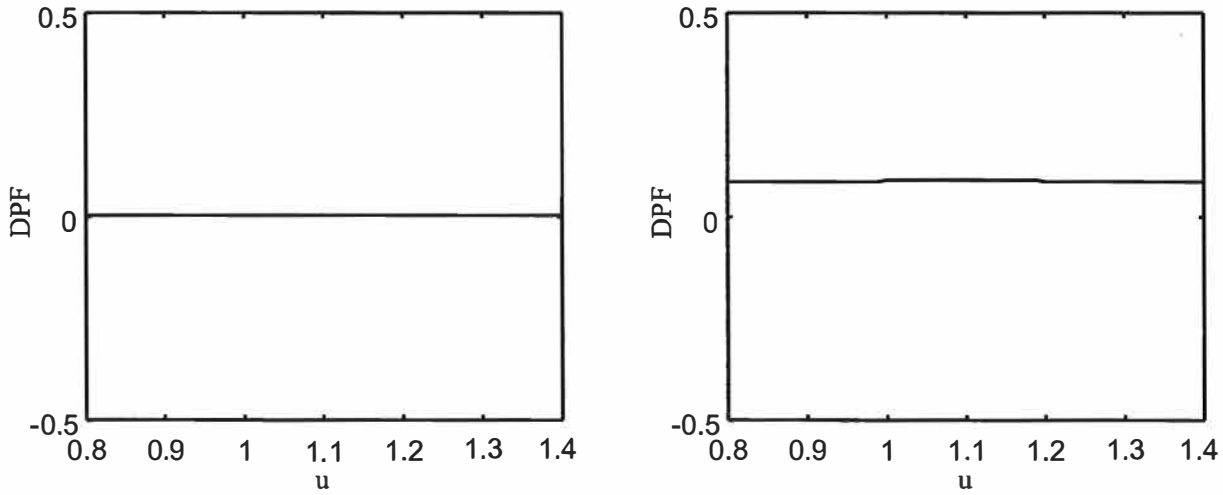
Since the normalized load impedance is again simply a function of u, k and Q_{s0}, the DPF determined from (4-9) is also a function of these parameters. The sensitivity of the DPF to these parameters is discussed below.

InductEV, Inc.
Exhibit 1008
Page 121

TABLE 4-7
FUNCTIONS OF THE NORMALIZED LOAD IMPEDANCE WITH COMPENSATED PICKUP

$\frac{1}{\omega C_p(\mathrm{Re}\,Z_{r0})}=\frac{1}{k^2Q_{s0}u}$	Series/parallel secondary
$\frac{\omega L_p}{\mathrm{Re}Z_{r0}}=\frac{u}{k^2Q_{s0}}$	Series/parallel secondary
$\mathrm{Re}\,Z_{rn}=\frac{\mathrm{Re}\,Z_r}{\mathrm{Re}Z_{r0}}=\begin{cases}\frac{u^4}{(u^2-1)^2Q_{s0}^2+u^2}\\ \frac{u^2}{(u^2-1)^2Q_{s0}^2+u^2}\end{cases}$	Series secondary Parallel secondary
$\mathrm{Im}\,Z_{rn}=\frac{\mathrm{Im}\,Z_r}{\mathrm{Re}Z_{r0}}=\begin{cases}\frac{-u^3(u^2-1)Q_{s0}}{(u^2-1)^2Q_{s0}^2+u^2}\\ \frac{-u^3[(u^2-1)Q_{s0}+1/Q_{s0}]}{(u^2-1)^2Q_{s0}^2+u^2}\end{cases}$	Series secondary Parallel secondary

Systems having both the primary and secondary uncompensated: The DPF of systems with both primary and secondary uncompensated is shown in Fig. 4-6 as a function of u for selected k. As can be seen, the power supply operates with poor DPF. In both loosely and well-coupled systems (low and high k), the DPF is close to zero as the power transfer of an uncompensated pickup is small in comparison to the reactive power of the primary winding.



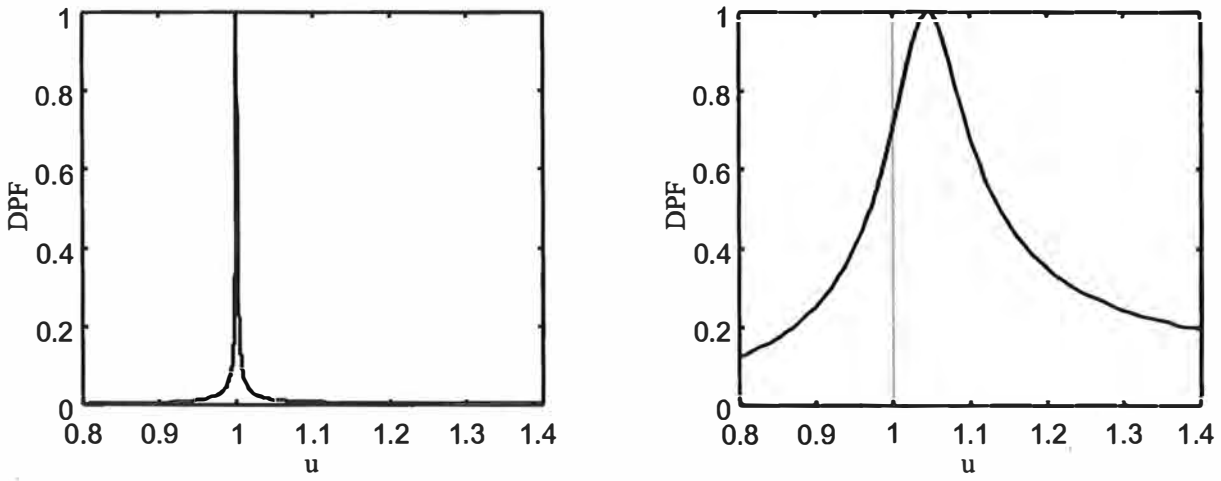
(a) k=0.05. (b) k=0.4.

Fig. 4-6. Sensitivity of DPF to u and k in systems having both the primary and secondary uncompensated.

Systems having a compensated primary and an uncompensated secondary: The poor DPF

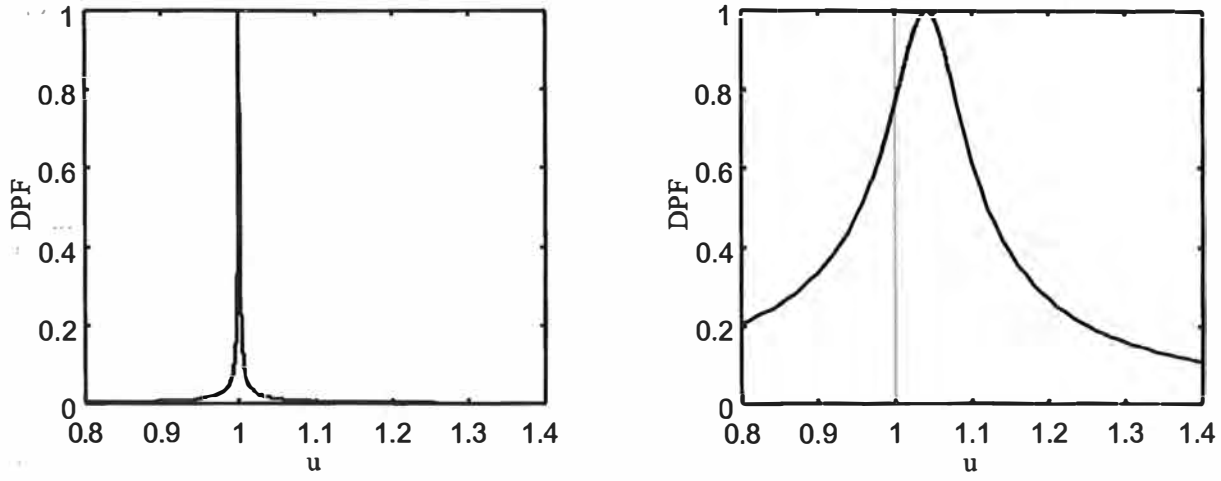
InductEV, Inc.
Exhibit 1008
Page 122

discussed above can be improved using primary compensation (as shown in Fig. 4-7). Both series and parallel-compensated primary topologies show similar effects. In loosely coupled systems, unity DPF can be achieved close to ω_0 (u=1). For well-coupled systems, the DPF at ω_0 is about 0.7 only due to the influence of the secondary pickup loading. In this case, unity DPF is achieved at a single frequency above ω_0 (u>1).



(i) k=0.05. (ii) k=0.4.

(a) Series primary.



(i) k=0.05. (ii) k=0.4.

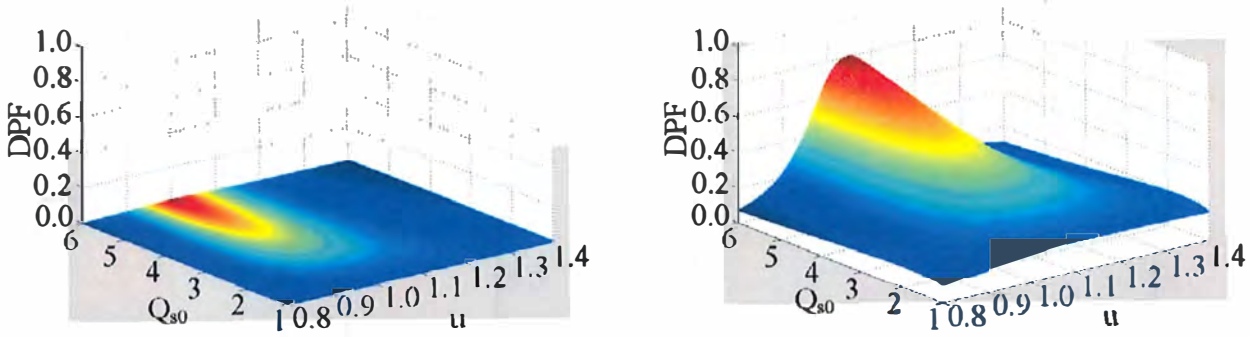
(b) Parallel primary.

Fig. 4-7. Sensitivity of DPF to u and k in systems having a compensated primary and an uncompensated secondary.

Systems having an uncompensated primary and a compensated secondary: The DPF of systems with an uncompensated primary and a compensated secondary are shown in Fig. 4-8 as a function of u and Q_{s0} for selected k. As expected, the power supply operates with a DPF less than unity. Once again, series and parallel secondary topologies exhibit similar features. In loosely coupled systems, the DPF is very close to zero as the power transfer is small. For well-coupled systems with high Q_s, the DPF

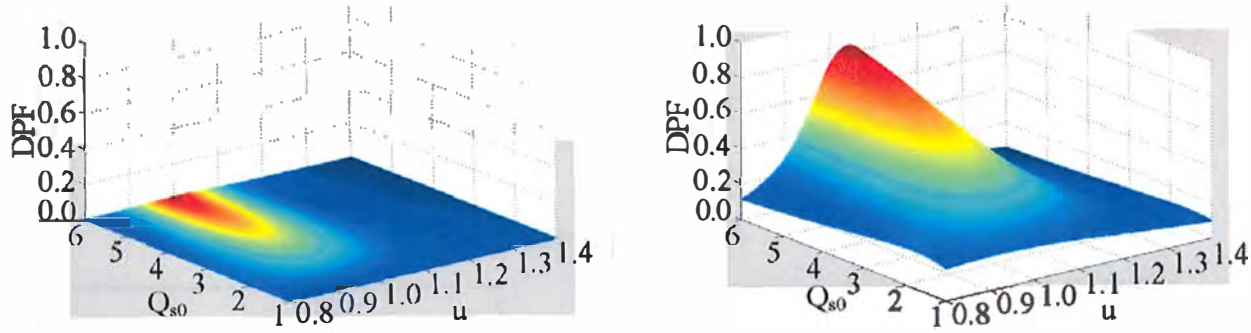
InductEV, Inc.
Exhibit 1008
Page 123

becomes higher because more power is transferred.



(i) k=0.05. (ii) k=0.4.

(a) Series secondary.



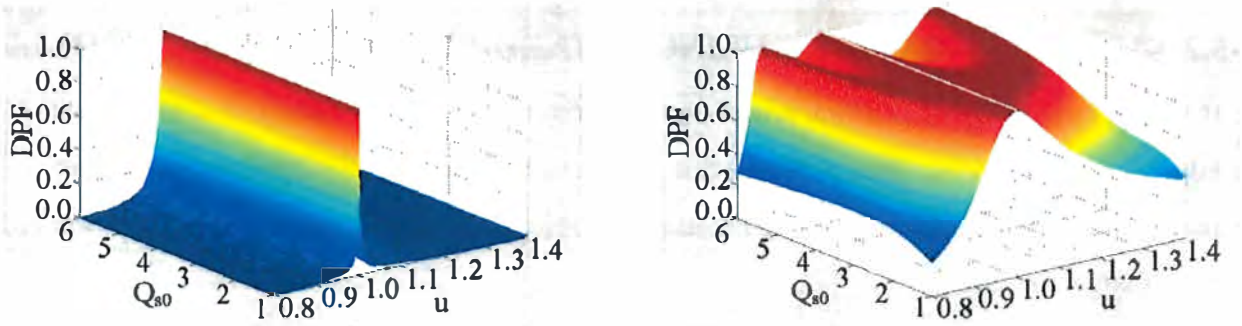
(i) k=0.05. (ii) k=0.4.

(b) Parallel secondary.

Fig. 4-8. Sensitivity of DPF to u, k and Q_{s0} in systems having an uncompensated primary and a compensated secondary.

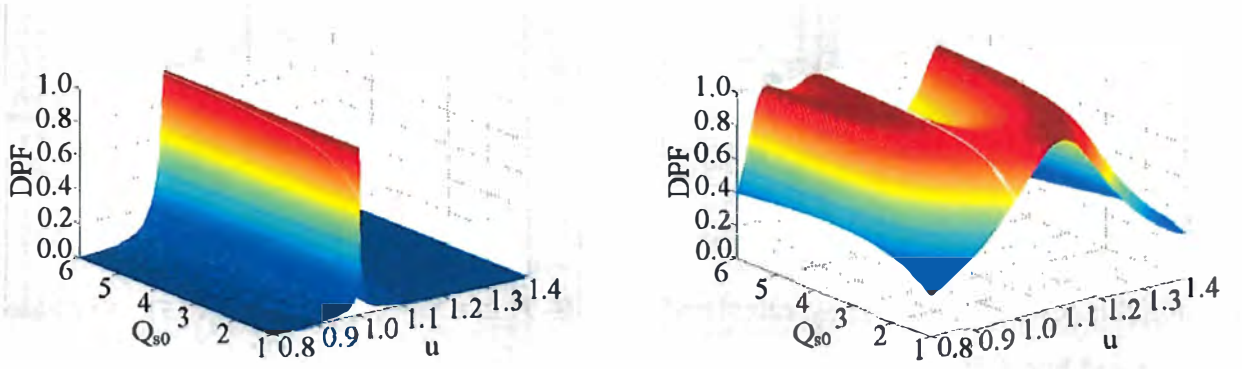
Systems having both the primary and secondary compensated: Poor DPF as shown in earlier systems can be improved with primary compensation. The four basic topologies (SS, SP, PP and PS) are compared in Fig. 4-9. In this figure, the DPF at ω_0 (u=1) is shown on the surfaces as a white line. Theoretically, the SS topology achieves the best results compared with the other topologies. The DPF of the SS topology at ω_0 is unity and independent of Q_s and k, but those of other three topologies are below unity and dependent on both Q_s and k. In addition, unity DPF is achieved only at one operating frequency if Q_s is low. When Q_s is high, unity DPF can be achieved at three operating frequencies. This bifurcation occurs at lower Q_s values as the magnetic coupling improves (high k). Furthermore, the operating frequency with unity DPF is not at ω_0 when either the primary or the secondary is parallel compensated (SP, PP and PS topologies).

InductEV, Inc.
Exhibit 1008
Page 124



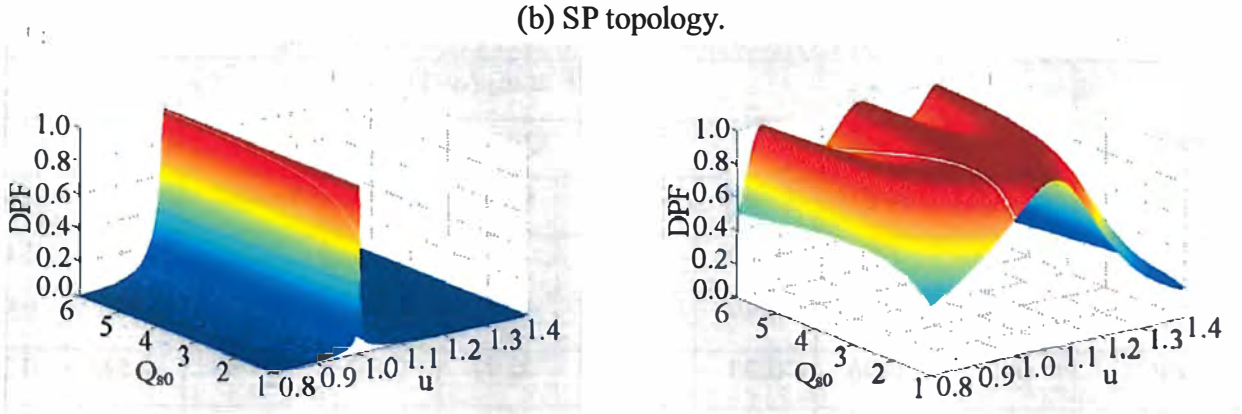
(i) k=0.05. (ii) k=0.4.

(a) SS topology.



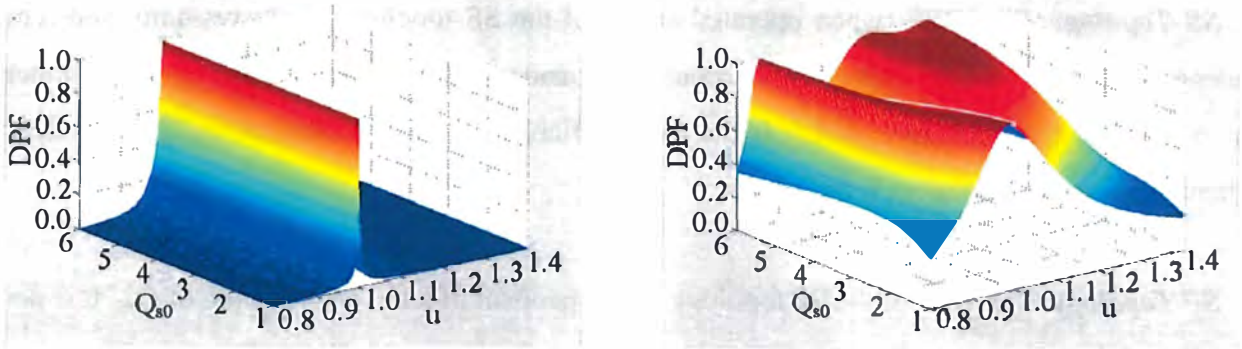
(i) k=0.05. (ii) k=0.4.

(b) SP topology.



(i) k=0.05. (ii) k=0.4.

(c) PP topology.



(i) k=0.05. (ii) k=0.4.

(d) PS topology.

Fig. 4-9. Sensitivity of DPF to u, k and Q_{s0} in systems having both the primary and secondary compensated.

InductEV, Inc.
Exhibit 1008
Page 125

4-5.2 SYSTEM BEHAVIOUR USING A FIXED-FREQUENCY CONTROLLER

If the operating frequency of the power supply is fixed at ω_0, the frequency detuning effects of the pickup are minimized. As shown above, this may result in a poor DPF if either the primary or the secondary is parallel compensated (SP, PP and PS topologies). A poor DPF requires the power supply to have a large VA rating.

For fixed-frequency operation at ω_0 (u=1), equation (4-8) can be calculated as:

$$\tan\theta_1(u=1)=\begin{cases}0 & \text{SS topology}\\ -\dfrac{1}{Q_{s0}} & \text{SP topology}\\ -k^2Q_{s0}+\dfrac{1-k^2}{Q_{s0}} & \text{PP topology}\\ -k^2Q_{s0} & \text{PS topology}\end{cases} \tag{4-10}$$

Using this result, the DPF at ω_0 calculated using (4-9) is a function of k and Q_{s0} as illustrated in Table 4-8 and Fig. 4-10.

TABLE 4-8
DPF OPERATING WITH FIXED FREQUENCY AT ω_0

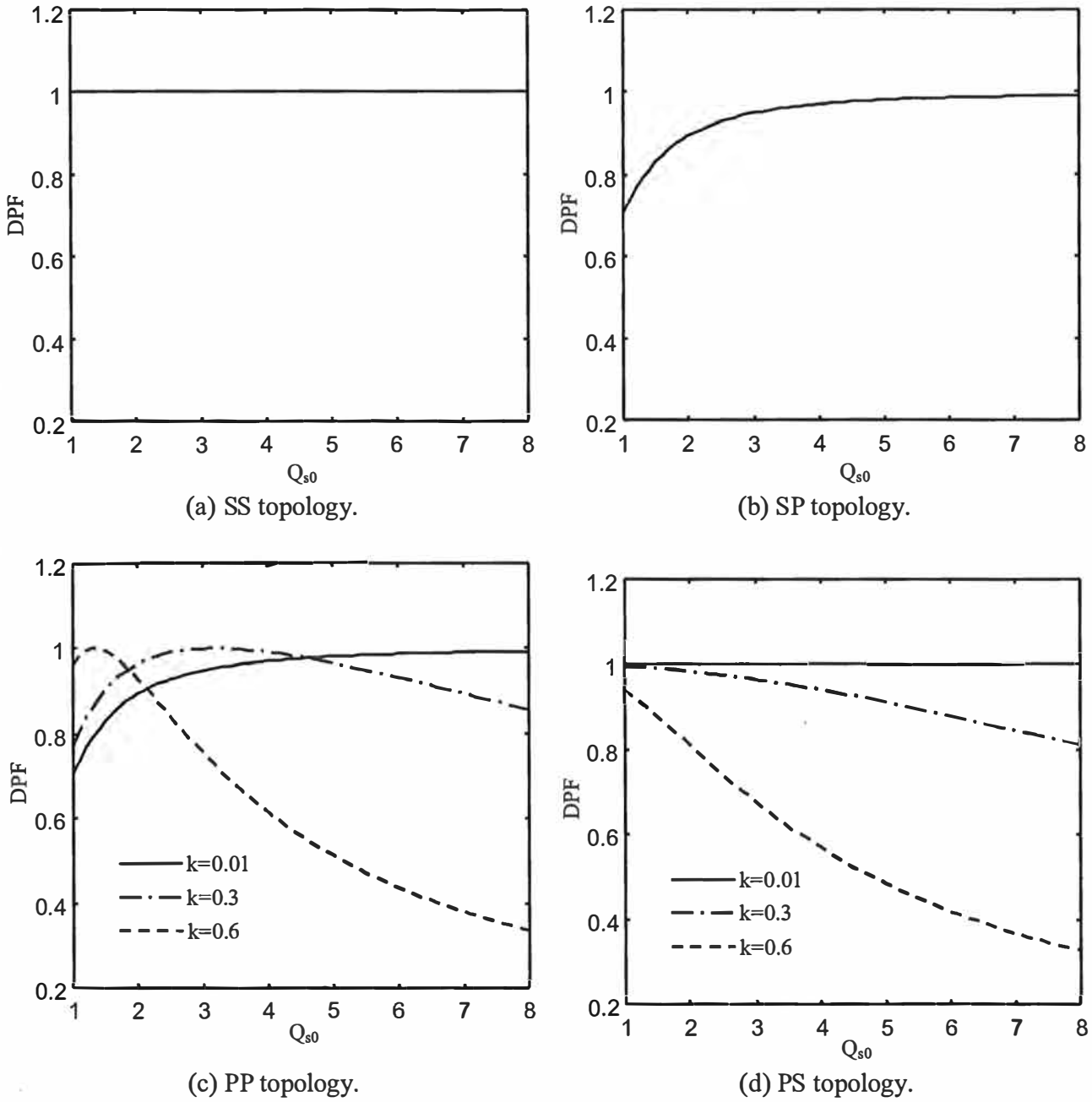
Topology	DPF at ω_0 (u=1)								
	Q_{s0}=2			Q_{s0}=5			Q_{s0}=8		
	k=0.01	k=0.3	k=0.6	k=0.01	k=0.3	k=0.6	k=0.01	k=0.3	k=0.6
SS	1.00	1.00	1.00	1.00	1.00	1.00	1.00	1.00	1.00
SP	0.89	0.89	0.89	0.98	0.98	0.98	0.99	0.99	0.99
PP	0.89	0.96	0.93	0.98	0.97	0.51	0.99	0.86	0.34
PS	1.00	0.98	0.81	1.00	0.91	0.49	1.00	0.81	0.33

SS Topology: The DPF (when operated at ω_0) of the SS topology is always unity and remains independent of k and Q_{s0}. This allows system performance to be maintained during misalignment of the electromagnetic structure, which is the most difficult parameter to control in ICPT applications where mechanical alignment is not used.

SP Topology: The DPF of the SP topology is independent ofk but is a function of Q_{s0}. It is poor at low Q_s, and becomes ever closer to unity as Q_s increases. Similar to the SS topology, the SP topology is independent of k allowing misalignment of the electromagnetic structure. Consequently, the performance of the SP topology is comparable to the SS topology providing Q_s is about 2 or larger that

InductEV, Inc.
Exhibit 1008
Page 126

is almost always true.



(a) SS topology. (b) SP topology.

(c) PP topology. (d) PS topology.

Fig. 4-10. DPF operating with fixed frequency at ω_0.

PP Topology: The DPF of the PP topology depends on both k and Q_s. The effects of Q_s and k are very complex. From (4-10) it can be seen that unity DPF can be achieved when:

$$k = \frac{1}{\sqrt{Q_{s0}^2 + 1}} \qquad \text{PP topology} \qquad (4\text{-}11)$$

This relationship is shown in Fig. 4-11 as a curve. As the magnetic coupling improves, Q_s must decrease to maintain unity DPF. The power transfer capability of an ICPT system can be improved by

InductEV, Inc.
Exhibit 1008
Page 127

enhancing k or increasing Q_s. However, to ensure good DPF in this case, a trade-off between k and Q_s is necessary.

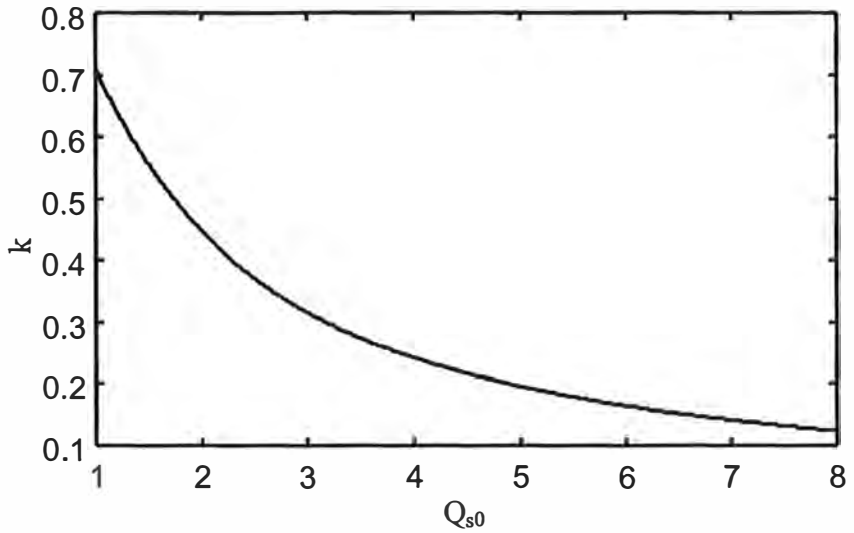


Fig. 4-11. Required relationship between k and Q_{s0} to achieve unity DPF at ω_0 for the PP topology.

Interestingly with low Q_s (around 2), as illustrated in Fig. 4-12, the DPF is close to unity across a wide range of k. At this condition, unity DPF is achieved when k is about 0.45. With higher Q_s, the DPF drops rapidly as k increases. For well-coupled systems where the variation of the magnetic coupling is large, it may be desirable to design the system with low Q_s. The contact-less electric vehicle battery charger discussed later in this thesis is designed with this in mind.

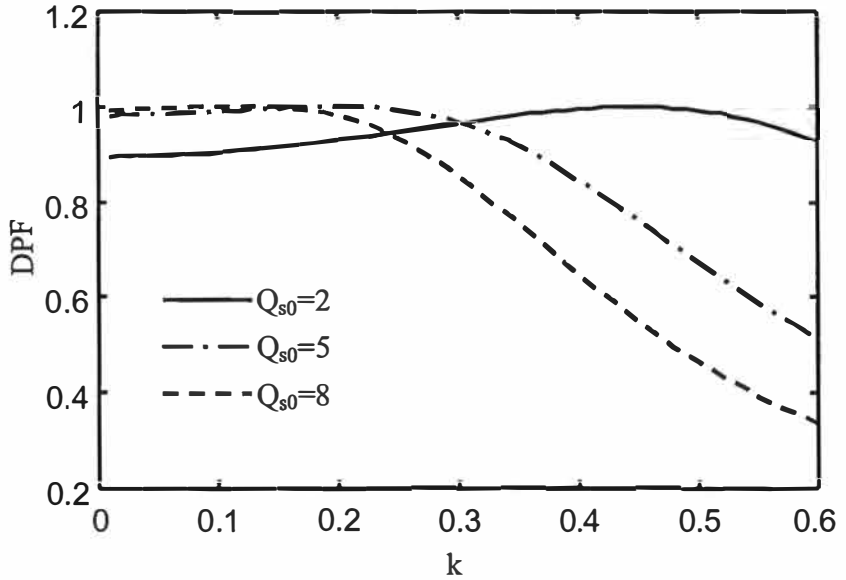


Fig. 4-12. Selection of Q_{s0} to improve DPF when operating at ω_0 over a wider range of k for the PP topology.

InductEV, Inc.
Exhibit 1008
Page 128

PS Topology: The DPF of the PS topology is the most sensitive of the topologies listed here to Q_s and k. The DPF becomes worse with increasing Q_s or improving k. This topology is thus a poor choice for well-coupled systems with high Q_s.

4-5.3 SYSTEM BEHAVIOUR USING A VARIABLE-FREQUENCY CONTROLLER

If the operating frequency of the power supply is controlled to achieve unity DPF, the necessary VA rating can be minimized. However, in such systems the pickup does not operate at the tuned frequency when either the primary or the secondary is parallel compensated (SP, PP and PS topologies) as stated earlier. If the frequency-detuning effect is large, the pickup may not be able to transfer enough power.

Under variable-frequency control, all of the four basic compensation topologies exhibit frequency bifurcation when Q_s is large. As a result, the system may shift between any of the possible operating frequencies. Naturally the controller operates at the frequency extremes (either the lowest or the highest operating point) where pickup frequency detuning can be very large resulting in significant loss of power transfer capability.

For variable-frequency operation with unity DPF, the operating frequency is the zero phase angle frequency of the load impedance and can be calculated by:

$$\mathrm{Im}\, Z_{in}(u,k,Q_{s0}) = 0 \quad \textbf{or} \quad \mathrm{Im}\, Y_{in}(u,k,Q_{s0}) = 0 \tag{4-12}$$

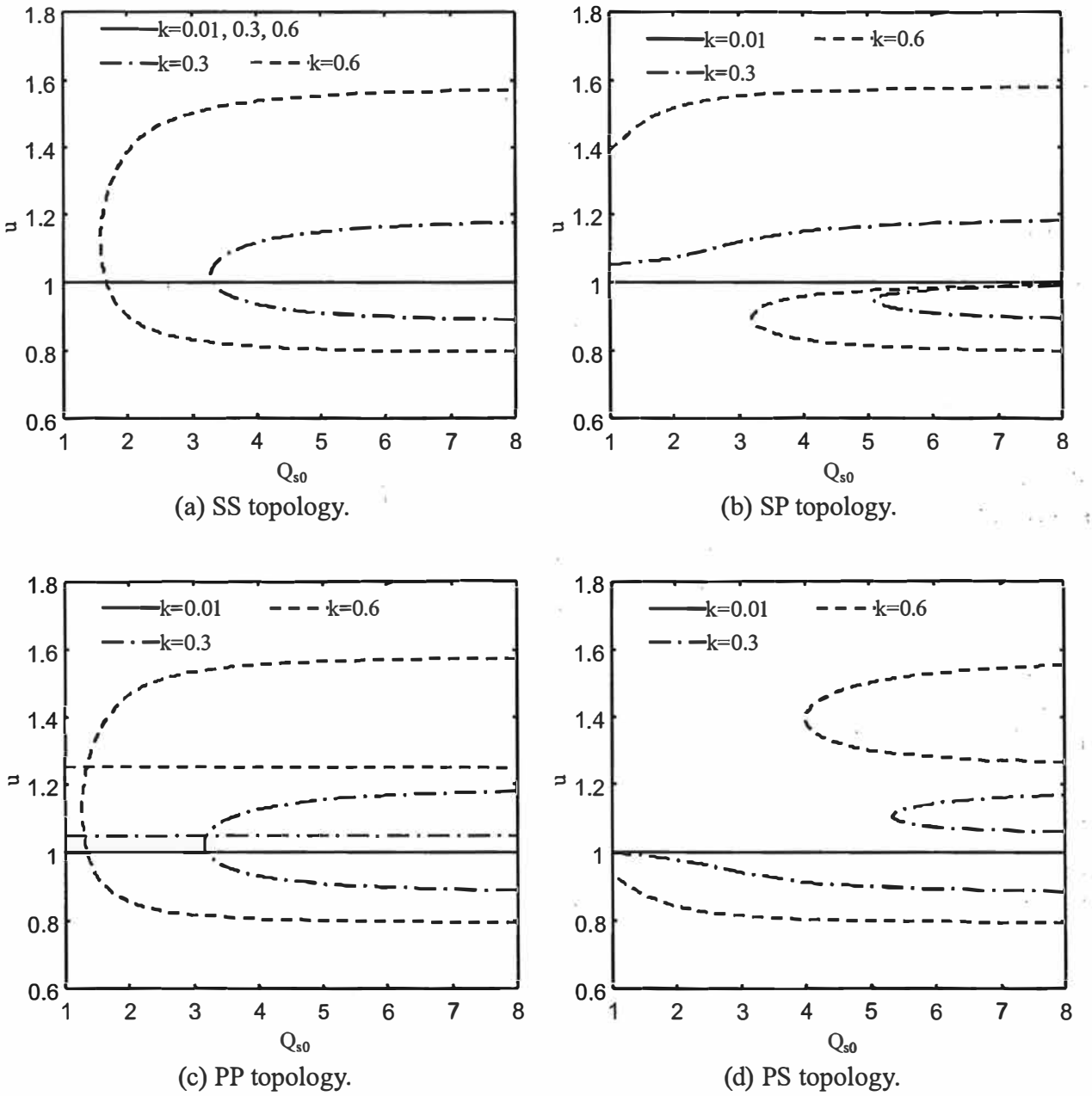
The operating frequency determined by (4-12) is a function of k and Q_{s0}. These topology dependent results are compared in Fig. 4-13. As expected, in all four basic topologies the operating frequency is closely at ω_0 for loosely coupled systems (low k), and bifurcation phenomenon is evident for well-coupled systems (high k) with high Q_s. In all cases, improving k results in the occurrence of bifurcation at lower Q_s.

SS topology: The SS topology once again is the most desirable as it can theoretically operate at ω_0 and as such assures maximum power transfer to the pickup. Moreover, this is achieved independent of k and Q_{s0}. Once bifurcation occurs there exists two additional operating modes above and below ω_0. Their frequency shifts from ω_0 increase with increasing k and Q_s, and may result in substantial frequency detuning of the pickup and as such a major drop in power transfer capability. It is necessary to avoid these two operating modes.

SP topology: All the three operating modes of the SP topology are dependent on k and Q_{s0}. This

InductEV, Inc.
Exhibit 1008
Page 129

topology has the worst light load behaviour (low Q_s in the bifurcation-free region) as the operating frequency can shift well above ω_0. In the region where bifurcation occurs, one of the three operating modes remains close to ω_0. If the system could be controlled to operate at this operating mode, detuning of the pickup would be minimized. Once again, the frequency shifts of the other two operating modes increase with increasing k and Q_s, and should be avoided.



(a) SS topology. (b) SP topology.

(c) PP topology. (d) PS topology.

Fig. 4-13. Operating frequency with unity DPF.

PP topology: In the bifurcation-free area, the operating frequency of the PP topology is independent of Q_{s0}. It can be shown that this frequency is a function of k given by:

InductEV, Inc.
Exhibit 1008
Page 130

$$u = \frac{1}{\sqrt{1-k^2}} \tag{4-13}$$

Consequently, the frequency shift increases with increasing k. This operating mode extends into the bifurcation region. The frequency shifts of the other two operating modes in the bifurcation region are normally larger and should be avoided.

PS topology: All the three operating modes of the PS topology also depend on k and Q_{s0}. The frequency shifts at light load (low Q_s in the bifurcation-free area) is comparable to the PP topology and less than that of the SP topology. Once bifurcation occurs, frequency shifts are significant in all three operating modes. It is desirable to avoid operation in this region.

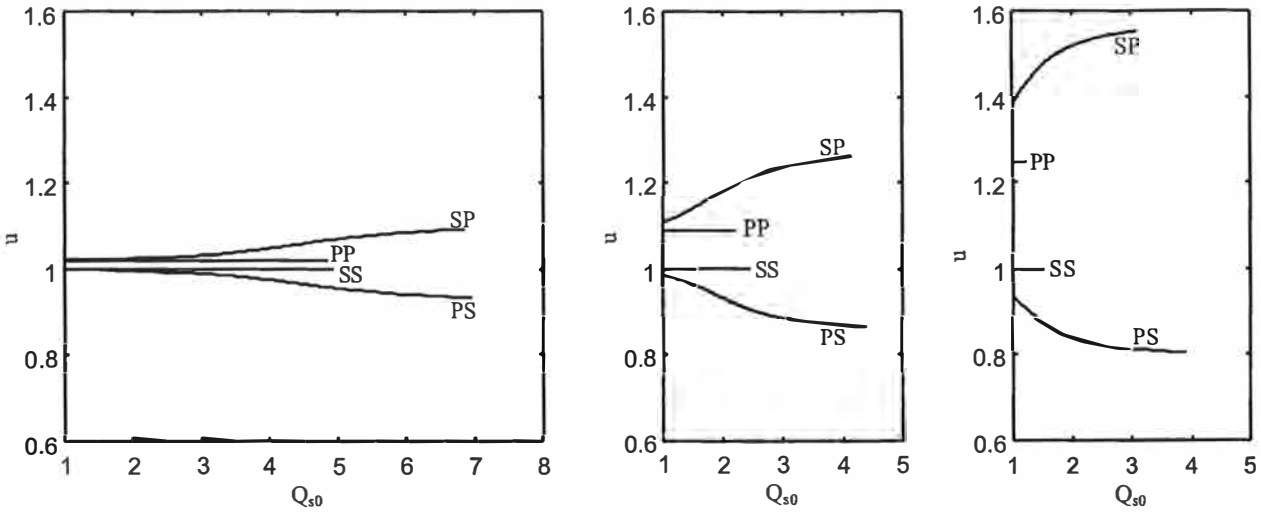
The bifurcation boundaries of the basic topologies are compared in Table 4-9 for selected k of 0.2, 0.4 and 0.6. Bifurcation appears when Q_{s0} is larger than the boundary value given in this table in each case. The corresponding primary quality factor (Q_{p0}) determined by (4-5) is also shown in the table. When the primary and secondary have the same compensation topology (SS and PP topologies), as can be seen in this table, the bifurcation boundary is very close to the simplified bifurcation criterion of $Q_{p0}>Q_{s0}$ (as discussed in section 2-5.5). For the other two topologies (SP and PS topologies), however, this simplified bifurcation criterion is not suitable, and bifurcation only occurs at a much larger Q_{s0}.

TABLE 4-9
BIFURCATION BOUNDARY FOR VARIABLE-FREQUENCY OPERATION WITH UNITY DPF

Topology	k=0.2	k=0.4	k=0.6
SS	Q_{p0}=5.05, Q_{s0}=4.95	Q_{p0}=2.55, Q_{s0}=2.45	Q_{p0}=1.79, Q_{s0}=1.55
SP	Q_{p0}=3.48, Q_{s0}=6.90	Q_{p0}=1.27, Q_{s0}=4.15	Q_{p0}=0.56, Q_{s0}=3.15
PP	Q_{p0}=4.95, Q_{s0}=4.85	Q_{p0}=2.39, Q_{s0}=2.20	Q_{p0}=1.42, Q_{s0}=1.25
PS	Q_{p0}=3.55, Q_{s0}=7.05	Q_{p0}=1.39, Q_{s0}=4.50	Q_{p0}=0.70, Q_{s0}=3.95

For bifurcation-free operation, the frequency shifts relative to ω_0 are compared in Fig. 4-14 for selected k. The SS topology as shown has no frequency shift. The SP topology has the largest frequency shift above ω_0. The PP topology also has a frequency shift above the ω_0, but is less than that of the SP topology. The PS topology has a frequency shift below ω_0. The absolute frequency shift of the PS topology at low Q_s is less than that of the PP topology. To minimize the pickup frequency detuning effects, the SS topology is the best choice, while the SP topology should be avoided, and the PS topology is a better choice than the PP topology.

InductEV, Inc.
Exhibit 1008
Page 131



(a) k=0.2. (b) k=0.4. (c) k=0.6.

Fig. 4-14. Frequency shifts for bifurcation-free operations.

4-5.4 DESIGN CONSIDERATIONS

It is usually assumed that a variable-frequency controlled ICPT system requires bifurcation-free operation, as it is very difficult for a standard variable-frequency controller to distinguish the different operating modes in the bifurcation region due to the fact that the operating frequency of each mode is load dependent. Using the load model developed in chapter 3, the bifurcation boundary can be determined to ensure bifurcation-free operation when a variable-frequency controller operating with unity DPF is used. The bifurcation boundary is a relation between k and Q_{s0}. With a given Q_{s0}, bifurcation occurs as k is improved over this boundary. For a given k, bifurcation occurs when Q_{s0} is increased across this boundary. The bifurcation boundary is topology dependent. With a given k, the maximum Q_{s0} of the SP and PS topologies for bifurcation-free operation is much higher than the SS and PP topologies.

The primary resonance design determined by (4-3) assumes the primary and secondary resonance is independent of each other. However, with improved k and increased Q_s the interactions between the primary and secondary resonant circuits may affect system behaviour significantly. This does not present a problem to the SS topology, but does for the other topologies. A series-compensated secondary reflects no reactance when operating at ω_0 as noted in section 3-7.1, and the primary can be completely tuned with the selected primary capacitance in series connection. However, a parallel-compensated secondary reflects a capacitive reactance when operating at this frequency, and this reflected reactance is not tuned by the selected primary capacitance. Both series and parallel-compensated secondary systems reflect a resistance representing the power transfer. Since this reflected resistance is in series with the primary coil, the selected primary capacitance is unable to tune

InductEV, Inc.
Exhibit 1008
Page 132

the reactance of the primary coil completely in a parallel-compensated primary system. The only exception is the PP topology, where complete tuning can be achieved if k and Q_s are carefully selected as explained in section 4-5.2.

Since the load resonant tank is not properly tuned, system operation will deviate from the design point. With a fixed-frequency controller operating at ω_0, the power supply will operate with a DPF less than unity. Using a variable-frequency controller operating with unity DPF, the operating frequency will shift away from ω_0 and bifurcation may occur. Such deviations are small when the loading effects of the secondary resonant circuit on the primary are negligible. This is true in loosely coupled system (low k) with low Q_s (no bifurcation).

With increased Q_s or improved k, the interactions between the primary and secondary resonant circuits can result in large frequency detuning of the pickup or poor DPF of the power supply. With a large frequency detuning, the assumption of operation about ω_0 is not valid. With a poor DPF, the desired constant primary current is not available when the required VA rating exceeds the capability of the selected power supply. In either case, the system will be unable to deliver the required power.

4-6 A PRACTICAL DESIGN EXAMPLE

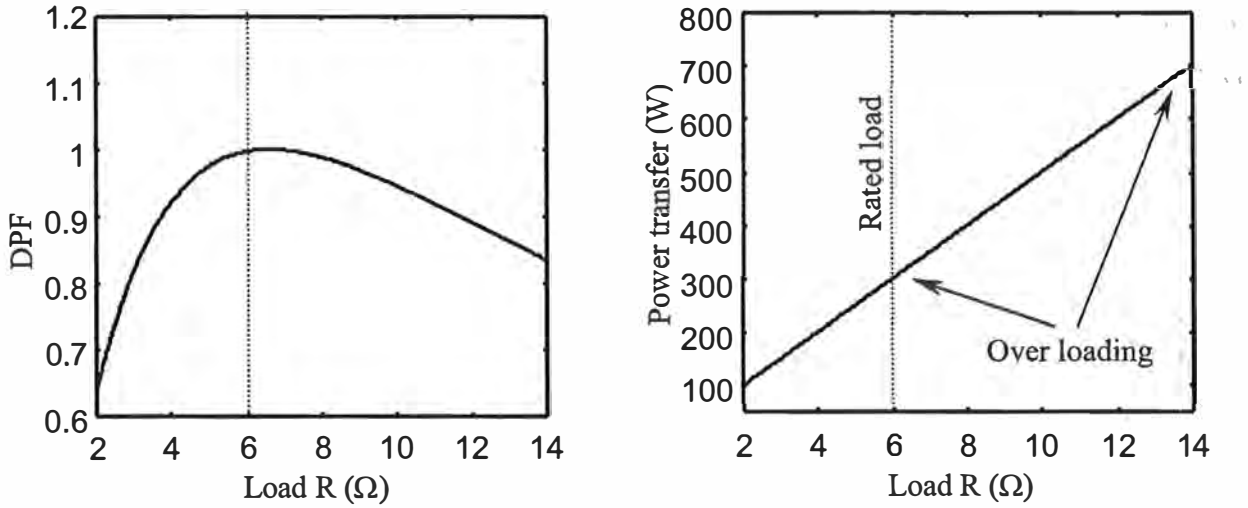
The contact-less electric vehicle battery charger discussed in section 3-11 was designed using the design methodology described in this chapter. The electromagnetic structure, the compensation topology, and the system parameters have been given in section 3-11. Using these parameters, the open circuit voltage (V_{oc}) was calculated as 239V, while the short circuit current (I_{sc}) was determined to be 71A. The maximum power transfer capability without secondary compensation is therefore given by $V_{oc}*I_{sc}/2$ to be 8.5kW. As this value is less than the required power transfer (P) of 30kW, secondary compensation is necessary. The compensation level (the secondary quality factor, Q_{s0}) as determined by $P/(V_{oc}*I_{sc})$ is about 1.8. The rated load is then calculated using (2-23) to be 6Ω. The secondary VA rating as determined by $\sqrt{1+Q_{s0}^2}$ *P is thus 62kVA.

The primary compensation capacitance (C_p) is calculated by (4-3). This primary capacitance is determined to compensate only the self-inductance of the primary coil. Without compensating the loading effects of the secondary resonant circuit on the primary coil, as noted in section 4-5, the system operation will deviate from the design point. For fixed-frequency operation at ω_0, the power supply will operate with a DPF less than unity. For variable-frequency operation with unity DPF, the operating frequency will shift away from ω_0. This section investigates and verifies such deviations for the above battery charger.

With a fixed-frequency controller operating at ω_0 (19.7 kHz), the DPF of the power supply and the

InductEV, Inc.
Exhibit 1008
Page 133

power transfer capability of the pickup assuming constant primary current are shown respectively in Fig. 4-15 (a) and (b). In these figures, the load is extended above rated load to illustrate complete system characteristics, but operation above rated load may be not possible due to the limit of the actual pickup VA rating. The DPF is determined from the phase relationship between the power supply output voltage and current. This phase relationship is calculated using the power supply load impedance developed in section 3-10.1 for the PP topology. The power transfer capability of the pickup when operated at ω_0 is calculated by (3-20). The power curve in this figure and the following similar figures were calculated assuming the primary current was controlled at 15A instead of the rated value of 150A for practical reasons, as this enables the theoretical curves to be verified in the laboratory. Although the primary current is reduced, all the system characteristics presented are identical except that the power level is scaled down by one-hundredth. Since the pickup operates at ω_0, the power curve shows a linear relationship to the load, and rated power of 300W is achieved at rated load.



(a) DPF (b) Power transfer capability (I_p=15A)

Fig. 4-15. DPF and power transfer capability of the contact-less electric vehicle battery charger using a fixed-frequency controller operating at ω_0.

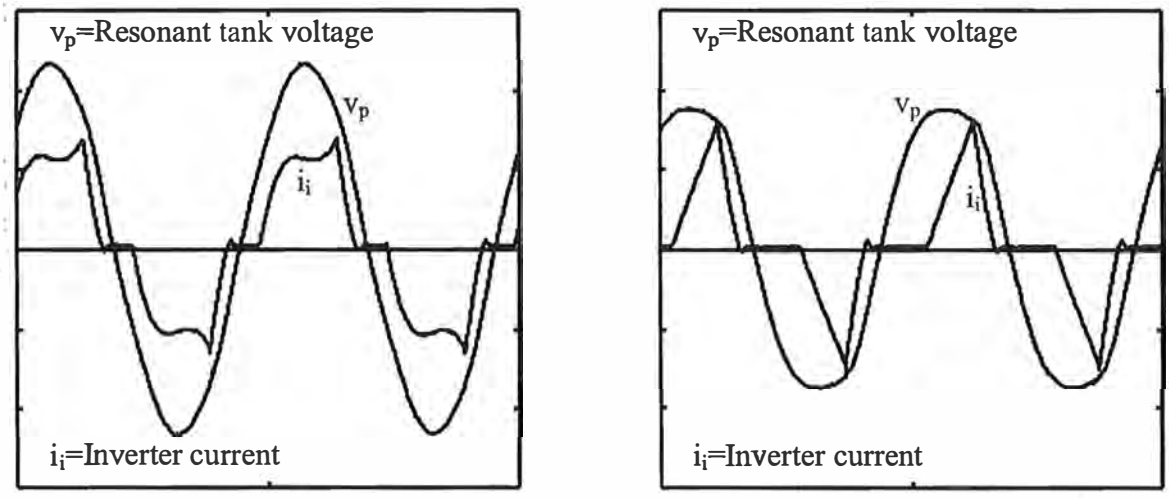
Since the choice of Q_{s0} is close to 2, as noted in section 4-5.2, the DPF of the power supply will be close to unity over a wide range of k allowing a larger tolerance to misalignment between the primary and secondary coils. The magnetic coupling coefficient (k) of the battery charger calculated by (2-1) is 0.45. The necessary Q_{s0} to achieve unity DPF for this coupling condition determined by (4-11) is 1.98 corresponding to a load of 6.6Ω, which is slightly larger than rated load of 6Ω as can be seen in Fig. 4-15 (a). At rated load, the DPF is slightly lower than unity. Due to a suitable choice of k and Q_{s0} for the selected PP topology, the interactions of the primary and secondary resonant circuits do not affect

InductEV, Inc.
Exhibit 1008
Page 134

the DPF of the power supply substantially for rated operation. However, the DPF of the power supply at light load conditions becomes very poor due to such interactions as Q_{s0} drops with the decreasing load.

As part of the experimental set-up, a voltage-fed full-bridge LCL-resonant inverter operating in discontinuous current mode was used to drive the designed system. This inverter will be investigated thoroughly in chapter 8. To simplify the discussion of the PP topology, the series inductor between the inverter and the primary parallel resonant tank is regarded as part of the power supply. As such, the system configuration is formed by a PP topology driven by this power supply. The DPF of the power supply is then determined by measuring the phase relationship between the discontinuous inverter current and the resonant tank voltage.

With the operating frequency controlled at ω_0 (19.7kHz, by manually adjusting the switching instant of the inverter), the measured waveform of the discontinuous inverter current (i_i) and the resonant tank voltage (v_p) are shown in Fig. 4-16 for rated load (6Ω) and a reduced load (3.8Ω). As shown, the fundamental inverter current and the resonant tank voltage are closely in phase at rated load, indicating a DPF close to unity. At the reduced load, there exists a significant phase angle, indicating a DPF less than unity. The inverter current waveform will be investigated further in chapter 8.



(a) Rated load (R=6Ω) (b) A reduced load (R=3.8Ω)

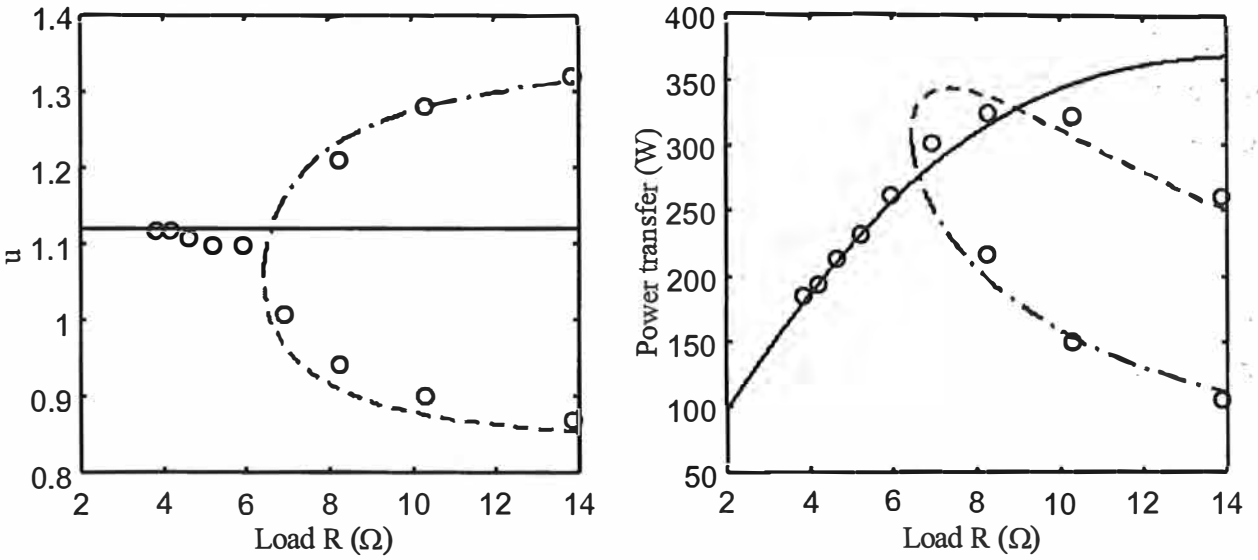
Fig. 4-16. Measured waveforms of the inverter current and the resonant tank voltage for the contact-less electric vehicle battery charger (operating at ω_0=19.7kHz).

Variable-frequency operation with unity DPF (zero-phase angle of the power supply load impedance) was achieved by controlling the inverter current (i_i) to follow the voltage (v_p) across the parallel-compensated primary winding. With this system, operating frequencies can be calculated from the power supply load impedance using:

InductEV, Inc.
Exhibit 1008
Page 135

$$\mathrm{Im}\, Z_t(\omega, R) = 0 \tag{4-14}$$

As shown in Fig. 4-17 (a), the frequencies at which zero-phase angle occurs are actually functions of the load. The power transfer capability when operated along these zero-phase angle frequency profiles can be calculated from (3-20) and are shown in Fig. 4-17 (b). As can be seen, bifurcation occurs as the load is increased slightly above rated load. The measured frequencies and power transfers are shown in Fig. 4-17 as circles at each of the measured loads. In practice, control perturbations and transients affect the operating frequency of the variable-frequency controller in the bifurcation region. In order to investigate and measure the system operating at the three different zero phase angle frequencies and thereby verify the theory, the converter was made to operate in this region by increasing the load beyond rated value while adjusting the turn-on interval of the inverter manually to force a shift between these operating frequencies. Under steady state conditions, the system was found to operate stably at either the lowest or highest zero phase angle frequency since perturbations that give a large positive phase angle will shift operation to the lowest zero phase angle frequency and perturbations that give a large negative phase angle will shift operation to the highest zero phase angle frequency. Stable operation at the middle zero phase angle frequency is not feasible without forcing the frequency (which was not possible with the controller used). As shown, the measured results closely follow the theoretical curves despite simplifications in the model that assume sinusoidal voltages and currents, and ignore losses in the capacitors and inductors.



(a) Operational frequency (b) Power transfer capability (I_p=15A)

Fig. 4-17. Operating frequency and power transfer capability of the contact-less electric vehicle battery charger using a variable-frequency controller operating with unity DPF.

Due to interactions between the primary and secondary resonant circuits, the operating frequency at

InductEV, Inc.
Exhibit 1008
Page 136

rated load (6Ω) is about 10% higher than ω_0. Since the pickup is detuned, the available power at rated load is only 266W. This is more than 10% lower than rated power of 300W.

4-7 CONCLUSIONS

A design methodology is described in this chapter for determination of the operating frequency, the primary current, the electromagnetic structure, the compensation requirement and the secondary quality factor. These design factors are inter-related and have to be selected properly to deliver the required power with minimum total cost.

The load model developed in chapter 3 was then used to evaluate system sensitivity to fundamental design parameters. When the primary compensation does not consider the interactions between the primary and secondary resonant circuits, it is found that the system deviates from design expectations due to influences of the secondary pickup on the primary. These influences depend on the compensation topology (SS, SP, PP and PS), the magnetic coupling coefficient (k) and the secondary quality factor (Q_s).

The influence of the interactions between the primary and secondary resonant circuits is not a problem for the SS topology (series primary and secondary), as the load resonant tank can be properly tuned. However, care must be taken when other topologies are used. With loose magnetic coupling (low k) and low Q_s, the loading effects of the secondary on the primary are negligible in comparison to the primary reactance. In this case, the system works very well since the primary and secondary resonant behaviour are virtually independent of each other. With improved magnetic coupling (high k) and increased Q_s, the secondary loading effect affects the primary resonant behaviour substantially. As a result, the system may operate with a poor displacement power factor under a fixed-frequency controller designed to operate at ω_0. For a variable-frequency controlled system operating with unity displacement power factor, the system may have significant pickup frequency detuning. With poor displacement power factor, the system operation may exceed the VA rating of the power supply. With large frequency detuning, the pickup may have a substantial drop in power transfer capability. In both cases, the system may be unable to deliver the required power.

Moreover, under variable-frequency control three operating modes may exist in the frequency spectrum, and as such the system may become uncontrollable. Bifurcation occurs when either the secondary quality factor or the magnetic coupling coefficient increase. Bifurcation limits are once again topology dependent. For well-coupled system (high k), bifurcation may occur with a Q_s less than 2.

The design methodology was applied to a practical example for contact-less electric vehicle battery

InductEV, Inc.
Exhibit 1008
Page 137

charging, and verified under fixed and variable frequency control respectively. The system behaviour is predicable, and clearly shows where improvements can be made.

REFERENCES

[1]. Gyu Bum Joun, B. H. Cho, "An energy transmission system for an artificial heart using leakage inductance compensation of transcutaneous transformer," *IEEE Transactions on Power Electronics,* vol. 13, pp. 1013-1022, Nov. 1998.

[2]. J. Lukacs, M. Kiss, I. Nagy, G. Gonter, R. Hadik, K. Kaszap, A. Tarsoly, "Inductive energy collection for electric vehicles," in *Conf. Rec. Fourth Power Electronics Conference*, 1981, pp. 71-81.

[3]. J. M. Barnard, J. A. Ferreira, J. D. van Wyk, "Sliding transformers for linear contactless power delivery," *IEEE Transactions on Industrial Electronics*, vol. 44, pp. 774-779, Dec. 1997.

[4]. A. Esser, H.-C. Skudelny, "A new approach to power supplies for robots," *IEEE Transactions on Industry Applications*, vol. 27, pp. 872-875, 1991.

[5]. A. Kawamura, K. Ishioka, J. Hirai, "Wireless transmission of power and information through one high-frequency resonant AC link inverter for robot manipulator applications," *IEEE Transactions on Industry Applications*, vol. 32, pp. 503-508, May-June 1996.

[6]. D. A. G. Pedder, A. D. Brown, J. A. Skinner, "A contactless electrical energy transmission system," *IEEE Transactions on Industrial Electronics*, vol. 46, pp. 23-30, Feb. 1999.

[7]. J. T. Boys, G. A. Covic, A. W. Green, "Stability and control of inductively coupled power transfer systems," *IEE Proceedings-Electric Power Applications*, vol. 147, pp. 37-43, Jan. 2000.

[8]. G. A. Covic, G. Elliott, O. H. Stielau, R. M. Green, J. T. Boys, "The design of a contact-less energy transfer system for a people mover system," in *Conf. Rec. International Conference on Power System Technology*, vol. 1, Dec. 2000, pp. 79-84.

[9]. Chwei-Sen Wang, G. A. Covic, O. H. Stielau, "General stability criterions for zero phase angle controlled loosely coupled inductive power transfer systems," in *Conf. Rec. The 27th Annual Conference of the IEEE Industrial Electronics Society,* vol. 2, 2001, pp. 1049-1054.

[10]. A. P. Hu, *Selected resonant converters for IPT power supplies*, PhD thesis, The Electrical and Electronics Engineering Department, The University of Auckland, Auckland, New Zealand, 2001, pp. 151-167.

[11]. A. W. Green, "Modelling a push-pull parallel resonant converter using generalised state-space averaging," *IEE Proceedings-Electric Power Applications*, vol. 140, pp. 350-356, Nov. 1993.

InductEV, Inc.
Exhibit 1008
Page 138

[12]. O. H. Stielau, G. A. Covic, "Design of loosely coupled inductive power transfer systems," in *Conf. Rec. International Conference on Power System Technology*, vol. 1, Dec. 2000, pp. 85-90.

[13]. J. B. Turner, G. W. Roth, "Regulator for inductively coupled power distributions system," *US-Patent No. 4914539*, Apr. 3, 1990.

[14]. A. W. Kelley, W. R. Owens, "Connectorless power supply for an aircraft-passenger entertainment system," *IEEE Transactions on Power Electronics*, vol. 4, pp. 348-354, July 1989.

[15]. J. T. Boys, A. W. Green, "Inductive power distribution system," *US-Patent No. 5293308*, Mar. 8, 1994.

[16]. A. W. Green, J. T. Boys, "An inductively coupled high-frequency power system for material handling applications," in *Conf. Rec. International Power Electronics*, vol. II, 1993, pp. 821-826.

[17]. J. T. Boys, G. A. Covic, Yongxiang Xu, "DC analysis technique for inductive power transfer pick-ups," *IEEE Power Electronics Letters*, vol. 1, pp. 51-53, June 2003.

[18]. J. T. Boys, G. A. Covic, J. E. James, "Switching frequencies in inductively coupled power transfer systems,' in C*onf. Rec. International Power Engineering Conference*, Nov. 2003.

[19]. J. T. Boys, G. A. Covic, G. A. J. Elliott, "Pick-up transformer for ICPT applications," *Electronics Letters*, vol. 38, pp. 1276-1278, Oct. 2002.

InductEV, Inc.
Exhibit 1008
Page 139

InductEV, Inc.
Exhibit 1008
Page 140

CHAPTER 5

TUNING TO IMPROVE POWER TRANSFER FOR VARIABLE-FREQUENCY SYSTEMS

5-1 Introduction
5-2 Primary tuning for unity DPF at rated load
5-3 Power transfer capability and bifurcation phenomenon
5-4 Bifurcation criteria
5-5 Discussion
5-6 Verification
5-7 Conclusions

5-1 INTRODUCTION

In variable-frequency systems, the operating frequency can vary from the desired pick-up tuned frequency (ω_0) with changes in load, thereby affecting the power transfer capability of the system. In this chapter, improvements in the system's power transfer capability are investigated by modifying the primary tuning assumed with the design methodology described in Chapter 4.

Modifying the secondary compensation capacitance also affects the system's power transfer characteristics, however this modification results in a change to the secondary resonant frequency. This is undesirable under the design methodology described in Chapter 4 since the required power transfer to the pickup can only be guaranteed whenever the secondary resonant circuit is tuned to the nominal operating frequency (ω_0). As previously shown, the load resonant tank tuning has a marked effect on the system's frequency deviations, consequently the focus of this chapter is the appropriate selection of the primary compensation capacitance (C_p) to minimise variations from ω_0 (over the operating load range).

Theoretically, an ideal solution could be achieved if C_p were able to be dynamically tuned [1]. However, this is normally not preferred in a practical system due to the complexity and cost of the control means necessary to achieve this. In this chapter, the aim is then to first select the best C_p that improves the tuning of the load resonant tank when operating at rated load. Following this the power transfer capability and bifurcation phenomenon under variable-frequency operation are investigated to find out the influences of the compensation topologies (SS, SP, PP and PS) as well as the fundamental parameters k (the magnetic coupling coefficient) and $Q_{s0,rated}$ (the secondary quality factor at ω_0 and rated load) determined with the design methodology described in Chapter 4. A general bifurcation

InductEV, Inc.
Exhibit 1008
Page 141

criterion is developed for each topology to ensure the system can deliver the necessary power stably over the full operating range. Finally the theory is verified using a practical design example. System behaviour under fixed-frequency operation is analysed in the following chapter.

5-2 PRIMARY TUNING FOR UNITY DPF AT RATED LOAD

In this chapter, all of the design parameters are assumed to be determined following the standard design process outlined in chapter 4 except the primary compensation capacitance (C_p). Thus the focus here is on using the load impedance model developed in section 3-10 to determine a suitable modification to C_p.

In order to minimize the VA rating of the power supply, it is desirable to operate at the zero phase angle frequency of the load impedance (Z_t). At this frequency, the load reactance (Im Z_t) seen by the power supply is zero, and the DPF of the power supply is unity. This zero phase angle frequency must be designed to equal ω_0 to ensure maximum power meets the required power. The design solution to achieve this objective can be determined using:

$$\operatorname{Im} Z_{t0} = \operatorname{Im} Z_t(\omega = \omega_0) = 0 \tag{5-1}$$

To meet this condition, C_p is designed here to compensate not only the self-inductance of the primary coil (L_p) but also the reflected impedance (Z_r). The necessary C_p as derived in Appendix H is:

$$C_p = \begin{cases} \dfrac{C_s L_s}{L_p} & \text{SS topology} \\ \dfrac{C_s L_s}{L_p}\left(\dfrac{1}{1-k^2}\right) & \text{SP topology} \\ \dfrac{C_s L_s}{L_p}\left(\dfrac{1-k^2}{Q_{s0}^2 k^4 + (1-k^2)^2}\right) & \text{PP topology} \\ \dfrac{C_s L_s}{L_p}\left(\dfrac{1}{Q_{s0}^2 k^4 + 1}\right) & \text{PS topology} \end{cases} \tag{5-2}$$

For a general analysis, a normalized primary compensation capacitance (C_{pn}) is defined here using the C_p assumed earlier with the design methodology described in chapter 4 (equation 4-3). Thus:

$$C_{pn} = \frac{C_p}{\dfrac{C_s L_s}{L_p}} \tag{5-3}$$

Substituting (5-2) into (5-3) results in:

InductEV, Inc.
Exhibit 1008
Page 142

$$C_{pn}=\begin{cases}1 & \text{SS topology}\\ \dfrac{1}{1-k^2} & \text{SP topology}\\ \dfrac{1-k^2}{Q_{s0}^2k^4+\left(1-k^2\right)^2} & \text{PP topology}\\ \dfrac{1}{Q_{s0}^2k^4+1} & \text{PS topology}\end{cases} \tag{5-4}$$

The value of C_{pn} as shown depends on three factors: the compensation topologies (SS, SP, PP and PS), the magnetic coupling coefficient (k) and the secondary quality factor (Q_{s0}) at ω_0. As expected, C_{pn} is unity when an SS topology is used and there is no need to modify C_p from the original tuning because the load resonant tank has been properly tuned (as noted in section 4-5). However, a different C_p ($C_{pn}\neq 1$) is necessary when the other three topologies are used.

As can be seen in (5-4), the selected primary and secondary compensation topologies play a large role in the correct choice of C_p. Since a series-compensated secondary reflects no reactance at ω_0, the primary inductance can be "tuned out" (independent of either k or Q_{s0}) using a series-connected capacitance in the primary network. Although this SS topology seems to be the best choice regarding primary resonance design, parallel compensation may be preferred in the primary and/or secondary resonant circuits for practical reasons [2-8]. The required C_p in these topologies (SP, PP and PS) is dependent on k. As a parallel-compensated secondary reflects a load-independent capacitive reactance at ω_0, the required C_p for a series tuned primary in this case (the SP topology) is independent of Q_{s0}. However, the required C_p for a parallel tuned primary (the PP and PS topologies) is a function of Q_{s0} and consequently load. The reflected impedance contains a real component representing the load in series with the primary self-inductance, and consequently parallel tuning of the primary coil is load dependent. It is impractical to allow C_p to vary with the load, thus C_p must be chosen for a selected load point. Given that the designer must ensure maximum power can be delivered, the logical choice is to select C_p for the rated power point. The required C_{pn} is thus:

$$C_{pn}=\begin{cases}1 & \text{SS topology}\\ \dfrac{1}{1-k^2} & \text{SP topology}\\ \dfrac{1-k^2}{Q_{s0,rated}^2k^4+\left(1-k^2\right)^2} & \text{PP topology}\\ \dfrac{1}{Q_{s0,rated}^2k^4+1} & \text{PS topology}\end{cases} \tag{5-5}$$

With this approach, the designed power should be delivered for all loading (Q_{s0}) variations within the design range.

InductEV, Inc.
Exhibit 1008
Page 143

As shown above, k and/or $Q_{s0,rated}$ must be included in the choice of C_p. In order to investigate the effects of k and $Q_{s0,rated}$ on the proposed primary resonance design, C_{pn} (as determined by (5-5)) is shown in Fig. 5-1 as a function of k, for $Q_{s0,rated}$ of 2, 5 and 10. While no change to the original tuning is required for the SS topology, the SP topology is shown to require a larger C_p with better coupling. The PP topology requires a slightly larger C_p for loose coupling with low $Q_{s0,rated}$, but needs a smaller C_p if the coupling is improved or $Q_{s0,rated}$ is increased. A smaller C_p is always required for the PS topology and the change becomes larger with better coupling or higher $Q_{s0,rated}$.

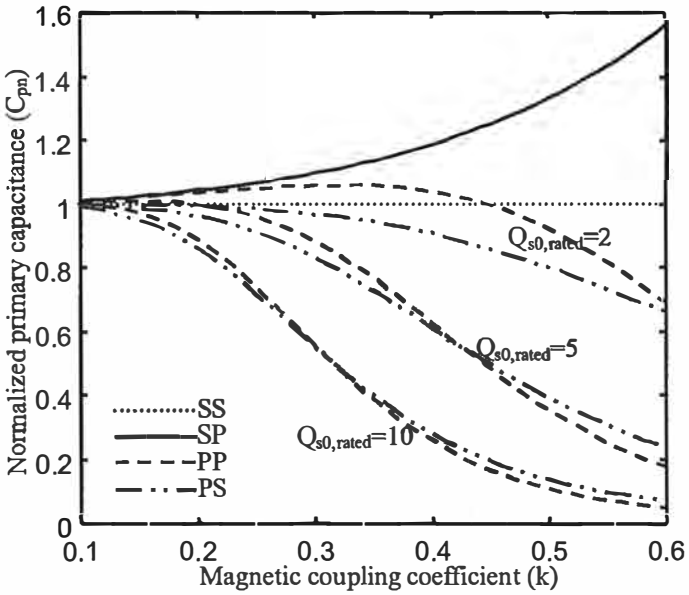


Fig. 5-1. Primary tuning for unity DPF at rated load.

To increase the power transfer capability of ICPT systems, effort has gone into improving the magnetic coupling between the primary and secondary, and coupling coefficients for single pickup applications of between 0.3 and 0.6 are often achievable [2], [8]. For multiple pickup applications, system constraints usually result in coupling coefficients of less than 0.1 per pickup [6], [7]. However, as discussed later in Chapter 9, the effect of all pickups together is often again equivalent to a single pickup with a coupling coefficient of about 0.2 to 0.5.

As shown in Fig 5-1, systems with such high coupling coefficients behave very differently to loosely coupled systems. For coupling coefficients of less than 0.2, the system can be considered loosely coupled and the original tuning gives a good result. However, as the coupling improves the system characteristics change substantially. This change is a strong function of both the system topology as well as $Q_{s0,rated}$ that could present a problem in SP, PP and PS topologies. With a $Q_{s0,rated}$ equal to 10, the PP and PS topologies start deviating from the loosely coupled theory at coupling coefficients exceeding about 0.2, while for lower $Q_{s0,rated}$ values of 2 the deviation only occurs at coupling coefficients exceeding about 0.5.

InductEV, Inc.
Exhibit 1008
Page 144

Practical ICPT systems are normally either loosely-middle coupled with medium-high Q_s or middle-well coupled with low-medium Q_s. Examples of C_{pn} are given in Table 5-1 for both systems assuming $Q_{s0,rated}$ of 10 (high Q_s) and 5 (medium Q_s). For loosely coupled high Q_s systems (k=0.1, $Q_{s0,rated}$=10), the required C_p is close to the original tuning (C_{pn}=1) as the reflected impedance is negligible. For middle coupled high Q_s systems (k=0.2, $Q_{s0,rated}$=10), the design can change by as much as 4% for an SP topology, 11% for a PP topology and 14% for a PS topology. For middle coupled medium Q_s systems (k=0.2, $Q_{s0,rated}$=5), the required C_p for the PP topology is again close to the original tuning, while the required change to C_p for the SP and PS topologies is about 4%. The well coupled medium Q_s systems (k=0.4, $Q_{s0,rated}$=5) change the design significantly by 19% for an SP topology, 38% for a PP topology and 39% for a PS topology.

TABLE 5-1
PRIMARY TUNING FOR UNITY DPF AT RATED LOAD

Topology	C_{pn}			
	$Q_{s0,rated}$=10		$Q_{s0,rated}$=5	
	k=0.1	k=0.2	k=0.2	k=0.4
SS	1	1	1	1
SP	1.01	1.04	1.04	1.19
PP	1.00	0.89	1.00	0.62
PS	0.99	0.86	0.96	0.61

From the above it can be seen that the original tuning works well for the SS topology, and for other topologies with low $Q_{s0,rated}$ (less than 2) or coupling coefficients less than 0.2. Special care needs to be taken when designing systems with either PP or PS topologies.

5-3 POWER TRANSFER CAPABILITY AND BIFURCATION PHENOMENON

In order to investigate the effects of the modified tuning on the power transfer capability, here the power transfer is normalized using the rated power determined at rated load ($Q_{s0,rated}$) and ω_0 (u=1). As noted in section 3-6 (equation 3-20), the power transfer to a secondary pickup is given by the square of the primary current (I_p) multiplied by the reflected resistance (Re Z_r). Assuming constant primary current, the normalized power P_n is then:

$$P_n = \frac{P}{P_{rated}} = \frac{(\mathrm{Re}\,Z_r)I_p^2}{(\mathrm{Re}\,Z_{r0,rated})I_p^2} = \frac{\mathrm{Re}\,Z_r}{\mathrm{Re}\,Z_{r0,rated}} = \left(\frac{\mathrm{Re}\,Z_r}{\mathrm{Re}\,Z_{r0}}\right)\left(\frac{\mathrm{Re}\,Z_{r0}}{\mathrm{Re}\,Z_{r0,rated}}\right) = (\mathrm{Re}\,Z_{rn})\left(\frac{\mathrm{Re}\,Z_{r0}}{\mathrm{Re}\,Z_{r0,rated}}\right) \qquad (5\text{-}6)$$

where (Re Z_{rn}) is the normalized reflected resistance, (Re Z_{r0}) is the reflected resistance at ω_0, and (Re

InductEV, Inc.
Exhibit 1008
Page 145

$Z_{r0,rated}$) is the rated reflected resistance at ω_0. These parameters are defined in section 3-7.

Substituting (3-26) into (5-6) results in:

$$P_n = (\mathrm{Re}\,Z_{rn})\left(\frac{\mathrm{Re}\,Z_{r0}}{\mathrm{Re}\,Z_{r0,rated}}\right) = (\mathrm{Re}\,Z_{rn})\left(\frac{\left(\frac{\omega_0 M^2}{L_s}\right)Q_{s0}}{\left(\frac{\omega_0 M^2}{L_s}\right)Q_{s0,rated}}\right) = (\mathrm{Re}\,Z_{rn})\left(\frac{Q_{s0}}{Q_{s0,rated}}\right) \tag{5-7}$$

Since (Re Z_{rn}) is a function of u and Q_{s0} as shown in (3-34), P_n is also a function of u and Q_{s0}. In addition, it is related to the specified rated load ($Q_{s0,rated}$).

To calculate P_n for variable-frequency systems, the operating frequency needs to be determined. Here it is assumed the power supply operates with unity DPF by allowing the frequency to vary with the load (Q_{s0}). At this frequency the phase angle of the load impedance (Z_t) is zero. Similar to the analysis in section 4-5.3, this operating frequency can be calculated using the normalized load impedance (Z_{tn}) by:

$$\mathrm{Im}\,Z_{tn}(u,k,Q_{s0}) = 0 \ \textbf{or}\ \mathrm{Im}\,Y_{tn}(u,k,Q_{s0}) = 0 \tag{5-8}$$

The normalized load impedance developed in section 3-10.2 can be reused providing the normalized reactance for C_p (defined as "$1/[\omega C_p(\mathrm{Re}\,Z_{r0})]$") is modified to include the changes proposed to C_p in this chapter. For convenience, the normalized load impedance is summarized in Table 5-2 with the function of each term given in Table 5-3. Here C_{pn} is unity for systems tuned using the approach described in Chapter 4 (hereafter labelled as "original tuning"). For systems using the modified tuning methodology proposed in section 5-2 (hereafter labelled as "modified tuning"), it is topology dependent as given by (5-5).

TABLE 5-2
NORMALIZED LOAD IMPEDANCES WITH COMPENSATED PICKUP

Series primary: $Z_{tn} = \frac{Z_t}{\mathrm{Re}\,Z_{r0}} = \mathrm{Re}\,Z_{tn} + j\,\mathrm{Im}\,Z_{tn}$	$\mathrm{Re}\,Z_{tn} = \mathrm{Re}\,Z_{rn}$
	$\mathrm{Im}\,Z_{tn} = -\frac{1}{\omega C_p(\mathrm{Re}\,Z_{r0})} + \frac{\omega L_p}{\mathrm{Re}\,Z_{r0}} + \mathrm{Im}\,Z_{rn}$
Parallel primary: $Z_{tn} = \frac{1}{Y_{tn}} = \frac{1}{\mathrm{Re}\,Y_{tn} + j\,\mathrm{Im}\,Y_{tn}}$	$\mathrm{Re}\,Y_{tn} = \frac{\mathrm{Re}\,Z_{rn}}{(\mathrm{Re}\,Z_{rn})^2 + \left(\frac{\omega L_p}{\mathrm{Re}\,Z_{r0}} + \mathrm{Im}\,Z_{rn}\right)^2}$
	$\mathrm{Im}\,Y_{tn} = \omega C_p(\mathrm{Re}\,Z_{r0}) - \frac{\frac{\omega L_p}{\mathrm{Re}\,Z_{r0}} + \mathrm{Im}\,Z_{rn}}{(\mathrm{Re}\,Z_{rn})^2 + \left(\frac{\omega L_p}{\mathrm{Re}\,Z_{r0}} + \mathrm{Im}\,Z_{rn}\right)^2}$

InductEV, Inc.
Exhibit 1008
Page 146

TABLE 5-3
FUNCTIONS OF THE NORMALIZED LOAD IMPEDANCE WITH MODIFIED TUNING

$\frac{1}{\omega C_p(\mathrm{Re}Z_{r0})} = \begin{cases} \frac{Q_{p0}}{uC_{pn}} = \frac{1}{uk^2Q_{s0}C_{pn}} \\ \left(\frac{1}{uC_{pn}}\right)\left(Q_{p0}+\frac{1}{Q_{s0}}\right) = \frac{1}{uk^2Q_{s0}C_{pn}} \end{cases}$	Series secondary. Parallel secondary.
$\frac{\omega L_p}{\mathrm{Re}Z_{r0}} = \begin{cases} uQ_{p0} = \frac{u}{k^2Q_{s0}} \\ u\left(Q_{p0}+\frac{1}{Q_{s0}}\right) = \frac{u}{k^2Q_{s0}} \end{cases}$	Series secondary. Parallel secondary.
$\mathrm{Re}Z_{rn} = \frac{\mathrm{Re}Z_r}{\mathrm{Re}Z_{r0}} = \begin{cases} \frac{u^4}{(u^2-1)^2Q_{s0}^2+u^2} \\ \frac{u^2}{(u^2-1)^2Q_{s0}^2+u^2} \end{cases}$	Series secondary. Parallel secondary.
$\mathrm{Im}Z_{rn} = \frac{\mathrm{Im}Z_r}{\mathrm{Re}Z_{r0}} = \begin{cases} \frac{-u^3(u^2-1)Q_{s0}}{(u^2-1)^2Q_{s0}^2+u^2} \\ \frac{-u^3[(u^2-1)Q_{s0}+1/Q_{s0}]}{(u^2-1)^2Q_{s0}^2+u^2} \end{cases}$	Series secondary. Parallel secondary.

With k and $Q_{s0,rated}$ determined using the design methodology described in Chapter 4, the normalized operating frequency (u) determined using (5-8) is a function of Q_{s0} (load) as shown in Fig. 5-2 to 5-9 for all four basic topologies (SS, SP, PP and PS). The normalized power transfer capability (P_n) when operating at this frequency calculated using (5-7) is also shown in Fig. 5-2 to 5-9. Here, the modified tuning is shown as solid lines, while dashed lines represent the original tuning. Bifurcation as shown is a common phenomenon in all topologies. Bifurcation occurs when Q_s is high, and improving k simply results in the appearance of bifurcation at lower Q_s.

In the analysis of each topology, the value of k is assumed to be 0.05, 0.2 and 0.4 to represent systems that are loosely coupled, middle coupled or well coupled. Typical loosely coupled systems are track-type ICPT systems, where the secondary pickup moves along a long track, and couples only with a small portion of the primary cable extended along the track. If in such systems, the primary is required to supply power to many secondary pickups distributed along the track, the coupling will increase and equivalently become mid-coupled or well-coupled systems (as noted later in Chapter 9). Typical mid-coupled or well-coupled systems are coil-type ICPT systems used in battery charging applications, where often both the primary and secondary are concentrated coils.

As expected, the frequency and power curves when tuned using the approach described in Chapter 4 ("original tuning") are independent of $Q_{s0,rated}$ in each topology as C_p is not load dependent. For the SS

InductEV, Inc.
Exhibit 1008
Page 147

topology, the modified tuning proposed in this chapter and the original tuning are identical. With the SP topology, the frequency and power curves for the modified tuning are also independent of $Q_{s0,rated}$. Here the independency to $Q_{s0,rated}$ arises from the fact that the required C_p is independent of load. In order to draw the power curves, $Q_{s0,rated}$ is arbitrary assumed to be close to, but still within the bifurcation boundary. Other values can be used for $Q_{s0,rated}$ but this only changes the scale of the power curves.

The PP and PS topologies with the modified tuning are more complex as the required C_p is load dependent. The frequency and power curves strongly depend on C_p, and it is assumed here that C_p is designed to achieve unity DPF at $Q_{s0,rated}$. The analysis here investigates three systems with different values of $Q_{s0,rated}$. The first system assumes $Q_{s0,rated}$ is well within the bifurcation boundary. The second system has $Q_{s0,rated}$ close to, but still within the bifurcation boundary. The third system has a value of $Q_{s0,rated}$ slightly higher so that bifurcation occurs at rated load. This later system is neither desirable nor practical and should be avoided as demonstrated by the effect this has a poor power transfer capability due to large frequency detuning.

The possible improvements in the power transfer capability that arise from the modified tuning depends on the system topology as well as k, Q_{s0} and $Q_{s0,rated}$ as discussed following.

SS Topology: As noted in section 4-5.3, the SS topology is theoretically the most desirable and there is no need to change C_p. Here operating at ω_0 is achievable for all loading conditions (any Q_s). In theory, there is no pickup frequency detuning providing the operation is constrained to the bifurcation-free region, and the power transfer capability increases linearly with the load as shown in Fig. 5-2. For the selected k of 0.05, 0.2 and 0.4, bifurcation occurs at Q_{s0} of about 20, 5 and 2.5, and as such $Q_{s0,rated}$ is selected as 18, 4.5 and 2.2 respectively to ensure maximum and stable power transfer.

SP Topology: Since the required change in C_p for the SP topology is independent of Q_{s0}, operating at ω_0 is achievable for all loading conditions (any Q_{s0}) as shown in Fig. 5-3. It is noted that the influences of k and Q_s on the operating frequency and the bifurcation phenomenon of the SS and SP topologies are similar. Both are able to operate at ω_0 under all loading conditions, which is a major improvement for the SP topology. The bifurcation boundary of the SP topology is slightly lower than that of the SS topology. For the selected k of 0.05, 0.2 and 0.4, bifurcation occurs at Q_{s0} of about 20, 4.9 and 2.3, and as such $Q_{s0,rated}$ is selected as 18, 4.5 and 2.2 respectively to ensure maximum and stable power transfer. Rated power is achieved (P_n=1) at $Q_{s0,rated}$ with the modified tuning, while the original tuning is unable to deliver rated power (P_n<1) due to pickup frequency detuning. The improvement in power transfer capability strongly depends on Q_{s0} and k. With a Q_{s0} much lower than $Q_{s0,rated}$, the improvement is negligible but becomes significant at $Q_{s0,rated}$ when k is high. With a k of

InductEV, Inc.
Exhibit 1008
Page 148

0.05, it is about 4% only and increases to 28% when k is 0.2, and 64% if k is 0.4.

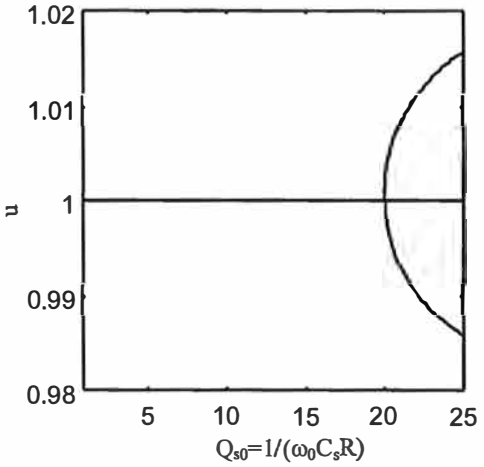
With the SS and SP topologies, one of the three operating modes in the bifurcation region shows no pickup frequency detuning. This could be exploited to deliver greater power providing a suitable variable-frequency controller could utilize this feature to enable stable operation within the bifurcation region and providing the VA rating of the secondary is not exceeded. However, pickup frequency detuning is unavoidable if the system chooses to operate in either of the other two operating modes.

PP Topology: Because C_p of the PP topology is selected to achieve unity DPF at rated load, operating at ω_0 is achievable only at $Q_{s0,rated}$ as shown in Fig. 5-4 to 5-6. In addition to k and Q_{s0}, the value of $Q_{s0,rated}$ affects the operating frequency and power transfer capability because the required C_p is dependent on $Q_{s0,rated}$. If $Q_{s0,rated}$ is within the bifurcation boundary, the modified tuning is able to reduce pickup frequency detuning, resulting in improved power transfer capability for all loading conditions up to and including rated load. With $Q_{s0,rated}$ at or within the bifurcation region, the modified tuning undesirably increases the pickup frequency detuning at all loading conditions within the bifurcation boundary and as such the pickup power transfer capability becomes lower. It is necessary to avoid this situation when using the modified tuning proposed in this chapter. To achieve this objective, a general bifurcation criterion is developed in section 5-4.

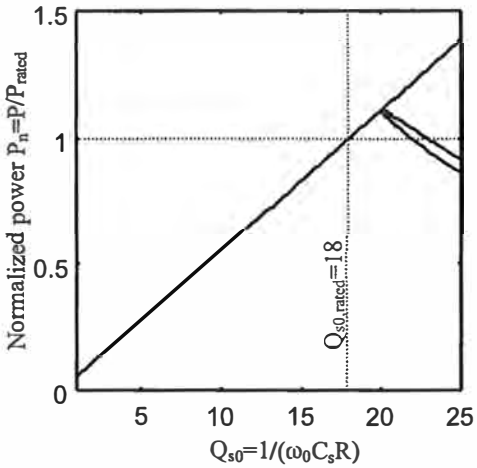
For this topology, the load (Q_{s0}) at which bifurcation occurs is higher than the original tuned system, resulting in a larger safety margin. This improvement is significant if the selected $Q_{s0,rated}$ is well within the bifurcation boundary. The bifurcation boundary of the PP topology is similar to the SP topology discussed above. For the selected k of 0.05, 0.2 and 0.4, bifurcation occurs also at Q_{s0} of about 20, 4.9 and 2.3. If $Q_{s0,rated}$ is well within the bifurcation boundary, the difference in the operating frequency and power transfer capability between the modified tuning and the original tuning is small or negligible below rated load. Once again the improvement in power transfer capability becomes significant when $Q_{s0,rated}$ is close to but within the bifurcation boundary in high k systems. With k of 0.05, this improvement is negligible. As k improves to 0.2, it is 3% only. At a k of 0.4, the improvement increases to about 15%.

PS Topology: Similar to the PP topology, the C_p of the PS topology is modified to achieve unity DPF at rated load and as such operating at ω_0 is only achieved at $Q_{s0,rated}$ as shown in Fig. 5-7 to 5-9. With $Q_{s0,rated}$ within the bifurcation boundary, the modified tuning is able to improve the power transfer capability under all loading conditions up to and including rated load. With systems where bifurcation occurs at $Q_{s0,rated}$, rated power is only available in the bifurcation area where the controller is normally unstable, thus this design should be avoided. A general bifurcation criterion is developed in section 5-4 to enable suitable values of k and $Q_{s0,rated}$ to be determined such that the system design is within the bifurcation boundary.

InductEV, Inc.
Exhibit 1008
Page 149

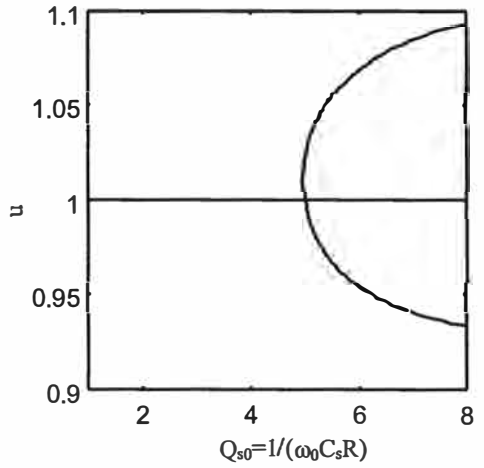


(i) Operating frequency.

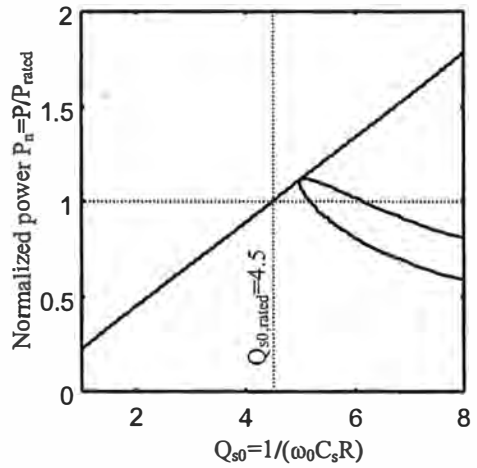


(ii) Power transfer capability.

(a) A loosely coupled system (k=0.05).

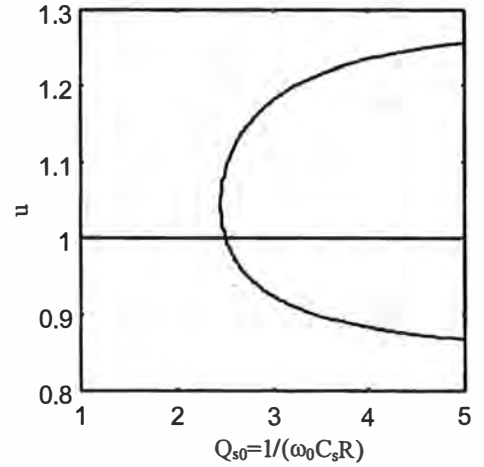


(i) Operating frequency.

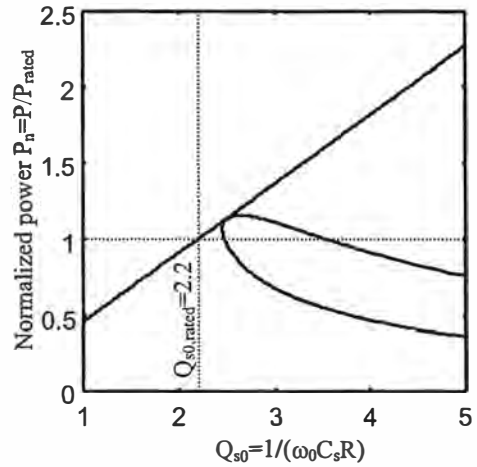


(ii) Power transfer capability.

(b) A mid-coupled system (k=0.2).



(i) Operating frequency.

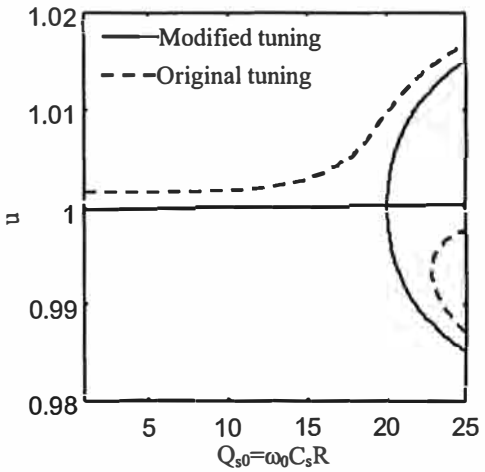


(ii) Power transfer capability.

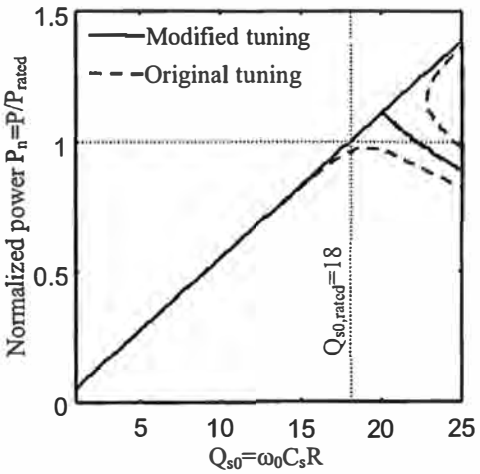
(c) A well-coupled system (k=0.4).

Fig. 5-2. SS topology - Operating frequency and power transfer capability under variable-frequency operation.

InductEV, Inc.
Exhibit 1008
Page 150

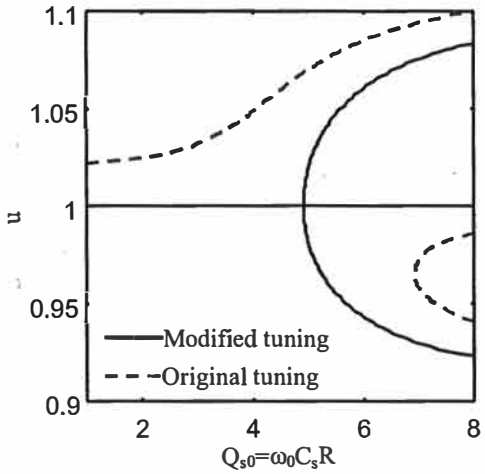


(i) Operating frequency.

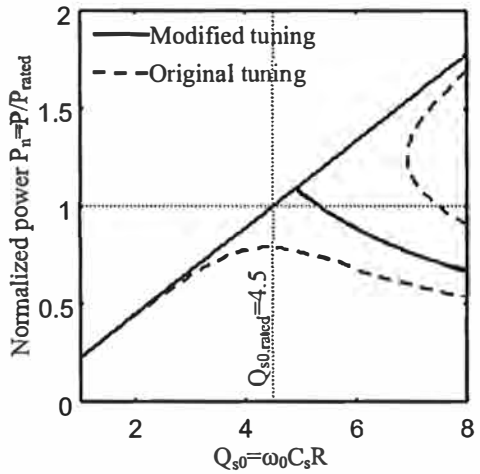


(ii) Power transfer capability.

(a) A loosely coupled system (k=0.05).

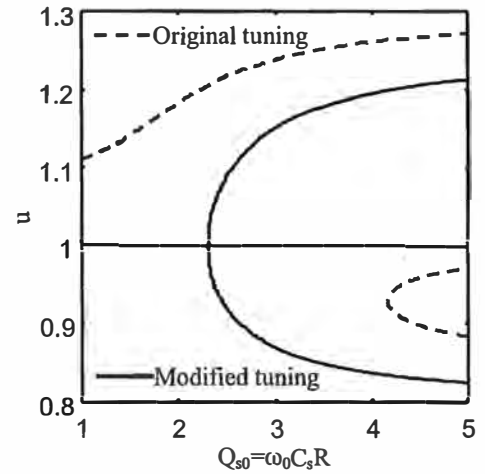


(i) Operating frequency.

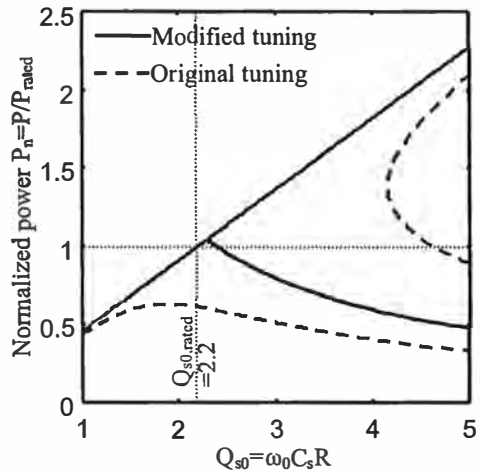


(ii) Power transfer capability.

(b) A mid-coupled system (k=0.2).



(i) Operating frequency.

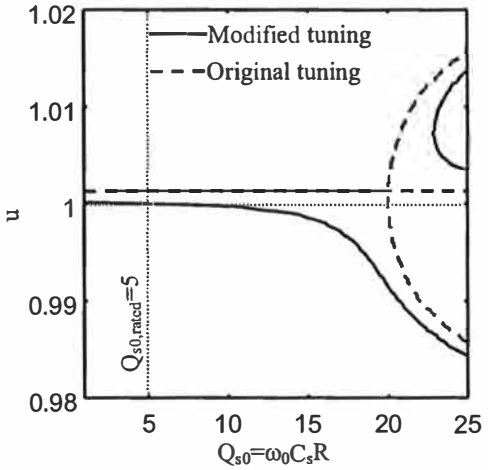


(ii) Power transfer capability.

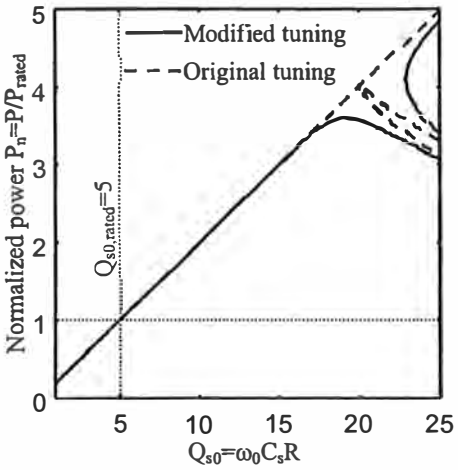
(c) A well-coupled system (k=0.4).

Fig. 5-3. SP topology - Operating frequency and power transfer capability under variable-frequency operation.

InductEV, Inc.
Exhibit 1008
Page 151

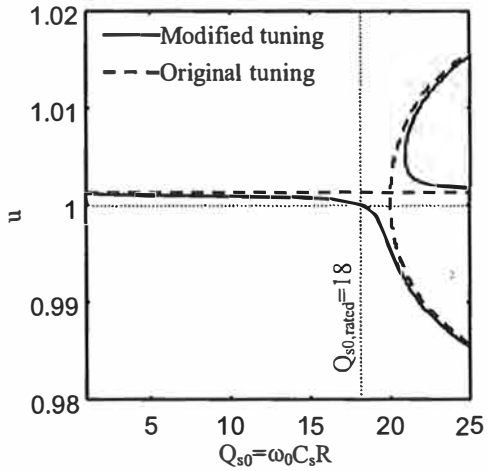


(i) Operating frequency.

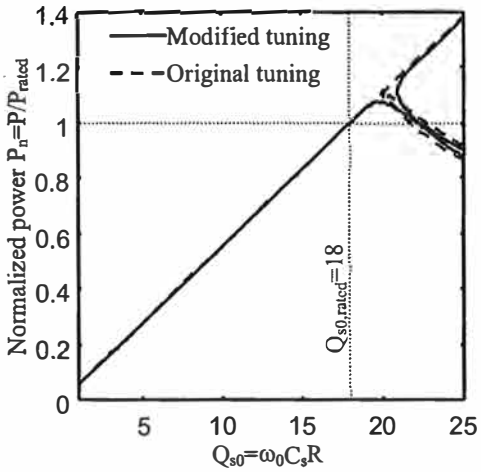


(ii) Power transfer capability.

(a) A system with $Q_{s0,rated}$ well within the bifurcation boundary.

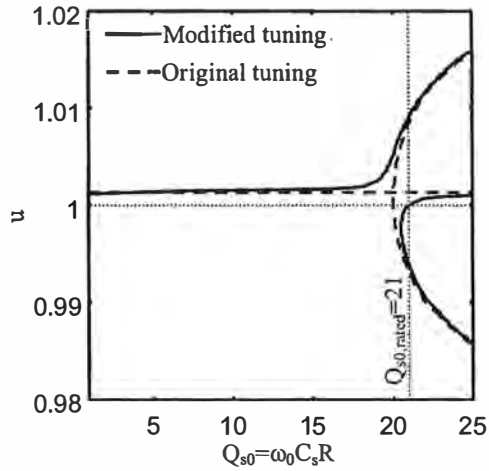


(i) Operating frequency.

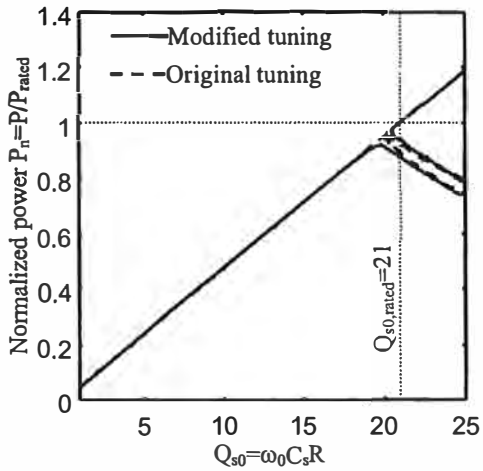


(ii) Power transfer capability.

(b) A system with $Q_{s0,rated}$ close to, but still within the bifurcation boundary.



(i) Operating frequency.

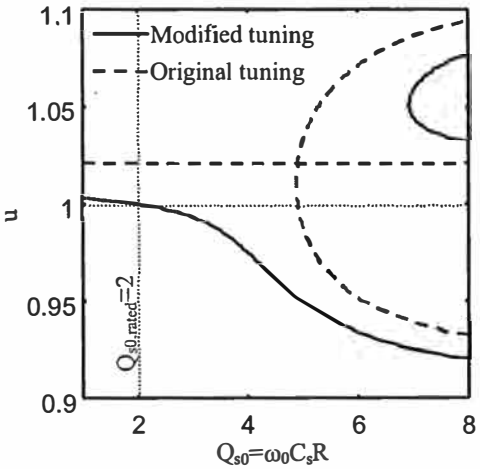


(ii) Power transfer capability.

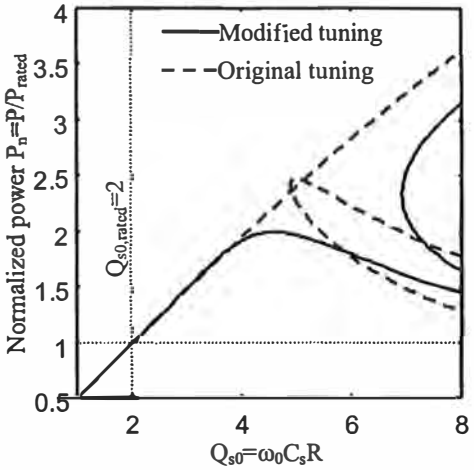
(c) A system where bifurcation occurs at $Q_{s0,rated}$.

Fig. 5-4. PP topology with loose coupling (k=0.05) - Operating frequency and power transfer capability under variable-frequency operation.

InductEV, Inc.
Exhibit 1008
Page 152

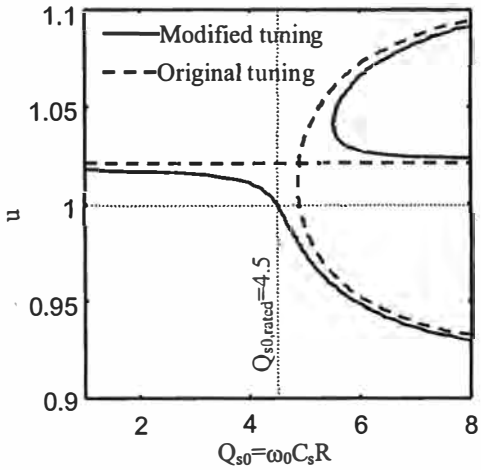


(i) Operating frequency.

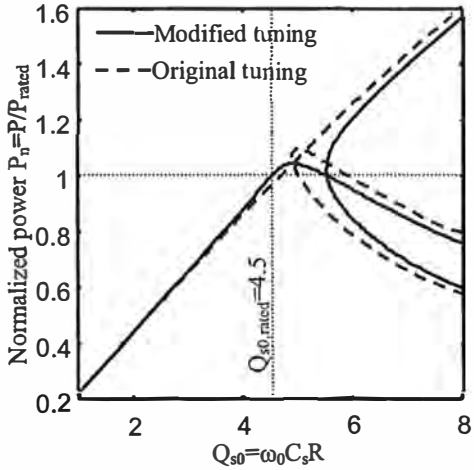


(ii) Power transfer capability.

(a) A system with $Q_{s0,rated}$ well within the bifurcation boundary.

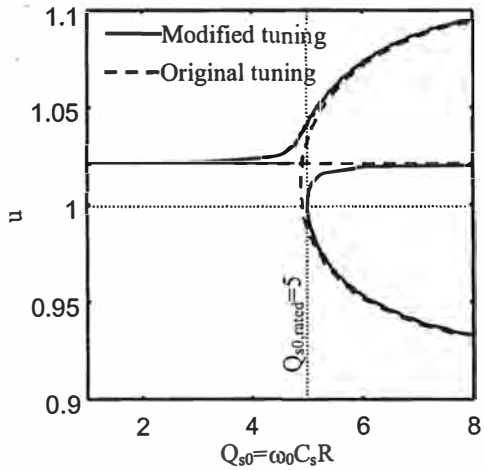


(i) Operating frequency.

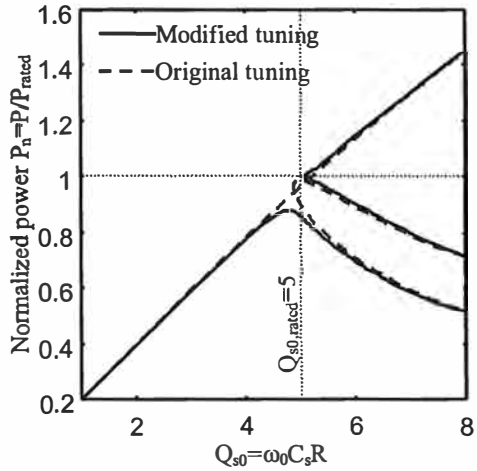


(ii) Power transfer capability.

(b) A system with $Q_{s0,rated}$ close to, but still within the bifurcation boundary.



(i) Operating frequency.

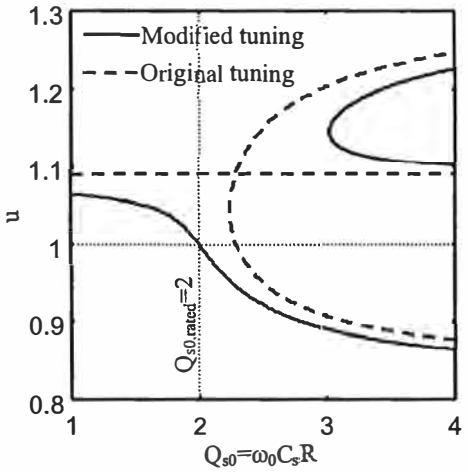


(ii) Power transfer capability.

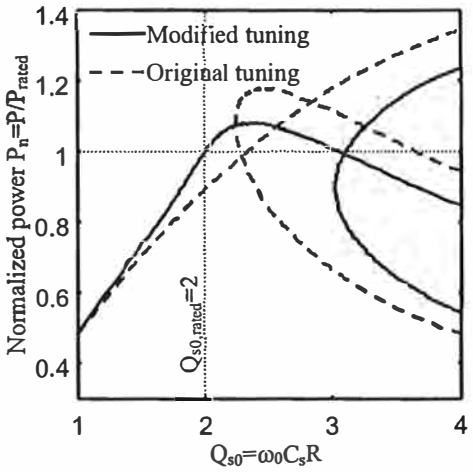
(c) A system where bifurcation occurs at $Q_{s0,rated}$.

Fig. 5-5. PP topology with middle coupling (k=0.2) - Operating frequency and power transfer capability under variable-frequency operation.

InductEV, Inc.
Exhibit 1008
Page 153

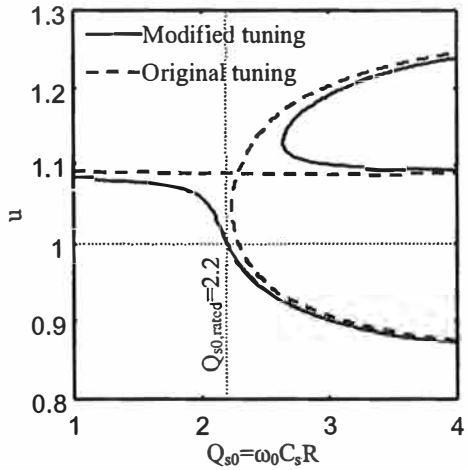


(i) Operating frequency.

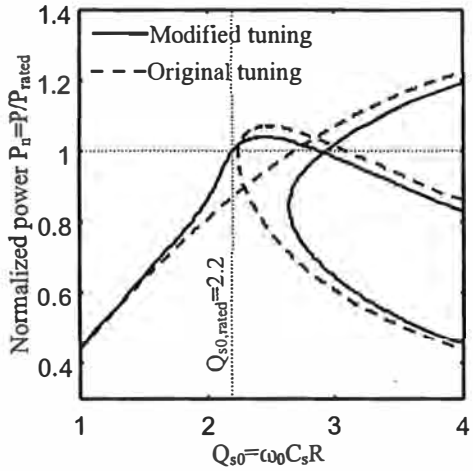


(ii) Power transfer capability.

(a) A system with $Q_{s0,rated}$ well within the bifurcation boundary.

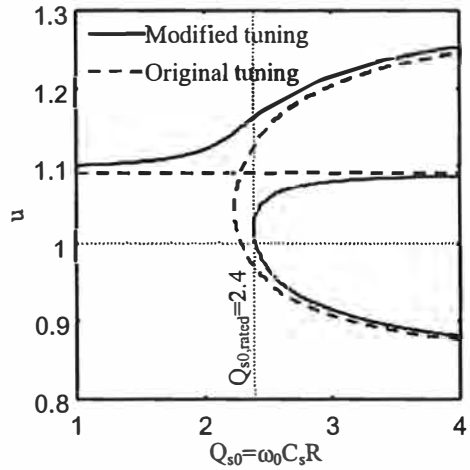


(i) Operating frequency.

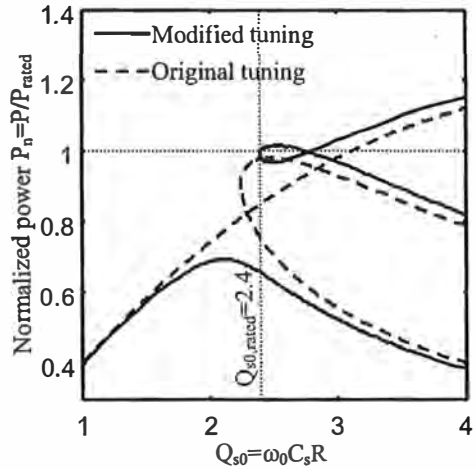


(ii) Power transfer capability.

(b) A system with $Q_{s0,rated}$ close to, but still within the bifurcation boundary.



(i) Operating frequency.

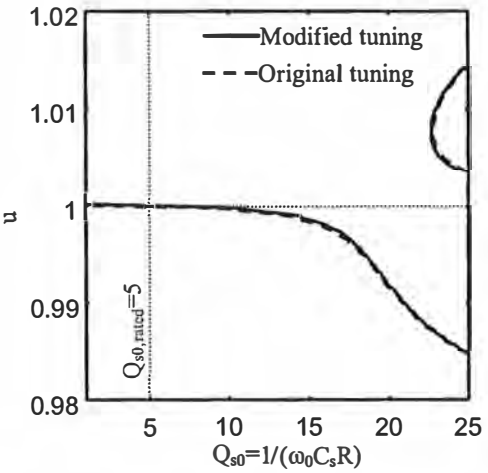


(ii) Power transfer capability.

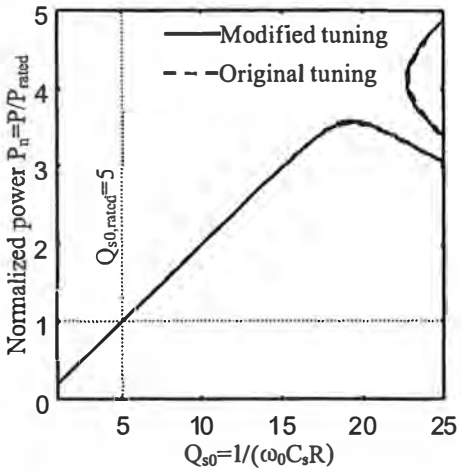
(c) A system where bifurcation occurs at $Q_{s0,rated}$.

Fig. 5-6. PP topology with good coupling (k=0.4) - Operating frequency and power transfer capability under variable-frequency operation.

InductEV, Inc.
Exhibit 1008
Page 154

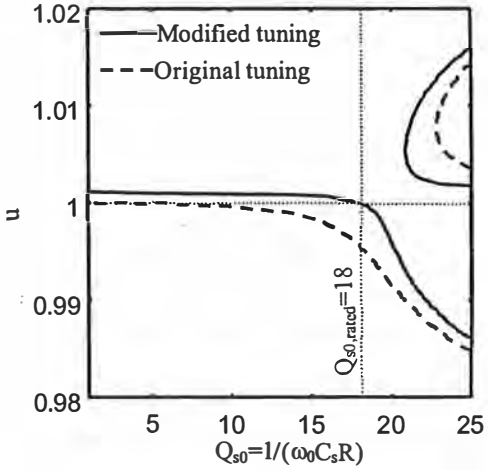


(i) Operating frequency.

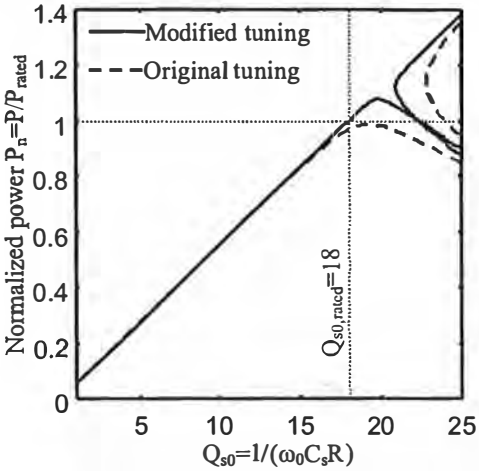


(ii) Power transfer capability.

(a) A system with $Q_{s0,rated}$ well within the bifurcation boundary.

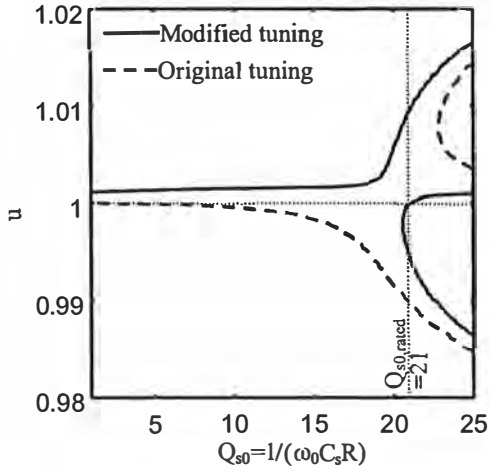


(i) Operating frequency.

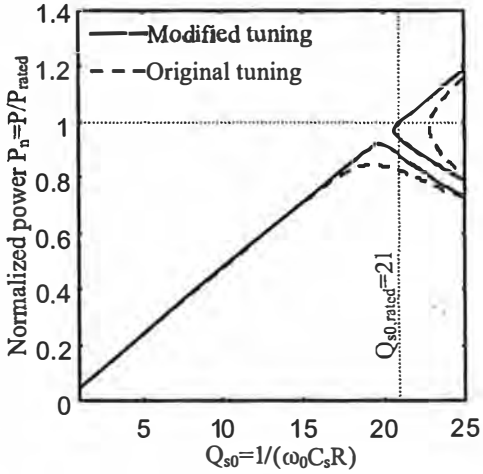


(ii) Power transfer capability.

(b) A system with $Q_{s0,rated}$ close to, but still within the bifurcation boundary.



(i) Operating frequency.

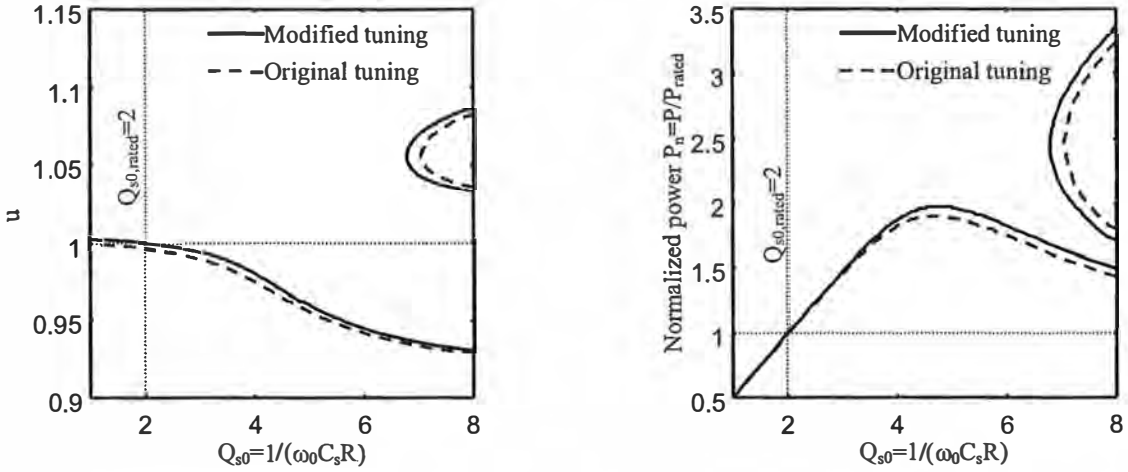


(ii) Power transfer capability.

(c) A system where bifurcation occurs at $Q_{s0,rated}$.

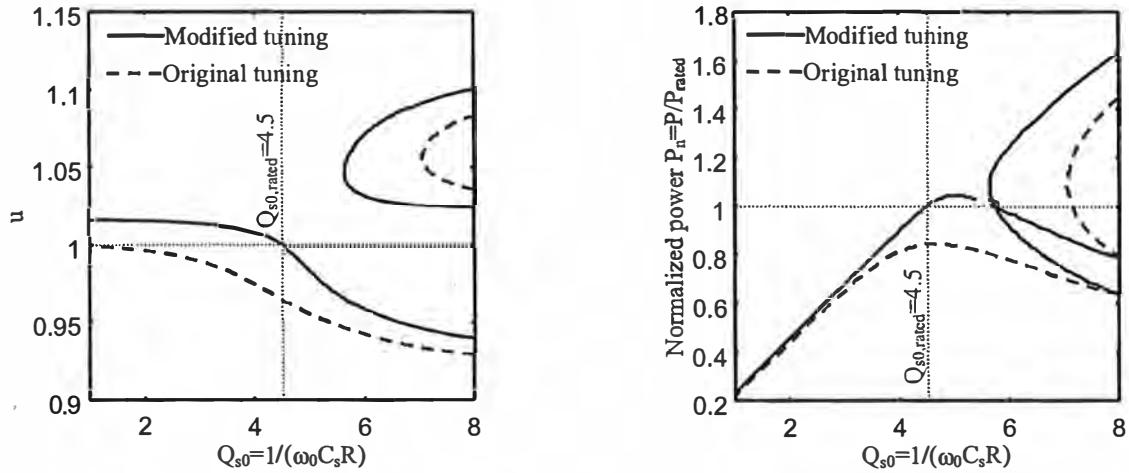
Fig. 5-7. PS topology with loose coupling (k=0.05) - Operating frequency and power transfer capability under variable-frequency operation.

InductEV, Inc.
Exhibit 1008
Page 155



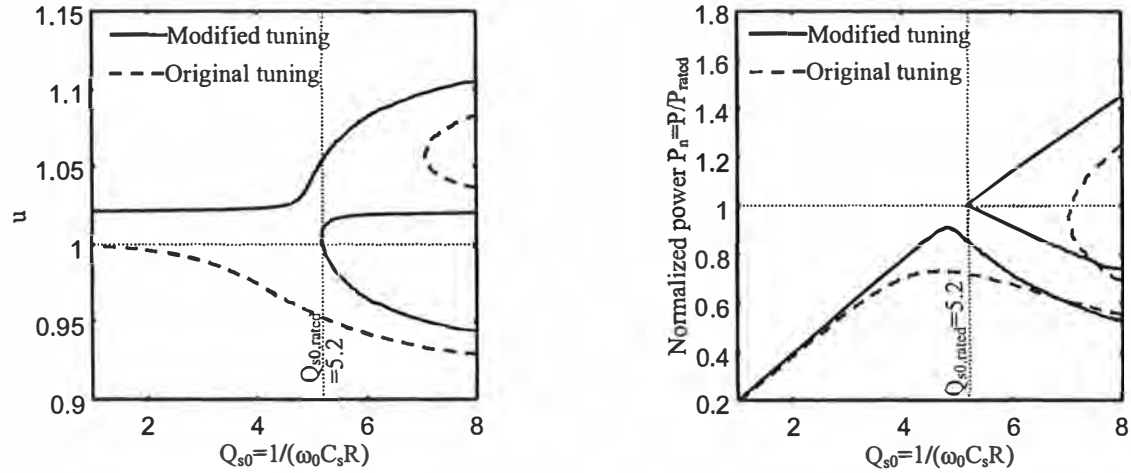
(i) Operating frequency. (ii) Power transfer capability.

(a) A system with $Q_{s0,rated}$ well within the bifurcation boundary.



(i) Operating frequency. (ii) Power transfer capability.

(b) A system with $Q_{s0,rated}$ close to, but still within the bifurcation boundary.

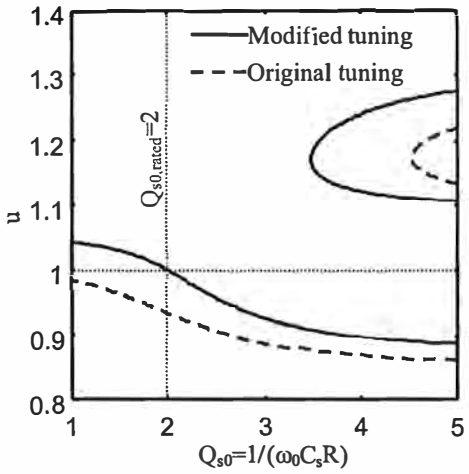


(i) Operating frequency. (ii) Power transfer capability.

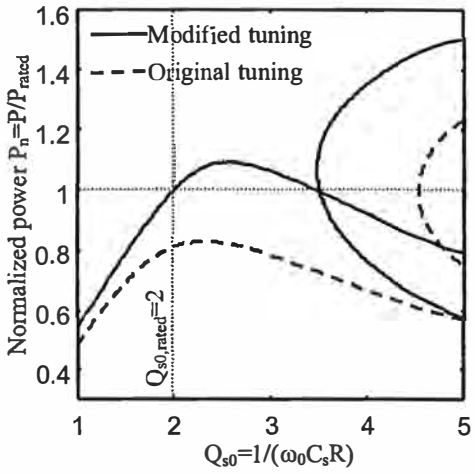
(c) A system where bifurcation occurs at $Q_{s0,rated}$.

Fig. 5-8. PS topology with middle coupling (k=0.2) - Operating frequency and power transfer capability under variable-frequency operation.

InductEV, Inc.
Exhibit 1008
Page 156

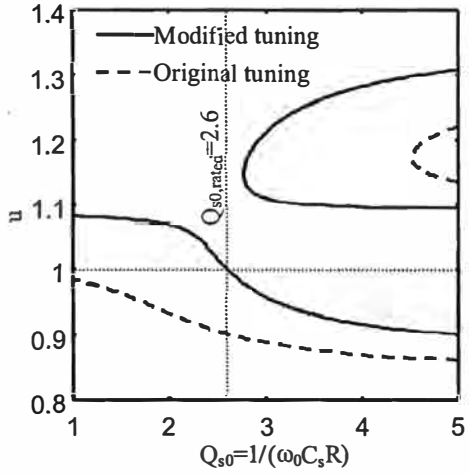


(i) Operating frequency.

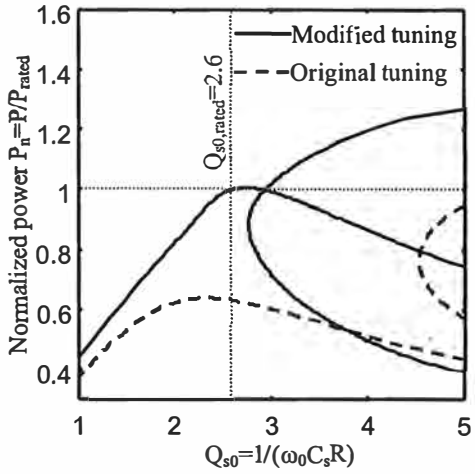


(ii) Power transfer capability.

(a) A system with $Q_{s0,rated}$ well within the bifurcation boundary.

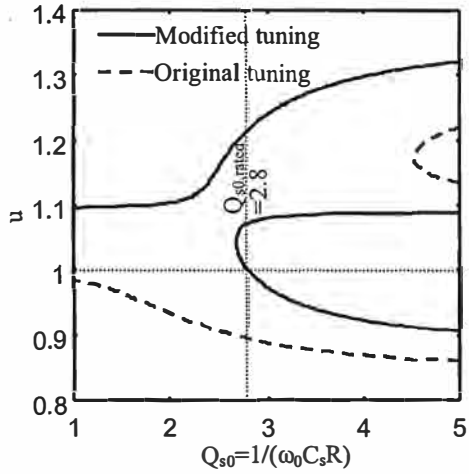


(i) Operating frequency.

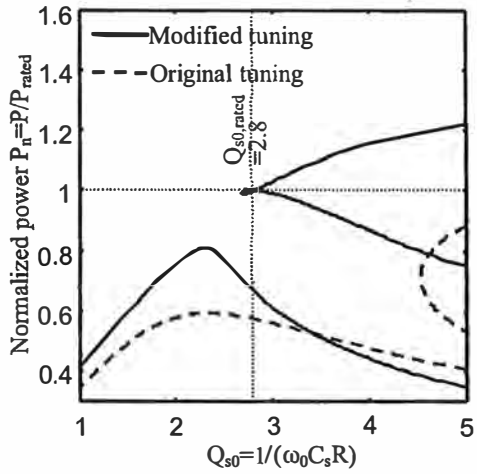


(ii) Power transfer capability.

(b) A system with $Q_{s0,rated}$ close to, but still within the bifurcation boundary.



(i) Operating frequency.



(ii) Power transfer capability.

(c) A system where bifurcation occurs at $Q_{s0,rated}$.

Fig. 5-9. PS topology with good coupling (k=0.4) - Operating frequency and power transfer capability under variable-frequency operation.

InductEV, Inc.
Exhibit 1008
Page 157

The bifurcation boundary of the PS topology is slightly higher than SP and PP topologies. For the selected k of 0.05, 0.2 and 0.4, bifurcation occurs at Q_{s0} of about 20, 5.1 and 2.7. If $Q_{s0,rated}$ is well within the bifurcation boundary, the improvement in power transfer capability is negligible below rated load in low k systems. This improvement becomes significant when $Q_{s0,rated}$ is close to but within the bifurcation boundary in high k systems. With a k of 0.05, 0.2 and 0.4, the improvement in power transfer capability under this condition is about 4%, 18% and 59% respectively.

With the SP and PS topologies, bifurcation appears at a lower Q_s in comparison to the original tuning. While this appears to be a disadvantage under variable-frequency control as the safety margin before bifurcation is reduced, the original tuning cannot transfer more power despite larger Q_s in the pickup design due to increased pickup frequency detuning. The maximum available power with the original tuning actually occurs at a Q_s below the bifurcation boundary of the modified tuning. Further increase of Q_s results in a drop of the power transfer.

5-4 BIFURCATION CRITERIA

According to above analysis, it is crucial to ensure the system design is within the bifurcation boundary when applying the modified tuning proposed in this chapter. In order to develop simple design criteria to identify the bifurcation boundary, it is assumed in this section that C_p is given by (5-2) and therefore changes with the load when the primary is parallel compensated. In consequence, the developed bifurcation criteria are valid for all loading conditions if the primary is series compensated (the SS and SP topologies) where the required C_p is independent of the load, but is applicable only at rated load in parallel compensated primary systems (the PP and PS topologies) since here C_p is selected at rated load as it is impractical to allow C_p to vary with the load. Because bifurcation only occurs with increasing load, it is shown in section 5-6 that designing the system to meet the bifurcation criterion at rated load (with a small safety margin) can ensure bifurcation-free operation for all loading conditions up to and including rated load.

As shown earlier in Fig. 5-2 to 5-9, the bifurcation criteria are topology dependent functions of k and Q_s. The theoretical analysis in this section investigates the full range of k and Q_s to develop general bifurcation criteria that can be used for any practical system design. For a given k (a specified electromagnetic structure), Q_s is allowed to vary in theory from a low value to a high value, and bifurcation appears if Q_s is greater than a boundary value determined by the bifurcation criteria. This process can be repeated with varying k values. The objective is to identify all theoretical k and Q_s where bifurcation occurs. The results can then be applied to any design where practical values of k and Q_s are known. Theoretically, a suitable trade-off between k and Q_s can be determined according to the

InductEV, Inc.
Exhibit 1008
Page 158

bifurcation criteria. In most designs, the electromagnetic structure is optimised to achieve the best k and here the bifurcation criteria can be used to determine the maximum allowable Q_s.

As noted in section 3-9, the fundamental design parameters k, Q_{p0} and Q_{s0} are related as:

$$Q_{p0} = \begin{cases} \dfrac{1}{k^2 Q_{s0}} & \text{series secondary} \\ \dfrac{1}{k^2 Q_{s0}} - \dfrac{1}{Q_{s0}} & \text{parallel secondary} \end{cases} \tag{5-9}$$

The bifurcation criteria can therefore be expressed in terms of Q_{p0} and Q_{s0} as well. In this section, the bifurcation criteria are developed first as relationships between Q_{p0} and Q_{s0}. They are then re-expressed in terms of k and Q_{s0} using (5-9).

Under ideal conditions, C_p can be assumed to be given by (5-2) so that pickup frequency detuning is eliminated at all loading conditions. Thus the normalized reactance of C_p (as derived in Appendix H) is a function of u, Q_{p0} and Q_{s0} given by:

$$\frac{1}{\omega C_p (\mathrm{Re}\, Z_{r0})} = \begin{cases} \dfrac{Q_{p0}}{u} & \text{series primary} \\ \dfrac{1+Q_{p0}^2}{uQ_{p0}} & \text{parallel primary} \end{cases} \tag{5-10}$$

When operating at the desired frequency that ensures unity DPF, the fundamental inverter output voltage and current of the power supply are in phase. This zero phase angle frequency can be calculated by determining the point at which the normalized load reactance is zero (Im Z_{tn}=0). However, for parallel-compensated primary systems, it is often mathematically easier to look at the normalized load susceptance (Im Y_{tn}=0). The normalized load impedance in Table 5-2 and 5-3 is once again used in this analysis with the normalized reactance of C_p replaced by (5-10).

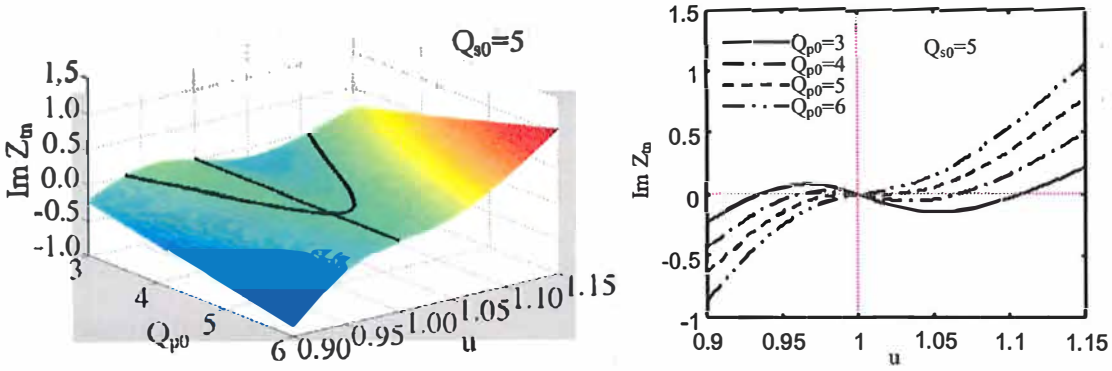
The normalized load reactance of series compensated primary systems (the SS and SP topologies) is shown in Fig. 5-10 as a function of u and Q_{p0}, with Q_{s0} fixed at 5. Similar graphs can be drawn for other values of Q_{s0}. The zero phase angle frequencies are shown as black lines on the surfaces. The cross-sections of these surfaces at selected values of Q_{p0} are also shown for comparison.

Generally, the SS and SP topologies exhibit similar features. The zero phase angle frequency is unique and identical to the secondary resonant frequency (u=1) if the primary quality factor is much larger than the secondary quality factor ($Q_p >> Q_s$). However, there are three zero phase angle frequencies when the primary quality factor is much lower than the secondary quality factor ($Q_p << Q_s$). One of these zero phase angle frequencies is identical to the secondary resonant frequency. The differences between these three zero phase angle frequencies increases as the primary quality factor Q_p

InductEV, Inc.
Exhibit 1008
Page 159

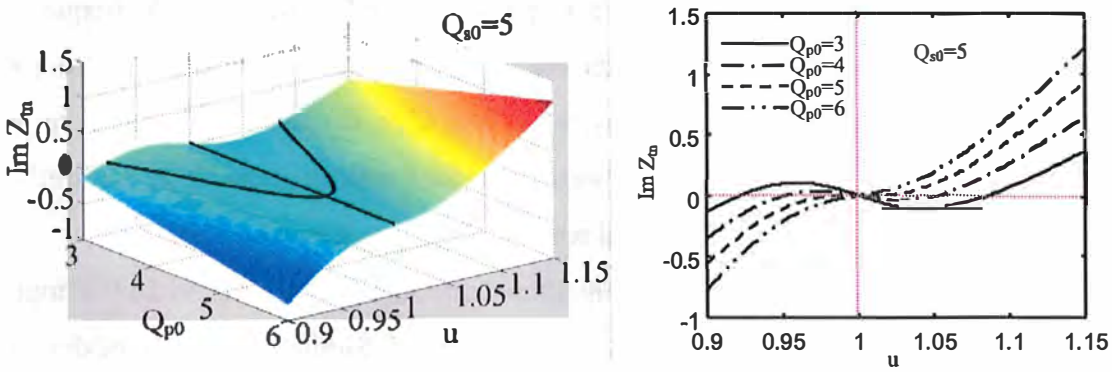
is reduced.

The normalized load susceptance of parallel-compensated primary systems is shown in Fig. 5-11. As shown, the PP and PS topologies have similar features to the afore mentioned SS and SP topologies. For all basic topologies, not only are the zero phase angle frequency curves similar, but also the normalized load reactance surfaces of series compensated primary systems are similar to the normalized load susceptance surfaces of parallel-compensated primary systems. Consequently, it is possible to develop a general analysis of the zero phase angle frequencies for all basic topologies (SS, SP, PP and PS). This approach is used in this section to develop general bifurcation criteria thereby enabling the bifurcation boundary conditions to be precisely specified.



(i) Surface function. (ii) Cross sections of the surface.

(a) SS topology.

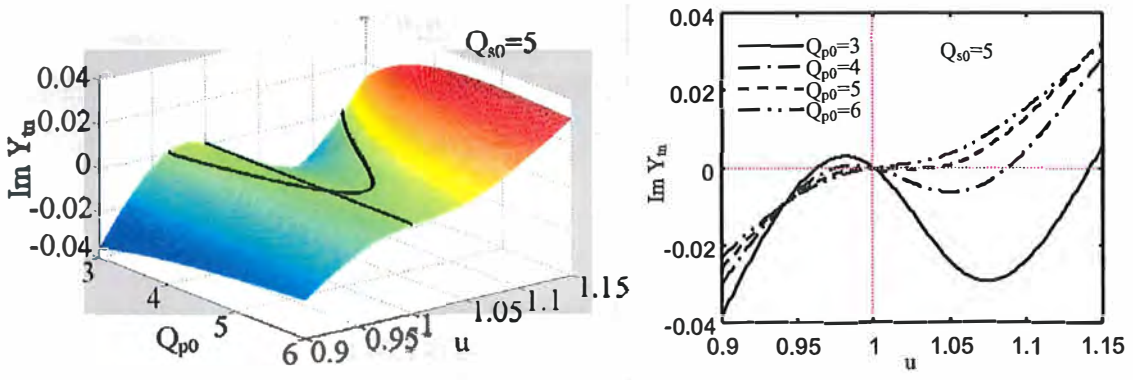


(i) Surface function. (ii) Cross sections of the surface.

(b) SP topology.

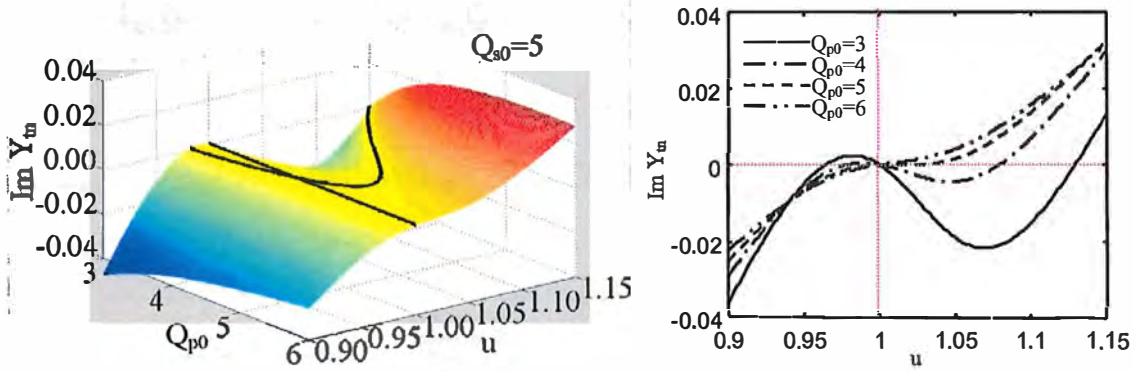
Fig. 5-10. Normalized load reactance.

InductEV, Inc.
Exhibit 1008
Page 160



(i) Surface function. (ii) Cross sections of the surface.

(a) PP topology.



(i) Surface function. (ii) Cross sections of the surface.

(b) PS topology.

Fig. 5-11. Normalized load susceptance.

The normalized load reactance for the SS and SP topologies and the normalized load susceptance for the PP and PS topologies can be represented as:

$$\mathrm{Im}Z_{tn} \text{ or } \mathrm{Im}Y_{tn} = \frac{\left(u^2-1\right)G\left(u,Q_{p0},Q_{s0}\right)}{D\left(u,Q_{p0},Q_{s0}\right)} \tag{5-11}$$

where the functions $G(u,Q_{p0},Q_{s0})$ and $D(u,Q_{p0},Q_{s0})$ are defined in Table 5-4 and (5-12) below for all basic topologies.

The factor (u^2-1) in (5-11) is zero at the secondary resonant frequency (u=1). This ensures system operation with zero-phase angle at the secondary resonant frequency. Since the factor (u^2-1) in (5-11) is negative when the operating frequency is below the secondary resonant frequency (u<1), and becomes positive when the operating frequency is above the secondary resonant frequency (u>1), it presents no bifurcation information. As shown in Table 5-4(a), the function $D(u,Q_{p0},Q_{s0})$ associated to each of the four basic topologies is always positive. It therefore carries no bifurcation information as well. Consequently, the bifurcation phenomenon, as shown in Fig. 5-10 and Fig. 5-11, will be inherent with the function $G(u,Q_{p0},Q_{s0})$.

For the four basic topologies, the function $G(u,Q_{p0},Q_{s0})$ is a polynomial of the form:

InductEV, Inc.
Exhibit 1008
Page 161

$$G(u,Q_{p0},Q_{s0}) = a_8u^8 + a_6u^6 + a_4u^4 + a_2u^2 + a_0 \tag{5-12}$$

The non-zero coefficients in (5-12) are given in Table 5-4(b). As shown, $G(u,Q_{p0},Q_{s0})$ is a bi-quadratic polynomial for the SS and SP topologies. For the PP and PS topologies, $G(u,Q_{p0},Q_{s0})$ is a bi-quartic polynomial.

TABLE 5-4
NORMALIZED FUNCTIONS IN (5-11)
(a) $D(u,Q_{p0},Q_{s0})$

SS&SP	$u(u^2-1)^2Q_{s0}^2 + u^3$
PP	$u\left\{u^2 + \left[(u^2-1)^2Q_{p0}Q_{s0}^2 + u^2Q_{p0} - (u^2-1)Q_{s0}\right]^2\right\}(1+Q_{p0}^2)$
PS	$u\left\{u^6 + \left[(u^2-1)^2Q_{p0}Q_{s0}^2 + u^2Q_{p0} - u^2(u^2-1)Q_{s0}\right]^2\right\}(1+Q_{p0}^2)$

(b) Coefficients of the polynomial $G(u, Q_{p0},Q_{s0})$ in (5-12)

SS	a_4	$Q_{p0}Q_{s0}^2 - Q_{s0}$
	a_2	$Q_{p0} - 2Q_{p0}Q_{s0}^2$
	a_0	$Q_{p0}Q_{s0}^2$
SP	a_4	$Q_{p0}Q_{s0}^2$
	a_2	$Q_{p0} - Q_{s0} - 2Q_{p0}Q_{s0}^2$
	a_0	$Q_{p0}Q_{s0}^2$
PP	a_8	$Q_{p0}^3Q_s^4$
	a_6	$-4Q_{p0}^3Q_{s0}^4 + 2Q_{p0}^3Q_{s0}^2 - 2Q_{p0}^2Q_{s0}^3 - Q_{p0}Q_{s0}^4$
	a_4	$6Q_{p0}^3Q_{s0}^4 - 4Q_{p0}^3Q_{s0}^2 + 5Q_{p0}^2Q_{s0}^3 + 3Q_{p0}Q_{s0}^4 - Q_{p0}Q_{s0}^2 - 2Q_{p0}^2Q_{s0} + Q_{p0}^3 + Q_{s0}^3$
	a_2	$-4Q_{p0}^3Q_{s0}^4 + 2Q_{p0}^3Q_{s0}^2 - 4Q_{p0}^2Q_{s0}^3 - 3Q_{p0}Q_{s0}^4 + Q_{p0}Q_{s0}^2 + Q_{p0}^2Q_{s0} - 2Q_{s0}^3 + Q_{s0}$
	a_0	$Q_{p0}^3Q_{s0}^4 + Q_{p0}^2Q_{s0}^3 + Q_{p0}Q_{s0}^4 + Q_{s0}^3$
PS	a_8	$Q_{p0}^3Q_{s0}^4 - 2Q_{p0}^2Q_{s0}^3 + Q_{p0}Q_{s0}^2$
	a_6	$-4Q_{p0}^3Q_{s0}^4 + Q_{p0} + 2Q_{p0}^3Q_{s0}^2 + 5Q_{p0}^2Q_{s0}^3 - Q_{p0}Q_{s0}^4 - Q_{p0}Q_{s0}^2 - 2Q_{p0}^2Q_{s0} + Q_{s0}^3$
	a_4	$6Q_{p0}^3Q_{s0}^4 + Q_{p0} - 4Q_{p0}^3Q_{s0}^2 - 4Q_{p0}^2Q_{s0}^3 + 3Q_{p0}Q_{s0}^4 - 2Q_{p0}Q_{s0}^2 + Q_{p0}^3 + Q_{p0}^2Q_{s0} - 2Q_{s0}^3 + Q_{s0}$
	a_2	$-4Q_{p0}^3Q_{s0}^4 + 2Q_{p0}^3Q_{s0}^2 + Q_{p0}^2Q_{s0}^3 - 3Q_{p0}Q_{s0}^4 + 2Q_{p0}Q_{s0}^2 + Q_{s0}^3$
	a_0	$Q_{p0}^3Q_{s0}^4 + Q_{p0}Q_{s0}^4$

The function $G(u,Q_{p0},Q_{s0})$ is shown in Fig. 5-12 for the four basic topologies (SS, SP, PP and PS). The white curves drawn on the surfaces of Fig. 5-12 represent zero values of the function $G(u,Q_{p0},Q_{s0})$. According to (5-11), these zero values correspond to either zero load reactance or susceptance. In consequence, two zero phase angle frequencies can be determined by these curves in addition to the secondary resonant frequency for each topology.

InductEV, Inc.
Exhibit 1008
Page 162

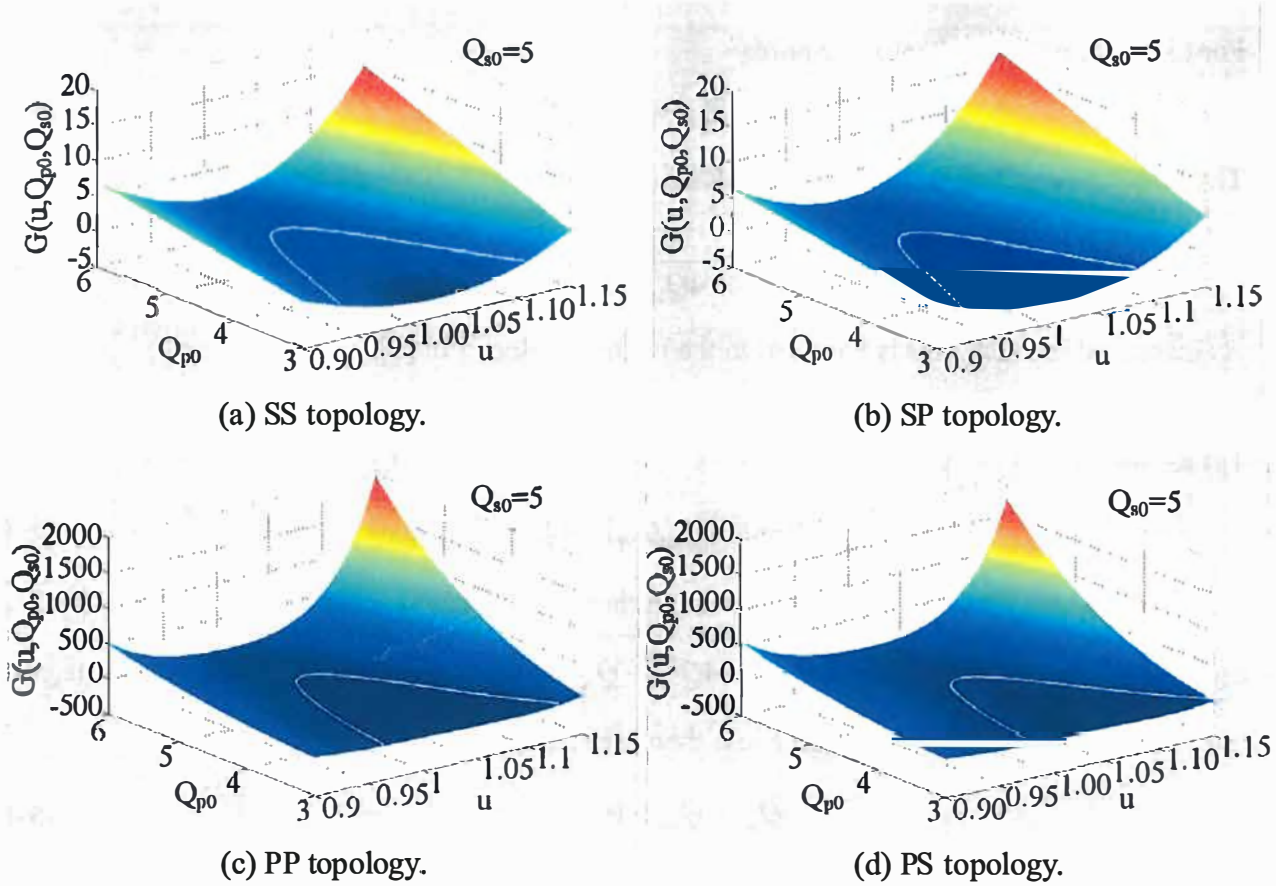


Fig. 5-12. Normalized function $G(u,Q_{p0},Q_{s0})$.

When the primary quality factor (Q_p) is much larger than the secondary quality factor (Q_s), the function $G(u,Q_{p0},Q_{s0})$ is positive across the frequency spectrum as shown in Fig. 5-12. However, the function $G(u,Q_{p0},Q_{s0})$ becomes negative around the secondary resonant frequency (u=1) if the primary quality factor is much lower than the secondary quality factor and as such two additional zero phase angle frequencies other than the secondary resonant frequency exist. To ensure the secondary resonant frequency is the only zero phase angle frequency, the function $G(u,Q_{p0},Q_{s0})$ must be greater than zero across the frequency spectrum. A general rule to avoid bifurcation is thus:

$$G(u,Q_{p0},Q_{s0})>0 \tag{5-13}$$

Normally both the primary and secondary quality factors are larger than unity. This makes the polynomial coefficient a_4 for SS and SP topologies positive so that if the bi-quadratic polynomial $G(u,Q_{p0},Q_{s0})$ is to be greater than zero, the discriminant:

$$\Delta = a_2^2 - 4a_4a_0 \tag{5-14}$$

must be less than zero.

Substituting the polynomial coefficients for the SS topology in Table 5-4 (b) into the discriminant (5-14) results in:

InductEV, Inc.
Exhibit 1008
Page 163

$$\Delta = \left(Q_{p0} - 2Q_{p0}Q_{s0}^2\right)^2 - 4Q_{p0}Q_{s0}^2\left(Q_{p0}Q_{s0}^2 - Q_{s0}\right) = Q_{p0}\left[Q_{p0}\left(1 - 4Q_{s0}^2\right) + 4Q_{s0}^3\right] \tag{5-15}$$

For (5-15) to become negative requires:

$$Q_{p0}\left(1 - 4Q_{s0}^2\right) + 4Q_{s0}^3 < 0 \tag{5-16}$$

The bifurcation criterion for the SS topology derived from (5-16) is then:

$$Q_{p0} > \frac{4Q_{s0}^3}{4Q_{s0}^2 - 1} \tag{5-17}$$

As discussed in 2-5.5, this is identical to the result developed in [9].

Substituting the polynomial coefficients for the SP topology in Table 5-4 (b) into the discriminant (5-14) results in:

$$\Delta = \left(Q_{p0} - Q_{s0} - 2Q_{p0}Q_{s0}^2\right)^2 - 4\left(Q_{p0}Q_{s0}^2\right)\left(Q_{p0}Q_{s0}^2\right) = \left(Q_{p0} - Q_{s0}\right)\left[Q_{p0}\left(1 - 4Q_{s0}^2\right) - Q_{s0}\right] \tag{5-18}$$

The secondary quality factor is normally larger than unity, and as such the term $(1 - 4Q_{s0}^2)$ in (5-18) is negative. As a result, the factor $Q_{p0}\left(1 - 4Q_{s0}^2\right) - Q_{s0}$ of the discriminat in (5-18) is also negative. Letting this discriminant (5-18) become less than zero results in:

$$Q_{p0} - Q_{s0} > 0 \tag{5-19}$$

The bifurcation criterion for the SP topology derived from (5-19) is thus:

$$Q_{p0} > Q_{s0} \tag{5-20}$$

The analytical bifurcation boundaries given by (5-17) and (5-20) respectively for the SS and SP topologies are shown in Fig. 5-13. The bifurcation boundary of the SS topology sits above the approximate bifurcation boundary given by $Q_{p0}>Q_{s0}$ in [6], [9-11] when the assumption of high Q_s is applied. In fact, the difference is negligible with high Q_s. With the SP topology, the analytical bifurcation boundary sits exactly at $Q_{p0}>Q_{s0}$.

The solutions of the general bifurcation rule (5-13) for the PP and PS topologies can be solved by the approach proposed by Ludovico Ferrari in 16th century [12], but is rather complicated and cumbersome. Alternatively, a numerical methodology can be used as shown in Fig. 5-14. Here, an iteration process is used over a practical range of Q_{s0} such as from 1 to 10 and a suitable frequency range of u around unity. In practical designs, Q_p is normally larger than Q_s to ensure bifurcation free operation [6], [10]. The numerical process starts from a significantly large Q_{p0} to make $G(u,Q_{p0},Q_{s0})$ positive across the frequency spectrum, and then reduces Q_{p0} by a small amount at each iteration step to verify whether $G(u,Q_{p0},Q_{s0})$ intersects with the axis $G(u,Q_{p0},Q_{s0})=0$, where bifurcation occurs. The iteration procedure stops when either the bifurcation boundary is found at a certain Q_{p0} or no bifurcation occurs for all Q_{p0} larger than zero.

InductEV, Inc.
Exhibit 1008
Page 164

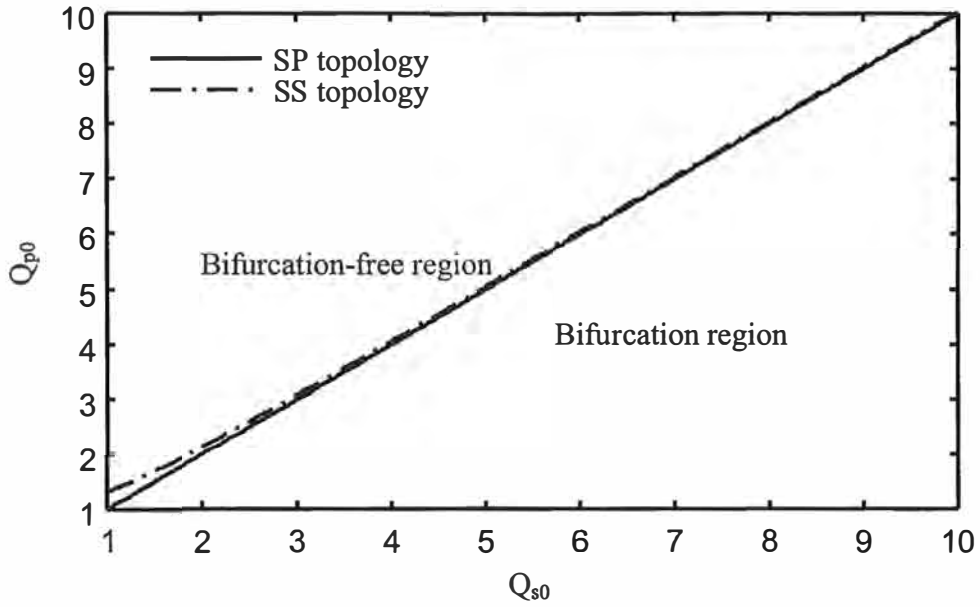


Fig. 5-13. Analytical bifurcation boundary for the SS and SP topologies.

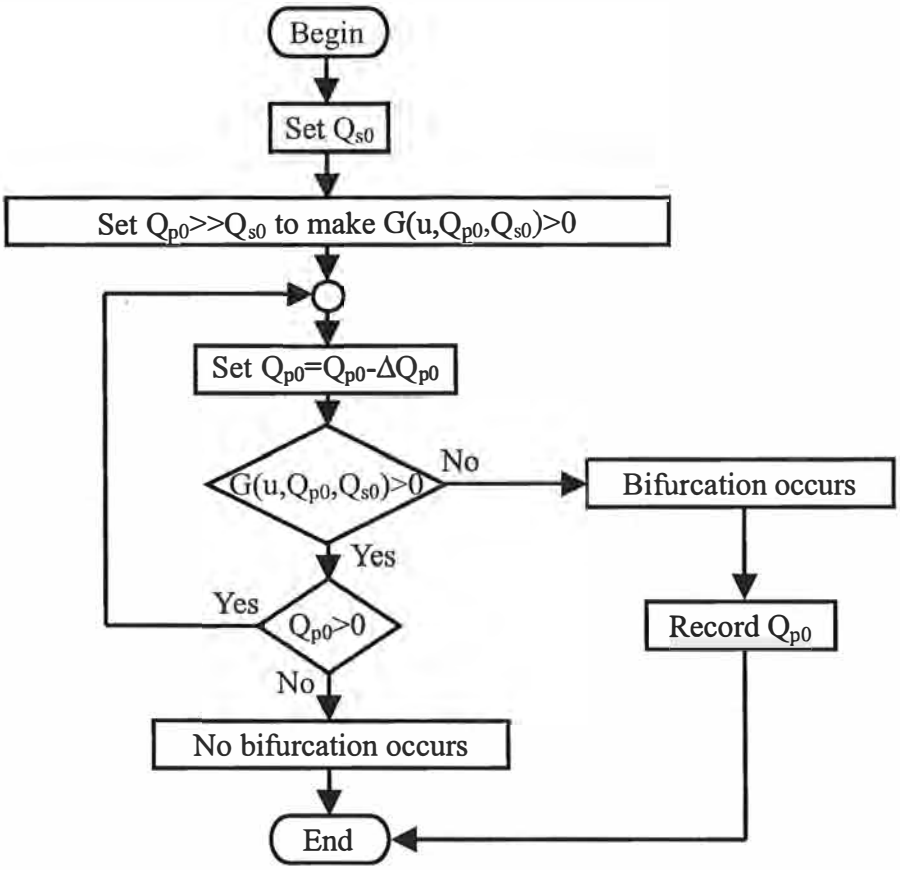


Fig. 5-14. Numerical algorithm for finding bifurcation boundary.

The numerical bifurcation boundaries are shown in Fig. 5-15 for the PP and PS topologies. It can be found that the numerical bifurcation boundary of the PP topology is identical to the analytical bifurcation boundary given by (5-20) for the SP topology and as such would be the exact analytical

InductEV, Inc.
Exhibit 1008
Page 165

bifurcation boundary. The numerical bifurcation boundary of the PS topology is below the approximate bifurcation boundary given by $Q_{p0}>Q_{s0}$. According to this numerical bifurcation boundary, if Q_{s0} is below 1.7 the system is free of bifurcation for any practical value of Q_{p0}. When Q_{s0} is above 1.7, the numerical bifurcation boundary of the PS topology is close to $Q_{p0}>Q_{s0}-1/Q_{s0}$.

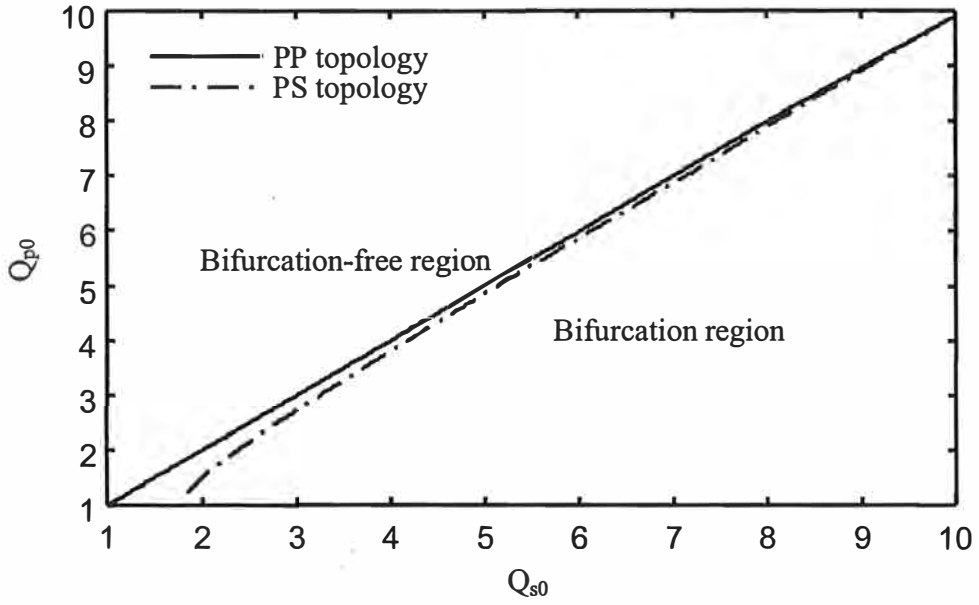


Fig. 5-15. Numerical bifurcation boundary for the PP and PS topologies.

A summary of the bifurcation criteria is given in Table 5-5 for four basic ICPT topologies. They are simple relations between the primary and secondary quality factors. According to above discussion, the bifurcation criteria given in this table for the SS, SP and PP topologies are exact analytical solutions, while that for the PS topology is an approximation.

Using (5-9), the bifurcation criteria can be expressed in terms k and Q_{s0} in Table 5-5.

If the magnetic coupling is very weak (k<<1), the bifurcation criteria given in Table 5-5 for the four basic topologies can be simplified to:

$$Q_{s0} < \frac{1}{k} \tag{5-21}$$

As noted in section 2-5.5, this result is identical to the analysis in [6], [9].

The bifurcation boundaries in terms of k and Q_{s0}, as given in Table 5-5, are compared in Fig. 5-16 for the four basic topologies. The maximum Q_{s0} for bifurcation-free operation decreases as k is improved. This boundary is topology dependent. For loosely coupled systems with a k of 0.1, the difference between the basic topologies is negligible, and bifurcation occurs in all topologies when Q_{s0} increases above 10. However, this difference increases with improved k. For example with a k of 0.6, bifurcation-free operation requires that Q_{s0} be below 1.3 for SP and PP topologies, 1.5 for the SS

InductEV, Inc.
Exhibit 1008
Page 166

topology, and 2 for the PS topology.

TABLE 5-5
BIFURCATION CRITERIA

	Standard derivation in terms of Q_{p0} and Q_{s0}	Re-expression in terms of k and Q_{s0}
SS	$Q_{p0} > \frac{4Q_{s0}^3}{4Q_{s0}^2 - 1}$	$Q_{s0} < \frac{\sqrt{1+\sqrt{1-k^2}}}{\sqrt{2}k}$
SP&PP	$Q_{p0} > Q_{s0}$	$Q_{s0} < \frac{\sqrt{1-k^2}}{k}$
PS	$\begin{cases} Q_{p0} > Q_{s0} - \frac{1}{Q_{s0}} & \text{if } Q_{s0} > 1.7 \\ \text{No bifurcation} & \text{if } Q_{s0} < 1.7 \end{cases}$	$\begin{cases} Q_{s0} < \frac{\sqrt{1+k^2}}{k} & \text{if } Q_{s0} > 1.7 \\ \text{No bifurcation} & \text{if } Q_{s0} < 1.7 \end{cases}$

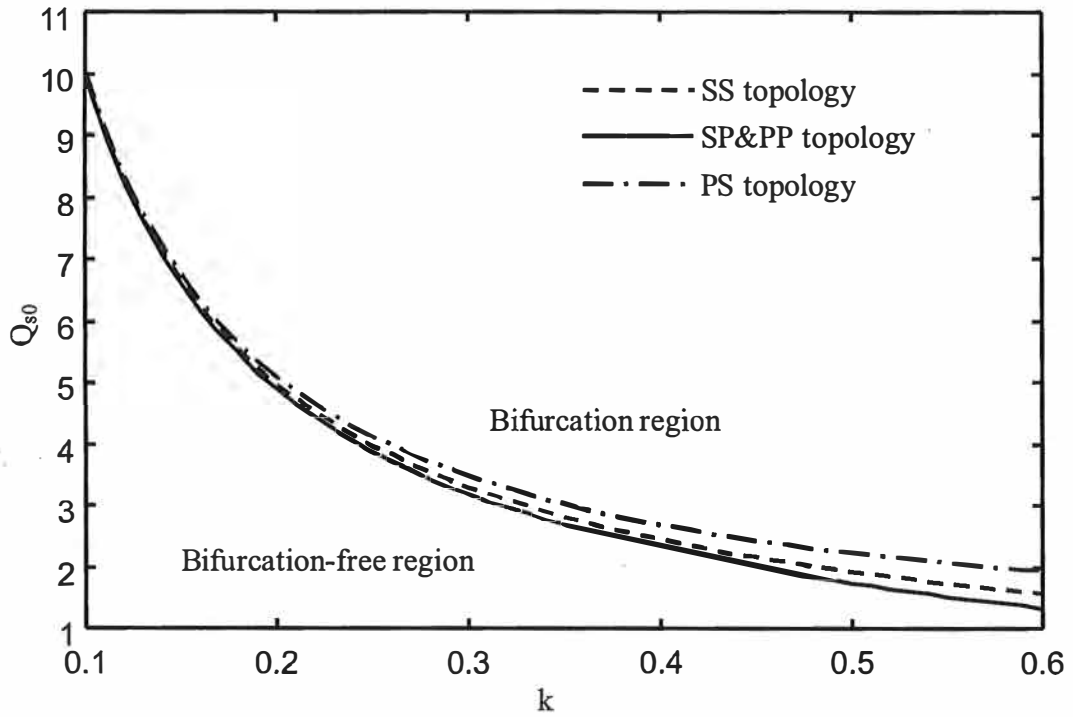


Fig. 5-16. Bifurcation boundary defined by k and Q_{s0} for the four basic topologies.

5-5 DISCUSSION

With k and $Q_{s0,rated}$ determined using the design methodology described in Chapter 4, the bifurcation criteria in Table 5-5 is used to evaluate the designed system under variable-frequency operation. This enables improvements in the power transfer capability (achieved as a result of modifying C_p to minimize pickup frequency detuning effects) to be determined. Here it is assumed that the power supply controller allows the operating frequency to vary such that unity DPF is achieved at

InductEV, Inc.
Exhibit 1008
Page 167

all times, thereby minimizing its required VA rating, size and cost. Consequently, in a single pickup system the required power supply VA rating equals the power transferred to the pickup.

The improvement in power transfer capability can be guaranteed with the modified tuning proposed in this chapter providing the bifurcation criterion is satisfied. If the designed system can not meet the bifurcation criterion, rated power is available only in the bifurcation region with both the original and modified tunings. Such a system is normally not desirable, and it is necessary to redesign the system to have lower k or $Q_{s0,rated}$ to force it to meet the bifurcation criterion.

The allowable $Q_{s0,rated}$ is strictly limited by k. In a loosely coupled system with k of 0.05, the maximum $Q_{s0,rated}$ is about 20 for all four basic topologies (SS, SP, PP and PS). With k improved to 0.2 for a middle coupled system, the maximum $Q_{s0,rated}$ reduces to about 5 for all topologies. In a well-coupled system with k of 0.4, the maximum $Q_{s0,rated}$ is close to 2.5 (2.5 for the SS topology, 2.3 for the SP and PP topologies, and 2.7 for the PS topology). Consequently, variable-frequency operation is not suitable for well-coupled (high k) systems with high $Q_{s0,rated}$. To avoid bifurcation, fixed-frequency operation may be considered. This is investigated in the following chapter.

The developed bifurcation criteria are valid for all loading conditions when the primary is series compensated, but are applicable only at rated load if the primary is parallel compensated. In this case, designing the system to meet the bifurcation criterion at rated load with a suitable safety margin assures bifurcation-free operation for all loading conditions up to and including rated load. This is a natural result as bifurcation only occurs with increasing load, as is verified in section 5-6 by a practical example.

Under the modified tuning scheme proposed in this chapter, when the primary is series-compensated (the SS and SP topologies), operation at ω_0 can theoretically be achieved independent of the load. In this case, pickup frequency detuning is minimized under all loading conditions. For parallel-compensated primary systems (the PP and PS topologies), operation at ω_0 is achieved only at rated operation. Consequently, pickup frequency detuning effects under lightly loading conditions cannot be avoided.

The improvement in the power transfer capability for selected examples are summarized in Table 5-6 to Table 5-8 for loosely coupled, middle coupled and well coupled systems respectively. The discussion focuses on the SP, PP and PS topologies, where modification of C_p is required. The improvement in the power transfer capability as expected depends on the compensation topology as well as k and $Q_{s0,rated}$. The required modification in C_p (as noted in section 5-2) for each case is given in these tables for comparison.

With loosely coupled systems, the original tuning works very well for all four basic topologies. Here the modified tuning and the original tuning are essentially identical since the required

InductEV, Inc.
Exhibit 1008
Page 168

modification of C_p is negligible as shown in Fig. 5-6. As expected, the improvement in the power transfer capability is very small or negligible.

For middle coupled systems, the original tuning also works well for the PP topology, and the SP and PS topologies with low $Q_{s0,rated}$. In these cases, the improvement in the power transfer capability with the modified tuning as shown in Table 5-7 is small. This improvement becomes more significant for the SP and PS topologies with higher $Q_{s0,rated}$. While it looks as if the modified tuning is useful here, the necessary change to C_p is small. To do this in practice requires good lifetime capacitance stability.

For well coupled systems as shown in Table 5-8, the improvement in the power transfer capability with the modified tuning can be up to about 15% for the PP topology, but again the required change in C_p is small and good lifetime capacitance stability is required. For the SP and PS topologies, the improvement in the power transfer capability can be more than 50% and the required change in C_p is significant.

The necessary C_p of this modified tuning depends on k, which may vary in practice due to misalignment of the electromagnetic structure. Moreover, the practical C_p selected may be different to the theoretical value due to manufacturing tolerances, aging or thermal effects. The influence of variations in capacitance and the misalignment in the electromagnetic structure are investigated in Chapter 7.

TABLE 5-6
IMPROVEMENT OF THE POWER TRANSFER CAPABILITY WITH THE MODIFIED TUNING FOR A LOOSELY COUPLED SYSTEM (k=0.05)

SP Topology.	Bifurcation criterion.	$Q_{s0}<20$		
	Rated load condition.	$Q_{s0,rated}=6$	$Q_{s0,rated}=12$	$Q_{s0,rated}=18$
	Modification in C_p.	$C_{pn}\sim1.00$		
	Improvement in power transfer.	0%	0%	4%
PP Topology.	Bifurcation criterion.	$Q_{s0}<20$		
	Rated load condition.	$Q_{s0,rated}=6$	$Q_{s0,rated}=12$	$Q_{s0,rated}=18$
	Modification in C_p.	$C_{pn}\sim1.00$		
	Improvement in power transfer.	0%	0%	0%
PS Topology.	Bifurcation criterion.	$Q_{s0}<20$		
	Rated load condition.	$Q_{s0,rated}=6$	$Q_{s0,rated}=12$	$Q_{s0,rated}=18$
	Modification in C_p.	$C_{pn}\sim1.00$		
	Improvement in power transfer.	0%	0%	3%

InductEV, Inc.
Exhibit 1008
Page 169

TABLE 5-7
IMPROVEMENT OF THE POWER TRANSFER CAPABILITY WITH THE MODIFIED TUNING FOR A MIDDLE COUPLED SYSTEM (k=0.2)

SP Topology.	Bifurcation criterion.	$Q_{s0}<4.9$		
	Rated load condition.	$Q_{s0,rated}=2$	$Q_{s0,rated}=3.5$	$Q_{s0,rated}=4.5$
	Modification in C_p.	$C_{pn}=1.04$		
	Improvement in power transfer.	1%	8%	28%
PP Topology.	Bifurcation criterion.	$Q_{s0}<4.9$		
	Rated load condition.	$Q_{s0,rated}=2$	$Q_{s0,rated}=3.5$	$Q_{s0,rated}=4.5$
	Modification in C_p.	$C_{pn}=1.04$	$C_{pn}=1.02$	$C_{pn}=1.01$
	Improvement in power transfer.	1%	2%	3%
PS Topology.	Bifurcation criterion.	$Q_{s0}<5.1$		
	Rated load condition.	$Q_{s0,rated}=2$	$Q_{s0,rated}=3.5$	$Q_{s0,rated}=4.5$
	Modification in C_p.	$C_{pn}=0.99$	$C_{pn}=0.98$	$C_{pn}=0.97$
	Improvement in power transfer.	1%	5%	18%

TABLE 5-8
IMPROVEMENT OF THE POWER TRANSFER CAPABILITY WITH THE MODIFIED TUNING FOR A WELL-COUPLED SYSTEM (k=0.4)

SP Topology.	Bifurcation criterion.	$Q_{s0}<2.3$		
	Rated load condition.	$Q_{s0,rated}=1.5$	$Q_{s0,rated}=2$	$Q_{s0,rated}=2.2$
	Modification in C_p.	$C_{pn}=1.19$		
	Improvement in power transfer.	16%	45%	64%
PP Topology.	Bifurcation criterion.	$Q_{s0}<2.3$		
	Rated load condition.	$Q_{s0,rated}=1.5$	$Q_{s0,rated}=2$	$Q_{s0,rated}=2.2$
	Modification in C_p.	$C_{pn}=1.10$	$C_{pn}=1.04$	$C_{pn}=1.01$
	Improvement in power transfer.	6%	12%	15%
PS Topology.	Bifurcation criterion.	$Q_{s0}<2.7$		
	Rated load condition.	$Q_{s0,rated}=1.5$	$Q_{s0,rated}=2$	$Q_{s0,rated}=2.6$
	Modification in C_p.	$C_{pn}=0.95$	$C_{pn}=0.91$	$C_{pn}=0.85$
	Improvement in power transfer.	9%	23%	59%

InductEV, Inc.
Exhibit 1008
Page 170

5-6 VERIFICATION

The design of the contact-less electric vehicle battery charger having a PP topology (previously described in section 3-11 and investigated in section 4-6) is now reconsidered using the modified tuning proposed in (5-2) for C_p. The controller is designed to operate with unity DPF. The operating frequency and power transfer capability are calculated for this operating condition, and then verified by experimental measurements.

With other design parameters unchanged, C_{pn} can be determined from the known k (of 0.45) and Q_{s0} (of 1.8) at rated load (of 6Ω). It is calculated to be 1.04. The modified tuning thus requires a C_p 4% higher than the original tuning. As a result, C_p needs to be increased from 2.20μF to 2.28μF.

Under variable frequency control where the controller is made to operate at the zero-phase angle of the power supply load impedance (at unity DPF as discussed in section 5-5), it is crucial with this modified tuning to ensure bifurcation-free operation for all loading conditions up to and including rated load. The primary quality factor (Q_{p0}) calculated using (5-9) is 2.19. The bifurcation criterion given by Table 5-5 (for the PP topology) is $Q_{p0}>Q_{s0}$. Since the calculated Q_{p0} satisfies this criterion, the system should not bifurcate for all normal operating loads, up to and including rated operation.

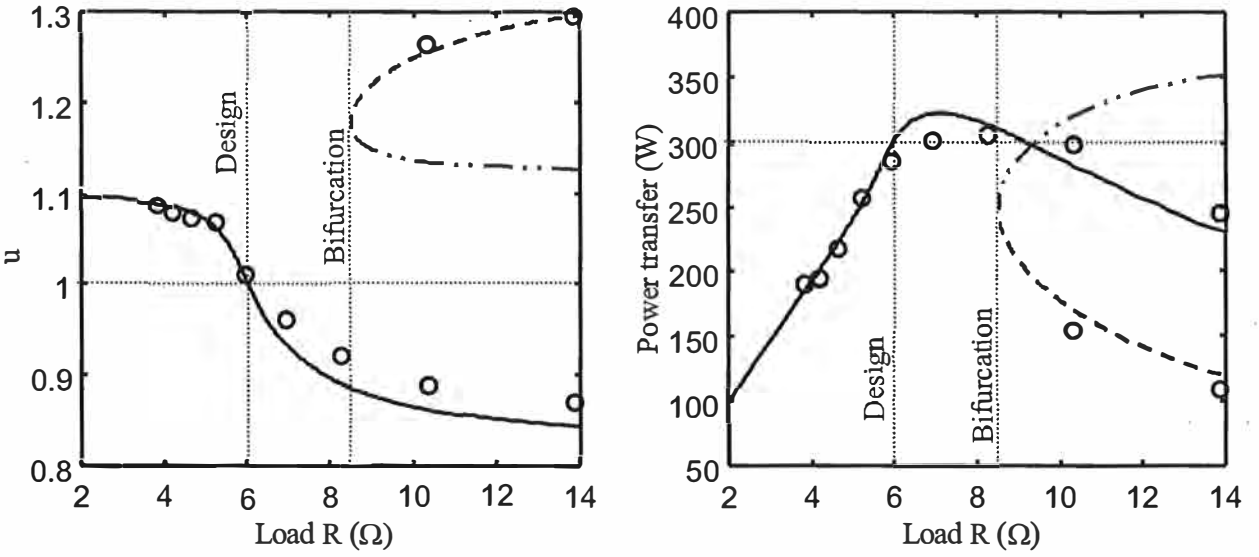
The bifurcation phenomenon and power transfer capability are shown in Fig. 5-17, where the operating frequency and power transfer curves are functions of the load extended into the bifurcation region. The measured operating frequencies and power transfers are shown in Fig. 5-17 as circles at each of the measured loads. As shown, the measured results closely follow theoretical curves.

Operation at ω_0 is achieved at rated load due to the modified tuning, and bifurcation is only apparent at higher loads, while the power transfer capability is equal to the desired power of 300W (30kW at rated primary current 150A) at rated load. With the original tuning, the power transfer at rated load condition is 266W. Here the change in C_p is only 4% and the improvement in power transfer capability is close to 13%.

At light loads, frequency detuning is unavoidable but it is less than that with the original tuning, where, as shown in Fig. 5-17 (b-i), the operating frequency is detuned more than 10% above ω_0 for all loads up to rated load. Because the pickup is better tuned, the power transfer capability at light loads is also higher than the original tuning.

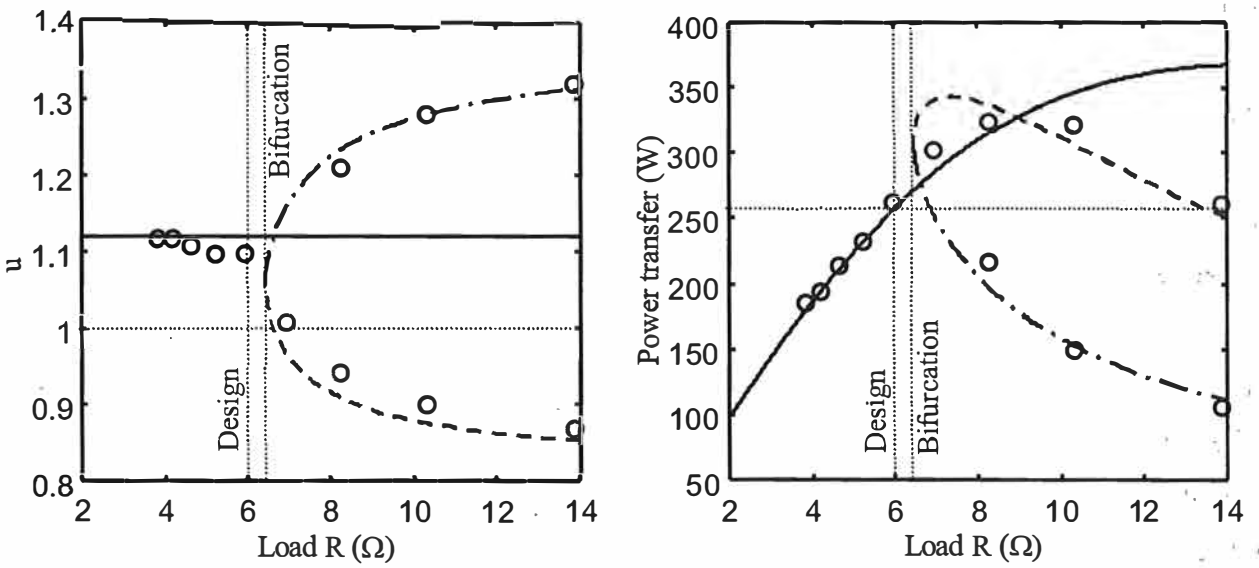
The maximum power point of the re-tuned system under bifurcation-free operation is achieved at a slightly higher load than 'rated' despite the operating frequency being a little lower than ω_0. This maximum power transfer capability as shown is 322W (32.2kW at rated primary current 150A). Beyond this point (as the load is increased further), the power transfer capability decreases because the operating frequency drops away from ω_0.

InductEV, Inc.
Exhibit 1008
Page 171



(i) Operational frequency. (ii) Power transfer capability (I_p=15A).

(a) Modified tuning.



(i) Operational frequency. (ii) Power transfer capability (I_p=15A).

(b) Original tuning.

Fig. 5-17. A contact-less electric vehicle battery charger with PP topology – Operating frequency and power transfer capability under variable-frequency operation (a comparison of the original and modified tuning schemes).

As discussed in section 5-3, the modified tuning for this PP topology also increases the bifurcation boundary resulting in a larger safety margin before bifurcation. The onset of bifurcation occurs at 6.4Ω with the original tuning. It increases by 33% to 8.5Ω due to the modified tuning. Fig. 5-17 also clearly shows why a variable-frequency controller requires a suitable safety margin to ensure bifurcation-free operation over all practical power demands. Once such a controller begins to operate within the bifurcation region, the potential power delivery varies significantly if the controller moves in operation between the highest and lowest operational frequencies.

InductEV, Inc.
Exhibit 1008
Page 172

5-7 CONCLUSIONS

In this chapter the primary tuning capacitance (C_p) was modified to compensate not only the self-inductance of the primary coil but also the loading effects of the secondary resonant circuit on the primary. All other design parameters determined by the design methodology described in Chapter 4 were left unchanged. Under variable-frequency operation with unity DPF, this modified tuning minimizes frequency-detuning effects in the pickup when operating at rated load, resulting in improved power transfer capability.

The magnitude of the change in C_p depends on the choices of the primary and secondary compensation topologies (SS, SP, PP and PS) as well as the fundamental design parameters k and Q_s. An SS topology does not require any change to C_p, whereas the SP topology requires a larger C_p with improved k. When the primary is parallel-compensated (the PP and PS topologies), C_p is a function of both k and Q_s. In this case, C_p needs to be selected for rated load to achieve the required power. The required modification in C_p could be as high as 20% in a middle coupled high Q_s system, or 40% in a well coupled medium Q_s system.

Bifurcation criteria were developed for each of the basic ICPT topologies. As shown bifurcation -free operation is ensured if a design satisfies the bifurcation criteria. It was found that the SP and PP topologies have identical bifurcation criteria, while those of the SS and PS topologies are different. The bifurcation criteria were found to be simple equations dependent on Q_p and Q_s. When Q_s is high, the bifurcation criteria of each topology can be simply stated as $Q_p > Q_s$. Since Q_p and Q_s are inversely related, ICPT systems will always bifurcate with increased loading (Q_s).

The bifurcation criteria can also be expressed in terms of k and Q_s allowing subtly different interpretations. Here it was noted that the maximum allowable Q_s decreases as k improves. With a k of 0.1, the maximum Q_s is about 10 in all topologies. With an increased k of 0.6, the maximum allowable Q_s before bifurcation drops to less than 2, but varies between the topologies.

With k and Q_s determined using the design methodology described in Chapter 4, the bifurcation criteria can be used to evaluate the potential improvement in the power transfer capability by modifying C_p. This improvement is guaranteed providing the bifurcation criterion is satisfied. If the bifurcation criterion is violated, both the original tuning and the modified tuning cannot transfer the designed power and the system should be redesigned to reduce either k or Q_s.

With systems that meet the bifurcation criteria with a large safety margin, the difference between the modified tuning and the original tuning is small, and the improvement in the power transfer capability is negligible. This improvement becomes more significant in systems that satisfy the

InductEV, Inc.
Exhibit 1008
Page 173

bifurcation criteria with a small safety margin.

For the SP and PS topologies with good coupling, the modified tuning can increase the power transfer capability by more than 50%. Here the required modification in C_p is significant, and should be used in practical systems. For the PP topology with good coupling, or the SP and PS topologies with middle coupling, the potential improvement in the power transfer capability is about 10% to 25%. In these cases, the required modification in C_p is small. This is achievable in practice if good lifetime capacitance stability is available.

In loosely coupled systems, the modified tuning and the original tuning are essentially identical as the required modification in C_p is negligible. For middle coupled systems, the original tuning also works well for the PP topology and the SP and PS topologies with low Q_s.

Both the theoretical power transfer capability and bifurcation phenomenon predicted for the modified tuning were verified by a practical example using a contact-less electric vehicle battery charger. The measurements were found to follow the calculated values closely. When the system is designed to satisfy the bifurcation criterion with a suitable safety margin, it is able to ensure bifurcation-free operation for all loading conditions up to and including rated load.

REFERENCES

[1]. J. B. Turner, "Autotuned resonant power source," *US-Patent No. 5006973*, Apr. 9, 1991.

[2]. T. Bieler, M. Perrottet, V. Nguyen, Y. Perriard, "Contactless power and information transmission," in *Conf. Rec. IEEE-IAS Annual Meeting*, vol. 1, 2001, pp. 83-88.

[3]. R. Laouamer, M. Brunello, J. P. Ferrieux, O. Normand, N. Buchheit, "A multi-resonant converter for noncontact charging with electromagnetic coupling," in *Conf. Rec. IEEE-IES Annual Conference*, vol. 2, 1997, pp. 792-797.

[4]. H. Abe, H. Sakamoto, K. Harada, "A noncontact charger using a resonant converter with parallel capacitor of the secondary coil," *IEEE Transactions on Industry Applications*, vol. 36, pp. 444-451, Mar./Apr. 2000.

[5]. A. Okuno, L. Gamage, M. Nakaoka, "Performance evaluations of high-frequency inverter-linked DC/DC converter with noncontact pickup coil," *IEEE Transactions on Industrial Electronics*, vol. 48, pp. 475-477, Apr. 2001.

[6]. J. T. Boys, G. A. Covic, A. W. Green, "Stability and control of inductively coupled power transfer systems," *IEE Proceedings - Electric Power Applicaions*, vol. 147, pp. 37-43, Jan. 2000.

InductEV, Inc.
Exhibit 1008
Page 174

[7]. G. A. Covic, G. Elliott, O. H. Stielau, R. M. Green, J. T. Boys, "The design of a contact-less energy transfer system for a people mover system," in *Conf. Rec. International Conference on Power System Technology*, vol. 1, Dec. 2000, pp. 79-84.

[8]. Chwei-Sen Wang, G. A. Covic, O. H. Stielau, "General stability criterions for zero phase angle controlled loosely coupled inductive power transfer systems," in *Conf. Rec. IEEE-IES Annual Conference*, vol. 2, 2001, pp. 1049-1054.

[9]. A. P. Hu, *Selected resonant converters for IPT power supplies*, PhD thesis, The Electrical and Electronics Engineering Department, The University of Auckland, Auckland, New Zealand, 2001, pp. 68-79.

[10]. O. H. Stielau, G. A. Covic, "Design of loosely coupled inductive power transfer systems," in *Conf. Rec. International Conference on Power System Technology*, vol. 1, Dec. 2000, pp. 85-90.

[11]. A. W. Green, J. T. Boys, "An inductively coupled high-frequency power system for material handling applications," in *Conf. Rec. International Power Electronics*, vol. II, 1993, pp. 821-826.

[12]. J. Gullberg, *Mathematics: From the Birth of Numbers*, W.W. Norton&Company, New York, 1997, pp. 320-324.

InductEV, Inc.
Exhibit 1008
Page 175

InductEV, Inc.
Exhibit 1008
Page 176

CHAPTER 6

TUNING TO IMPROVE DPF FOR FIXED-FREQUENCY SYSTEMS

6-1 Introduction
6-2 System behaviour with primary tuning for unity DPF at rated load
6-3 Primary tuning for load independent unity DPF
6-4 Discussion
6-5 Design examples
6-6 Verification
6-7 Conclusions

6-1 INTRODUCTION

This chapter investigates a method by which the displacement power factor (DPF) of an ICPT power supply operating under fixed frequency operation can be improved. When the frequency of the power supply is fixed to the nominal frequency (ω_0), primary tuning does not affect the power transfer capability to the pickup loads providing the supply can maintain the primary current constant under all loading conditions. However the DPF of the power supply may be well below unity if its load resonant tank is not properly tuned. Consequently, this Chapter focuses on suitable variations to the primary tuning with the design methodology described in Chapter 4.

The modified primary tuning proposed in Chapter 5 for variable frequency systems is investigated first. Here the design ensures unity DPF at rated load. However many practical ICPT systems are found to operate for considerable periods of time under lightly load conditions, thus ideally DPF should be improved under all loading conditions (up to and including rated load). An alternative tuning option is therefore investigated that aims to achieve load independent unity DPF.

6-2 SYSTEM BEHAVIOUR WITH PRIMARY TUNING FOR UNITY DPF AT RATED LOAD

It is assumed in this section that the primary compensation capacitance (C_p) is modified using (5-2) so that unity DPF is assured at rated load for fixed-frequency systems operating at ω_0. As noted in section 5-2, the original tuning assumed with the design methodology described in Chapter 4 works

InductEV, Inc.
Exhibit 1008
Page 177

well for the SS topology. Here unity DPF is achieved independent of the load and there is no need to modify C_p. This section thus focuses on the SP, PP and PS topologies, where the original tuning does not have unity DPF and modification of C_p is required.

Similar to the analysis in section 4-5.1, the phase angle between the fundamental components of the output voltage and current of the power supply can be calculated using the normalized load impedance (Z_{tn}) as:

$$\tan\theta_1 = \frac{\mathrm{Im}Z_{tn}}{\mathrm{Re}Z_{tn}} \text{ or } \tan\theta_1 = \frac{-\mathrm{Im}Y_{tn}}{\mathrm{Re}Y_{tn}} \tag{6-1}$$

The DPF of the power supply can then be determined from this phase angle as:

$$\mathrm{DPF} = \cos\theta_1 \tag{6-2}$$

Thus under fixed frequency operation at ω_0 (u=1), equation (6-1) can be calculated (using the normalized load impedance given in Table 5-2 and Table 5-3) as:

$$\tan\theta_1(u=1) = \begin{cases} \left(\frac{1}{k^2 Q_{s0}}\right)\left(1-k^2-\frac{1}{C_{pn}}\right)=0 & \text{SP topology} \\ -k^2 Q_{s0} C_{pn} + \left(\frac{1-k^2}{Q_{s0}}\right)\left(\frac{1-C_{pn}+k^2 C_{pn}}{k^2}\right) & \text{PP topology} \\ -k^2 Q_{s0} C_{pn} + \left(\frac{1}{k^2 Q_{s0}}\right)\left(1-C_{pn}\right) & \text{PS topology} \end{cases} \tag{6-3}$$

where the normalized primary compensation capacitance C_{pn} is summarized in Table 6-1 for both the original tuning and the modified tuning. For the PP and PS topologies, the required C_{pn} with the modified tuning is a function of the load (Q_{s0}=$Q_s(\omega=\omega_0)$ equals "$\omega_0 C_s R$" for a parallel pickup and "$1/(\omega_0 C_s R)$" for a series pickup), and it is assumed here that C_{pn} is selected for rated operation ($Q_{s0,rated}$). It should be noted that as the operating frequency is fixed at ω_0 (u=1), the operating secondary quality factor Q_s equals Q_{s0} under all conditions.

With the phase angle determined by (6-3), the DPF of the power supply can be calculated using (6-2). They are functions of k, Q_{s0} and C_{pn}. As shown in Table 6-1, C_{pn} is a function of k for the SP topology, and depends on both k and $Q_{s0,rated}$ for the PP and PS topologies. Influences of this modified tuning on DPF are topology dependent as shown in Fig. 6-1 to Fig. 6-3. In these figures, the modified design is labelled "modified tuning", and the system designed using the methodology described in Chapter 4 is labelled "original tuning". The modified tuning and the original tuning are compared for loosely coupled (low k), mid-coupled (middle k), and well-coupled (high k) systems. For the PP and PS topologies, the difference between high and low $Q_{s0,rated}$ systems are identified.

InductEV, Inc.
Exhibit 1008
Page 178

TABLE 6-1
A SUMMARY OF C_{pn} FOR THE ORIGINAL TUNING AND THE MODIFIED TUNING FOR UNITY DPF AT RATED LOAD

Topologies	C_{pn}	
	Original tuning	Modified tuning
SS	1	1
SP	1	$\frac{1}{1-k^2}$
PP	1	$\frac{1-k^2}{Q_{s0,rated}^2 k^4 + (1-k^2)^2}$
PS	1	$\frac{1}{Q_{s0,rated}^2 k^4 + 1}$

SP Topology: In the SP topology, the DPF is independent of k under both the original and modified tuning. As shown in Fig. 6-1, the modified tuning has unity DPF at all loads (Q_s). The improvement in DPF under lightly loading conditions (low Q_s) is more significant. When Q_s is high, the DPF of the original system is very close to unity, and the difference between this system and that resulting from the modified tuning is negligible.

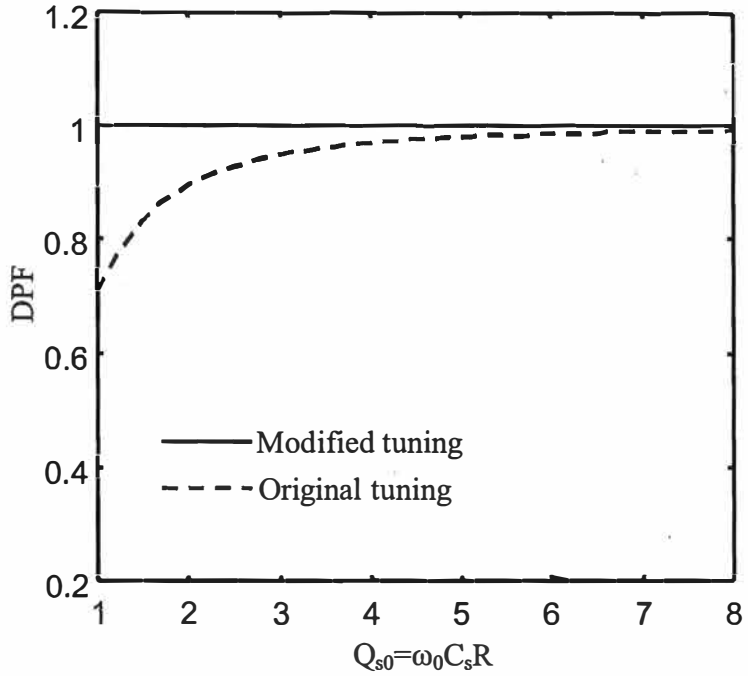
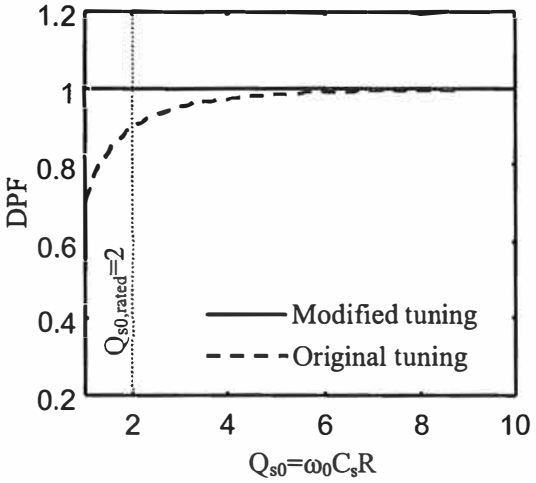
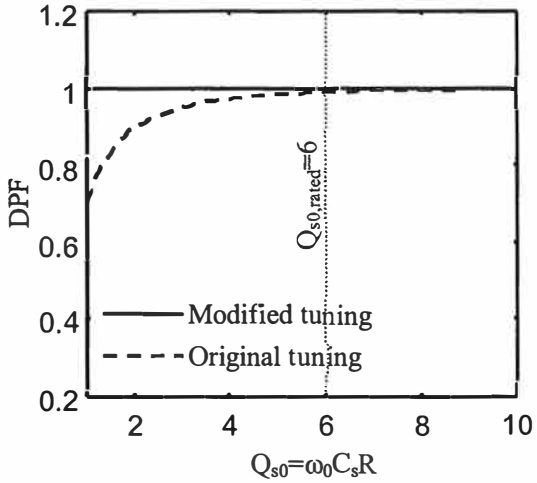


Fig. 6-1. SP topology - DPF under fixed-frequency operation at ω_0 assuming modified primary tuning to achieve unity DPF at rated load.

InductEV, Inc.
Exhibit 1008
Page 179

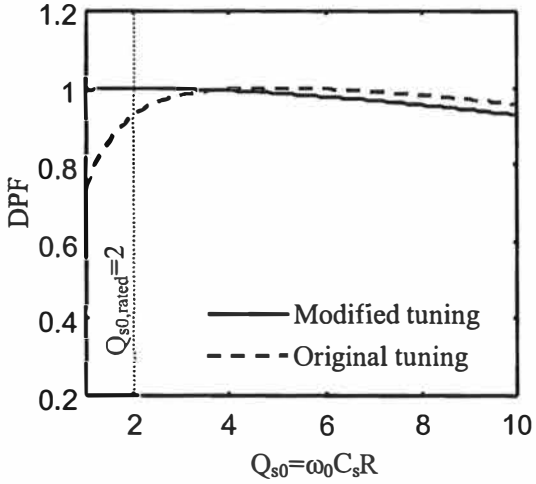


(i) Low $Q_{s0,rated}$ pickup.

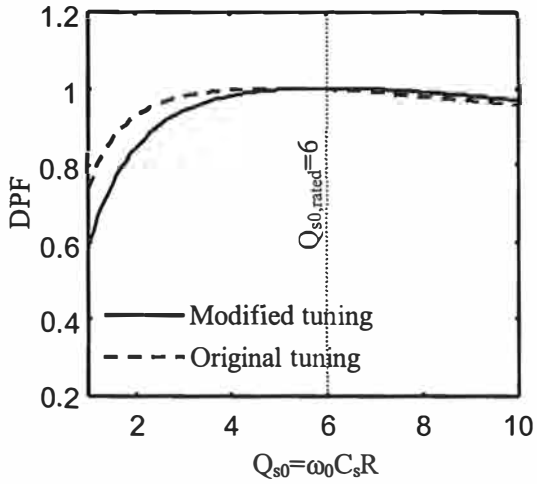


(ii) High $Q_{s0,rated}$ pickup.

(a) Loosely coupled systems (k=0.05).

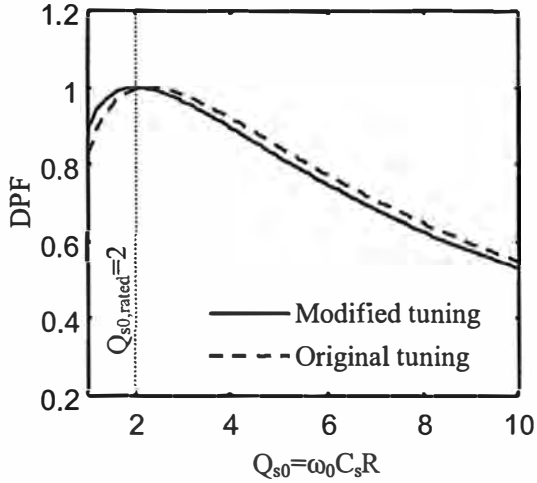


(i) Low $Q_{s0,rated}$ pickup.

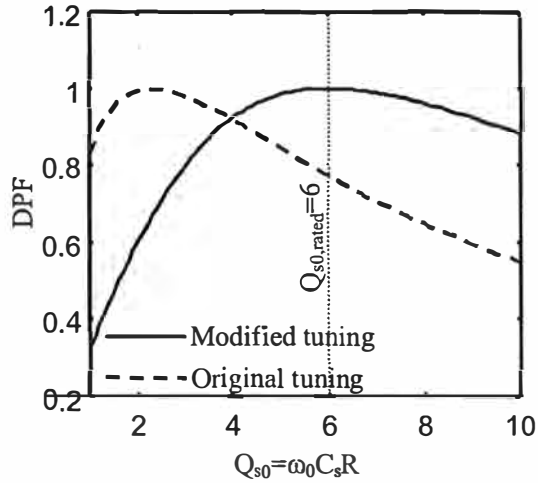


(ii) High $Q_{s0,rated}$ pickup.

(b) Mid-coupled systems (k=0.2).



(i) Low $Q_{s0,rated}$ pickup.

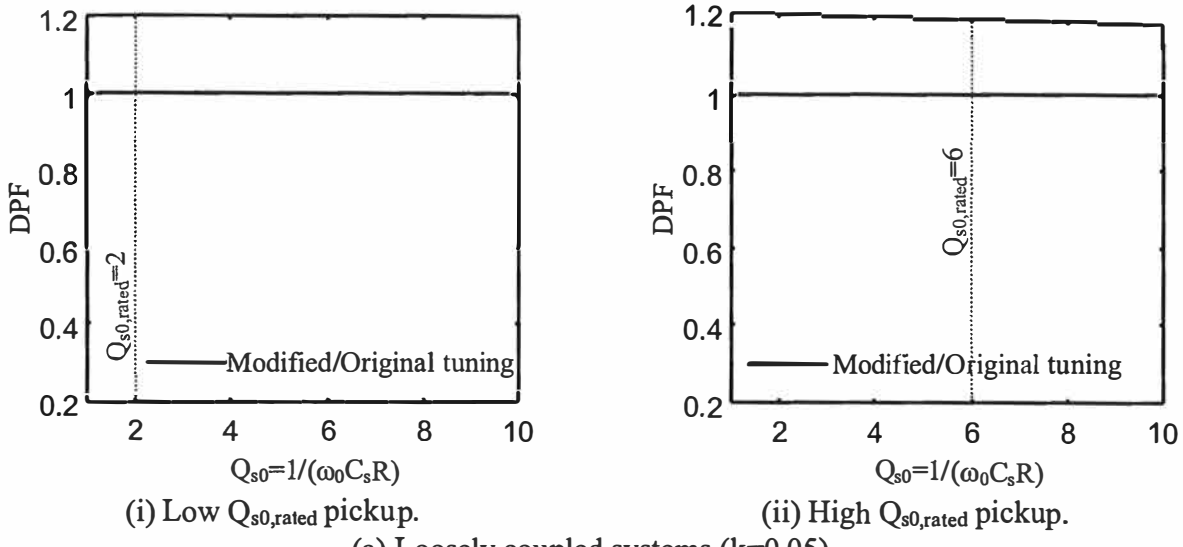


(ii) High $Q_{s0,rated}$ pickup.

(c) Well-coupled systems (k=0.4).

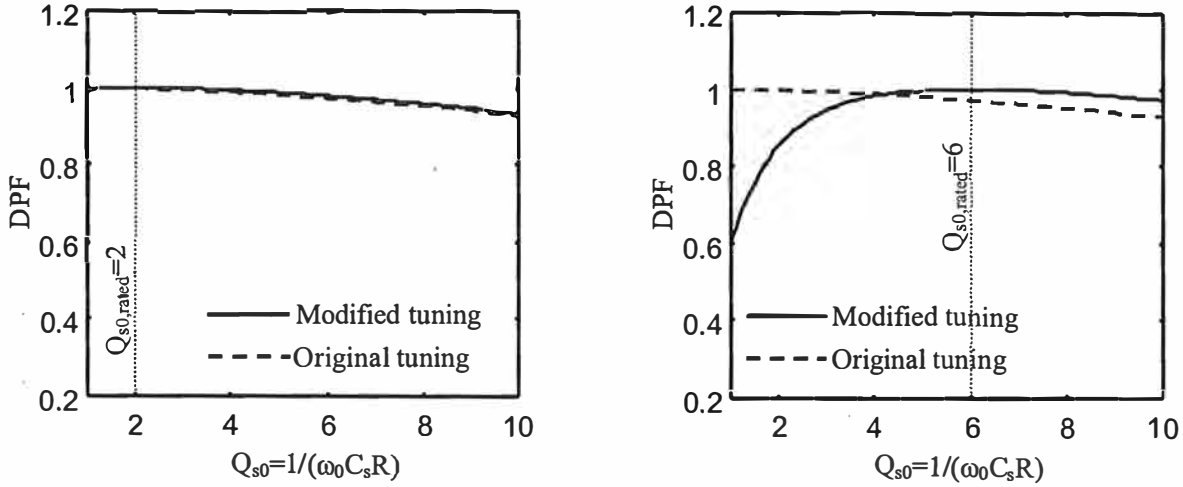
Fig. 6-2. PP topology - DPF under fixed-frequency operation at ω_0 assuming modified primary tuning to achieve unity DPF at rated load.

InductEV, Inc.
Exhibit 1008
Page 180



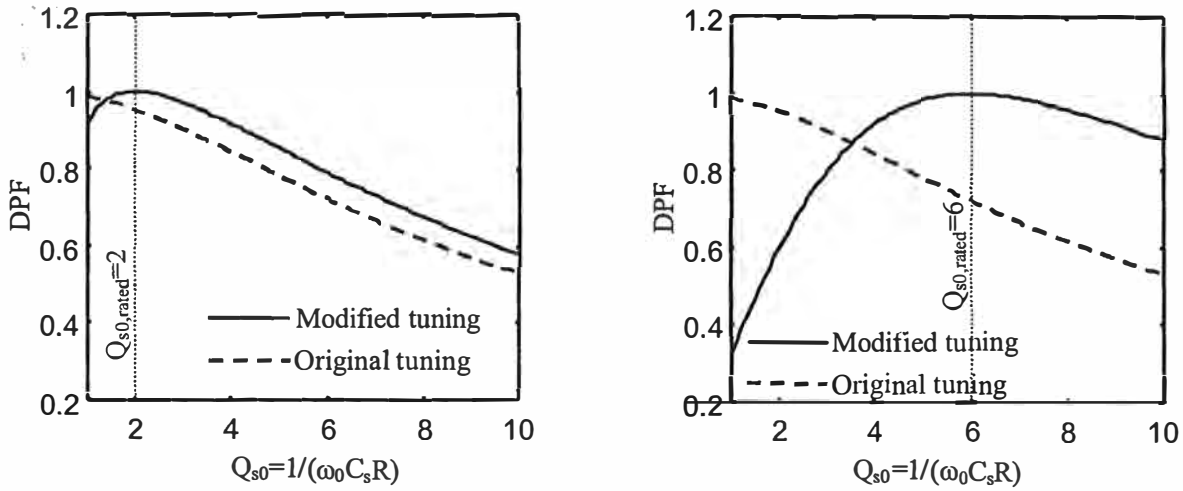
(i) Low $Q_{s0,rated}$ pickup. (ii) High $Q_{s0,rated}$ pickup.

(a) Loosely coupled systems (k=0.05).



(i) Low $Q_{s0,rated}$ pickup. (ii) High $Q_{s0,rated}$ pickup.

(b) Mid-coupled systems (k=0.2).



(i) Low $Q_{s0,rated}$ pickup. (ii) High $Q_{s0,rated}$ pickup.

(c) Well-coupled systems (k=0.4).

Fig. 6-3. PS topology - DPF under fixed-frequency operation at ω_0 assuming modified primary tuning to achieve unity DPF at rated load.

InductEV, Inc.
Exhibit 1008
Page 181

PP Topology: The original and modified tuning schemes are identical at the following condition:

$$Q_{s0,rated} = \frac{\sqrt{1-k^2}}{k} \tag{6-4}$$

Interestingly, this is the bifurcation boundary given in Table 5-5. It occurs at larger Q_s in loosely coupled systems. With a k of 0.05, 0.2 and 0.4, the original tuning achieves unity DPF at Q_s of 20, 4.9 and 2.3 respectively.

The degree of influence of the proposed modified tuning on DPF depends strongly on $Q_{s0,rated}$ as shown in Fig. 6-2. If $Q_{s0,rated}$ equals the value given in (6-4), the original tuning and the modified tuning are identical. With $Q_{s0,rated}$ below this value, the modified tuning improves the DPF for all loading conditions up to and including rated load. When $Q_{s0,rated}$ is above this value, the modified tuning improves the DPF only when Q_s is close to $Q_{s0,rated}$, but undesirably decreases the DPF at lower Q_s values.

PS Topology: With this topology, the original tuning has a DPF below unity for all normal Q_s, and the modified tuning achieves unity DPF only at $Q_{s0,rated}$ as shown in Fig. 6-3. The influences of k and Q_s on the DPF of the original tuning are quite different between the PP and PS topologies (as discussed in section 4-5.2). However, here with the suggested modified tuning the two topologies have similar characteristics. The DPF under lightly loading conditions (corresponding to lower Q_s) can however be poor when k is good and $Q_{s0,rated}$ is high. Overall the shift is desirable since the improvement in DPF at rated load minimizes the required VA rating of the power supply. The change is more significant in well-coupled systems with high $Q_{s0,rated}$. In order to improve the DPF for all loading conditions up to and including rated load, an alternative primary tuning option is proposed in the following section.

6-3 PRIMARY TUNING FOR LOAD INDEPENDENT UNITY DPF

In the previous section, it was noted that unity DPF could be achieved under all loading conditions only in series tuned primary systems using the tuning methodology described. In this section, a new primary tuning methodology is proposed that makes the load reactance (Im Z_t) equal to zero under all loading conditions in order to achieve load independent unity DPF for both series and parallel tuned primary systems. For parallel tuned primaries this is possible only with suitable modifications to the primary compensation capacitance and/or the operating frequency assumed with the design methodology described in Chapter 4. Influences of such modifications on the power transfer capability and the required secondary VA rating are investigated in order to identify the required operating conditions when using the modified systems to transfer rated power.

InductEV, Inc.
Exhibit 1008
Page 182

6-3.1 PRIMARY CAPACITANCE AND OPERATING FREQUENCY

The required primary compensation capacitance (C_{pn}) and the operating frequency (u) (derived in Appendix I) to achieve the above stated objectives are given in Table 6-2. In respect to the SP, PP and PS topologies, they are functions of k and independent of Q_{s0}. The latter independency ensures that unity DPF is possible under all load conditions.

As expected, there is no need to change either C_p or the operating frequency for the SS topology, while the SP topology requires a different C_p identical to the modified tuning proposed in section 5-2. The PP topology does not change C_p but requires a different operating frequency, while the PS topology needs to change both C_p and the operating frequency.

It should be noted that the required changes to the operating frequency for the PP and PS topologies will necessarily affect the power transfer capability and needs to be considered carefully when using the modified primary tuning methodology. This is investigated in section 6-3.2.

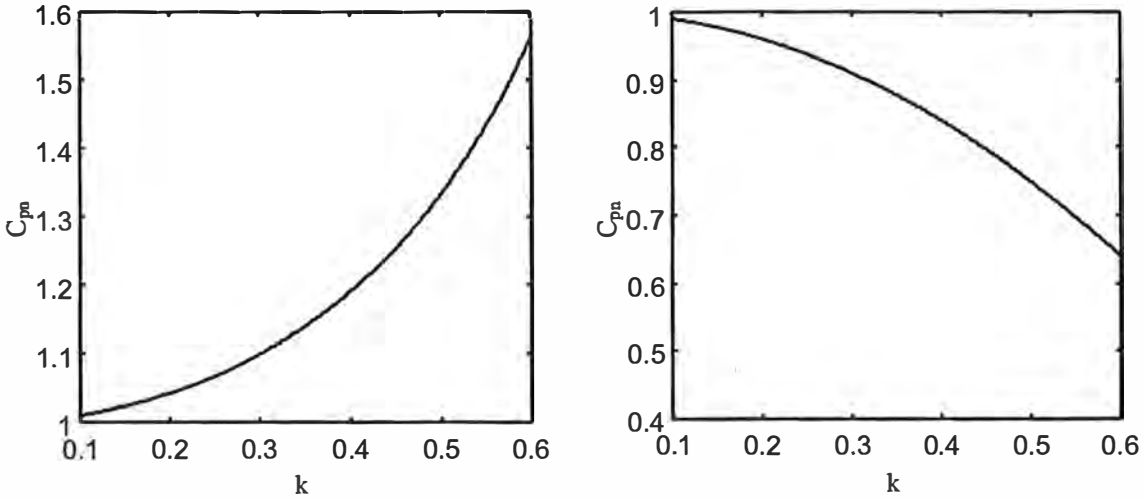
TABLE 6-2
NORMALIZED PRIMARY COMPENSATION CAPACITANCE AND OPERATING FREQUENCY REQUIRED TO ACHIEVE LOAD INDEPENDENT UNITY DPF

Topology	Normalized Primary Capacitance (C_{pn})	Normalized Operating Frequency (u)
SS	1	1
SP	$\frac{1}{1-k^2}$	1
PP	1	$\frac{1}{\sqrt{1-k^2}}$
PS	$1-k^2$	$\frac{1}{\sqrt{1-k^2}}$

The influence of k on the required change to C_p is shown in Fig. 6-4 for the SP and PS topologies (SS and PP topologies do not require a different C_p). The SP topology requires a larger C_p, while the PS topology needs a smaller C_p. The necessary change is small in loosely coupled systems, but becomes quite significant in well-coupled systems. With k of 0.6 the SP topology requires a 56% larger C_p value, while the PS topology needs a 36% smaller C_p value.

The required changes to the operating frequency are identical in both the PP and PS topologies as shown in Fig. 6-5. Here, it is necessary to deliberately operate at a frequency above ω_0 (u>1). The required change is small in loosely coupled (low k) systems, but becomes significant with improving k.

InductEV, Inc.
Exhibit 1008
Page 183



(a) SP topology. (b) PS topology.

Fig. 6-4. Influences of k to the required change in C_p to achieve load independent unity DPF.

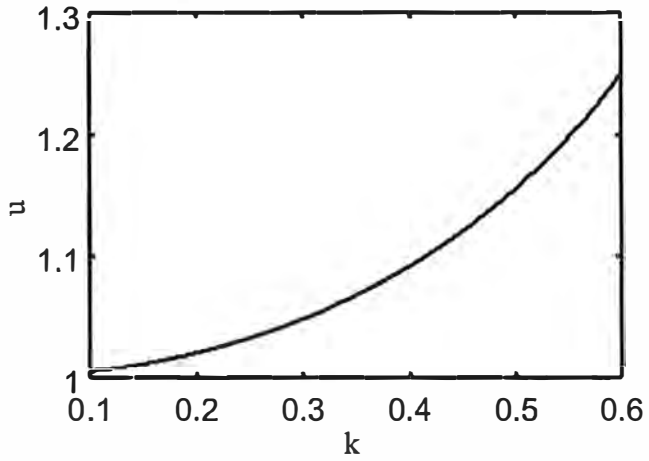


Fig. 6-5. Influence of k to the required change in ω to achieve load independent unity DPF (the PP and PS topologies).

6-3.2 POWER TRANSFER CAPABILITY AND SECONDARY VA RATING

The SS and SP topologies do not require a change to the operating frequency, and as such this tuning approach does not influence the power transfer capability or the required secondary VA rating. Furthermore, these tuning options are identical to those proposed in section 6-2 and have therefore been fully discussed already.

Consequently, this section focuses only on the PP and PS topologies, where operating above ω_0 is required. The behaviours of these systems are shown in Fig. 6-6 and 6-7. Here each system using the design methodology described in Chapter 4 is shown using dashed lines (labelled as "original tuning"), while all systems using the primary compensation capacitance and operating frequency given in Table 6-2 are shown as solid lines (labelled as "modified tuning").

InductEV, Inc.
Exhibit 1008
Page 184

Under the modified tuning suggested, the operating frequency shifts above ω_0 by increasing amounts as the coupling increases. With k of 0.2, 0.3 and 0.4, this shift in ω_0 is about 2%, 5% and 9% respectively. These percentage changes in ω_0 reflects the percentage changes in Q_s under all loading conditions, since for the PP topology "$Q_s=uQ_{s0}$" while in the PS topology "$Q_s=Q_{s0}/u$".

The need to deliberately detune the operating frequency above ω_0 for the PP and PS topologies in order to achieve load independent unity DPF affects the power transfer capability of the pickup. If the primary current is assumed constant, such influences can be quantified using the normalized power (P_n) defined in (5-7) using the rated power determined at rated load ($Q_{s0,rated}$) and ω_0 (u=1). Here P_n is determined to be a function of k, Q_{s0} and the specified rated load ($Q_{s0,rated}$) given by:

$$P_n = \begin{cases} \dfrac{1-k^2}{1-k^2+k^4Q_{s0}^2}\left(\dfrac{Q_{s0}}{Q_{s0,rated}}\right) & \text{PP topology} \\ \dfrac{1}{1-k^2+k^4Q_{s0}^2}\left(\dfrac{Q_{s0}}{Q_{s0,rated}}\right) & \text{PS topology} \end{cases} \tag{6-5}$$

For a general analysis, the secondary current, secondary voltage and required secondary VA rating are normalized here using the rated values determined at rated load and ω_0. The normalized secondary current and voltage can be calculated using Table 3-1 as:

$$I_{sn} = \frac{I_s}{I_{s0,rated}} = \begin{cases} \dfrac{\sqrt{\left(1-k^2+k^2Q_{s0}^2\right)^2+\left(1-k^2\right)^3Q_{s0}^2}}{\left(1-k^2+k^4Q_{s0}^2\right)\sqrt{1+Q_{s0,rated}^2}} & \text{PP topology} \\ \dfrac{Q_{s0}\sqrt{1-k^2+k^4Q_{s0}^2}}{\left(1-k^2+k^4Q_{s0}^2\right)Q_{s0,rated}} & \text{PS topology} \end{cases} \tag{6-6}$$

and

$$V_{sn} = \frac{V_s}{V_{s0,rated}} = \begin{cases} \dfrac{Q_{s0}\sqrt{\left(1-k^2\right)\left(1-k^2+k^4Q_{s0}^2\right)}}{\left(1-k^2+k^4Q_{s0}^2\right)Q_{s0,rated}} & \text{PP topology} \\ \dfrac{\sqrt{Q_{s0}^2+\left(1-k^2\right)\left(1-k^2Q_{s0}^2\right)^2}}{\left(1-k^2+k^4Q_{s0}^2\right)\sqrt{1+Q_{s0,rated}^2}} & \text{PS topology} \end{cases} \tag{6-7}$$

The normalized VA rating required for the pickup coil (VA_{sn}) is then:

$$VA_{sn} = \frac{VA_s}{VA_{s0,rated}} = I_{sn}V_{sn} \tag{6-8}$$

The normalized power (P_n), secondary current (I_{sn}), secondary voltage (V_{sn}) and required secondary VA rating (VA_{sn}) are shown in Fig. 6-6 and 6-7 by arbitrarily selecting $Q_{s0,rated}$ as 5. In loosely coupled

InductEV, Inc.
Exhibit 1008
Page 185

(low k) systems, the original tuning works well and the required change to C_p and the operating frequency is negligible. For such systems, there is essentially no difference between the original and modified tuning. For mid-coupled systems with k of about 0.2, rated power is achieved with the modified tuning but at a Q_{s0} slightly above $Q_{s0,rated}$. In well-coupled systems with k of about 0.4, the modified tuning cannot achieve rated power, and the system should be redesigned to have lower $Q_{s0,rated}$. A practical well-coupled low Q_s system (k=0.45, $Q_{s0,rated}$=1.8) for contact-less electric vehicle battery charging is discussed later in section 6-5.

With k of 0.3, rated power is achieved with the modified tuning at Q_{s0} of about 7.5 in the PP topology. At this operating condition, the secondary current and voltage increase by 27% and 22%, requiring a secondary VA rating increase of 55%. For the PS topology, rated power is achieved at Q_{s0} of about 6, and here the secondary current and voltage increases by 9% and 4% respectively, so that the required secondary VA rating increases by 14%. Generally, the PP topology requires a larger secondary VA rating than the PS topology when this modified tuning methodology is applied.

The power transfer capability of the original tuned system increases linearly with Q_{s0}, while that of the modified tuning increases but at a decreasing rate with Q_{s0} until it reaches a maximum point after which it drops. This maximum power point can be determined by:

$$\frac{dP_n}{dQ_{s0}} = 0 \qquad \text{PP and PS topologies} \qquad (6\text{-}9)$$

Substituting (6-5) into (6-9), the maximum power point is found to be:

$$Q_{s0} = \frac{\sqrt{1-k^2}}{k^2} \qquad \text{PP and PS topologies} \qquad (6\text{-}10)$$

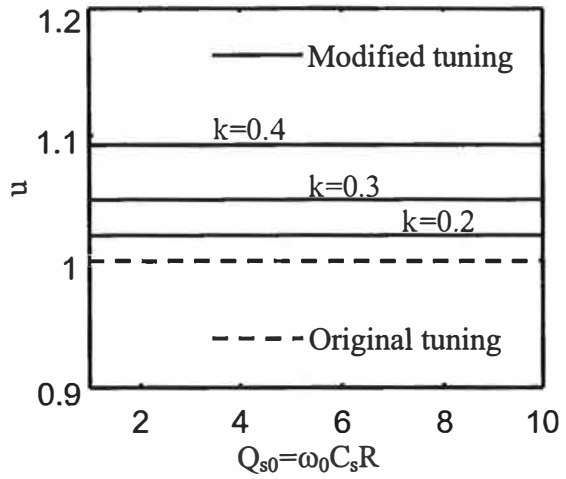
and

$$P_n = \begin{cases} \left(\dfrac{\sqrt{1-k^2}}{2k^2}\right)\left(\dfrac{1}{Q_{s0,rated}}\right) & \text{PP topology} \\ \left(\dfrac{1}{2k^2\sqrt{1-k^2}}\right)\left(\dfrac{1}{Q_{s0,rated}}\right) & \text{PS topology} \end{cases} \qquad (6\text{-}11)$$

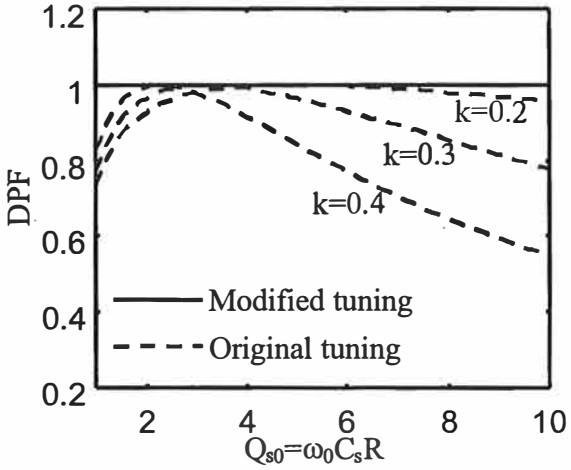
Assuming rated power can just be achieved with the modified tuning at the maximum power point, then replacing P_n with unity, $Q_{s0,rated}$ can be determined using (6-11) to be:

$$Q_{s0,rated} = \begin{cases} \dfrac{\sqrt{1-k^2}}{2k^2} & \text{PP topology} \\ \dfrac{1}{2k^2\sqrt{1-k^2}} & \text{PS topology} \end{cases} \qquad (6\text{-}12)$$

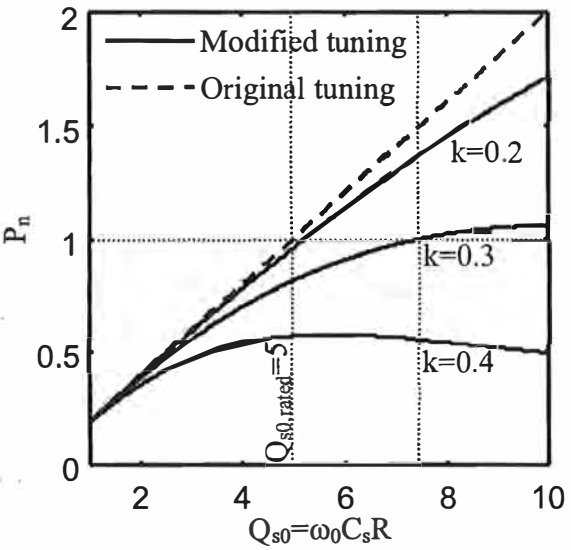
InductEV, Inc.
Exhibit 1008
Page 186



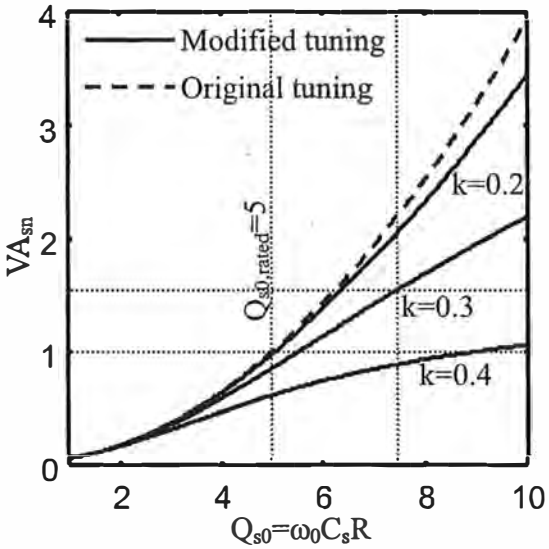
(a) Operating frequency.



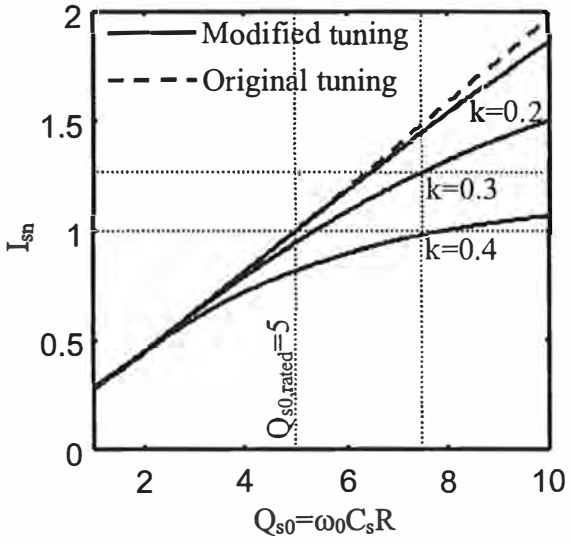
(b) DPF.



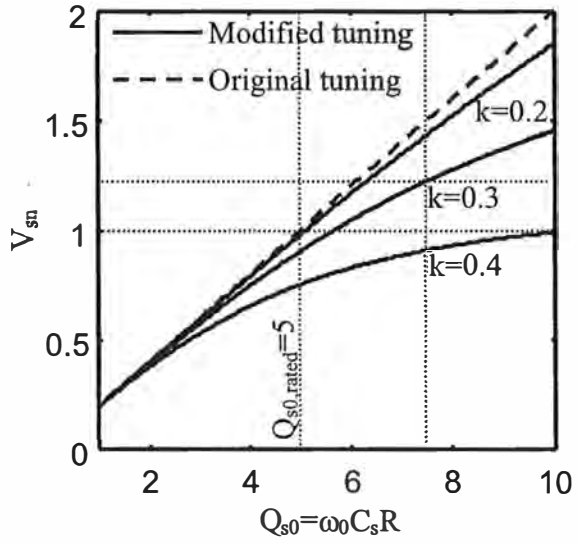
(c) Power transfer capability.



(d) Required secondary VA rating.



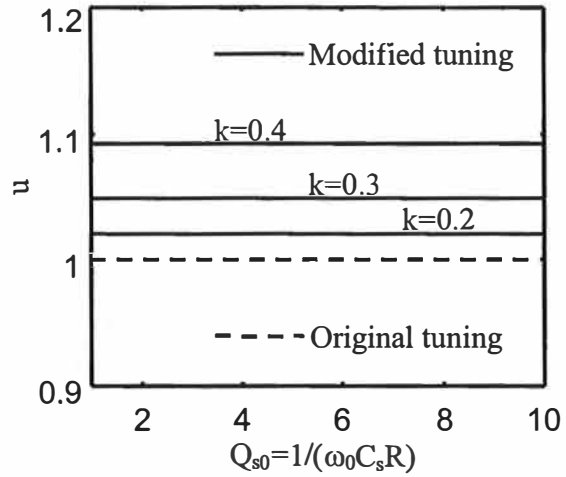
(e) Secondary current.



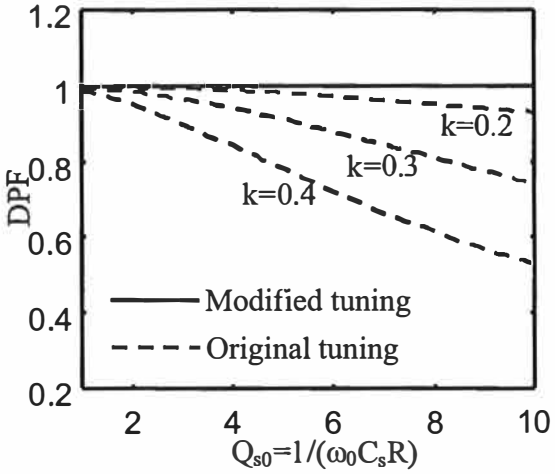
(f) Secondary voltage.

Fig. 6-6. PP topology – System behaviour under fixed-frequency operation ($Q_{s0,rated}=5$).

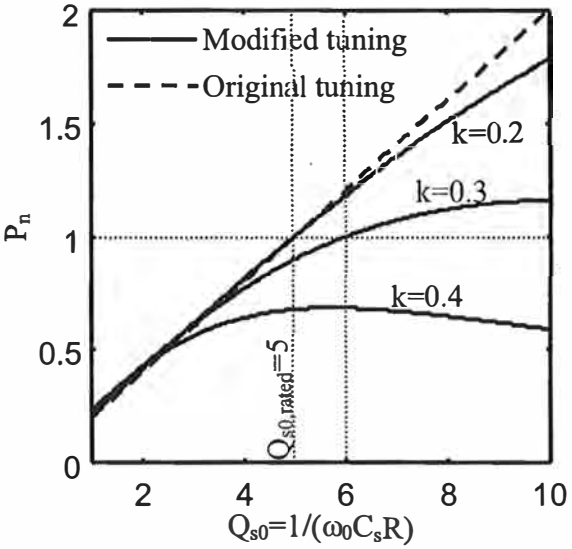
InductEV, Inc.
Exhibit 1008
Page 187



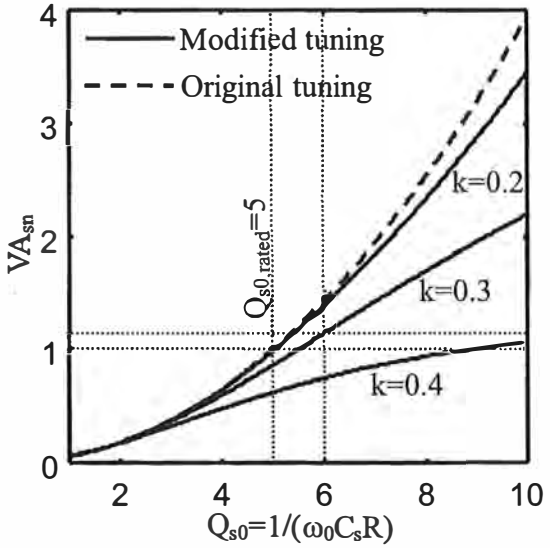
(a) Operating frequency.



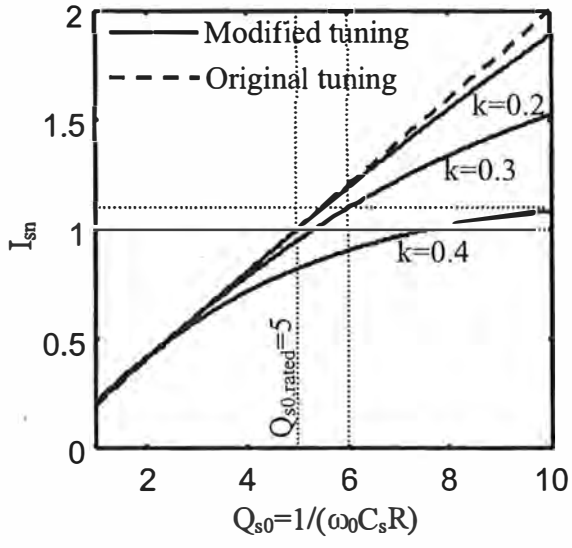
(b) DPF.



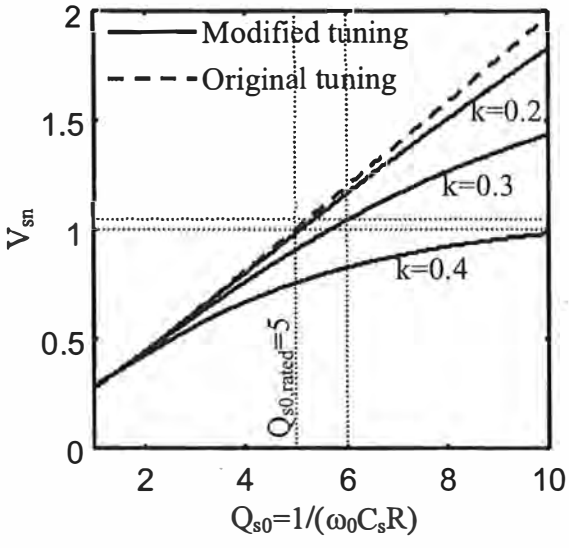
(c) Power transfer capability.



(d) Required secondary VA rating.



(e) Secondary current.



(f) Secondary voltage.

Fig. 6-7. PS topology – System behaviour under fixed-frequency operation ($Q_{s0,rated}=5$).

InductEV, Inc.
Exhibit 1008
Page 188

Equation (6-12) determines the maximum $Q_{s0,rated}$ for a given coupling k when using the modified tuning methodology to achieve load independent unity DPF for both the PP and PS topologies. This is shown in Fig. 6-8. For a given coupling k, it is necessary to ensure $Q_{s0,rated}$ is within the shaded region to ensure rated power can be achieved. The PS topology allows slightly larger $Q_{s0,rated}$ than the PP topology. For both topologies, a trade-off between k and $Q_{s0,rated}$ is necessary. In a mid-coupled system with k of 0.2, the maximum $Q_{s0,rated}$ is more than 10. The maximum $Q_{s0,rated}$ in a well-coupled system with k of 0.4 is much lower at about 3. Track-type systems are normally loosely-middle coupled with medium-high Q_s, while coil-type systems are normally middle-well coupled with low-medium Q_s, as such this characteristic suits practical ICPT systems since a well coupled high Q_s system would rarely if ever exist in practice.

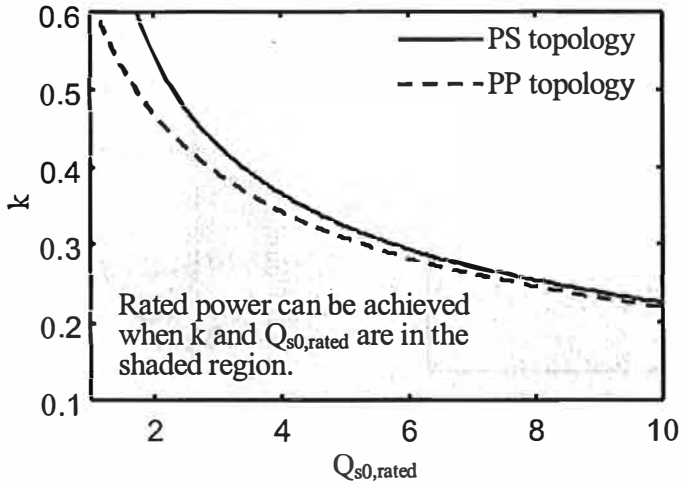
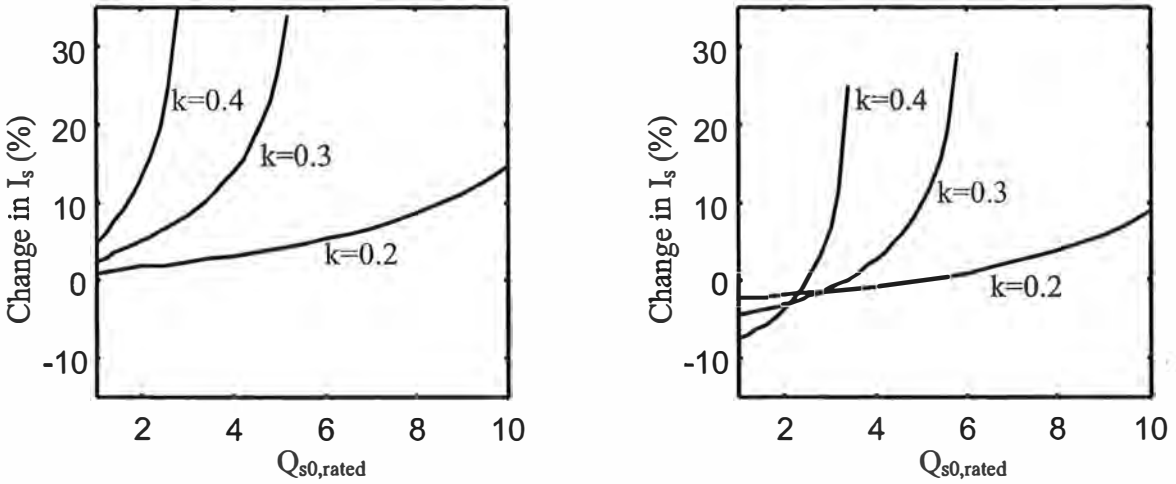


Fig. 6-8. Limit of k and $Q_{s0,rated}$ when using the modified tuning to achieve load independent unity DPF.

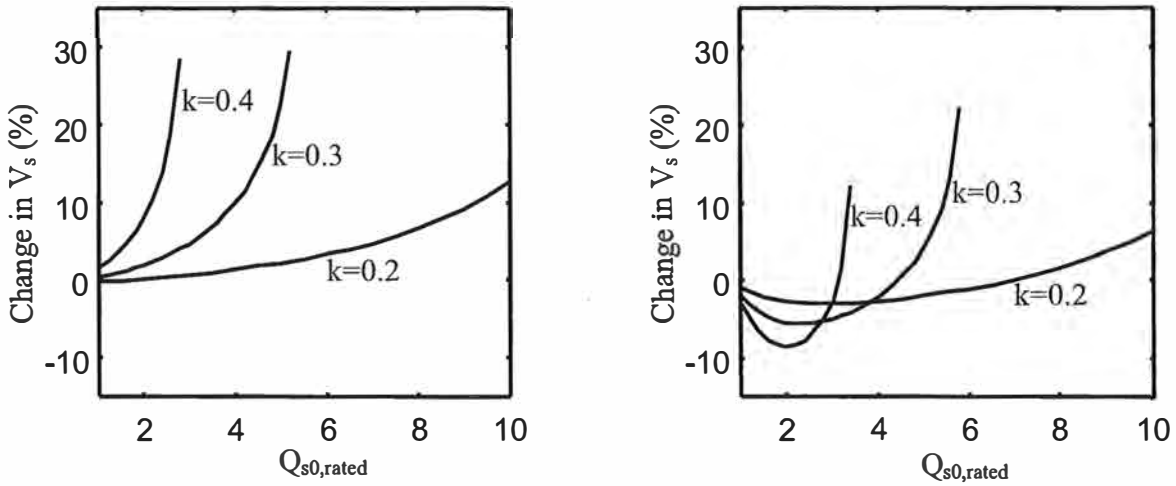
With the modified tuning applied, the changes in the secondary current, secondary voltage, required secondary VA rating when operating at rated power are shown in Fig. 6-9 for the PP and PS topologies. Here k is arbitrarily selected as 0.2, 0.3 and 0.4. In each case, the changes are calculated for all possible values of $Q_{s0,rated}$ within the shaded region in Fig. 6-8. For each value of k, the required Q_{s0} to achieve rated power (P_n=1) is calculated using (6-5). The secondary current, secondary voltage and required secondary VA rating at this new operating condition are then determined using (6-6), (6-7) and (6-8). These changes strongly depend on k and $Q_{s0,rated}$. For systems using a PP topology, the required secondary VA rating with the modified tuning is always higher than the original tuning. This increase is small for loosely coupled systems with reasonable $Q_{s0,rated}$, or well-coupled systems with low $Q_{s0,rated}$, but can be more than 50% for well-coupled systems with high $Q_{s0,rated}$. It is also found that the increase in the secondary voltage is less than the secondary current.

InductEV, Inc.
Exhibit 1008
Page 189



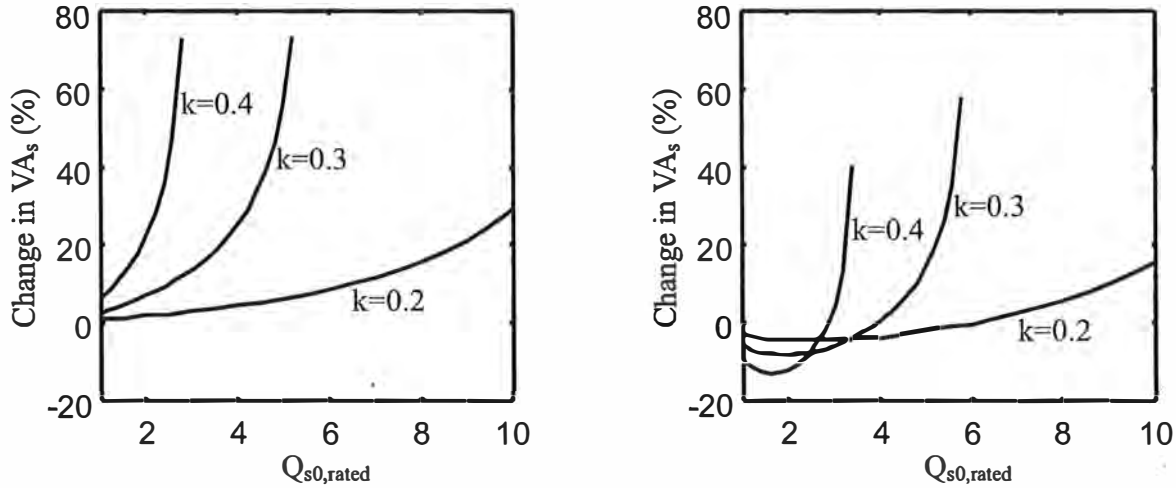
(i) PP topology. (ii) PS topology.

(a) Change in the secondary current.



(i) PP topology. (ii) PS topology.

(b) Change in the secondary voltage.



(i) PP topology. (ii) PS topology.

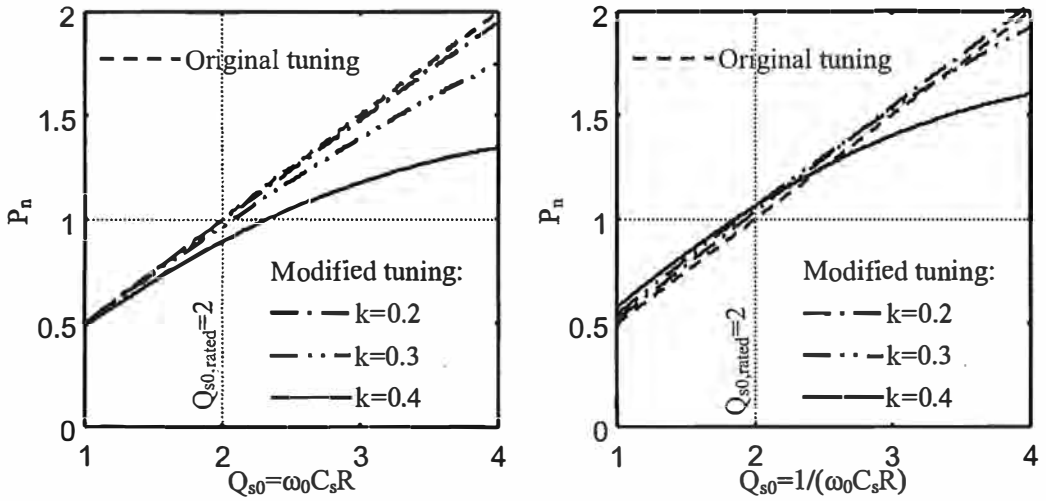
(b) Change in the required secondary VA rating.

Fig. 6-9. Changes in the secondary current, secondary voltage, and required secondary VA rating under rated power operation when using the modified tuning to achieve load independent unity DPF.

InductEV, Inc.
Exhibit 1008
Page 190

For systems using a PS topology, the required secondary VA rating with the modified tuning is less than the PP topology, and can be lower than the original tuning in loosely coupled systems with reasonable $Q_{s0,rated}$, or well-coupled systems with low $Q_{s0,rated}$. The decrease in the required secondary VA rating can be more than 10% for well-coupled systems with low $Q_{s0,rated}$. It is also noted that the decrease in the secondary voltage is more than the decreases shown in the secondary current.

The power transfer capability of systems with low $Q_{s0,rated}$ is illustrated in Fig. 6-10 where $Q_{s0,rated}$ is assumed to be 2. As can be seen, rated power is achieved with the modified tuning at a Q_{s0} higher than $Q_{s0,rated}$ for the PP topology, but for the PS topology interestingly it is at a Q_{s0} lower than $Q_{s0,rated}$. Consequently, the required secondary VA rating of the PS topology with the modified tuning is reduced.



(a) PP topology. (b) PS topology.

Fig. 6-10. Power transfer capability under fixed-frequency operation ($Q_{s0,rated}$=2).

6-4 DISCUSSION

In order to ensure maximum power transfer capability is achievable in a pickup, it is desirable to operate the system at or near the tuned frequency (ω_0). It is also desirable to operate the power supply with a DPF close to unity in order to minimize the required VA rating while maximizing the efficiency. As shown, load independent unity DPF is achievable at ω_0 for the SS topology using the original tuning (assumed with the design methodology described in Chapter 4). Load independent unity DPF is also achievable at ω_0 for the SP topology providing the original tuning is modified using the approach proposed in Chapter 5. Consequently, series-compensated primary systems (the SS and SP topologies) are good topologies for fixed-frequency systems.

Parallel-compensated primary systems (PP and PS topologies) may be required in an application for practical reasons. In such systems, the modified tuning proposed in section 6-2 achieves unity DPF at

InductEV, Inc.
Exhibit 1008
Page 191

ω_0 at rated load only. Since the DPF is less than unity at light load, the efficiency of the power supply is also lower. In order to improve this efficiency, it is desirable to have unity DPF under all loading conditions. This is achievable using the modified tuning proposed in section 6-3, but then it is necessary to deliberately raise the operating frequency above ω_0. Both the power transfer capability and the required secondary VA rating are affected, as the pickup is not operating at the designed frequency. Rated power can still be delivered in the majority of ICPT systems, however there is now a trade-off between the system k and the maximum allowable Q_s when using this tuning scheme. Typical track-type ICPT systems are loosely coupled with reasonable Q_s, while coil-type ICPT systems are well coupled with low Q_s. In such systems, the required secondary VA rating increases slightly in a PP topology, but favourably decreases in a PS topology. In well-coupled systems with low Q_s, the PS topology ensures unity DPF under all load conditions with pickup VA requirement reduced by more than 10%. With this modified tuning, the required secondary VA rating for the PS topology is always less than the PP topology, and as such would be the preferred choice.

The above analysis assumes constant resonant parameters (C_p, C_s, L_p, L_s and M). In practice, the capacitance values (C_p and C_s) are affected by aging, thermal effects and manufacturing tolerance, while the coupling parameters (L_p, L_s and M) vary due to misalignment of the electromagnetic structure. Influences of such variations on the sensitivity of systems using the modified tuning approaches proposed here are investigated further in Chapter 7.

6-5 DESIGN EXAMPLES

The options proposed above for improving DPF under fixed-frequency operation are considered in this section for the design of the contact-less electric vehicle battery charger (described in sections 3-11 and 4-6). Both PP and PS topologies are investigated.

PP topology: Under fixed-frequency operation at ω_0 (f_0=19.7kHz), unity DPF is achieved with the original tuning when Q_{s0} is 1.98 (6.6Ω) determined using (6-4) from the known k (of 0.45). Here the DPF at rated load (6Ω, $Q_{s0,rated}$=1.8) is slightly lower than unity. To achieve unity DPF at rated load as described in section 6-2, the required C_{pn} calculated using Table 6-1 is 1.04 requiring C_p to be 4% larger than the original tuning. The improvement in the DPF with the modified tuning is shown in Fig. 6-11 compared to the original tuned system. At rated operation, the improvement with this modification is not significant, because the DPF of the original system is close to unity due to the values of k and $Q_{s0,rated}$. However, under lightly loaded conditions, the improvement in DPF is more significant but still remains well below unity.

The tuning approach suggested in section 6-3 for achieving load independent unity DPF can also be

InductEV, Inc.
Exhibit 1008
Page 192

used here without compromising the rated power delivery because the system k of 0.45 and $Q_{s0,rated}$ of 1.8 are within the shaded region in Fig. 6-8 for the PP topology. The required C_{pn} determined using Table 6-2 is unity thus C_p does not need to change. However the normalized operating frequency ($u=\omega/\omega_0$) is 1.12 and the operating frequency needs to be raised 12% above ω_0 at 22.1kHz. While the overall power transfer capability is affected (as shown in Fig. 6-12(a) due to pickup frequency detuning effects), rated power transfer of 300W now occurs at Q_{s0} of 2.3 (R=7.6Ω) rather than 1.8 (R=6Ω). The required secondary VA rating (shown in Fig. 6-12(b)) increases by 33% from 620 VA to 825VA as a result of the increased Q_{s0} for rated power delivery (labelled as $Q'_{s0,rated}$).

PS topology: Under fixed-frequency operation at ω_0, the DPF with the original tuning at $Q_{s0,rated}$ (shown in Fig. 6-13) is less than unity. To achieve unity DPF at $Q_{s0,rated}$ as proposed in section 6-2, the required C_{pn} calculated using Table 6-1 is 0.88, and C_p needs to be reduced from 2.20μF by 12% to 1.94μF. With this scheme, however, the DPF under lightly loaded operation is sacrificed, and is notably worse than the original system.

As the system k and $Q_{s0,rated}$ are within the shaded region in Fig. 6-8, the tuning approach suggested in section 6-3 can be applied to achieve load independent unity DPF while ensuring rated power transfer. The required C_{pn} calculated using Table 6-2 is 0.80 and a 20% smaller C_p of 1.76μF is required. Similar to the PP topology, the operating frequency needs to be raised 12% above ω_0 to 22.1kHz. The resulting DPF is shown in Fig. 6-13. The power transfer capability with this modified tuning is compared with the original tuning in Fig. 6-14(a). Under the original tuning rated power is achieved at $Q_{s0,rated}$ of 1.8 (R=1.8Ω), while under the modified tuning rated power is achieved at a smaller Q_{s0} of 1.64 (R=2Ω), labelled as $Q'_{s0,rated}$. Consequently, the required secondary VA rating reduces by 14% from 620VA to 533VA (as shown in Fig. 6-14(b)).

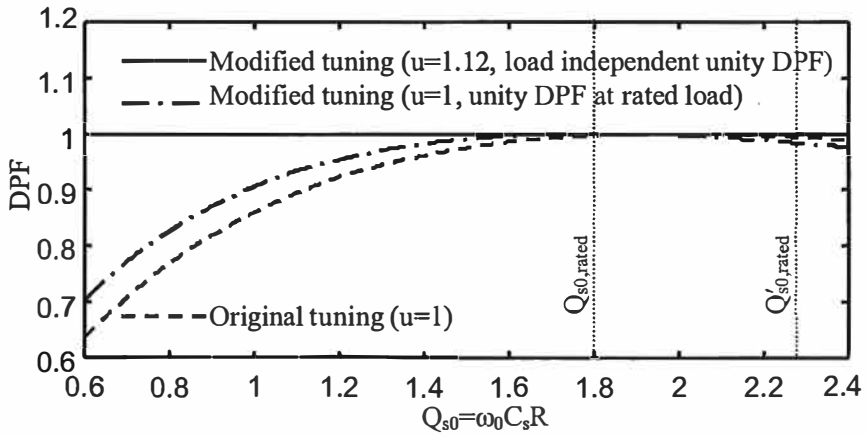
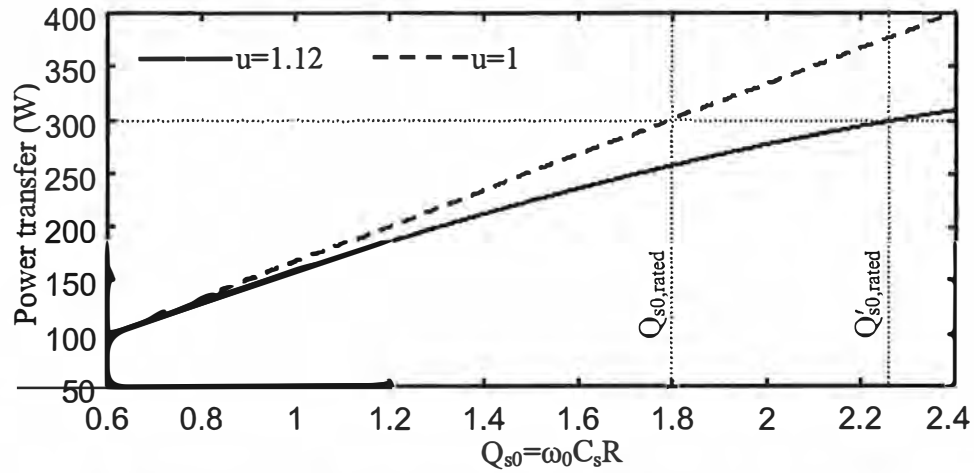
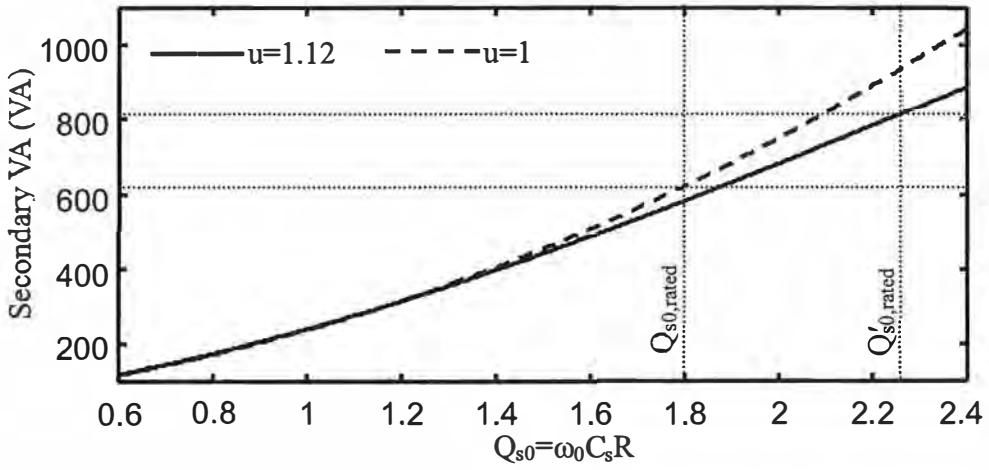


Fig. 6-11. A contact-less electric vehicle battery charger with PP topology – DPF under fixed-frequency operation (a comparison of the original and modified tuning schemes).

InductEV, Inc.
Exhibit 1008
Page 193



(a) Power transfer capability (I_p=15A).



(b) Required secondary VA rating (I_p=15A).

Fig. 6-12. A contact-less electric vehicle battery charger with PP topology – Power transfer capability and required secondary VA rating under fixed-frequency operation (a comparison of the original and modified tuning schemes).

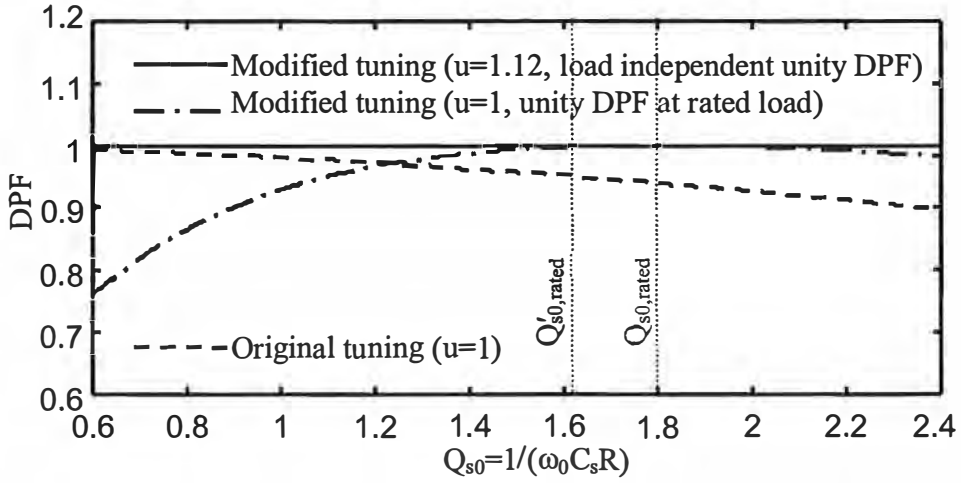
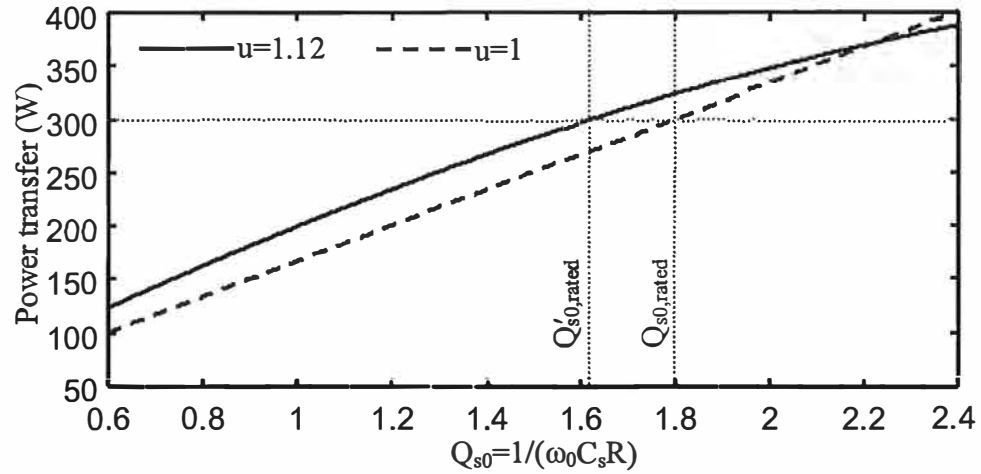
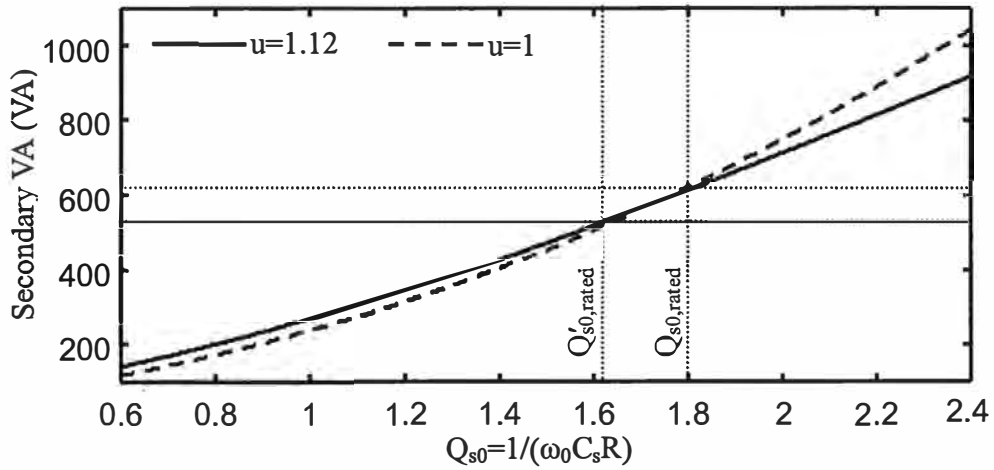


Fig. 6-13. A contact-less electric vehicle battery charger with PS topology – DPF under fixed-frequency operation (a comparison of the original and modified tuning schemes).

InductEV, Inc.
Exhibit 1008
Page 194



(b) Power transfer capability (I_p=15A).



(c) Required secondary VA rating (I_p=15A).

Fig. 6-14. A contact-less electric vehicle battery charger with PS topology – Power transfer capability and required secondary VA rating under fixed-frequency operation (a comparison of the original and modified tuning schemes).

6-6 VERIFICATION

The test system (described in section 4-6) was used to verify the design examples with the modified tuning to achieve load independent unity DPF applied (as discussed above).

The DPF of the power supply was determined by measuring the phase relationship between the discontinuous inverter current (i_i) and the resonant tank voltage (v_p). The measured waveforms of i_i and v_p at the measured loads are shown in Fig. 6-15 (for the PP topology) and Fig. 6-17 (for the PS topology). The fundamental inverter current is closely in phase with the resonant tank voltage for all loads. The measured and predicted power and secondary VA are illustrated in Fig. 6-16 (for the PP topology) and Fig. 6-18 (for the PS topology). Measurements are shown as circles, while the calculated values are shown as solid lines. These results verify the theoretical analysis.

InductEV, Inc.
Exhibit 1008
Page 195

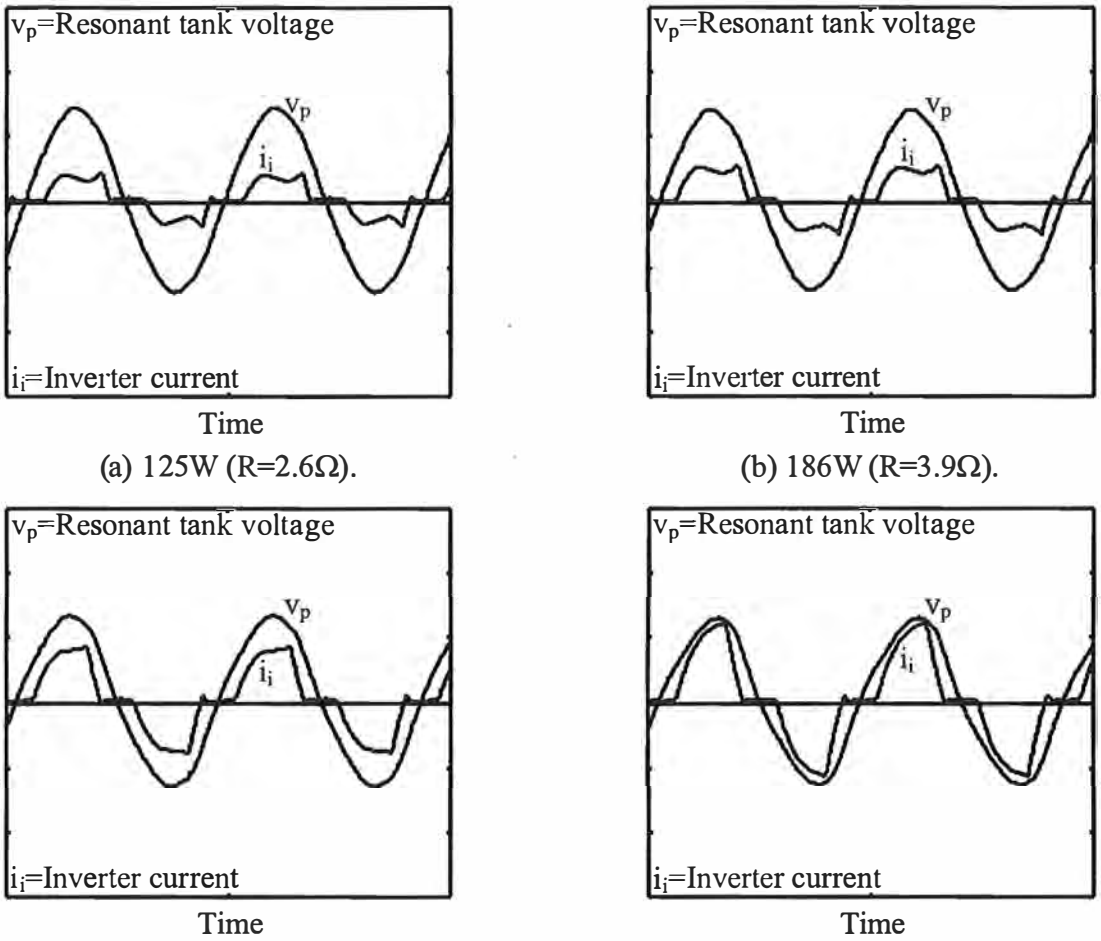


Fig. 6-15. A contact-less electric vehicle battery charger with PP topology, using the modified tuning to achieve load independent unity DPF (C_{pn}=1, u=1.12) - Measured waveforms of the inverter current (i_i) and the resonant tank voltage (v_p).

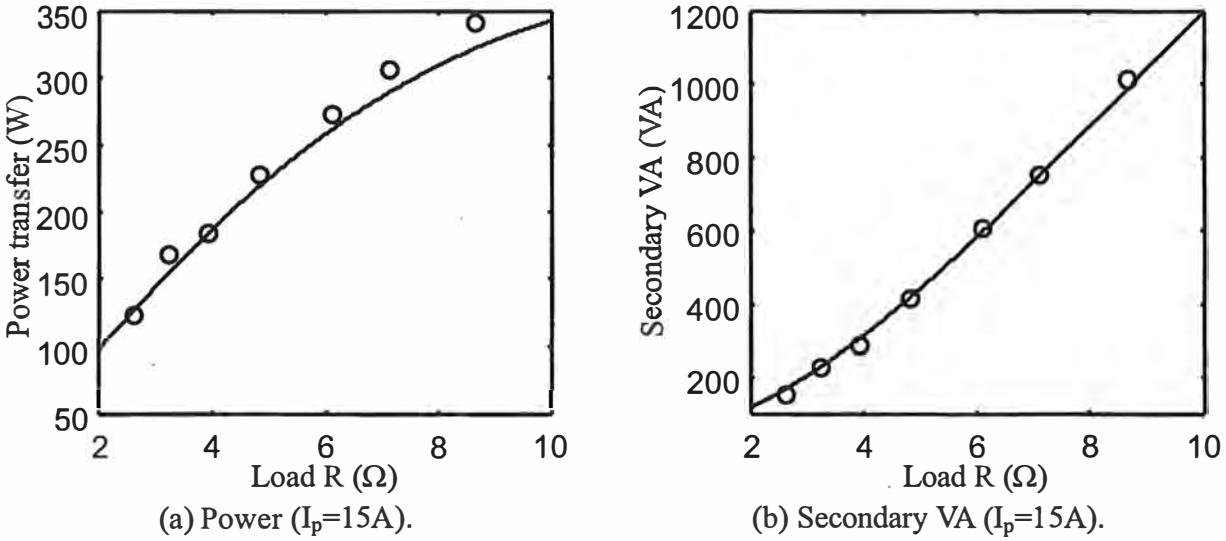


Fig. 6-16. A contact-less electric vehicle battery charger with PP topology, using the modified tuning to achieve load independent unity DPF (C_{pn}=1, u=1.12) - Measured and calculated power and secondary VA.

InductEV, Inc.
Exhibit 1008
Page 196

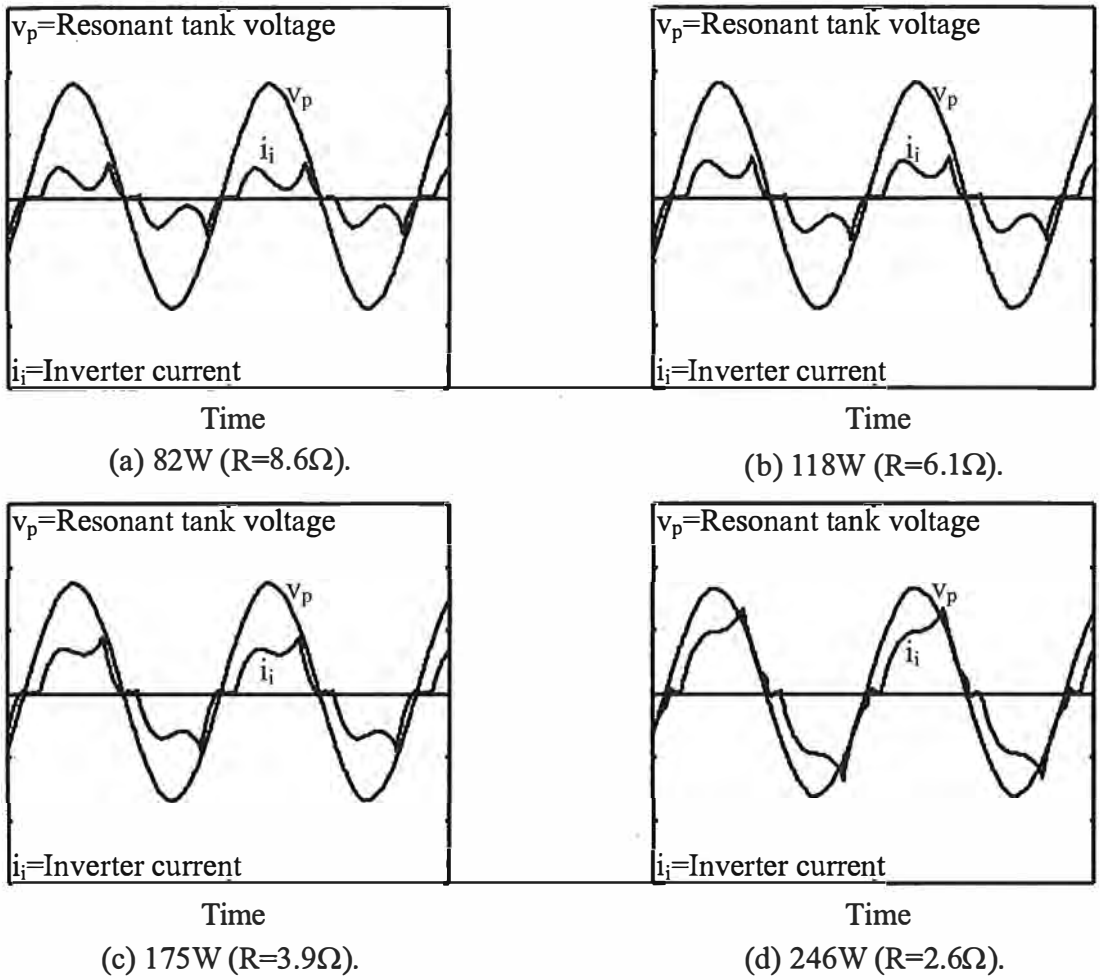


Fig. 6-17. A contact-less electric vehicle battery charger with PS topology, using the modified tuning to achieve load independent unity DPF (C_{pn}=0.8, u=1.12) - Measured waveforms of the inverter current (i_i) and the resonant tank voltage (v_p).

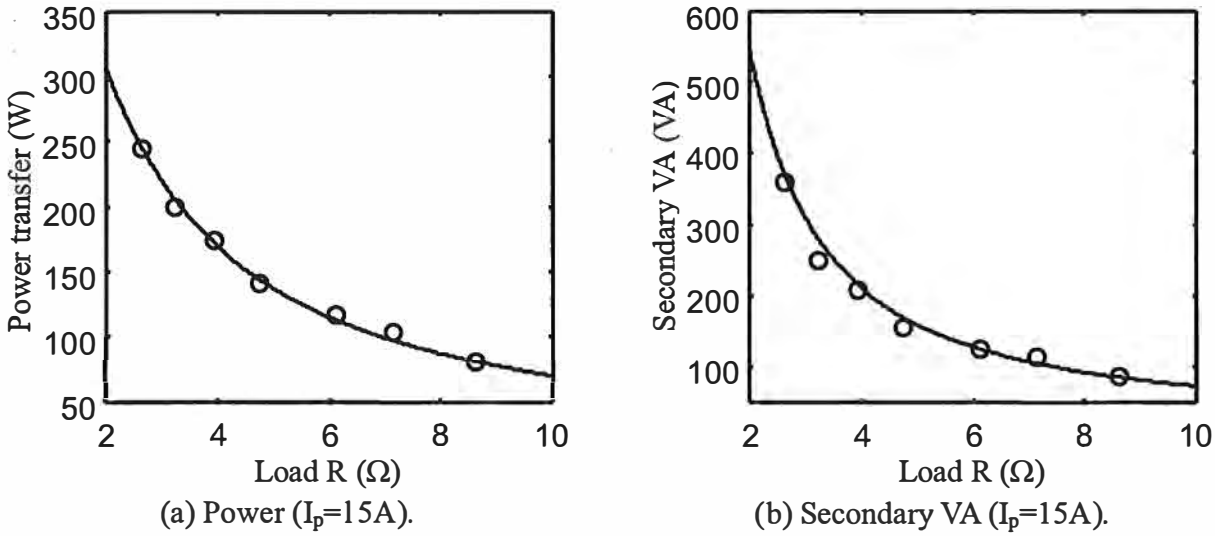


Fig. 6-18. A contact-less electric vehicle battery charger with PS topology, using the modified tuning to achieve load independent unity DPF (C_{pn}=0.8, u=1.12) - Measured and calculated power and secondary VA.

InductEV, Inc.
Exhibit 1008
Page 197

6-7 CONCLUSIONS

In this chapter, the primary tuning was modified to improve the displacement power factor (DPF) of the power supply under fixed-frequency operation. With series-compensated primary systems (the SS and SP topologies), load independent unity DPF was found to be achievable at ω_0 ensuring maximum power transfer capability to the pickup. Therefore they are desirable choices for fixed-frequency systems. Due to practical considerations, parallel-compensated primary systems (the PP and PS topologies) may be required and here if the system is constrained to operate at ω_0 unity DPF is achievable only at rated load.

Load independent unity DPF can be achieved in parallel-tuned primary systems providing the operation frequency is deliberately increased above ω_0. This affects the power transfer capability of the pickups and the required secondary VA rating but does not necessarily impact on rated power delivery. Rated power can still be achieved in the majority of ICPT systems that are either loosely coupled systems with reasonable Q_s, or well-coupled systems with low Q_s.

The theory was verified on a practical contact-less electric vehicle battery charging system. The measurements closely follow the predictions.

InductEV, Inc.
Exhibit 1008
Page 198

CHAPTER 7

A SENSITIVITY ANALYSIS OF SYSTEMS USING THE PROPOSED PRIMARY TUNING SCHEMES

7-1 Introduction
7-2 Fundamentals of the sensitivity analysis
7-3 Compensation capacitor selection
7-4 The influence of variations in primary capacitance
7-5 The influence of variations in secondary capacitance
7-6 The influence of misalignment in the electromagnetic structure
7-7 Discussion
7-8 Conclusions

7-1 INTRODUCTION

The design approaches proposed in chapters 4, 5 and 6 assume all components are ideal. This is not true in the real world where real components have losses, parasitics, tolerances and operating variations. This chapter investigates the influence of variations in the primary and secondary compensation capacitances (C_p and C_s) as well as misalignment of the electromagnetic structure (variations in the coupling parameters L_p, L_s and M) in order to determine the relative sensitivity of the various tuning schemes described, while at the same time indicate practical design considerations that should minimize the influence of such variations on the power transfer capability to the pickup and the displacement power factor (DPF) of the power supply.

In order to determine the extent of practical variations that should be considered, this chapter considers the choice of suitable compensation capacitors based on typical high frequency power capability in addition to thermal and lifetime stability. The degree of misalignment and the resulting variations in coupling parameters between the primary and secondary depends on the configuration of the electromagnetic structure and the ICPT application. Typical misalignment and the resulting variations of the coupling parameters are discussed in this context.

The sensitivity of the DPF, the operating frequency and the power transfer capability to variations in C_p, C_s, L_p, L_s and M are compared for systems designed using the original tuning (assumed with the design methodology described in Chapter 4), the modified tuning to achieve unity DPF at rated load (Chapter 5 for variable-frequency systems, and section 6-2 for fixed-frequency systems), and the modified tuning to achieve load independent unity DPF (section 6-3).

As previously shown, the behaviour of an ICPT system depends strongly on the sensitivity of the

InductEV, Inc.
Exhibit 1008
Page 199

load resonant tank (seen by the power supply), which can be characterised by the fundamental design parameters k (the magnetic coupling coefficient) and Q_s (the secondary quality factor). Practical ICPT systems are normally well coupled (high k) with low Q_s or loosely coupled (low k) with reasonable Q_s. In this chapter, a well-coupled electric vehicle battery charger and a loosely coupled monorail material handling system are used for the sensitivity analysis. Both fixed and variable-frequency operations are investigated.

7-2 FUNDAMENTALS OF THE SENSITIVITY ANALYSIS

The sensitivity analysis in this chapter focuses on variations in C_p, L_p, M, C_s and L_s. The fundamental influences of such variations on the power transfer capability and the DPF are discussed in this section for both fixed and variable frequency systems.

As described in earlier chapters, the power transferred from the primary to the secondary is the reflected resistance multiplied by the square of the primary current as given by:

$$P = (\mathrm{Re}\, Z_r) I_p^2 \tag{7-1}$$

where the reflected impedance (Z_r) is given by:

$$Z_r = \frac{\omega^2 M^2}{Z_s} \tag{7-2}$$

with the secondary impedance (Z_s) given by:

$$Z_s = \begin{cases} j\omega L_s + \dfrac{1}{j\omega C_s} + R & \text{series secondary} \\ j\omega L_s + \dfrac{1}{j\omega C_s + \dfrac{1}{R}} & \text{parallel secondary} \end{cases} \tag{7-3}$$

The DPF of the power supply can be determined as:

$$\mathrm{DPF} = \cos\left(\tan^{-1} \frac{\mathrm{Im}\, Z_t}{\mathrm{Re}\, Z_t}\right) \tag{7-4}$$

where the load impedance (Z_t) is given by:

$$Z_t = \begin{cases} \dfrac{1}{j\omega C_p} + j\omega L_p + Z_r & \text{series primary} \\ \dfrac{1}{j\omega C_p + \dfrac{1}{j\omega L_p + Z_r}} & \text{parallel primary} \end{cases} \tag{7-5}$$

InductEV, Inc.
Exhibit 1008
Page 200

As shown, the power transfer capability depends on ω, M, C_s L_s and R, but is independent of C_p and L_p. It is proportional to the square of M and ω, and therefore changes in either of these parameters will have a significant impact on power transfer. The influence that C_s and L_s have on the power transfer capability needs to be considered by investigating their influence on Z_s. In particular, an increase in L_s directly increases Z_s while also detuning the pickup, resulting in reduced power transfer capability, and vice versa. Variations in C_s, however, have a similar but less direct impact. This sensitivity analysis is further complicated by the fact that Z_s depends on the compensation topology of the pickup and is a complex variable depending on ω and R.

DPF depends on L_p, C_p, M, C_s and L_s. The influence of these parameters on DPF needs to be considered by investigating their influence on Z_t which is dependent on both the primary and secondary compensation topologies, and is also a function of ω and R.

According to above, in fixed-frequency systems, variations in C_p and L_p in fixed-frequency systems do not affect the power transfer capability of the pickup providing the primary current (I_p) is controlled constant. The main influence is on the DPF of the power supply. However, variations in ω, M, C_s and L_s affect both the DPF and the power transfer. Thus for the tuning scheme suggested in section 6-3 where ω has been increased to achieve load independent unity DPF, its sensitivity to M, C_s and L_s relative to other schemes is of particular interest.

Under variable-frequency operation, the operating frequency is allowed to vary so that the power supply operates with unity DPF. Variations in C_p, L_p, M, C_s and L_s therefore affect both the operating frequency and the power transfer.

A complete sensitivity analysis is out of the scope of this thesis. This chapter instead focuses on comparing the various tuning schemes discussed in this thesis to determine their relative sensitivities to those component variations.

7-3 COMPENSATION CAPACITOR SELECTION

In an ICPT system, the compensation capacitors must work with high frequency alternating voltage and current. A major consideration when choosing these capacitors is their high frequency power capability, since the apparent power in the compensation networks is usually large. Good capacitance stability is also often required as the system is usually highly sensitive to capacitance variations.

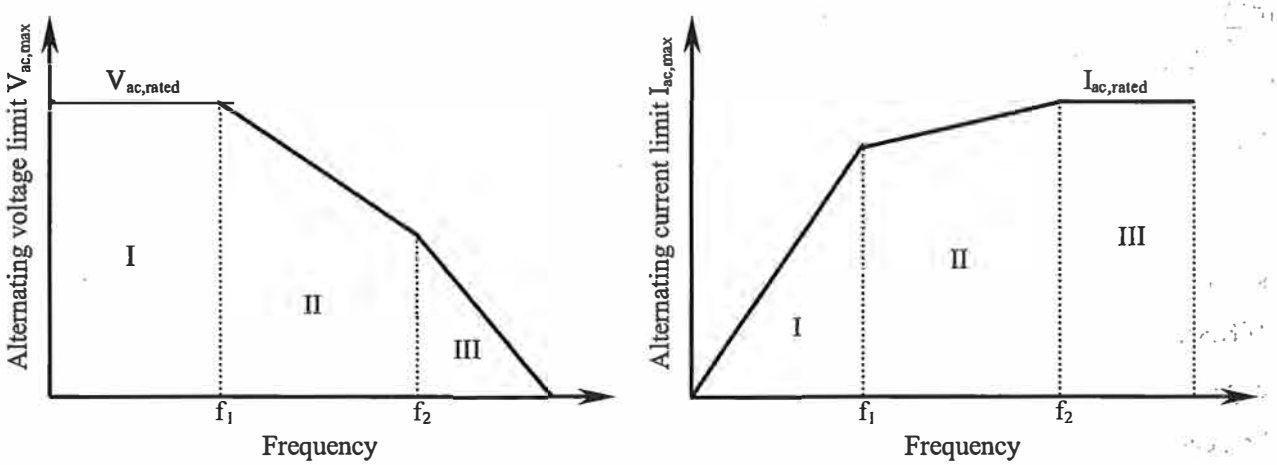
There are three basic types of capacitors: the electrolytic (aluminium and tantalum), the plastic film, and the ceramic. Electrolytic capacitors are normally polarized. The dielectric layers of polar electrolytic capacitors are arranged so that the current is blocked in only one direction, and as such these cannot be used as compensation capacitors in an ICPT system. As such, the following discussion

InductEV, Inc.
Exhibit 1008
Page 201

focuses on plastic film and ceramic types.

The ability of a capacitor to withstand alternating voltage and current is dependent on the operating frequency. This is discussed following by separating the voltage and current limits into three frequency ranges labelled as 'I', 'II' and 'III' in Fig. 7-1, where f_1 and f_2 can be characterised for any particular capacitor as shown in Appendix J.

Below f_1 (Region I), the allowable alternating voltage and current are limited by the dielectric strength of the capacitor. The applied alternating voltage should not exceed the rated ac voltage ($V_{ac,rated}$) and the maximum allowable alternating current is less than the rated ac current ($V_{ac,rated}$). Between f_1 and f_2 (Region II), the allowable alternating voltage and current are less than rated values due to the limitation of the thermal dissipation capability of the capacitor. Above f_2 (Region III), the resistances of the leads, the metal layers, and the soldered and welded joints limit the allowable alternating voltage and current. The applied alternating current should not exceed $I_{ac,rated}$, and the maximum permissible alternating voltage is less than $V_{ac,rated}$.



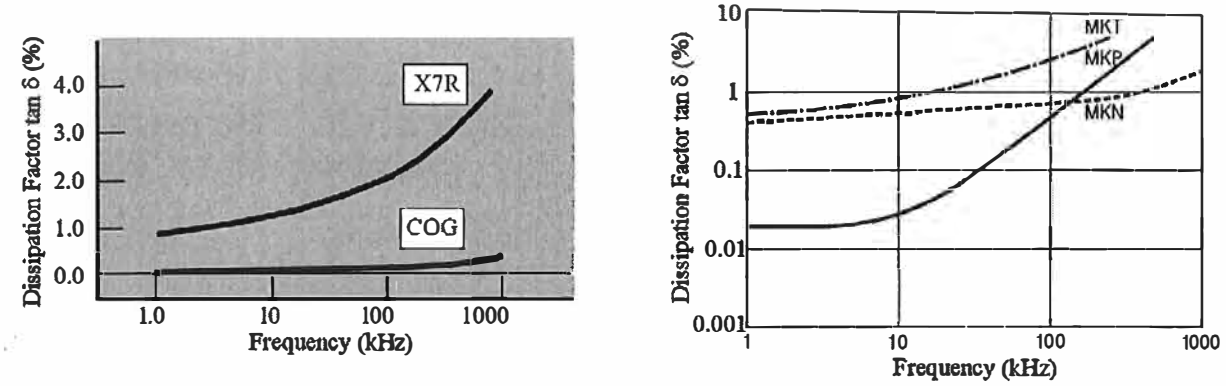
(a) Alternating voltage limit. (b) Alternating current limit.

Fig. 7-1. High frequency power capability of capacitors.

Typical frequency dependences of the dissipation factor of ceramic and plastic film capacitors are shown in Fig. 7-2. The dissipation factor of both capacitor types increases with frequency. Below 100kHz, Class I ceramic capacitors and polypropylene plastic film capacitors have the lowest dissipation factors.

Typical capacitance tolerances of the plastic film and ceramic capacitors are compared in Table 7-1 for selected manufacturers. Generally, better tolerance can be achieved for ceramic capacitors.

InductEV, Inc.
Exhibit 1008
Page 202



(a) Ceramic capacitors (Source: NOVACAP) – Class I (COG), Class II (X7R).

(b) Plastic film capacitors (Source: EPCOS) – Polyester (MKT/MKN), Polypropylene (MKP).

Fig. 7-2. Typical frequency dependence of the dissipation factor (tan δ) of capacitors.

TABLE 7-1
TYPICAL CAPACITANCE TOLERANCE OF PLASTIC FILM AND CERAMIC CAPACITORS

Manufacturer	Capacitance Tolerance	
	Plastic Film Capacitors	**Ceramic Capacitors**
EPCOS (Siemens Matsushita)	±5%,±10%,±20%	±1%,±5%,±10%
NIPPON (Marcon)	±3%,±5%,±10%	±20%
WIMA	±5%,±10%,±20%	N.A.
NOVACAP	N.A.	±1%,±5%,±10%

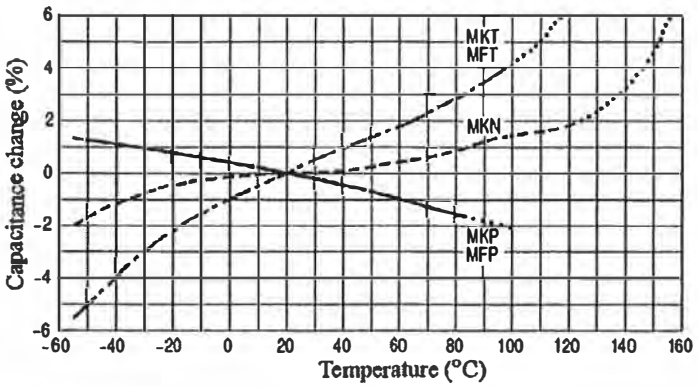
Typical temperature dependences of the capacitance of plastic film and ceramic capacitors are shown in Fig. 7-3. Polyester film capacitors have positive temperature coefficients (MKT, MFT and MKN), such that their capacitance increases with increasing temperature, while polypropylene film capacitors have negative temperature coefficients (MKP and MFP). Class II ceramic capacitors have bad capacitance stability with changing temperature, while Class I ceramic capacitors are comparable to the plastic film capacitor.

Typical long-term capacitance changes in plastic film capacitors are shown in Table 7-2. These are close to the manufacturing tolerances.

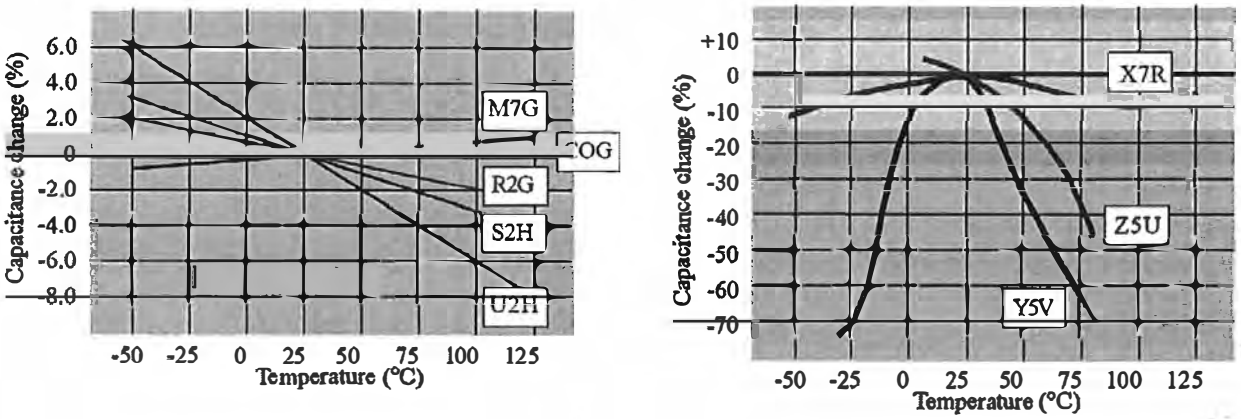
Class I ceramic capacitors use non-ferroelectric (paraelectric) materials and virtually have no significant aging characteristics. The aging phenomenon occurs predominantly in Class II ceramic capacitors that use ferroelectric materials especially with a high dielectric constant. Typical capacitance aging characteristics are shown in Fig. 7-4 for Class II ceramic capacitors.

The voltage dependences of the capacitance of typical polyester plastic film capacitors and Class II ceramic capacitors are compared in Fig. 7-5. The polyester capacitor has good capacitance stability with changing voltage, while that of the Class II ceramic capacitor is worse. High voltage dependence results in large non-linear distortion in the alternating voltage and current associated with the capacitor.

InductEV, Inc.
Exhibit 1008
Page 203



(a) Plastic film capacitors (Source: EPCOS) – Polyester (MKT/MFT/MKN), Polypropylene (MKP/MFP).



(i) Class I. (ii) Class II.

(b) Ceramic capacitors (Source: NOVACAP).

Fig. 7-3. Typical temperature dependence of the capacitance.

TABLE 7-2

LONG TERM CAPACITANCE CHANGE OF PLASTIC FILM CAPACITORS

Manufacturer	Plastic film capacitors
EPCOS (Siemens Matsushita)	±3%
NIPPON (Marcon)	±5%
WIMA	±3%

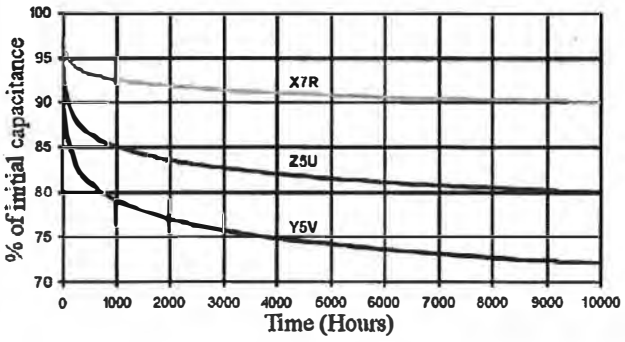


Fig. 7-4. Typical aging (time dependence of the capacitance) – Class II ceramic capacitors (Source: American Technical Ceramics).

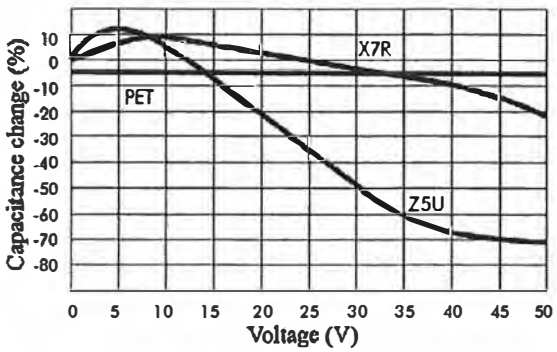


Fig. 7-5. Typical voltage dependence of the capacitance (Source: WIMA) – Polyester plastic film capacitors (PET), Class II ceramic capacitors (X7R/Z5U).

InductEV, Inc.
Exhibit 1008
Page 204

Additional characteristics of plastic film and ceramic capacitors are compared in Table 7-3. The ceramic capacitor has a significantly larger dielectric constant and as such can achieve a higher capacitance per unit volume. However, the plastic film capacitor has a larger range of available capacitance values. The plastic film capacitor also has less dielectric absorption, equivalent series resistance (ESR), and non-linear distortion. Low ESR is a desirable characteristic for capacitors used for high-frequency/high-current ac applications.

According to above discussion, plastic film capacitors are well suited for compensation capacitors in an ICPT system. The polypropylene capacitor in particular has good power capability and lifetime capacitance stability.

TABLE 7-3
TYPICAL CHARACTERISTICS OF PLASTIC FILM AND CERAMIC CAPACITORS (SOURCE: WIMA)

	Plastic film capacitors		Ceramic capacitors	
	Polyester	Polypropylene	NPO (Class I)	X7R (Class II)
Dielectric constant (1kHz, 23°C)	3.3	2.2	12 to 40	700 to 2000
Capacitance range	1000pF to 10μF	100pF to 10μF	1pF to 0.01μF	100pF to 2.2μF
Dielectric absorption (%)	0.5	0.05 to 0.1	0.6	2.5
ESR	low	very low	low	moderate to high
Non-linear distortion	very low	very low	low	high

7-4 THE INFLUENCE OF VARIATIONS IN PRIMARY CAPACITANCE

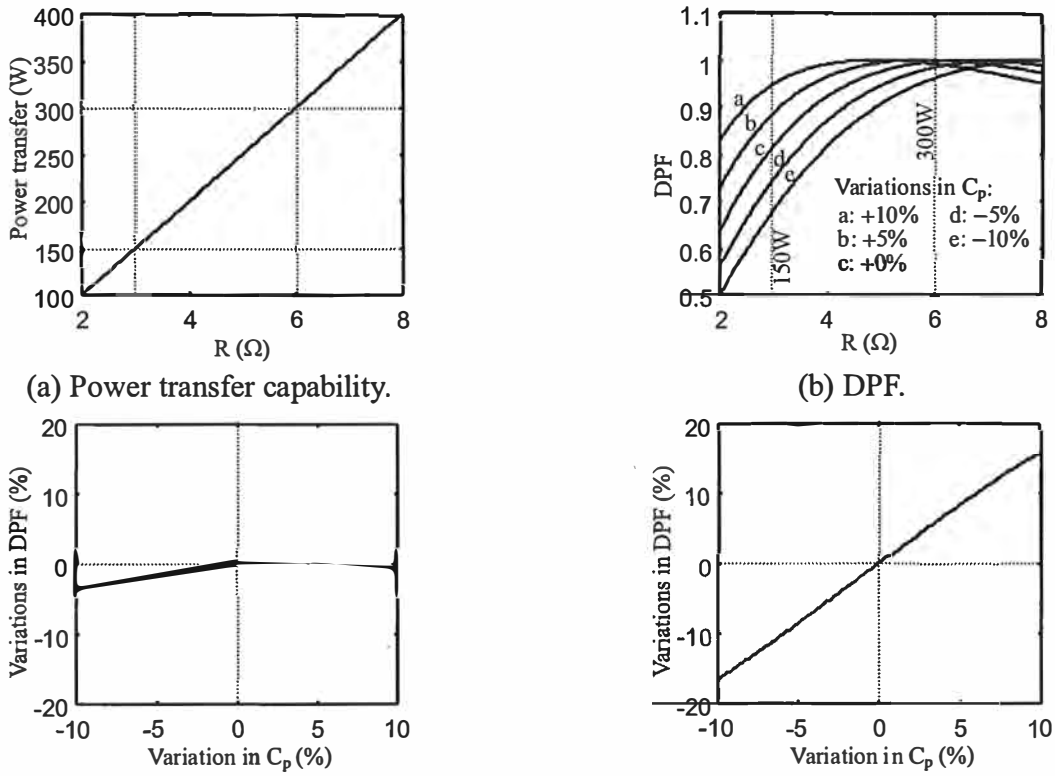
7-4.1 FIXED-FREQUENCY SYSTEMS

A well-coupled system (electric vehicle battery charging) – This example is described in sections 3-11, 4-6, 5-6 and 6-6. The influence of variations in C_p, when using the tuning scheme proposed in Chapter 4 (here after noted as "original tuning"), is illustrated in Fig. 7-6.

With the frequency fixed at ω_0 (u=1) and the primary current controlled at 15A, the power transfer capability of the system is independent of variations in C_p. The loading condition to achieve rated power of 300W is about 6Ω as shown in Fig. 7-6(a). Percentage variations in DPF as a result of variations in C_p can be determined from Fig. 7-6(b), and for rated load are shown in Fig. 7-6(c). For comparison, the sensitivity of the DPF at a reduced power (150W) is shown in Fig. 7-6(d). At rated power DPF remains close to unity having a small sensitivity to variations in C_p. At reduced power, it is well below unity and has a much higher sensitivity due to increased primary quality factor (Q_p).

InductEV, Inc.
Exhibit 1008
Page 205

Interestingly, the DPF is more sensitive to decreases than increases in C_p.



(a) Power transfer capability.

(b) DPF.

(c) Sensitivity of the DPF at 300W.

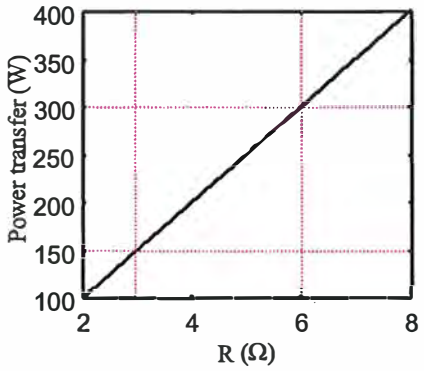
(d) Sensitivity of the DPF at 150W.

Fig. 7-6. Original tuning (C_{pn}=1, u=1) – The influence of variations in C_p for an electric vehicle battery charger under fixed-frequency operation (k=0.45, $Q_{s0,rated}$=1.8, PP topology, I_p=15A).

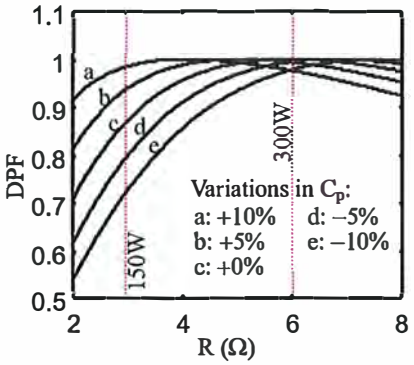
The influence of variations in C_p when using the tuning scheme proposed in section 6-2 (here after noted as "modified tuning for unity DPF at rated load") is illustrated in Fig. 7-7. The operating frequency is also fixed at ω_0. The power transfer capability is therefore identical to the original tuned system. The sensitivity of the DPF to variations in C_p is similar to the original system operating at both rated and light load.

The influence of variations in C_p when using the tuning scheme proposed in section 6-3 (here after noted as "modified tuning for load independent unity DPF") is illustrated in Fig. 7-8. Here the operating frequency is deliberately increased above ω_0 (u=1.12) resulting in reduced power transfer capability to the pickup as described in Chapter 6 and shown in Fig. 7-8(a). Relative to Fig. 7-6(a) and 7-7(a), the loading condition at which rated power (300W) is achieved is 7.6Ω since a higher operating Q_s is necessary. The influence on the DPF can be determined from Fig. 7-8(b). The sensitivity when operating at 300W is once again similar to the original tuning scheme as shown in Fig. 7-8(c). However, the system is less sensitive at light load. Increases and decreases in C_p have identical influences on the DPF at all loading conditions as shown in Fig. 7-8(d).

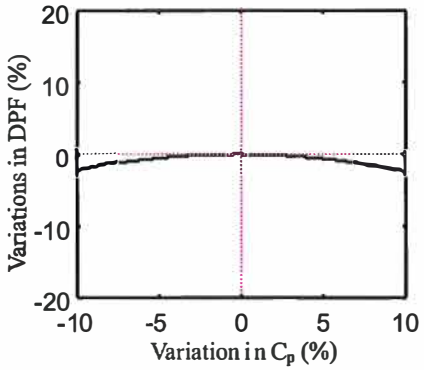
InductEV, Inc.
Exhibit 1008
Page 206



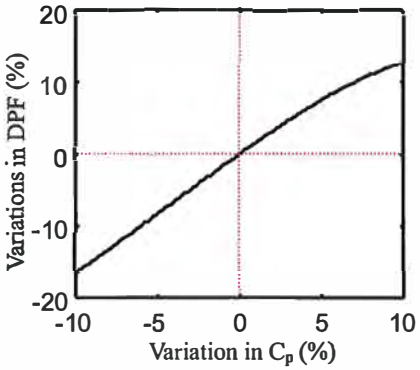
(a) Power transfer capability.



(b) DPF.

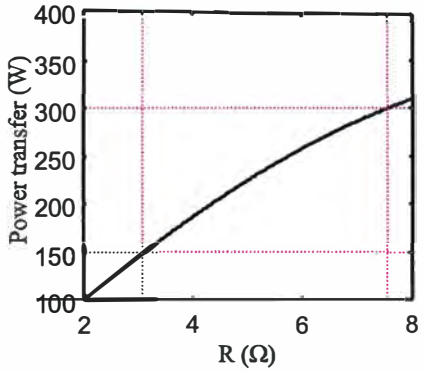


(c) Sensitivity of the DPF at 300W.

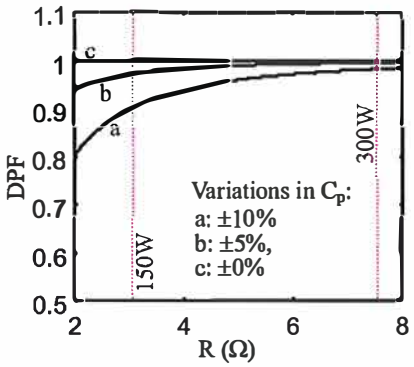


(d) Sensitivity of the DPF at150W.

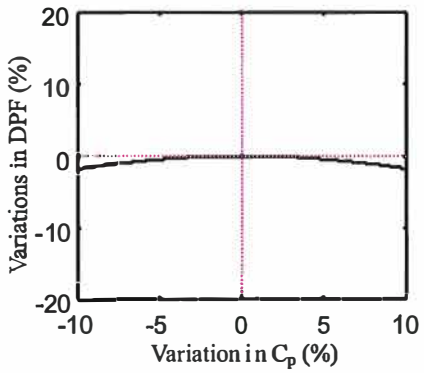
Fig. 7-7. Modified tuning for unity DPF at rated load (C_{pn}=1.04, u=1) – The influence of variations in C_p for an electric vehicle battery charger under fixed-frequency operation.



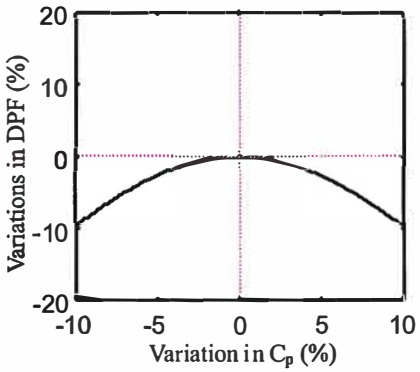
(a) Power transfer capability.



(b) DPF.



(c) Sensitivity of the DPF at 300W.



(d) Sensitivity of the DPF at150W.

Fig. 7-8. Modified tuning for load independent unity DPF (C_{pn}=1, u=1.12) – The influence of variations in C_p for an electric vehicle battery charger under fixed-frequency operation.

InductEV, Inc.
Exhibit 1008
Page 207

A loosely coupled system (monorail material handling) – This example is described in [1,2]. The power supply generates a 10-kHz current in the track magnetic circuit. The magnetic circuit is coupled to multiple secondary vehicles and the power transferred to these vehicles is then conditioned to produce a stable supply on the vehicle capable of driving travelling motors. In this example only one vehicle is considered.

The electromagnetic structure is shown in Fig. 7-9. In this system, a single turn primary winding without magnetic material is constructed using parallel cables extending along the track. The secondary winding uses several turns of coil wound on a ferrite core that concentrates the flux generated by the primary current flowing in the track.

Both the primary and secondary of the monorail material handling system are parallel compensated (PP topology). A summary of the system parameters [1,2] is given in Table 7-4. With the selected secondary capacitance of 0.38μF, the secondary resonant frequency is calculated as 10.2kHz. As the pickup winding is magnetically coupled with only a small portion of the extended primary coil, the magnetic coefficient (k) is only 0.086. The primary current is controlled constant at 54A, and the rated power is 800W ($Q_{s0,rated}$=4.7, R=192Ω).

When using the tuning scheme proposed in section 6-2 to achieve unity DPF at rated load while operating at ω_0 (u=1), the required C_{pn} calculated using Table 6-1 is 1.007. As such the required change to the original tuning is negligible.

When using the tuning scheme proposed in section 6-3 to achieve load independent unity DPF, the required C_{pn} is unity and the operating frequency calculated using Table 6-2 is 1.004. Again the necessary change to the original tuning is negligible. The following sensitivity analysis therefore focuses only on the original tuned system (C_{pn}=1, u=1), as this is representative of all tuning schemes.

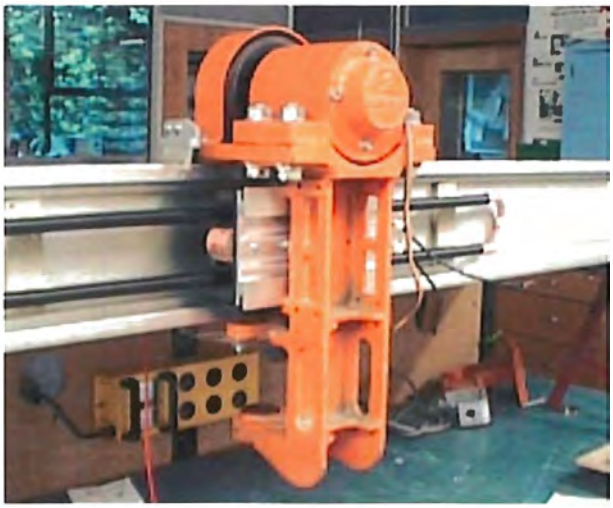


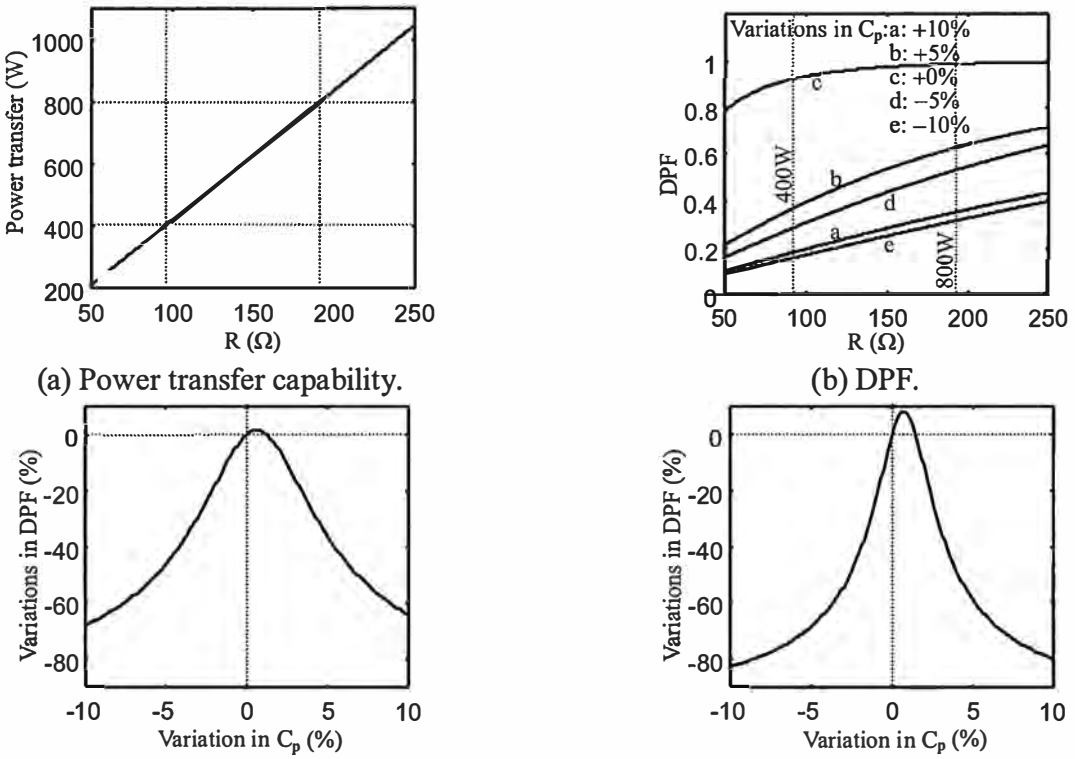
Fig. 7-9. Electromagnetic structure of the monorail material handling system.

InductEV, Inc.
Exhibit 1008
Page 208

TABLE 7-4
PARAMETERS OF THE MONORAIL MATERIAL HANDLING SYSTEM

Nominal frequency (f_0, secondary resonant frequency)	10.2kHz
Primary track current (I_p)	54A
Primary track inductance (L_p)	123μH
Primary track compensation capacitance (C_p)	1.96μF
Pickup mutual inductance (M)	24μH
Secondary pickup self-inductance (L_s)	634μH
Secondary pickup compensation capacitance (C_s)	0.38μF
Secondary pickup rated load (R)	192Ω
Secondary quality factor ($Q_{s0,rated}$)	4.7
Secondary pickup rated power (P)	800W
Magnetic coefficient (k)	0.086

The influence of variations in C_p is illustrated in Fig. 7-10. Here both increases and decreases in C_p have similar influences on the DPF. Because of higher Q_p, the sensitivity of the DPF to variations in C_p is much higher compared to the well-coupled system noted earlier. Similarly, this sensitivity increases under lightly loaded conditions. For reliable operation C_p should not change by more than about 2%. This is difficult to achieve as noted in section 7-3.



(a) Power transfer capability.

(b) DPF.

(c) Sensitivity of the DPF at 800W.

(d) Sensitivity of the DPF at 400W.

Fig. 7-10. The influence of variations in C_p for a monorail material handling system under fixed-frequency operation (k=0.086, $Q_{s0,rated}$=4.7, PP topology, C_{pn}=1, u=1).

InductEV, Inc.
Exhibit 1008
Page 209

7-4.2 VARIABLE-FREQUENCY SYSTEMS

A well-coupled system (electric vehicle battery charging) – The influence of variations in C_p for the original system (C_{pn}=1) is illustrated in Fig. 7-11. The operating frequency and power transfer capability when C_{pn} is unity are shown as solid lines. In this design case, bifurcation occurs slightly above rated load. The operating frequency is independent of load providing the operation is restricted within the bifurcation-free area. This load independent frequency (u=1.12) is above ω_0 and as such the pickup does not operate at the maximum power point.

An increase of C_{pn} above unity has two major effects. Firstly, the emergence of bifurcation is at a higher load. Secondly, the operating frequency at light loads becomes closer to ω_0 resulting in higher power transfer capability. The operating frequency at rated load equals ω_0 when C_{pn} is 1.04.

A decrease of C_{pn} below unity also results in the occurrence of bifurcation at higher load. However, the operating frequency for all loading conditions up to rated load shifts further away from ω_0 resulting in lower power transfer capability, which is undesirable.

Assuming operation is restricted within the bifurcation-free region, the loading conditions to achieve rated power (300W) can be determined from the power curves. The operating frequencies at these loading conditions calculated from the frequency curve are shown in Fig. 7-11(c-i). For comparison, the sensitivity of the operating frequency at a reduced power (150W) to variations in C_p is shown in Fig. 7-11(c-ii). This sensitivity is significant at rated power, and becomes slightly lower at reduced power because of reduced secondary quality factor (Q_s).

Fig. 7-12 shows the influence of variations in C_p when using the modified tuning scheme for unity DPF at rated load as described in Chapter 5 for variable-frequency systems. Here the designed C_p using (5-4) is 4% larger than the original tuning. Similar characteristics to the original system (noted in Fig. 7-11) are found.

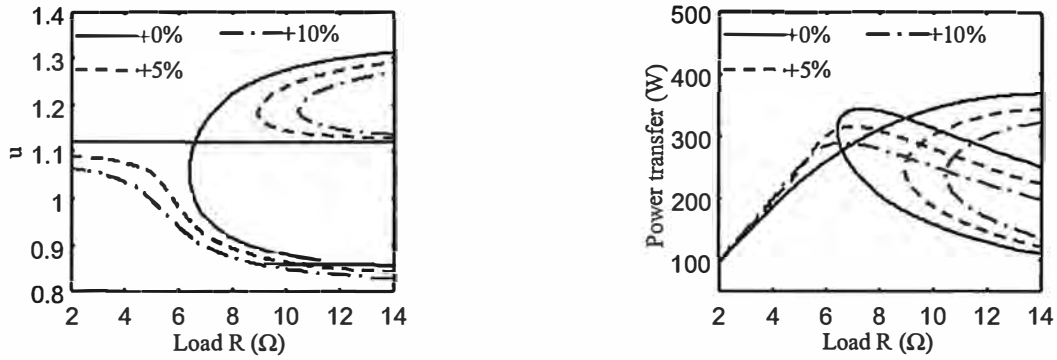
A loosely coupled system (monorail material handling) – As described in section 7-4.1, the difference between the original tuning and the modified tuning for unity DPF at rated load is negligible as the required change to C_p calculated using (5-4) is very small. As such, the analysis here only focuses on the original system (C_{pn}=1), since the trends are representative of both tuning schemes. Fig. 7-13 shows the influence of variations in C_p.

With a k of 0.086, the maximum Q_{s0} for bifurcation-free operation determined using the bifurcation criterion (Table 5-5 for the PP topology) is 11.6. Since the monorail material handling system with $Q_{s0,rated}$ of 4.7 is well within the bifurcation boundary, it does not bifurcate within normal operating conditions.

With the theoretical C_p, the operating frequency is close to ω_0 (u=1) for all loading conditions. An

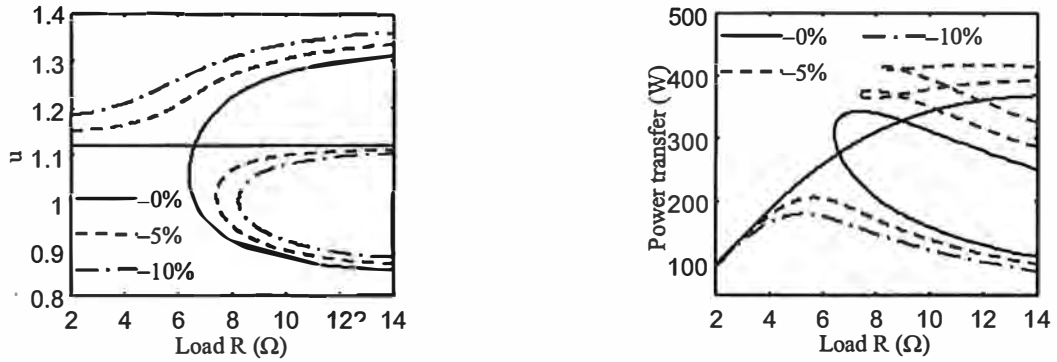
InductEV, Inc.
Exhibit 1008
Page 210

increase in C_p results in a shift in the operating frequency below ω_0 ($u<1$), while decreasing C_p shifts the operating frequency above ω_0 ($u>1$). The change in operating frequency is similar at all loading conditions and causes the pickup to become detuned. Consequently the power transfer capability to the pickup reduces. In comparison to well-coupled systems (noted in Fig. 7-11 and 7-12), this sensitivity to variations in C_p is lower.



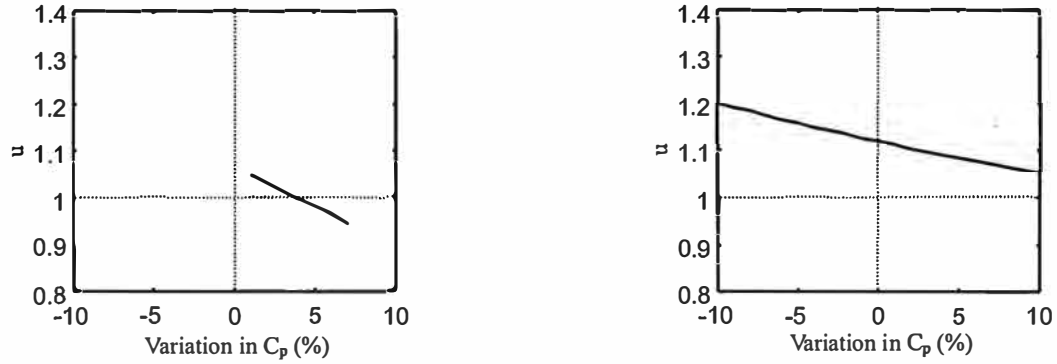
(i) Operational frequency. (ii) Power transfer capability.

(a) Increases in C_p.



(i) Operational frequency. (ii) Power transfer capability.

(b) Decreases in C_p.

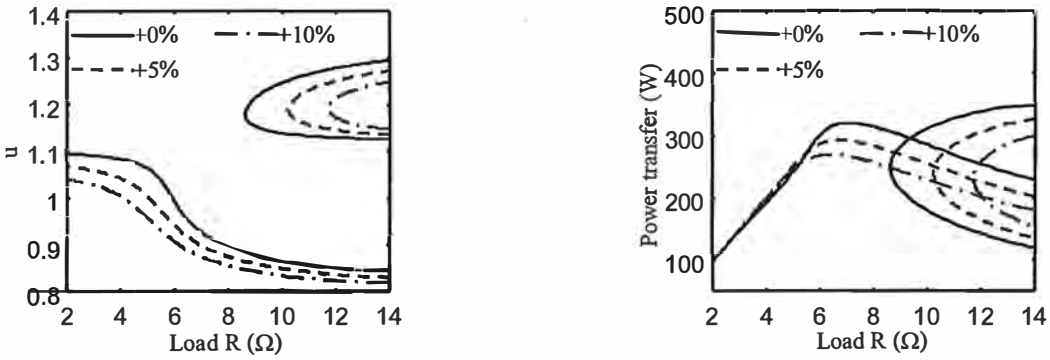


(i) Operating at 300W. (ii) Operating at 150W.

(c) Sensitivity of the operating frequency.

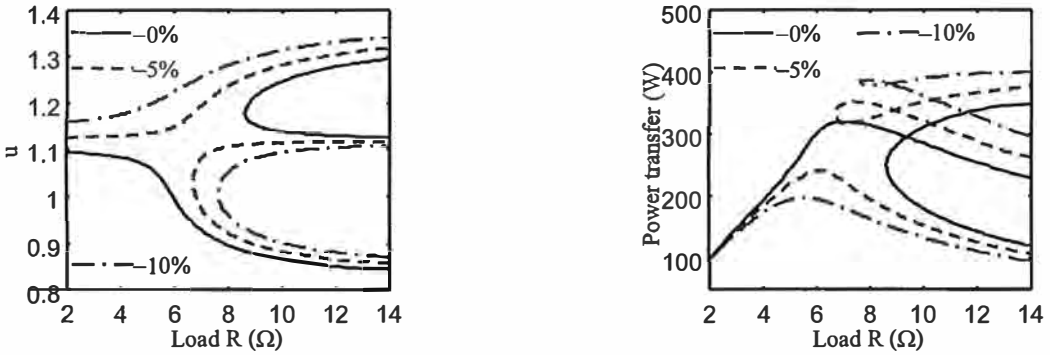
Fig. 7-11. Original tuning (C_{pn}=1) – The influence of variations in C_p for an electric vehicle battery charger under variable-frequency operation (k=0.45, $Q_{s0,rated}$=1.8, PP topology, I_p=15A).

InductEV, Inc.
Exhibit 1008
Page 211



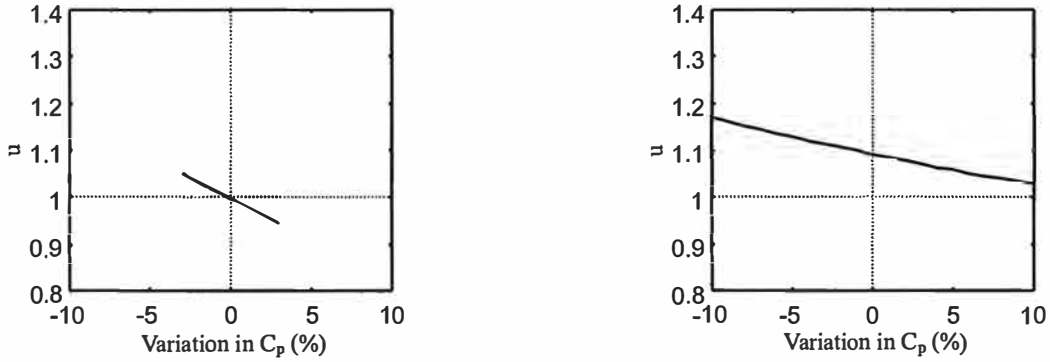
(i) Operational frequency. (ii) Power transfer capability.

(a) Increases in C_p.



(i) Operational frequency. (ii) Power transfer capability.

(b) Decreases in C_p.



(i) Operating at 300W. (ii) Operating at 150W.

(c) Sensitivity of the operating frequency.

Fig. 7-12. Modified tuning for unity DPF at rated load (C_{pn}=1.04) – The influence of variations in C_p for an electric vehicle battery charger under variable-frequency operation.

7-5 THE INFLUENCE OF VARIATIONS IN SECONDARY CAPACITANCE

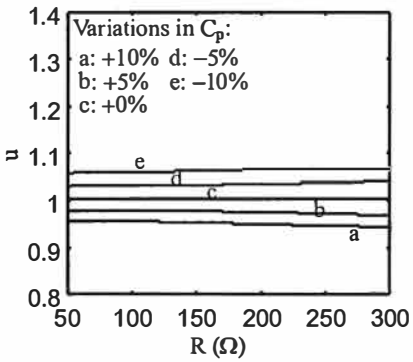
7-5.1 FIXED-FREQUENCY SYSTEMS

A well-coupled system (electric vehicle battery charging) – The influence of variations in C_s are illustrated in Fig. 7-14 for the original tuned system. As discussed in section 7-2, variations in C_s affect

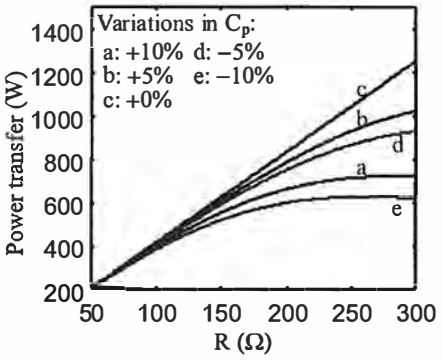
InductEV, Inc.
Exhibit 1008
Page 212

both the DPF and the power transfer capability, but here the influences are found to be small over all loading conditions. Fig. 7-15 shows the influence of variations in C_s when using the modified tuning scheme for unity DPF at rated load. Similar to the original tuned system, both the DPF and the power transfer have low sensitivity to variations in C_s under all loading conditions. Fig. 7-16 shows the influence of variations in C_s when using the modified tuning for load independent unity DPF. In this case, the influence on the power transfer capability is significant. An increase in C_s results in lower power transfer capability as the pickup resonant frequency moves further away from the operating frequency (u), while decreases in C_s improve the power transfer capability since the secondary tuned frequency moves closer to u. The influence on the DPF is however small, especially at light load. Interestingly, increases and decreases in C_s have an identical influence on the DPF. Overall, the sensitivity of the DPF to variations in C_s is small irrespective of load.

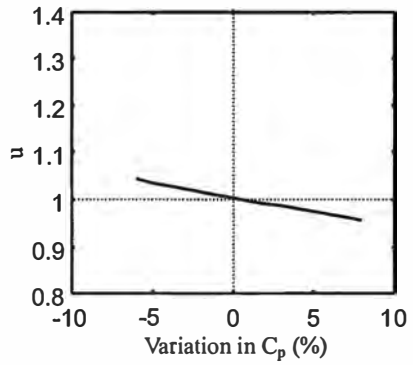
A loosely coupled system (monorail material handling) – As shown in Fig. 7-17, variations in C_s have significant influence on both the DPF and the power transfer capability because of higher Q_p and Q_s.



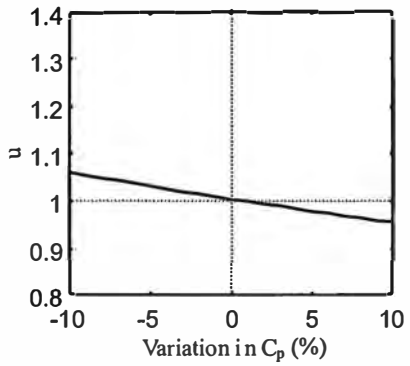
(a) Operating frequency.



(b) Power transfer capability.



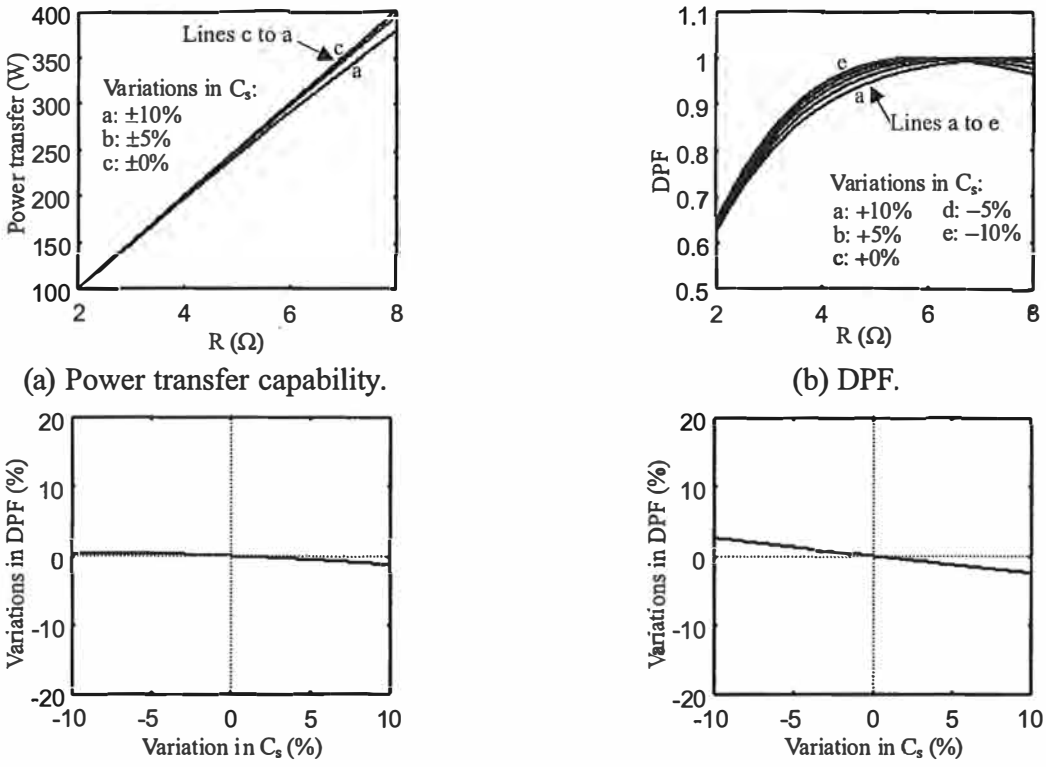
(c) Sensitivity of u at 800W.



(d) Sensitivity of u at 400W.

Fig. 7-13. The influence of variations in C_p for a monorail material handling system under variable-frequency operation (k=0.086, $Q_{s0,rated}$=4.7, PP topology, C_{pn}=1, I_p=54A).

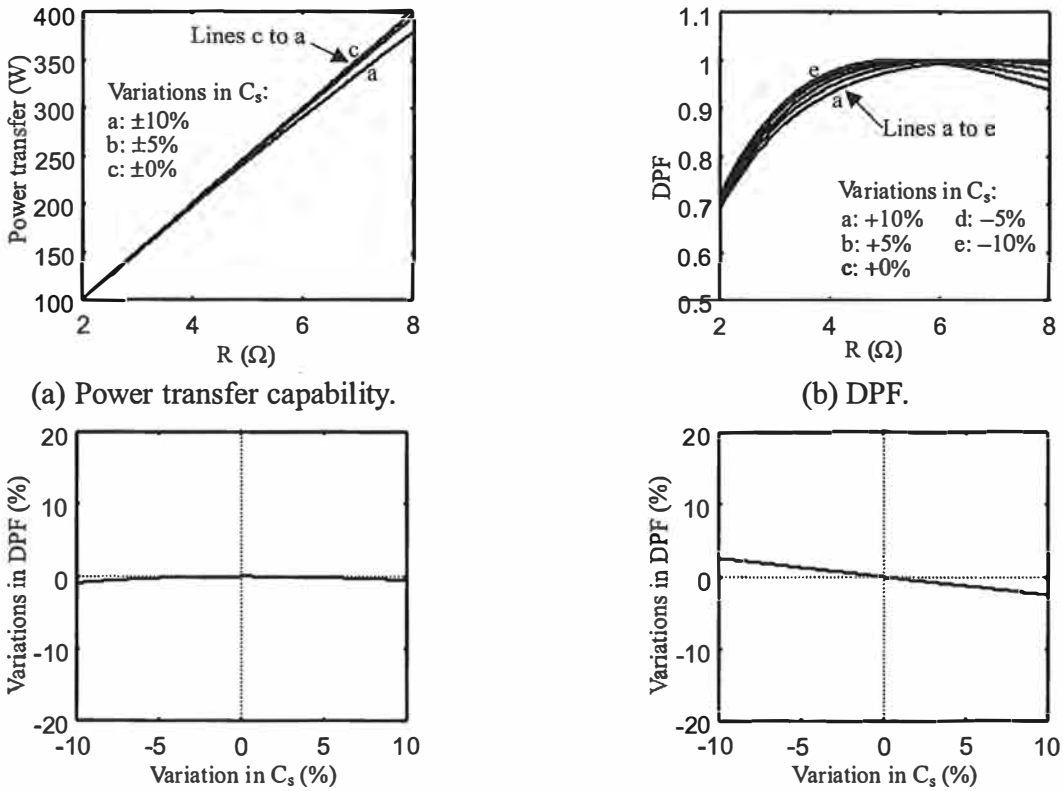
InductEV, Inc.
Exhibit 1008
Page 213



(a) Power transfer capability. (b) DPF.

(c) Sensitivity of the DPF at 300W. (d) Sensitivity of the DPF at 150W.

Fig. 7-14. Original tuning (C_{pn}=1, u=1) – The influence of variations in C_s for an electric vehicle battery charger under fixed-frequency operation (k=0.45, $Q_{s0,rated}$=1.8, PP topology, I_p=15A).

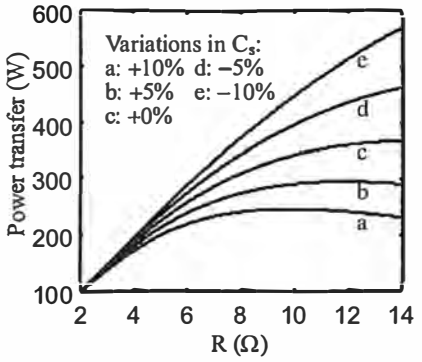


(a) Power transfer capability. (b) DPF.

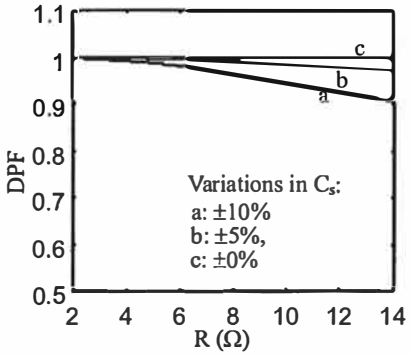
(c) Sensitivity of the DPF at 300W. (d) Sensitivity of the DPF at150W.

Fig. 7-15. Modified tuning for unity DPF at rated load (C_{pn}=1.04, u=1) – The influence of variations in C_s for an electric vehicle battery charger under fixed-frequency operation.

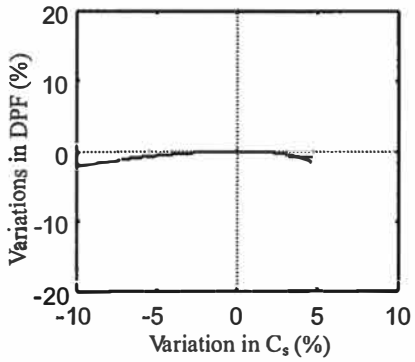
InductEV, Inc.
Exhibit 1008
Page 214



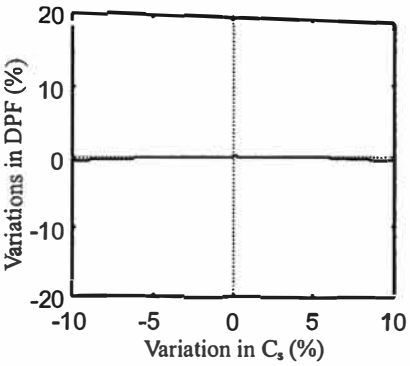
(a) Power transfer capability.



(b) DPF.

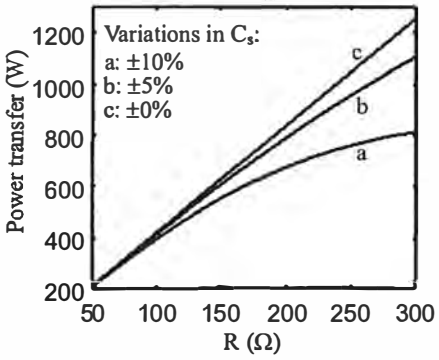


(c) Sensitivity of the DPF at 300W.

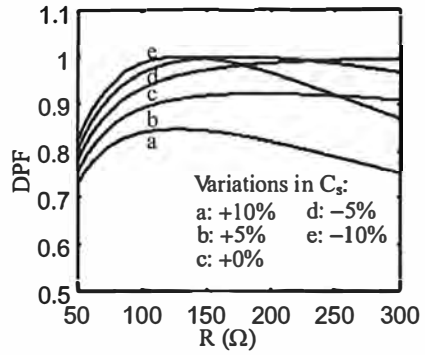


(d) Sensitivity of the DPF at150W.

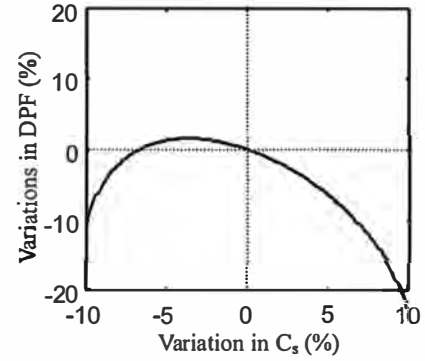
Fig. 7-16. Modified tuning for load independent unity DPF (C_{pn}=1, u=1.12) – The influence of variations in C_s for an electric vehicle battery charger under fixed-frequency operation.



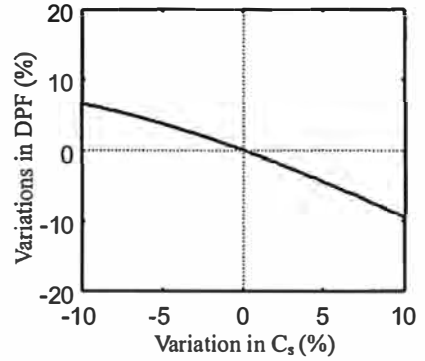
(a) Power transfer capability.



(b) DPF.



(c) Sensitivity of the DPF at 800W.



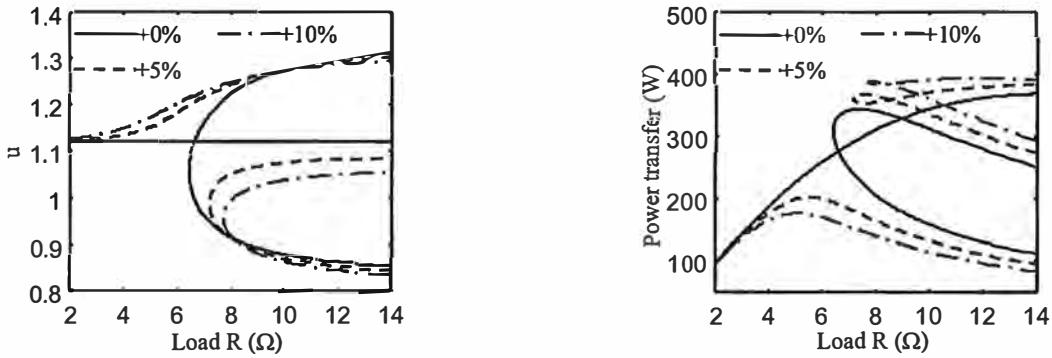
(d) Sensitivity of the DPF at 400W.

Fig. 7-17. The influence of variations in C_s for a monorail material handling system under fixed-frequency operation (k=0.086, $Q_{s0,rated}$=4.7, PP topology, C_{pn}=1, u=1).

InductEV, Inc.
Exhibit 1008
Page 215

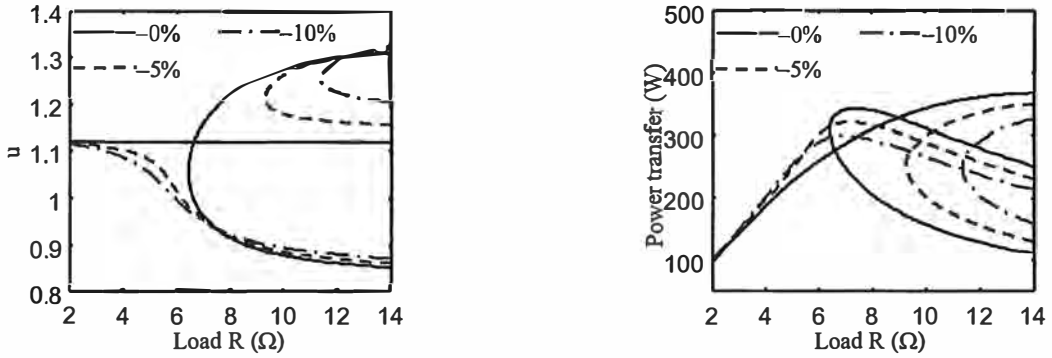
7-5.2 VARIABLE-FREQUENCY SYSTEMS

A well-coupled system (electric vehicle battery charging) – The influence of variations in C_s are shown in Fig. 7-18 for the original tuned system. The effects of decreasing C_s are similar to those found when C_p is increased, and vice versa. However, the actual sensitivity of the operating frequency to variations in C_s is lower than that found with variations in C_p.



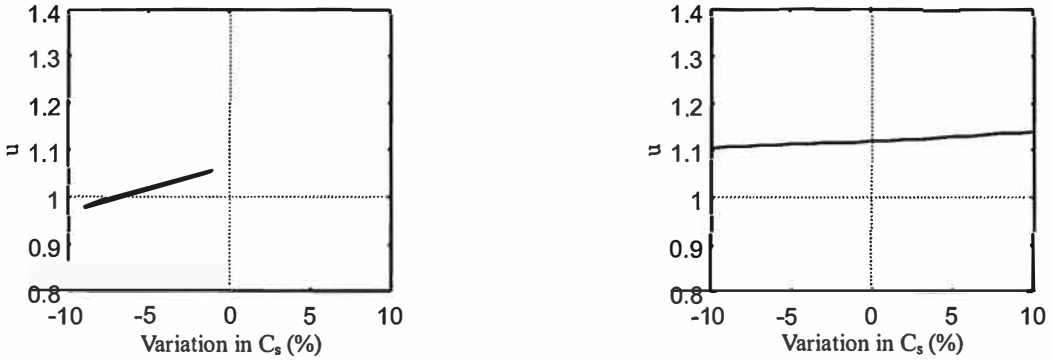
(i) Operational frequency. (ii) Power transfer capability.

(a) Increases in C_s.



(i) Operational frequency. (ii) Power transfer capability.

(b) Decreases in C_s.



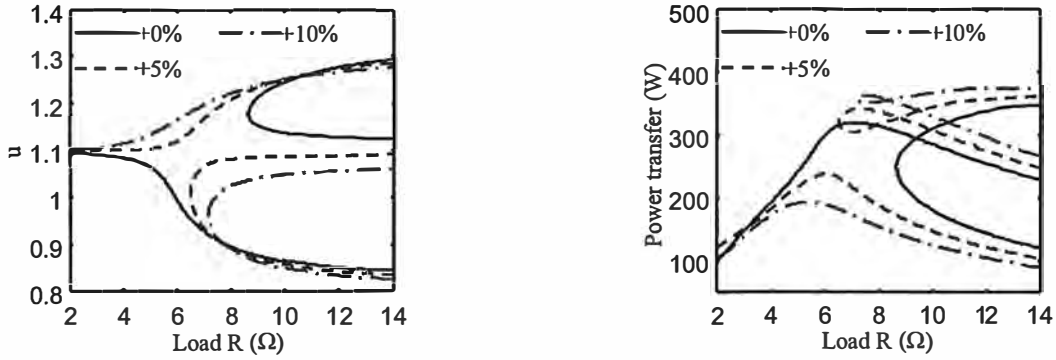
(i) Operating at 300W. (ii) Operating at 150W.

(c) Sensitivity of the operating frequency.

Fig. 7-18. Original tuning (C_{pn}=1) – The influence of variations in C_s for an electric vehicle battery charger under variable-frequency operation (k=0.45, $Q_{s0,rated}$=1.8, PP topology, I_p=15A).

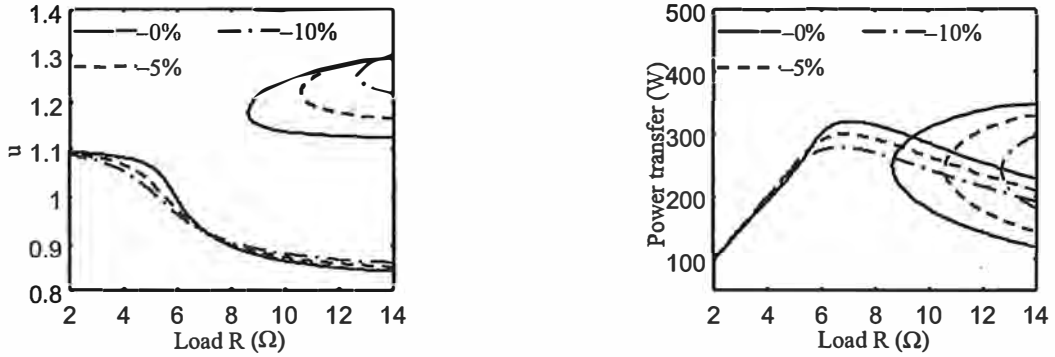
InductEV, Inc.
Exhibit 1008
Page 216

Fig. 7-19 shows the influence of variations in C_s when using the modified tuning scheme for unity DPF at rated load. Once again, similar characteristics to the original tuned system are found.



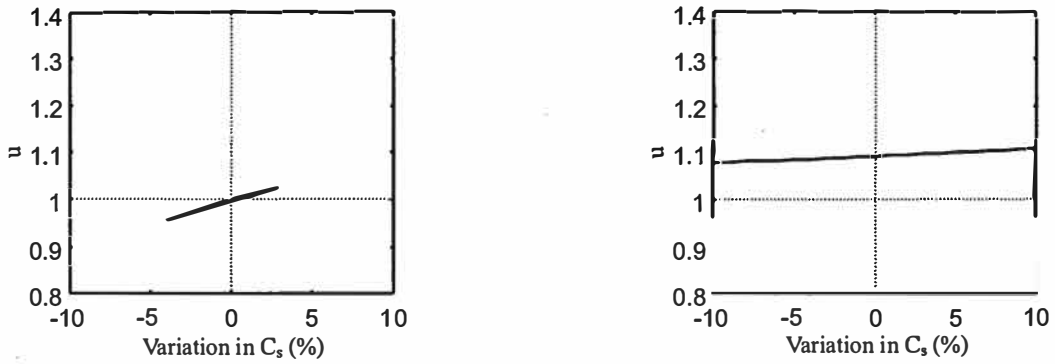
(i) Operational frequency. (ii) Power transfer capability.

(a) Increases in C_s.



(i) Operational frequency. (ii) Power transfer capability.

(b) Decreases in C_s.



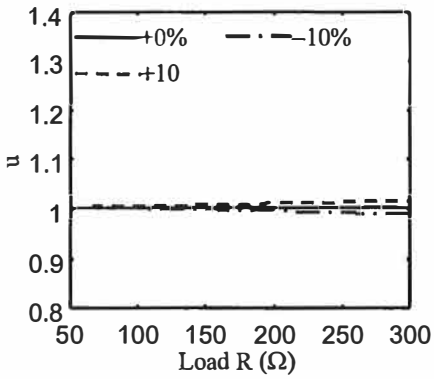
(i) Operating at 300W. (ii) Operating at 150W.

(c) Sensitivity of the operating frequency.

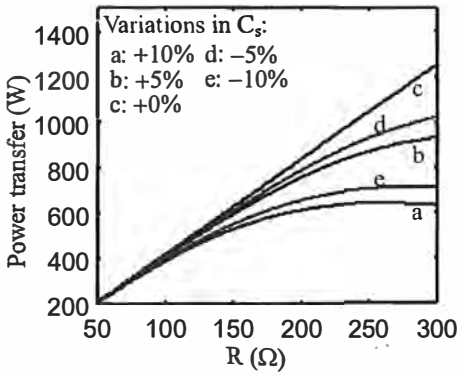
Fig. 7-19. Modified tuning for unity DPF at rated load (C_{pn}=1.04) – The influence of variations in C_s for an electric vehicle battery charger under variable-frequency operation (k=0.45, $Q_{s0,rated}$=1.8, PP topology, I_p=15A).

A loosely coupled system (monorail material handling) – Fig. 7-20 shows the influence of variations in C_s. The influence on the operating frequency is negligible since the loading effects of the pickup on the primary can be neglected. However, the influence on the power transfer capability is significant as the operating Q_s is high and is therefore highly sensitive to pickup tuning.

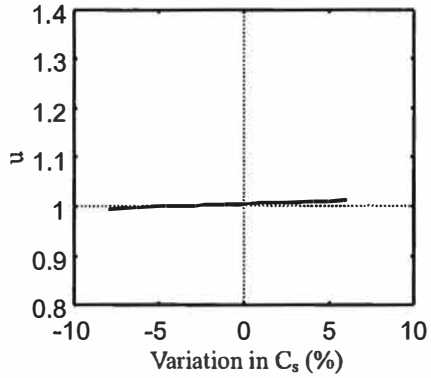
InductEV, Inc.
Exhibit 1008
Page 217

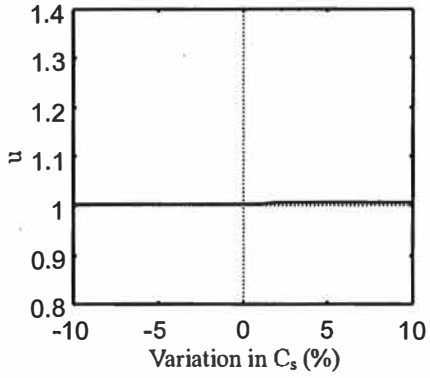


(a) Operating frequency.



(b) Power transfer capability.





(c) Sensitivity of the operating frequency at 800W. (d) Sensitivity of the operating frequency at 400W.

Fig. 7-20. The influence of variations in C_s for a monorail material handling system under variable-frequency operation (k=0.086, $Q_{s0,rated}$=4.7, PP topology, C_{pn}=1, I_p=54A).

7-6 THE INFLUENCE OF MISALIGNMENT IN THE ELECTROMAGNETIC STRUCTURE

The amount of misalignment in the electromagnetic structure depends on how the primary and secondary are aligned. Both mechanical and electrical guiding methodologies can be used. For contact-less battery charging of portable consumer products, the product can be designed to sit in a pocket of the battery charger and as such to minimize the misalignment. For the monorail material handling system discussed above, the primary coil is fixed on a rail while the secondary pickup is fixed to a bogie that is guided on the same rail to minimize misalignment. In automatic guided vehicle applications and in contact-less electric vehicle battery charging systems (such as that discussed earlier), vehicles are normally electrically guided in position and may have "significant" misalignment.

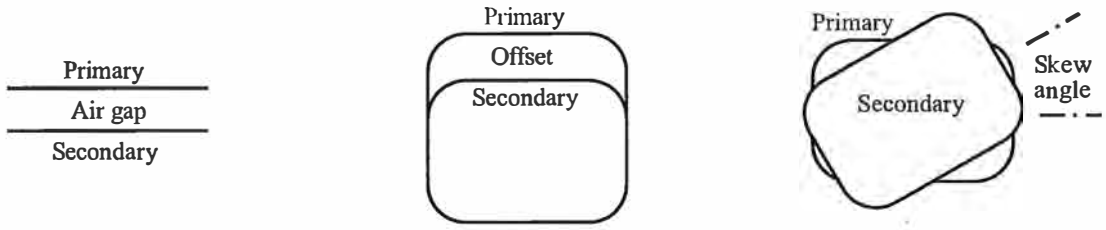
The misalignment of the electromagnetic structure results in variations to the coupling parameters (L_p, L_s and M). In fixed-frequency systems, such variations affect the DPF and the power transfer capability. In variable-frequency systems, the main influences of this misalignment are on the operating frequency and the power transfer capability. These influences are investigated in this

InductEV, Inc.
Exhibit 1008
Page 218

section.

7-6.1 COUPLING PARAMETER VARIATIONS IN AN ELECTRIC VEHICLE BATTERY CHARGER

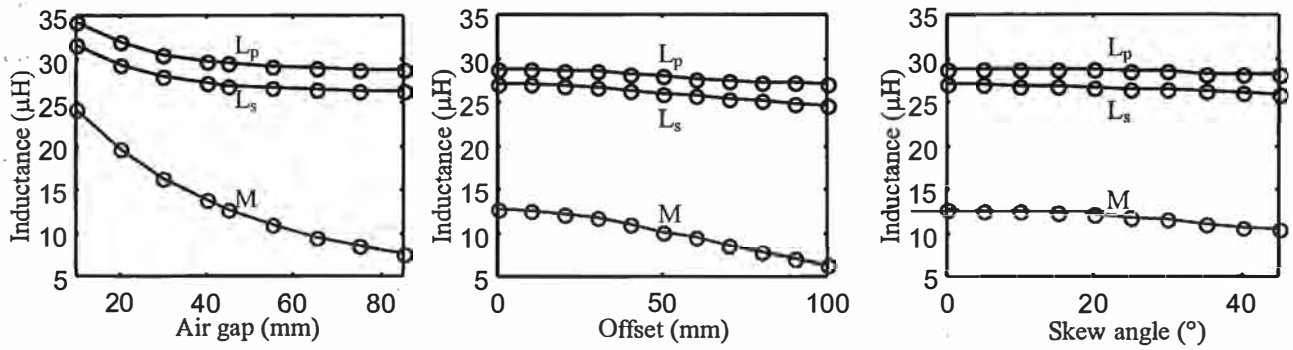
For the contact-less electric vehicle battery charger used in examples throughout this thesis and designed earlier in section 4-6, misalignment of the electromagnetic structure can be defined as variations in air gap, offset and skew angle as shown in Fig. 7-21. A vehicle with a flat tire results in smaller air gap. As the vehicle stops at the charging station, offset and skew angle between the primary and secondary while limited are in practice unavoidable.



(a) Air gap. (b) Offset. (c) Skew angle.

Fig. 7-21. Misalignment of the contact-less electric vehicle battery charging system.

The primary and secondary self-inductances as well as the mutual inductance were measured for selected air gap, offset and skew angle (measurements are shown in Fig. 7-22 as circles). Increases in all of these factors result in a drop in the coupling parameters. Variations in the air gap are the most significant in comparison to the offset and skew angle as a result of the magnetic design in this system (as shown in Fig. 7-23). As the air gap increases from 10mm to 85mm, the mutual inductance drops to less than a third. The drop of the primary and secondary self-inductance is relatively smaller. Due to the symmetry of the primary and secondary electromagnetic structure, the effects of the skew angle are small.



(a) Air gap. (b) Offset. (c) Skew angle.

Fig. 7-22. Measurement of the effects of misalignment on coupling parameters for the contact-less electric vehicle battery charger.

InductEV, Inc.
Exhibit 1008
Page 219

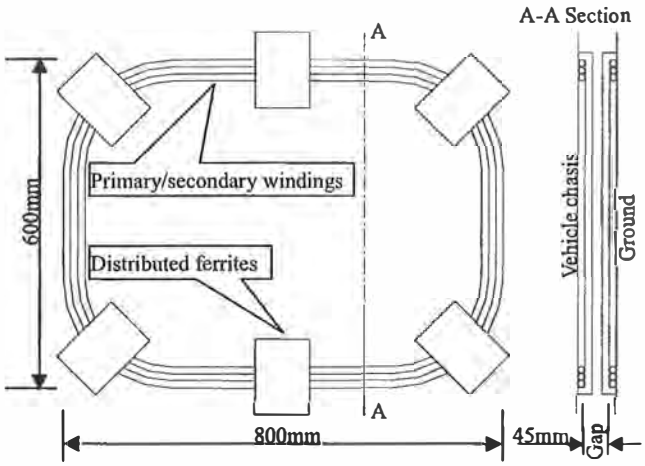


Fig. 7-23. Symmetry of the electromagnetic structure of the battery charger.

7-6.2 FIXED-FREQUENCY SYSTEMS

A well-coupled system (electric vehicle battery charging) – The influence on power and DPF of variations in the coupling parameters (L_p, L_s and M) are illustrated in Fig. 7-24 to 7-32 for each tuning scheme discussed in this thesis. The DPF has a small sensitivity to variations in L_p at rated load for all tuning schemes, but becomes more sensitive at light load due to increased Q_p. Here, systems using the modified tuning for load independent unity DPF have the lowest sensitivity.

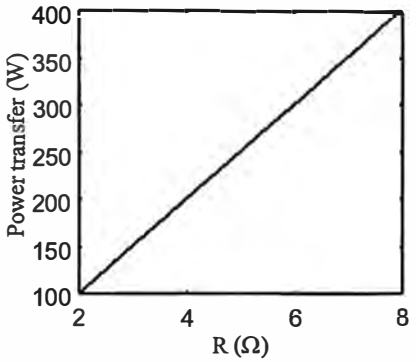
The variation in L_s has moderate influences on both the DPF and the power transfer capability in all tuning schemes. Overall, the sensitivity of the DPF to variations in L_s is small under all loading conditions. An increase in L_s results in lower power transfer capability, and as such a higher operating Q_s is required for the same power transfer. In practice, increases in L_s are almost always accompanied by increases in M that are more than enough to compensate for this power drop.

As expected, variations in M influence both the DPF and the power transfer capability in all tuning schemes. In percentage terms, this influence is moderate, however M can change significantly with misalignment so that the influence on DPF and power can be quite large. A decrease in M results in lower power transfer capability and therefore a higher operating Q_s is required for the same power transfer. The sensitivity of the DPF to variations in M is small at rated load, but becomes more sensitive at light load due to increased Q_p. Systems using the modified tuning for load independent unity DPF have the lowest sensitivity at light load.

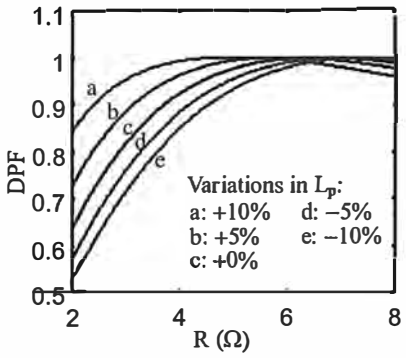
A loosely coupled system (monorail material handling) – The influence of variations in the coupling parameters are shown in Fig. 7-33 to 7-35. The DPF is highly sensitive to variations in L_p because Q_p is high. The sensitivity of DPF to variations in L_s is significant at rated load, and becomes lower at light load due to reduced influence of the pickup on the primary. The sensitivity of DPF to variations in M is small. Variations in M and L_s have significant influences on the power transfer

InductEV, Inc.
Exhibit 1008
Page 220

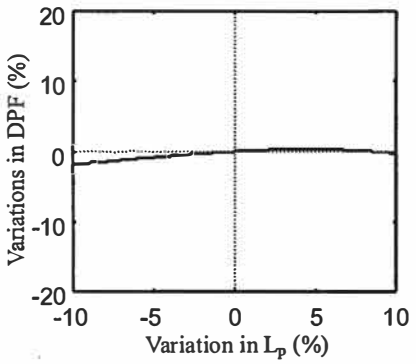
capability because of Q_s.



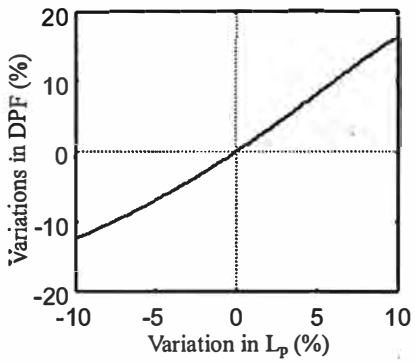
(a) Power transfer capability.



(b) DPF.

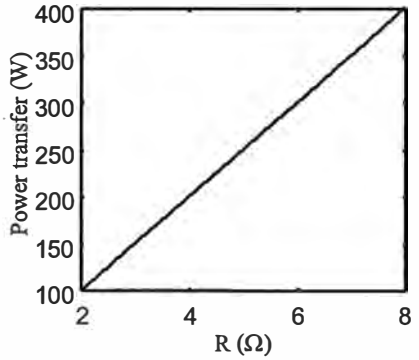


(c) Sensitivity of the DPF at 300W.

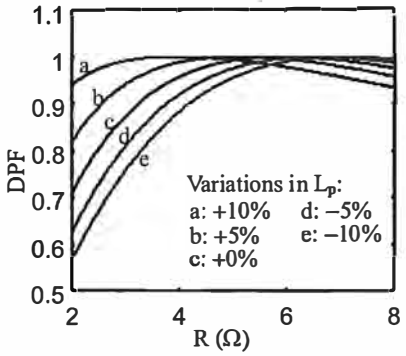


(d) Sensitivity of the DPF at 150W.

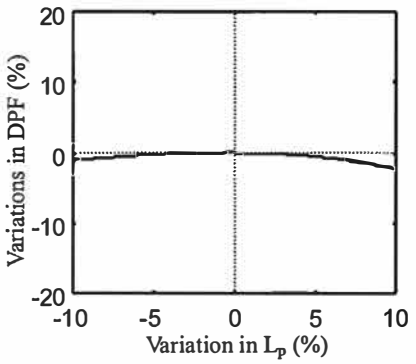
Fig. 7-24. Original tuning (C_{pn}=1, u=1) – The influence of variations in L_p for an electric vehicle battery charger under fixed-frequency operation (k=0.45, $Q_{s0,rated}$=1.8, PP topology, I_p=15A).



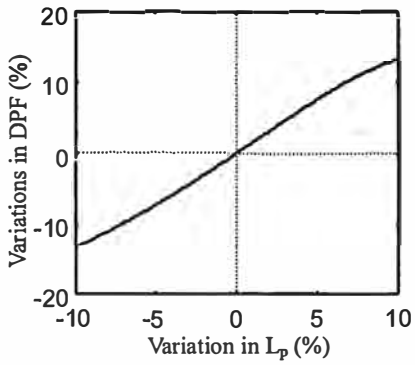
(a) Power transfer capability.



(b) DPF.



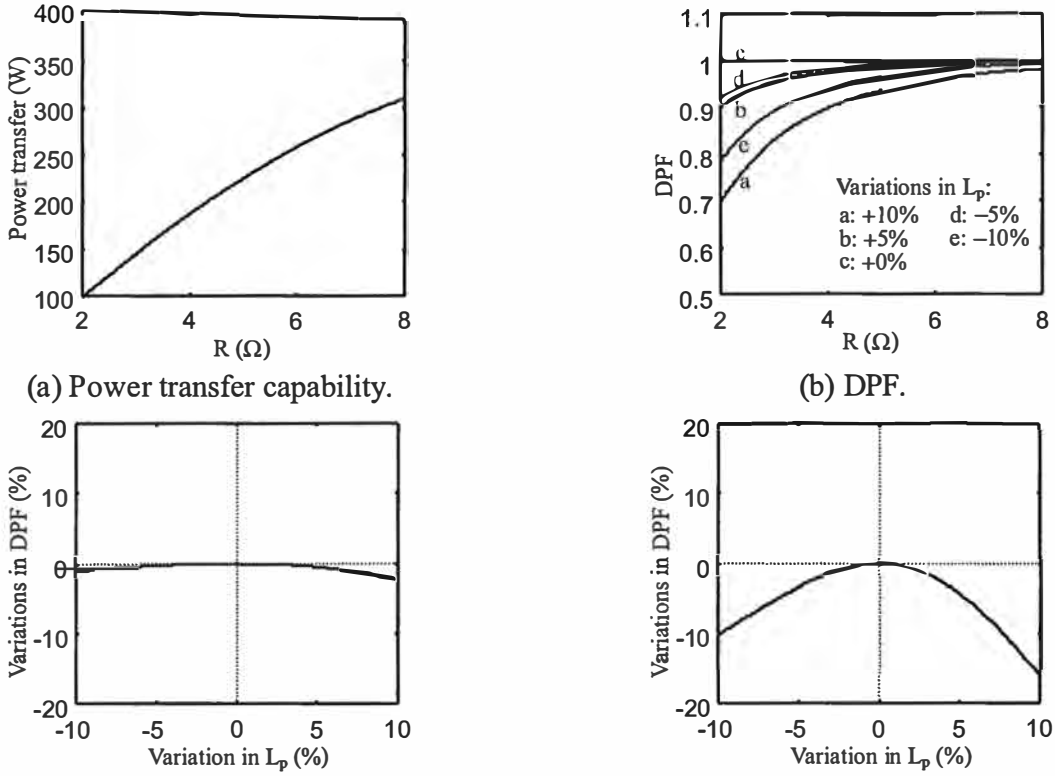
(c) Sensitivity of the DPF at 300W.



(d) Sensitivity of the DPF at150W.

Fig. 7-25. Modified tuning for unity DPF at rated load (C_{pn}=1.04, u=1) – The influence of variations in L_p for an electric vehicle battery charger under fixed-frequency operation.

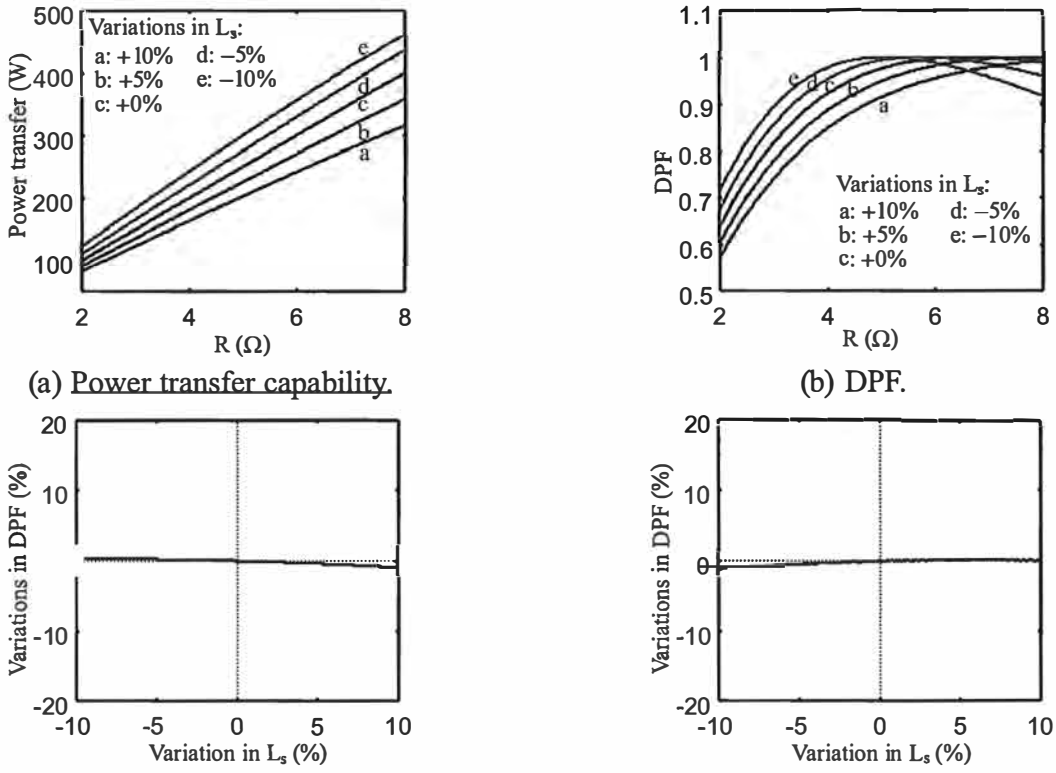
InductEV, Inc.
Exhibit 1008
Page 221



(a) Power transfer capability. (b) DPF.

(c) Sensitivity of the DPF at 300W. (d) Sensitivity of the DPF at150W.

Fig. 7-26. Modified tuning for load independent unity DPF (C_{pn}=1, u=1.12) – The influence of variations in L_p for an electric vehicle battery charger under fixed-frequency operation.

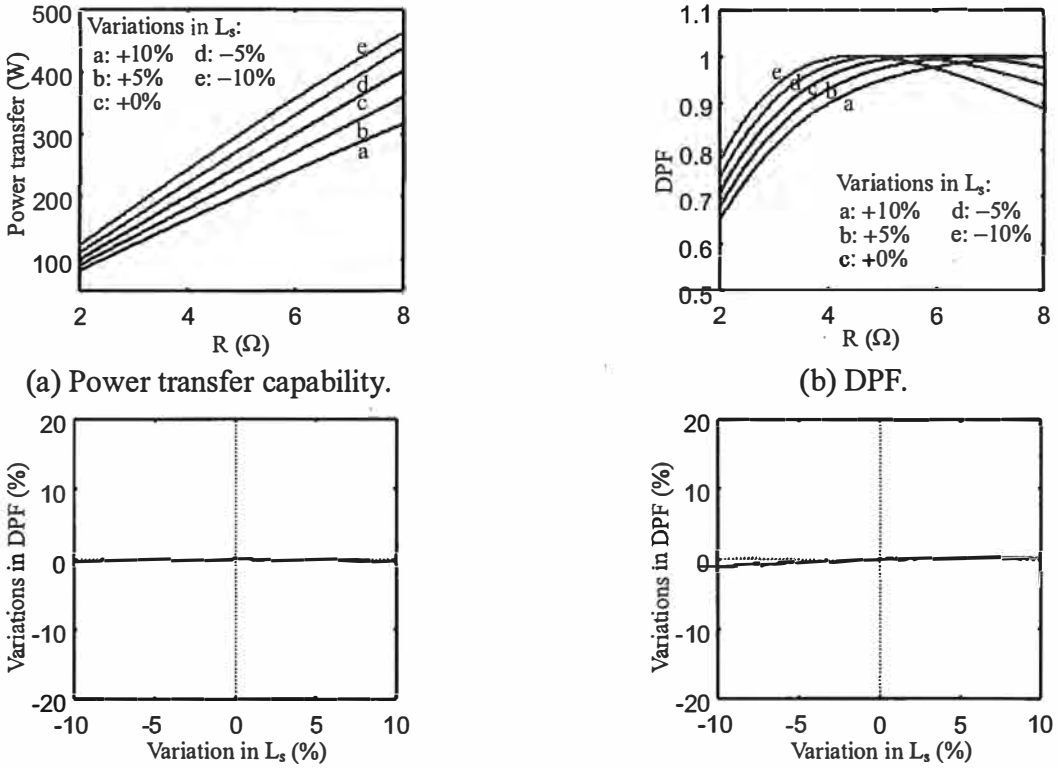


(a) Power transfer capability. (b) DPF.

(c) Sensitivity of the DPF at 300W. (d) Sensitivity of the DPF at 150W.

Fig. 7-27. Original tuning (C_{pn}=1, u=1) – The influence of variations in L_s for an electric vehicle battery charger under fixed-frequency operation (k=0.45, $Q_{s0,rated}$=1.8, PP topology, I_p=15A).

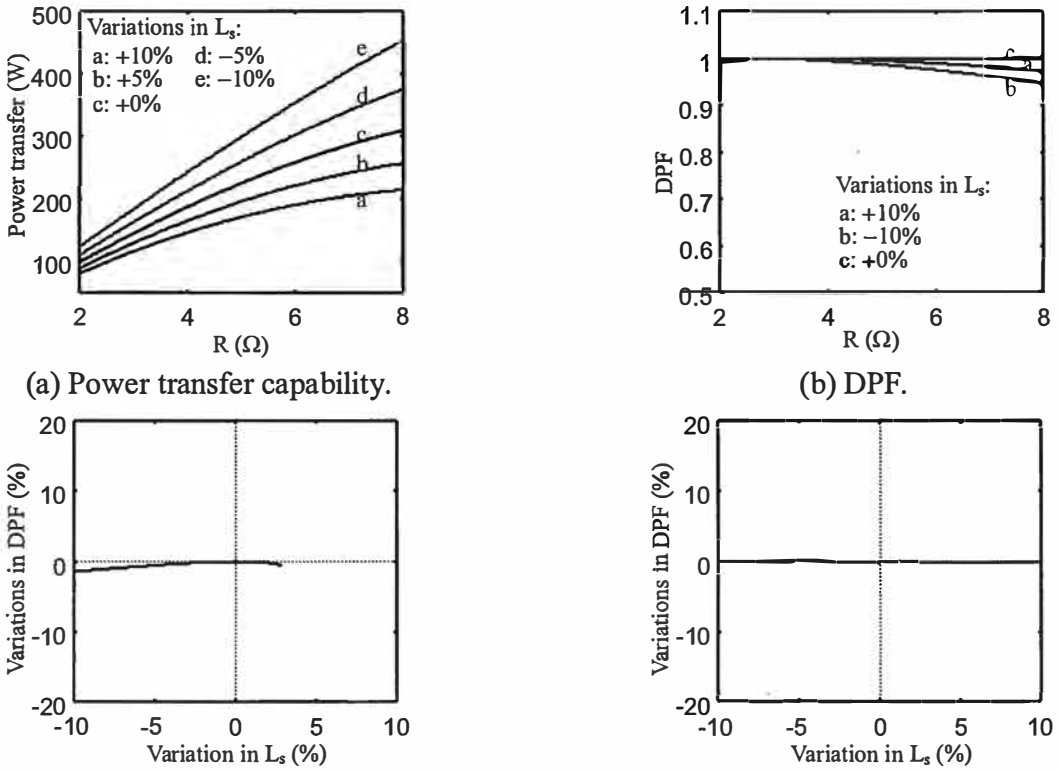
InductEV, Inc.
Exhibit 1008
Page 222



(a) Power transfer capability. (b) DPF.

(c) Sensitivity of the DPF at 300W. (d) Sensitivity of the DPF at150W.

Fig. 7-28. Modified tuning for unity DPF at rated load (C_{pn}=1.04, u=1) – The influence of variations in L_s for an electric vehicle battery charger under fixed-frequency operation.

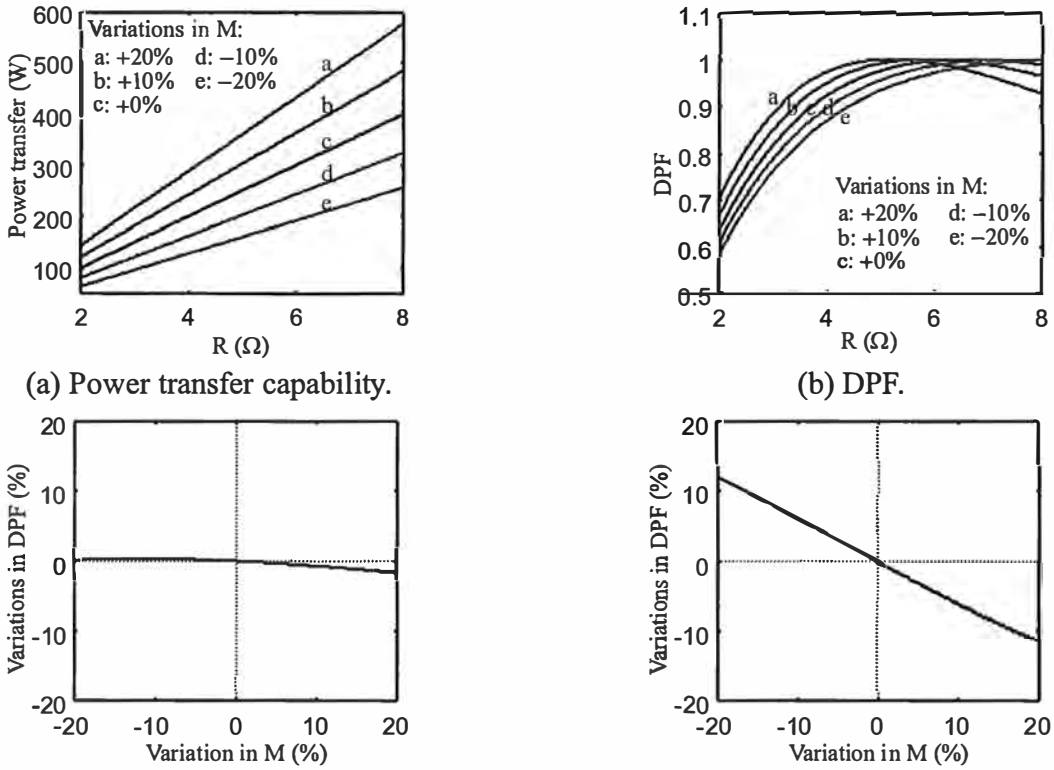


(a) Power transfer capability. (b) DPF.

(c) Sensitivity of the DPF at 300W. (d) Sensitivity of the DPF at150W.

Fig. 7-29. Modified tuning for load independent unity DPF (C_{pn}=1, u=1.12) – The influence of variations in L_s for an electric vehicle battery charger under fixed-frequency operation.

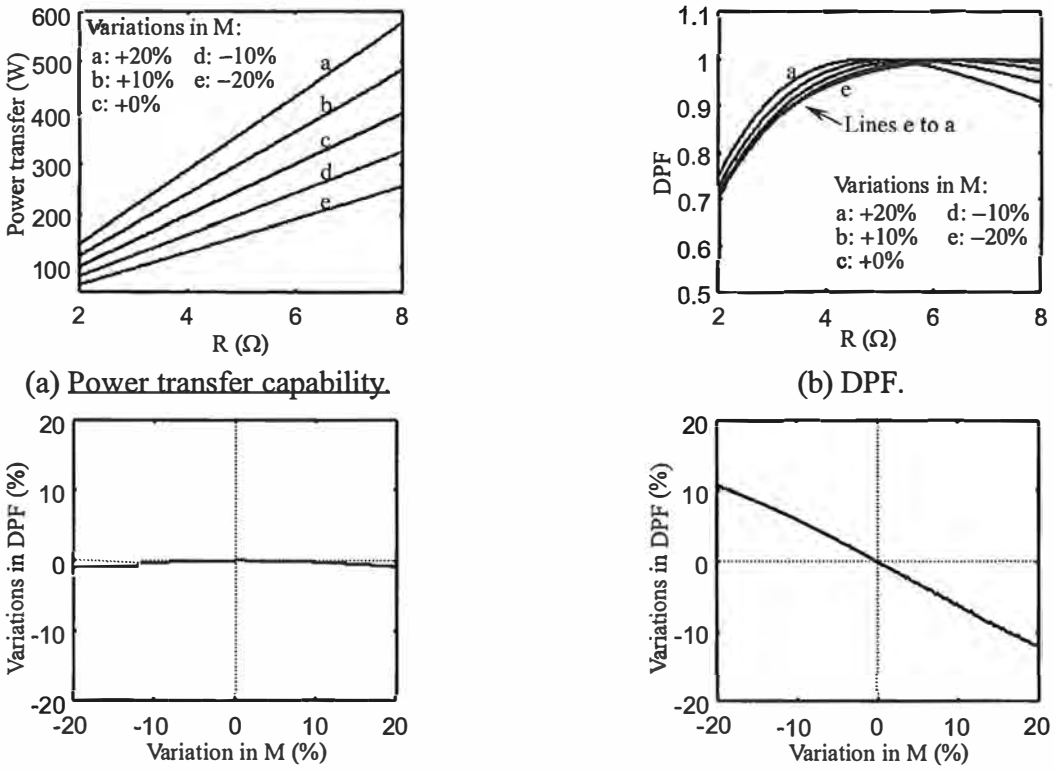
InductEV, Inc.
Exhibit 1008
Page 223



(a) Power transfer capability. (b) DPF.

(c) Sensitivity of the DPF at 300W. (d) Sensitivity of the DPF at 150W.

Fig. 7-30. Original tuning (C_{pn}=1, u=1) – The influence of variations in M for an electric vehicle battery charger under fixed-frequency operation (k=0.45, $Q_{s0,rated}$=1.8, PP topology, I_p=15A).

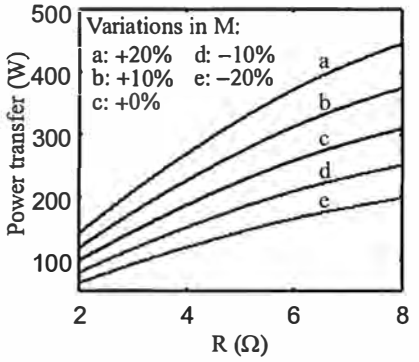


(a) Power transfer capability. (b) DPF.

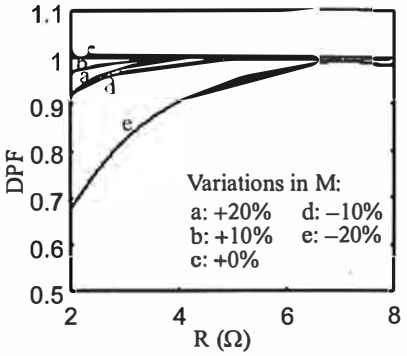
(c) Sensitivity of the DPF at 300W. (d) Sensitivity of the DPF at150W.

Fig. 7-31. Modified tuning for unity DPF at rated load (C_{pn}=1.04, u=1) – The influence of variations in M for an electric vehicle battery charger under fixed-frequency operation.

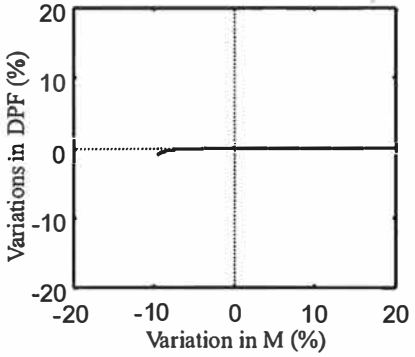
InductEV, Inc.
Exhibit 1008
Page 224



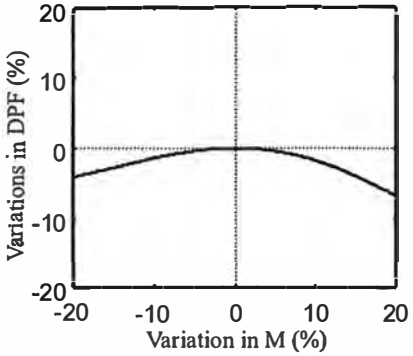
(a) Power transfer capability.



(b) DPF.

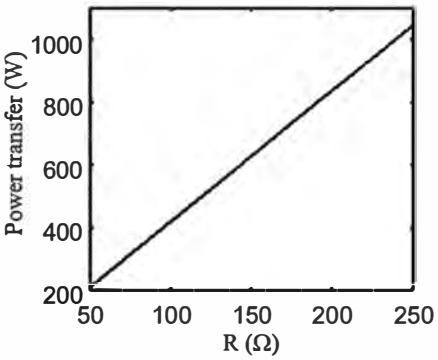


(c) Sensitivity of the DPF at 300W.

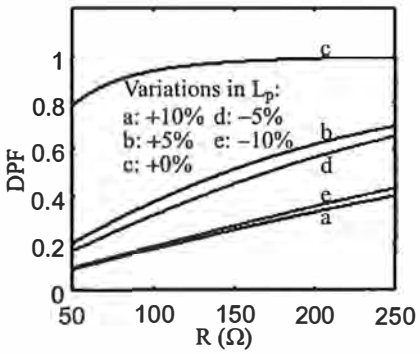


(d) Sensitivity of the DPF at150W.

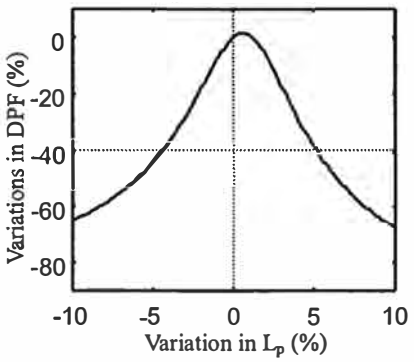
Fig. 7-32. Modified tuning for load independent unity DPF (C_{pn}=1, u=1.12) – The influence of variations in M for an electric vehicle battery charger under fixed-frequency operation.



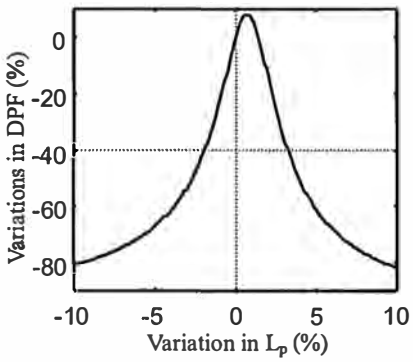
(a) Power transfer capability.



(b) DPF.



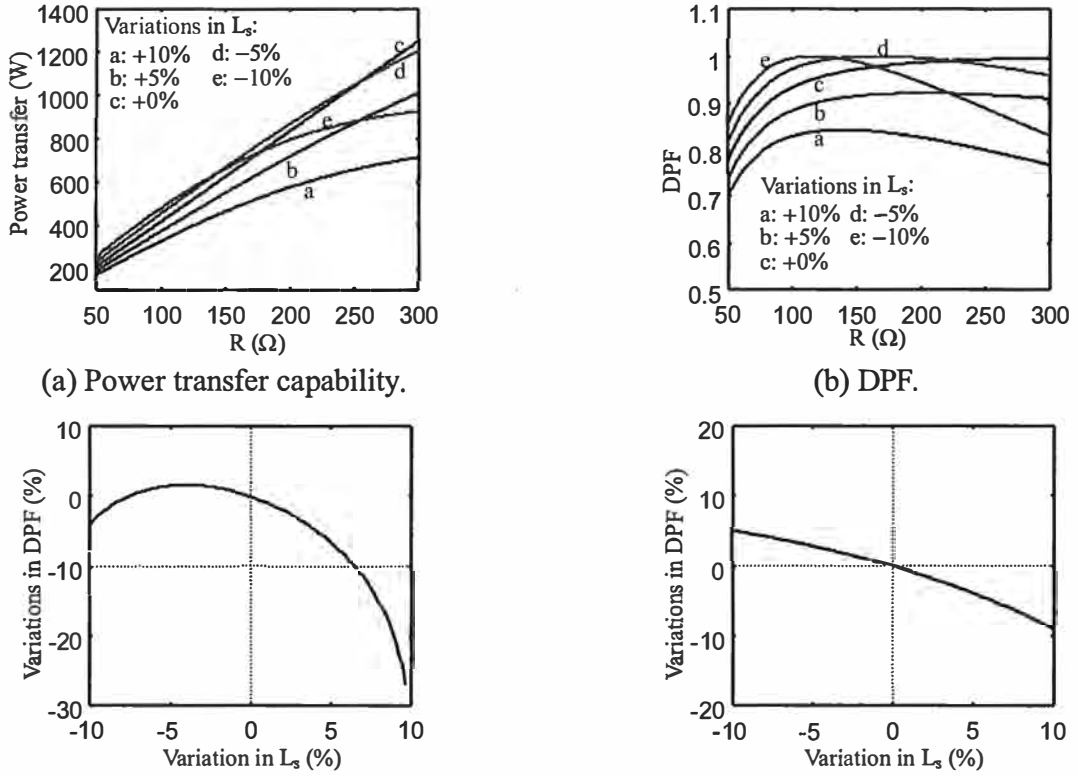
(c) Sensitivity of the DPF at 800W.



(d) Sensitivity of the DPF at 400W.

Fig. 7-33. The influence of variations in L_p for a monorail material handling system under fixed-frequency operation (k=0.086, $Q_{s0,rated}$=4.7, PP topology, C_{pn}=1, u=1).

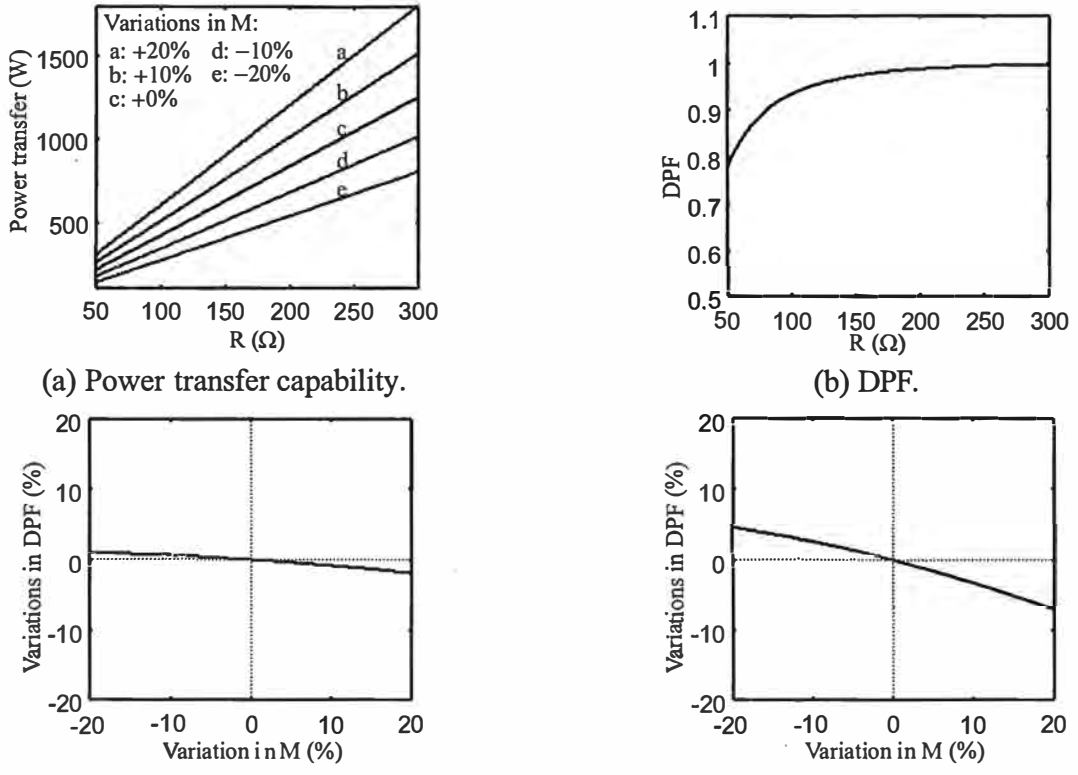
InductEV, Inc.
Exhibit 1008
Page 225



(a) Power transfer capability. (b) DPF.

(c) Sensitivity of the DPF at 800W. (d) Sensitivity of the DPF at 400W.

Fig. 7-34. The influence of variations in L_s for a monorail material handling system under fixed-frequency operation (k=0.086, $Q_{s0,rated}$=4.7, PP topology, C_{pn}=1, u=1).



(a) Power transfer capability. (b) DPF.

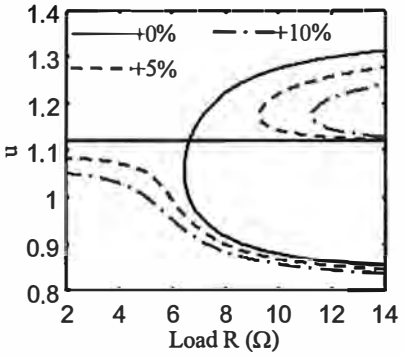
(c) Sensitivity of the DPF at 800W. (d) Sensitivity of the DPF at 400W.

Fig. 7-35. The influence of variations in M for a monorail material handling system under fixed-frequency operation (k=0.086, $Q_{s0,rated}$=4.7, PP topology, C_{pn}=1, u=1).

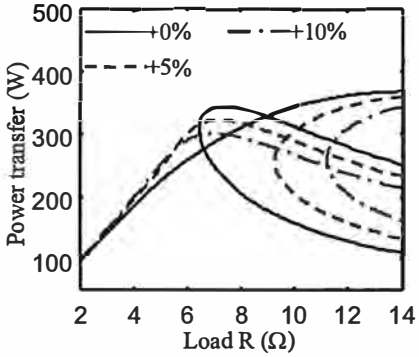
InductEV, Inc.
Exhibit 1008
Page 226

7-6.3 VARIABLE-FREQUENCY SYSTEMS

A well-coupled system (electric vehicle battery charging) – The influence on operating frequency and power of variations in the coupling parameters are shown in Fig. 7-36 to 7-41. The original and modified tuning schemes exhibit similar sensitivities. Variations in L_p have a similar influence to that seen with variations in C_p. Here, the power transfer capability is highly sensitive to decreases in L_p. The sensitivity of the operating frequency to variations in L_p is significant at rated power, and becomes slightly lower at reduced load because of lower Q_s.

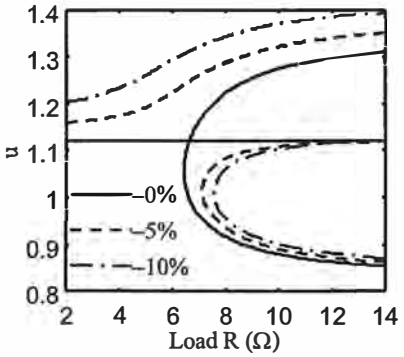


(i) Operational frequency.

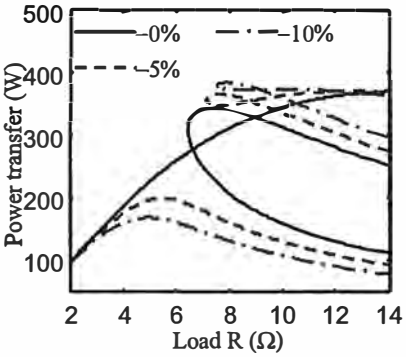


(ii) Power transfer capability.

(a) Increases in L_p.

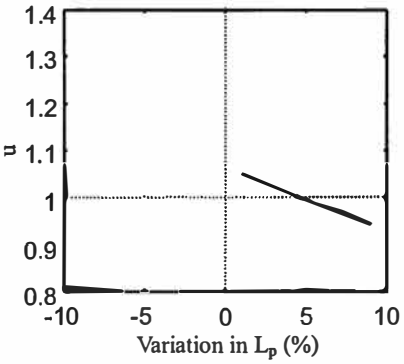


(i) Operational frequency.

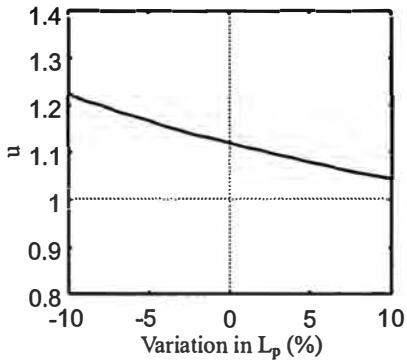


(ii) Power transfer capability.

(b) Decreases in L_p.



(i) Operating at 300W.

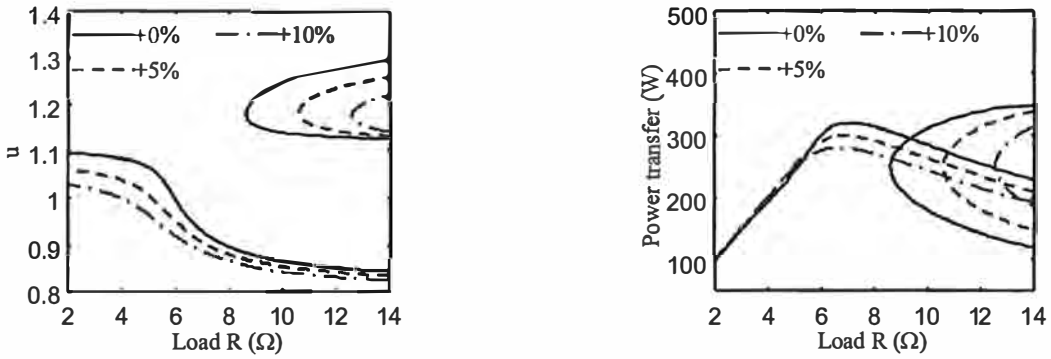


(ii) Operating at 150W.

(c) Sensitivity of the operating frequency.

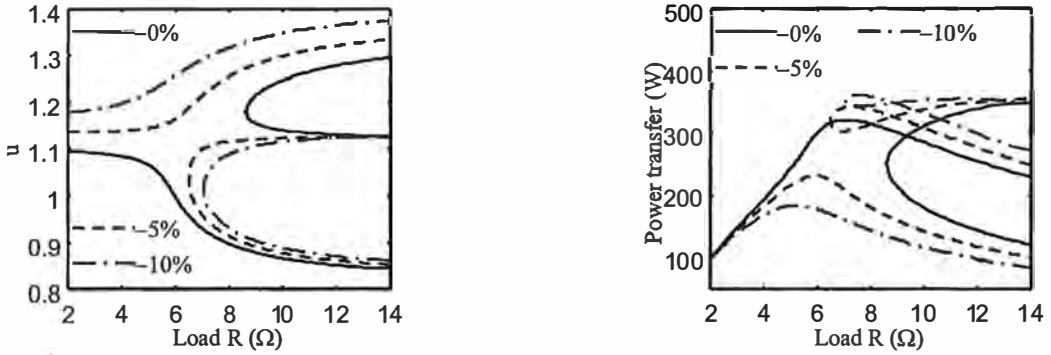
Fig. 7-36. Original tuning (C_{pn}=1) – The influence of variations in L_p for an electric vehicle battery charger under variable-frequency operation (k=0.45, $Q_{s0,rated}$=1.8, PP topology, I_p=15A).

InductEV, Inc.
Exhibit 1008
Page 227



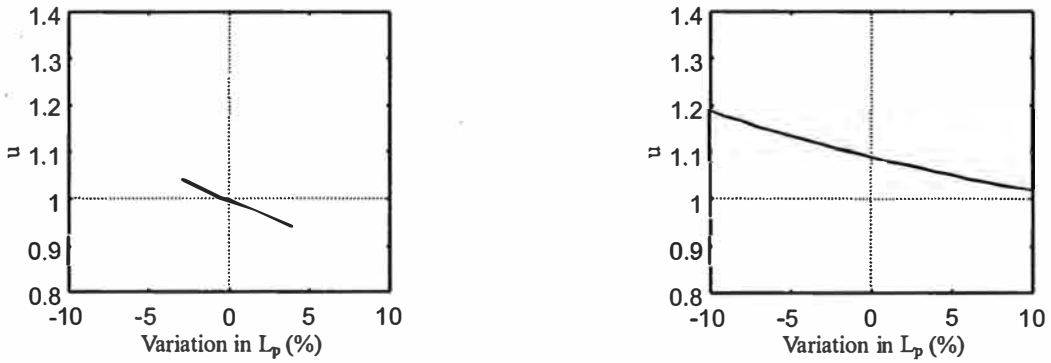
(i) Operational frequency. (ii) Power transfer capability.

(a) Increases in L_p.



(i) Operational frequency. (ii) Power transfer capability.

(b) Decreases in L_p.



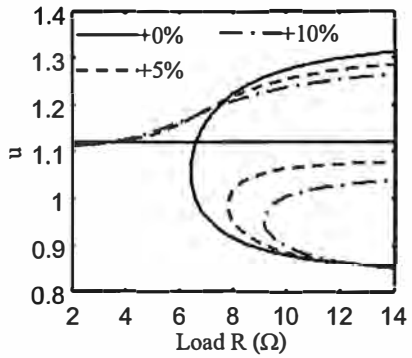
(i) Operating at 300W. (ii) Operating at 150W.

(c) Sensitivity of the operating frequency.

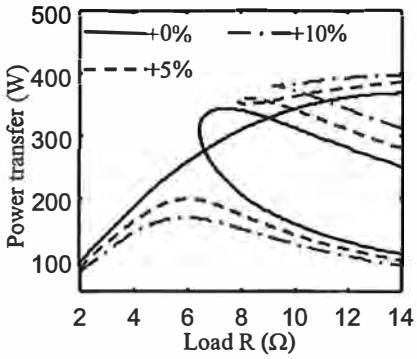
Fig. 7-37. Modified tuning for unity DPF at rated load (C_{pn}=1.04) – The influence of variations in L_p for an electric vehicle battery charger under variable-frequency operation (k=0.45, $Q_{s0,rated}$=1.8, PP topology, I_p=15A).

InductEV, Inc.
Exhibit 1008
Page 228

Variations in L_s have similar effects to that seen with variations in C_s. Here, the power transfer capability is highly sensitive to increases in L_s. The sensitivity of the operating frequency to variations in L_s is less than that seen with variations in L_p, especially at light load where the sensitivity is negligible because the frequency shift can be neglected.

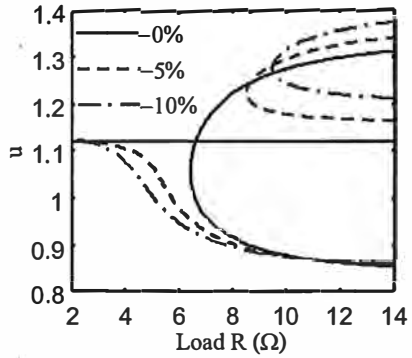


(i) Operational frequency.

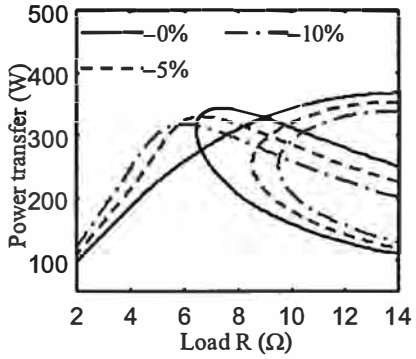


(ii) Power transfer capability.

(a) Increases in L_s.

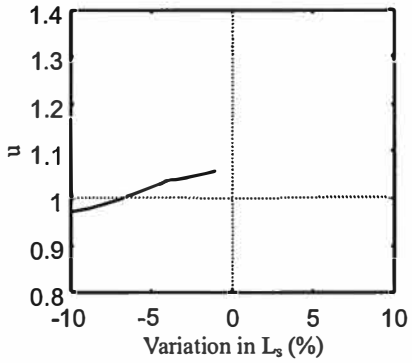


(i) Operational frequency.

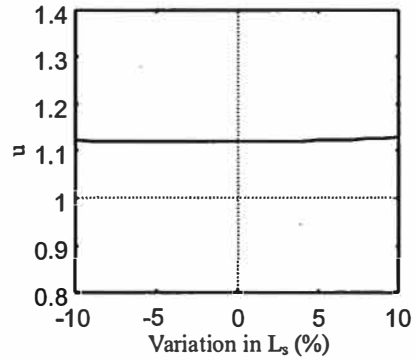


(ii) Power transfer capability.

(b) Decreases in L_s.



(i) Operating at 300W.

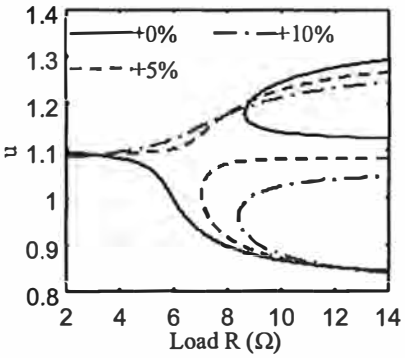


(ii) Operating at 150W.

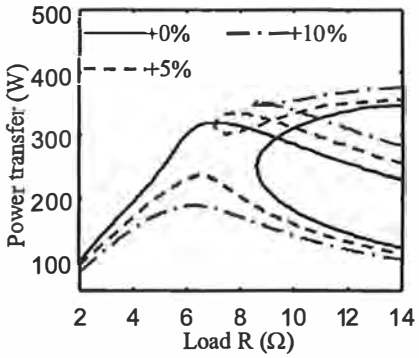
(c) Sensitivity of the operating frequency.

Fig. 7-38. Original tuning (C_{pn}=1) – The influence of variations in L_s for an electric vehicle battery charger under variable-frequency operation (k=0.45, $Q_{s0,rated}$=1.8, PP topology, I_p=15A).

InductEV, Inc.
Exhibit 1008
Page 229

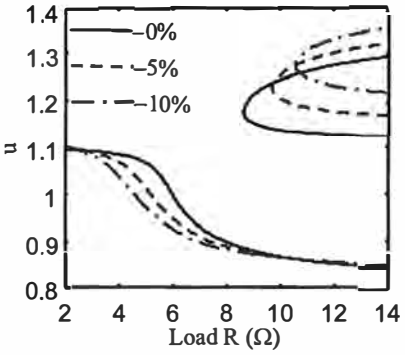


(i) Operational frequency.

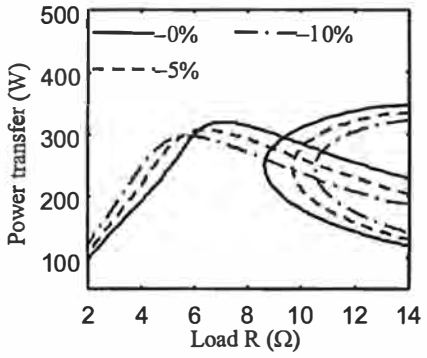


(ii) Power transfer capability.

(a) Increases in L_s.

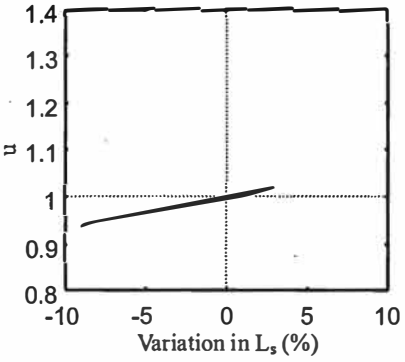


(i) Operational frequency.

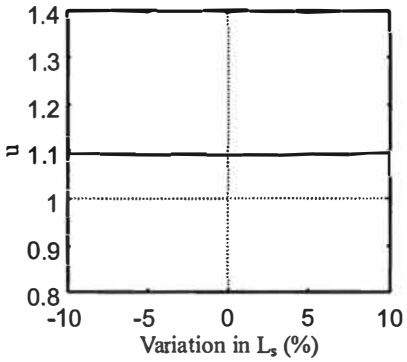


(ii) Power transfer capability.

(b) Decreases in L_s.



(i) Operating at 300W.



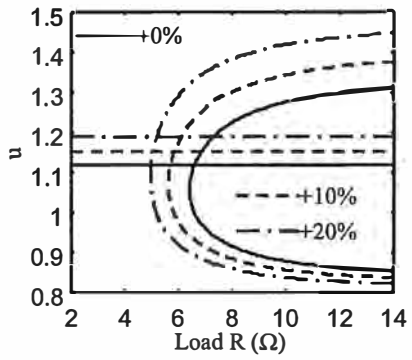
(ii) Operating at 150W.

(c) Sensitivity of the operating frequency.

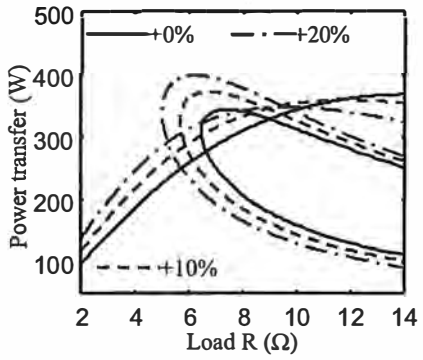
Fig. 7-39. Modified tuning for unity DPF at rated load (C_{pn}=1.04) – The influence of variations in L_s for an electric vehicle battery charger under variable-frequency operation (k=0.45, $Q_{s0,rated}$=1.8, PP topology, I_p=15A).

InductEV, Inc.
Exhibit 1008
Page 230

As expected, variations in M have a significant influence on the power transfer capability. An increase in M results in improved power transfer capability as well as the occurrence of bifurcation at a light load. Decreasing M results in reduced power transfer capability and the appearance of bifurcation at higher load. Because of changes in the loading effects of the pickup, the sensitivity of the operating frequency to variations in M is higher than that seen with variations in L_s for all loading conditions.

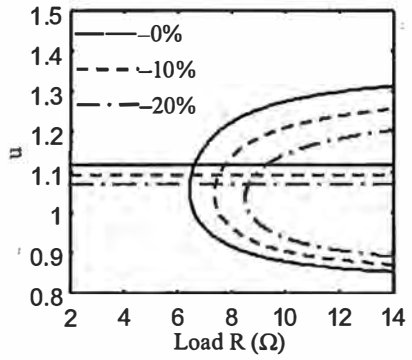


(i) Operational frequency.

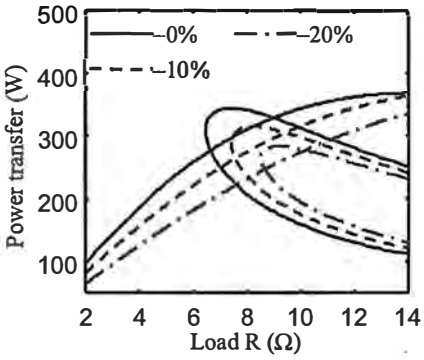


(ii) Power transfer capability.

(a) Increases in M.

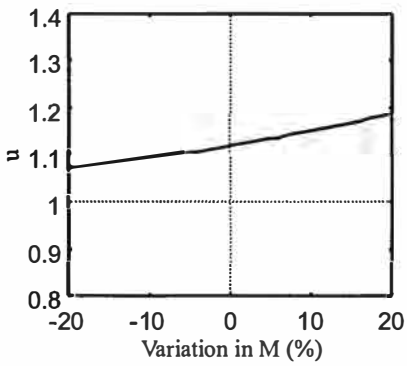


(i) Operational frequency.



(ii) Power transfer capability.

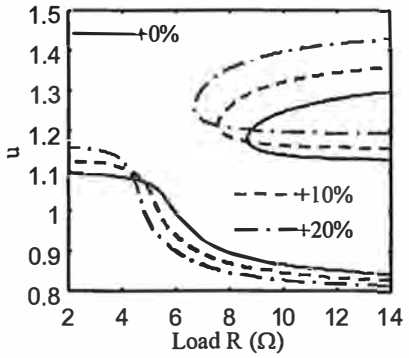
(b) Decreases in M.



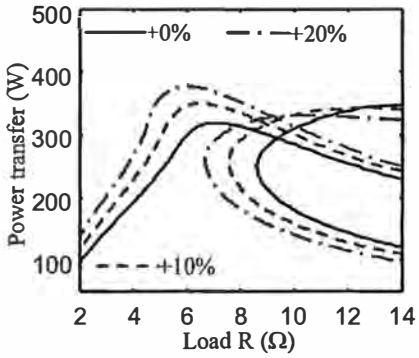
(c) Sensitivity of the operating frequency operating at 150W.

Fig. 7-40. Original tuning (C_{pn}=1) – The influence of variations in M for an electric vehicle battery charger under variable-frequency operation (k=0.45, $Q_{s0,rated}$=1.8, PP topology, I_p=15A).

InductEV, Inc.
Exhibit 1008
Page 231

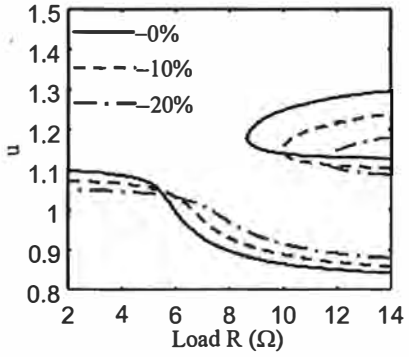


(i) Operational frequency.

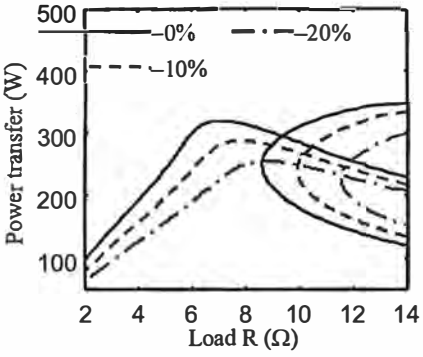


(ii) Power transfer capability.

(a) Increases in M.

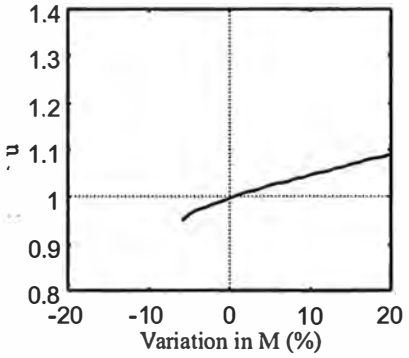


(i) Operational frequency.

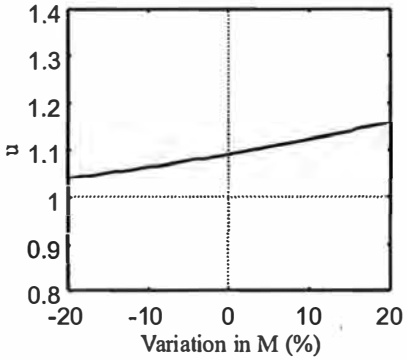


(ii) Power transfer capability.

(b) Decreases in M.



(i) Operating at 300W.



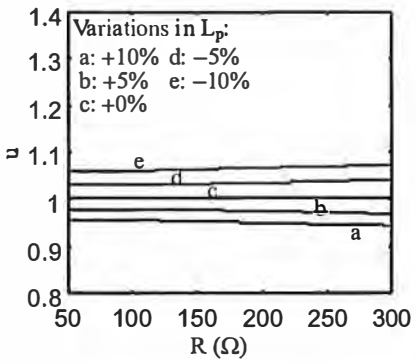
(ii) Operating at 150W.

(c) Sensitivity of the operating frequency.

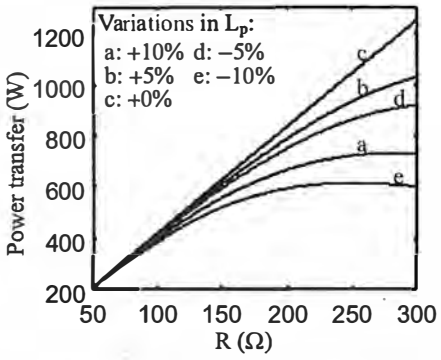
Fig. 7-41. Modified tuning for unity DPF at rated load (C_{pn}=1.04) – The influence of variations in M for an electric vehicle battery charger under variable-frequency operation (k=0.45, $Q_{s0,rated}$=1.8, PP topology, I_p=15A).

A loosely coupled system (monorail material handling) –The influence on operating frequency and power of variations in the coupling parameters are shown in Fig. 7-42 to 7-44. The operating frequency is sensitive to variations in L_p, while its insensitivity to variations in L_s and M is small as the loading effects of the pickup are insignificant. The power transfer capability is quite sensitive to variations in each coupling parameter since Q_s is high.

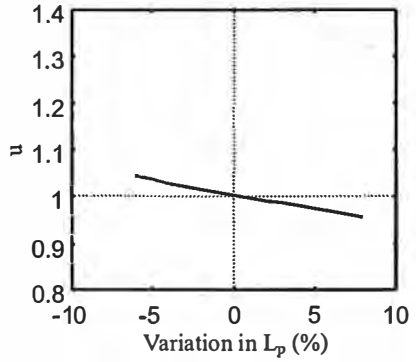
InductEV, Inc.
Exhibit 1008
Page 232



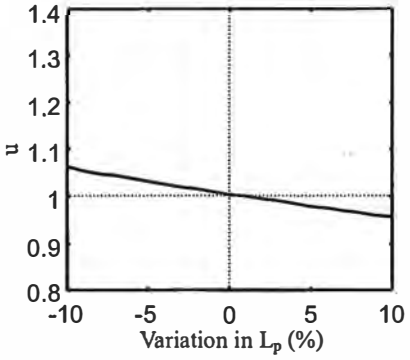
(a) Operating frequency.



(b) Power transfer capability.

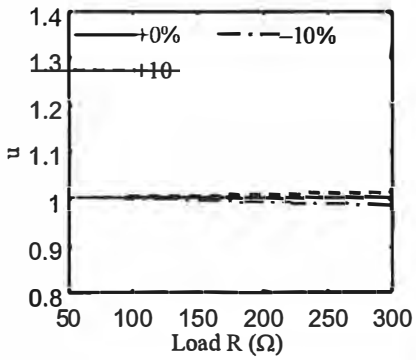


(c) Sensitivity of the operating frequency at 800W.

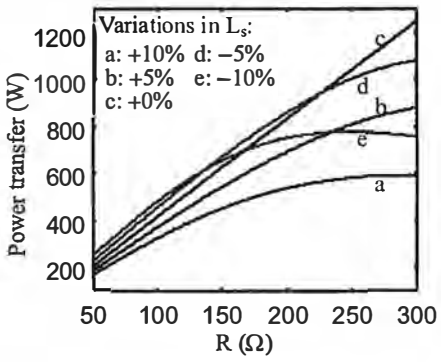


(d) Sensitivity of the operating frequency at 400W.

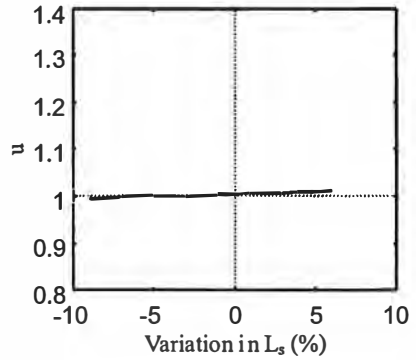
Fig. 7-42. The influence of variations in L_p for a monorail material handling system under variable-frequency operation (k=0.086, $Q_{s0,rated}$=4.7, PP topology, C_{pn}=1, I_p=54A).



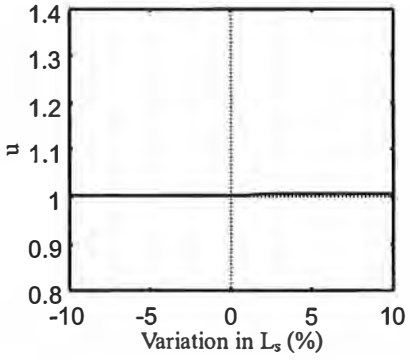
(a) Operating frequency.



(b) Power transfer capability.



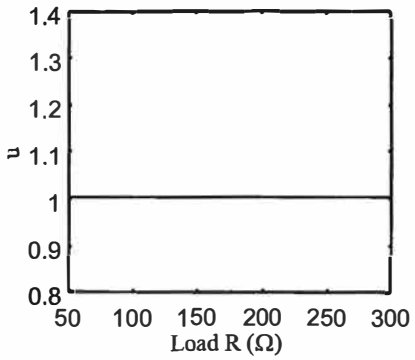
(c) Sensitivity of the operating frequency at 800W.



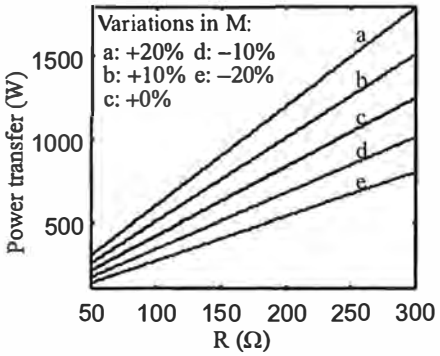
(d) Sensitivity of the operating frequency at 400W.

Fig. 7-43. The influence of variations in L_s for a monorail material handling system under variable-frequency operation (k=0.086, $Q_{s0,rated}$=4.7, PP topology, C_{pn}=1, I_p=54A).

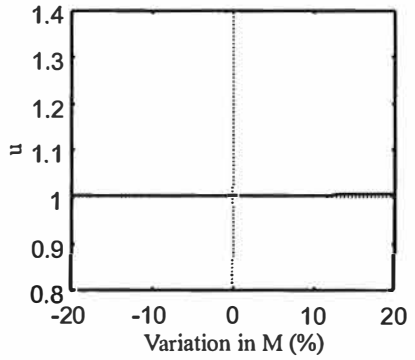
InductEV, Inc.
Exhibit 1008
Page 233



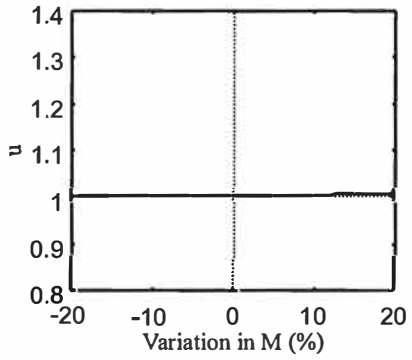
(a) Operating frequency.



(b) Power transfer capability.



(c) Sensitivity of the operating frequency at 800W.



(d) Sensitivity of the operating frequency at 400W.

Fig. 7-44. The influence of variations in M for a monorail material handling system under variable-frequency operation (k=0.086, $Q_{s0,rated}$=4.7, PP topology, C_{pn}=1, I_p=54A).

7-7 DISCUSSION

A comparison of the various sensitivity analyses for variations in C_p, C_s, L_p, L_s and M are summarized in Table 7-5 to 7-8. Here, all of the tuning schemes discussed in this thesis are compared. Influences on the DPF, the power transfer capability and the operating frequency are classified here into: "Very High (>50%)", "High (<50%)", "Moderate (<30%)", "Low (<15%)" and "Very Low (<5%)" according to the percentage changes found when each of the parameters of interest is varied by ±10%. In all cases, the original tuning and the modified tunings are essentially identical and therefore are not separated.

For loosely coupled systems under fixed-frequency operation, the DPF is highly sensitive to variations in C_p and L_p. This can result in very poor DPF requiring a larger VA rating for the power supply. In consequence, fixed-frequency operation is not a good choice when variations in C_p or L_p are large. With variable-frequency control, the operating frequency is also sensitive to variations in C_p and L_p. This has moderate influences on the power transfer capability. Variations in C_s, L_s and M also have moderate influences on the power transfer capability in both fixed and variable-frequency systems. Overall, in order to minimize the VA rating of the power supply, variable-frequency operation is a good choice for loosely coupled systems.

InductEV, Inc.
Exhibit 1008
Page 234

For well-coupled systems under fixed-frequency operation, the sensitivity of DPF to variations in C_s, C_p, L_p, L_s and M is small at rated power in all three tuning schemes. The sensitivity becomes higher under lightly loading conditions. Here, the modified tuning for load independent unity DPF has lower sensitivity, but the sensitivity of the power transfer capability to variations in C_s becomes higher, requiring a careful choice of the type and grade of capacitor used here. Variations in L_s have a significant impact on the power transfer capability for all tuning schemes. However, as noted in Fig. 7-22, if L_s increases M increases faster to compensate its influence on power transfer.

TABLE 7-5
SENSITIVITY OF DPF TO VARIATIONS IN C_P, C_S, L_P, L_S AND M UNDER FIXED-FREQUENCY OPERATION (PP TOPOLOGY)

		Well-coupled systems			Loosely coupled systems
		Original tuning	Modified tuning for unity DPF at rated load	Modified tuning for load independent unity DPF	
C_p	Rated power	Very Low	Very Low	Very Low	Very High
	Light power	Moderate	Moderate	Low	Very High
C_s	Rated power	Very Low	Very Low	Very Low	Moderate
	Light power	Very Low	Very Low	Very Low	Moderate
L_p	Rated power	Very Low	Very Low	Very Low	Very High
	Light power	Moderate	Moderate	Low	Very High
L_s	Rated power	Very Low	Very Low	Very Low	Moderate
	Light power	Very Low	Very Low	Very Low	Low
M	Rated power	Very Low	Very Low	Very Low	Very Low
	Light power	Moderate	Moderate	Low	Low

TABLE 7-6
THE INFLUENCE OF VARIATIONS IN C_S, L_S AND M ON THE POWER TRANSFER CAPABILITY UNDER FIXED-FREQUENCY OPERATION (PP TOPOLOGY)

		Well-coupled systems			Loosely coupled systems
		Original tuning	Modified tuning for unity DPF at rated load	Modified tuning for load independent unity DPF	
C_s	Rated power	Low	Low	High	Moderate
	Light power	Low	Low	Low	Low
L_s	Rated power	High	High	High	Moderate
	Light power	Moderate	Moderate	Moderate	Moderate
M	Rated power	Moderate	Moderate	Moderate	Moderate
	Light power	Moderate	Moderate	Moderate	Moderate

InductEV, Inc.
Exhibit 1008
Page 235

TABLE 7-7
SENSITIVITY OF THE OPERATING FREQUENCY TO VARIATIONS IN C_P, C_S, L_P, L_S AND M UNDER VARIABLE-FREQUENCY OPERATION (PP TOPOLOGY)

		Well-coupled systems		Loosely coupled systems
		Original tuning	Modified tuning for unity DPF at rated load	
C_p	Rated power	High	High	Moderate
	Light power	Moderate	Moderate	Low
C_s	Rated power	Moderate	Moderate	Very Low
	Light power	Very Low	Very Low	Very Low
L_p	Rated power	High	High	Moderate
	Light power	Moderate	Moderate	Low
L_s	Rated power	Moderate	Moderate	Very Low
	Light power	Very Low	Very Low	Very Low
M	Rated power	Moderate	Moderate	Very Low
	Light power	Low	Low	Very Low

TABLE 7-8
THE INFLUENCE OF VARIATIONS IN C_P, C_S, L_P, L_S AND M ON THE POWER TRANSFER CAPABILITY UNDER VARIABLE-FREQUENCY OPERATION (PP TOPOLOGY)

		Well-coupled systems		Loosely coupled systems
		Original tuning	Modified tuning for unity DPF at rated load	
C_p	Increase	Low	Low	Moderate
	Decrease	High	High	Moderate
C_s	Increase	High	High	Moderate
	Decrease	Low	Low	Moderate
L_p	Increase	Low	Low	Moderate
	Decrease	High	High	Moderate
L_s	Increase	High	High	Moderate
	Decrease	Low	Low	Moderate
M	Increase	Moderate	Moderate	Moderate
	Decrease	Moderate	Moderate	Moderate

For well-coupled systems under variable-frequency operation, the original and modified tuning schemes have similar sensitivity. The operating frequency is sensitive to variations in C_p and L_p, particularly with increased output power. Such variations in the operating frequency result in reduced

InductEV, Inc.
Exhibit 1008
Page 236

power transfer capability, and as such rated power may be unavailable. Importantly, the power transfer capability is particularly sensitive to decreases in C_p and L_p as well as increases in C_s and L_s. If it were possible to have positive variations in C_p and L_p and negative variations in C_s and L_s, the impact on system operation would be minimized.

The sensitivity analysis in this chapter focused on two typical systems, one of which was a well-coupled contact-less electric vehicle battery charger and the other a loosely coupled monorail material handling system. Both examples use PP topologies. Similar sensitivities can be found using other topologies (SS, SP and PS), but such an extended analysis is beyond the scope of this thesis.

7-8 CONCLUSIONS

The sensitivity of the displacement power factor (DPF), the operating frequency and the power transfer capability to variations in the primary and secondary compensation capacitances (C_p and C_s) as well as the misalignment of the electromagnetic structure (variations in the coupling parameters M, L_p and L_s) were investigated in this chapter for both fixed and variable-frequency systems. It was found that systems designed using the tuning schemes proposed in Chapter 5 (for variable-frequency systems) and Chapter 6 (for fixed-frequency systems) have similar sensitivities to that found with those tuned using the approach described in Chapter 4. The exception is the tuning scheme for load independent unity DPF proposed in section 6-3 (for fixed-frequency systems). Here, the sensitivity of its DPF at light load is lower than all other tuning schemes, however, its power transfer is particularly sensitive to increases in C_s, and therefore requires this capacitor to be carefully selected for temperature and lifetime stability.

REFERENCES

[1]. J. T. Boys, G. A. Covic, A. W. Green, "Stability and control of inductively coupled power transfer systems," *IEE Proceedings-Electric Power Applications*, vol. 147, pp. 37-43, Jan. 2000.

[2]. A. W. Green, J. T. Boys, "10 kHz inductively coupled power transfer-concept and control," in *Conf. Rec. Power Electronics and Variable-Speed Drives*, 1994, pp. 694-699.

InductEV, Inc.
Exhibit 1008
Page 237

InductEV, Inc.
Exhibit 1008
Page 238

CHAPTER 8

INVESTIGATING AN LCL RESONANT INVERTER FOR ICPT APPLICATIOMS

8-1 Introduction
8-2 Overview of the system
8-3 Capability of the inverter
8-4 Capability of the resonant tank
8-5 Steady state power flow analysis
8-6 Verification
8-7 Conclusions

8-1 INTRODUCTION

Throughout this thesis, an LCL resonant inverter has been used to verify the proposed theory. This chapter investigates the suitability of this LCL resonant inverter for ICPT applications.

Resonant inverters are popular for applications such as induction heating [1]. Induction heating inverters in the 10 to 100 kHz frequency range can be used for ICPT applications, but the design considerations are very different due to the difference in load characteristics. When analysing such inverters, the load is normally represented as a resistor in series with the primary inductance, but in many practical ICPT systems the reflected reactance due to secondary resonance is comparable to the primary inductance [2-5]. Consequently, in order to analyse ICPT systems accurately, the secondary resonant circuit needs to be solved simultaneously with the primary resonant network.

Sinusoidal ac analysis (fundamental mode analysis) is commonly used to analyse resonant inverters [1][3][5][6]. This approach is suitable for determining steady state characteristics, but is unable to identify the transient response or non-linear features. Alternatively, time domain analysis using differential equations can be used [7]. However, this approach becomes too complex to be solved analytically when combining the primary and secondary resonant circuits of an ICPT system.

In this chapter, the inverter is modelled using time domain differential equations, while sinusoidal ac analysis is used to model the resonant tank (the impedance model developed in Chapter 3). A power flow balance between the inverter and the resonant tank determines the steady state operation, enabling the inverter to be designed to achieve maximum power transfer to the load. The analysis is verified using a design example for contact-less electric vehicle battery charging.

InductEV, Inc.
Exhibit 1008
Page 239

8-2 OVERVIEW OF THE SYSTEM

This section introduces the fundamental operation of the LCL resonant inverter, and summarizes the proposed analytical procedure used in the following sections to match the inverter to the resonant tank for maximum power transfer to the load.

8-2.1 OPERATING MODES OF THE LCL RESONANT INVERTER

The schematic in Fig. 8-1 shows an ICPT system using an LCL resonant inverter. The switching power supply used here is a full-bridge inverter fed by a dc voltage (V_d). The inductance of the primary winding (L_p), its primary parallel compensation capacitor (C_p), together with the series inductor L_m form the LCL resonant circuit. Either series or parallel compensation can be used for the secondary, with the advantages of each topology discussed in section 2-3. In this system, a parallel topology was chosen for the secondary compensation.

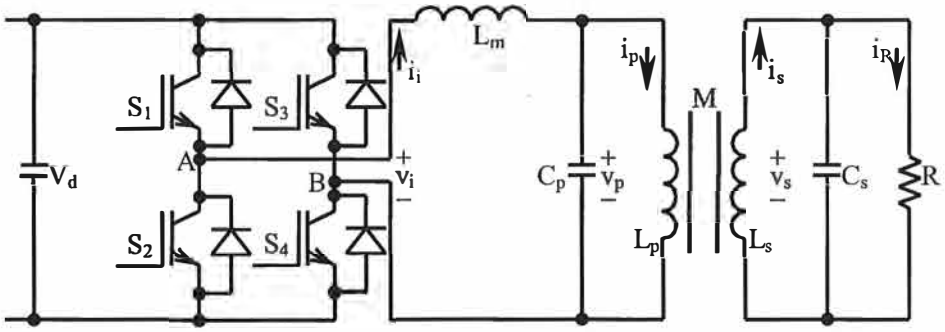


Fig. 8-1. Circuit diagram of an ICPT system driven by an LCL resonant inverter.

The inverter can be controlled using either a fixed or a variable-frequency controller. The advantages and disadvantages of fixed and variable-frequency operations have been discussed in section 2-5.

LCL resonant inverters can be operated with either continuous or discontinuous current. Continuous current operation has been reported in detail for induction heating applications under variable- frequency operation [1], and for ICPT applications under fixed-frequency operation [8]. Discontinuous current operation, however, has not been investigated thoroughly in the literature. Consequently, this chapter investigates a variable frequency controlled LCL resonant inverter operating with discontinuous current.

In continuous current mode, the inverter is controlled to always ensure a path for the inverter current. This can be achieved by using the voltage amplification effect described in [1]. With this design the resonant tank voltage is much larger than the output inverter voltage, and the inverter

InductEV, Inc.
Exhibit 1008
Page 240

current becomes nearly sinusoidal as shown in Fig. 8-2 (a). For optimal inverter efficiency, the frequency is controlled so that the inverter current is in phase with the inverter output voltage. Switching losses are virtually non-existent, and very high operating frequencies can be achieved. Power regulation can be achieved by varying the frequency as described in [1], but the resulting switching losses need to be considered carefully.

In discontinuous current mode the inverter is switched so that the inverter current drops to zero and stays there for a finite period during each half cycle as shown in Fig. 8-2 (b). The biggest advantage is that turn-on losses are eliminated, and only conduction and turn-off losses need to be considered.



(a) Continuous current mode. (b) Discontinuous current mode.

Fig. 8-2. Inverter voltage and current waveforms for the LCL resonant inverter.

It is further possible to control the switches so that inverter current is minimised. This is achieved by ensuring the inverter voltage always has the same polarity as the resonant tank voltage. With v_p positive, only S_1 and S_4 are allowed to turn on, while S_2 and S_3 will only be turned on if v_p is negative. Figure 8-3 shows current and voltage waveforms for half a cycle.

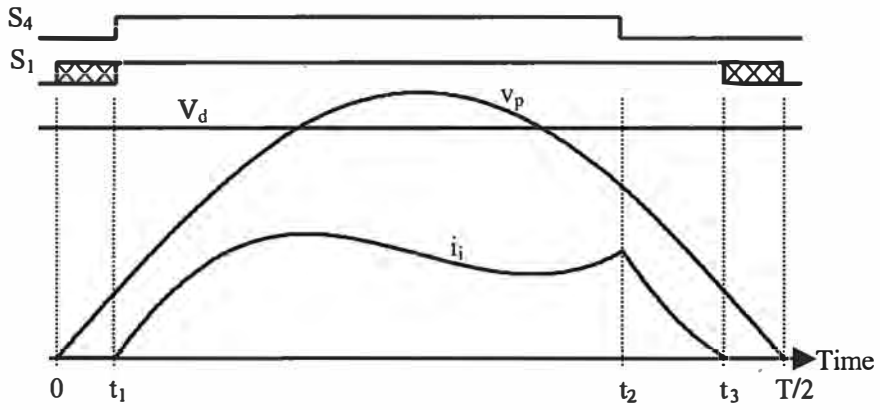


Fig. 8-3. Switching control of the LCL resonant inverter in discontinuous current mode.

To ensure discontinuous current, t_2 has to be early enough to ensure that the current will drop back to zero before the end of the half cycle. Since the resonant tank voltage v_p provides the voltage to drive the inverter current back to zero, t_2 is a strong function of v_p (t_2 must reduce as v_p reduces).

Power control is mainly achieved by varying t_1. As t_1 increases, the inverter current drops resulting in lower power. With only turn-off and conduction losses, a trade-off between the switching and conduction losses is necessary. Using modern IGBT modules, conduction losses are equal to turn-off

InductEV, Inc.
Exhibit 1008
Page 241

losses at switching frequencies around 20kHz. With such devices, this would be the best practical operating frequency to maximize the inverter's efficiency.

8-2.2 AN ANALYTICAL PROCEDURE FOR SYSTEM DESIGN

To facilitate analysis and design of the system, a four-step process is followed:

Step1: Firstly an inverter model is developed in which the resonant tank (the electromagnetic structure, the primary and secondary compensations as well as the load) is modelled as a sinusoidal voltage source. With this simplification, the inverter current waveform as well as the inverter output power can be determined as a function of the resonant tank voltage.

Step 2: Once the inverter current waveform is known, the fundamental component of the inverter current is calculated. Of particular importance is the phase relationship between the inverter current and the resonant tank voltage.

Step 3: Next the impedance model developed in Chapter 3 is used to model the resonant tank (the electromagnetic structure, the primary and secondary compensations as well as the load). If all parameters are known, the model can be used to calculate the power and phase relationships of the resonant tank.

Step 4: Finally the two models are combined, and the steady state operating point is determined using power flow balance between the inverter and the resonant tank.

8-3 CAPABILITY OF THE INVERTER

The output power of the inverter can be calculated from the output voltage (v_i) and current (i_i). The amplitude of the rectangular inverter output voltage equals the dc bus voltage (V_d), while the pulse width is controllable by the switching instants t_1 and t_2. The waveform of the inverter output current is dependent on not only the switching instants and the dc bus voltage, but also the resonant tank voltage (v_p) and the series inductance (L_m). An inverter model is developed in this section to investigate influences of these parameters on the capability of the inverter.

8-3.1 THE INVERTER MODEL

In the inverter model shown in Figure 8-4, all primary and secondary resonant tank components are replaced by a single sinusoidal voltage source v_p. This is a valid simplification for high Q resonant systems, where the resonant tank voltages are very close to sinusoidal.

InductEV, Inc.
Exhibit 1008
Page 242

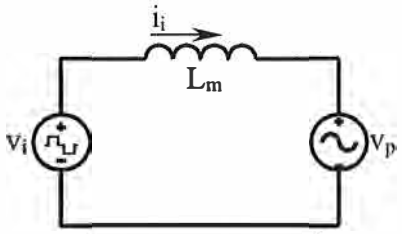


Fig. 8-4. Simplified model of the LCL resonant inverter.

The resonant tank voltage is given by:

$$v_p(t) = \hat{V}_p \sin \omega t \tag{8-1}$$

The inverter voltage depends on the states of the switches, and is equal to:

$$v_i(t) = \begin{cases} v_p(t), & 0 < t < t_1 \\ V_d, & t_1 < t < t_2 \\ 0, & t_2 < t < t_3 \\ v_p(t), & t_3 < t < T/2 \end{cases} \tag{8-2}$$

With this inverter model, the inverter current (i_i) can be determined from:

$$v_i(t) - v_p(t) = L_m \frac{di_i(t)}{dt} \tag{8-3}$$

During the time interval from t_1 to t_2, the inverter current solved from (8-3) is:

$$i_i(t) = \frac{V_d}{L_m}(t - t_1) + \frac{\hat{V}_p}{\omega L_m}[\cos \omega t - \cos \omega t_1] \qquad t_1 < t < t_2 \tag{8-4}$$

During the freewheeling period after t_2, the inverter current solved from (8-3) is:

$$i_i(t) = \frac{V_d}{L_m}(t_2 - t_1) + \frac{\hat{V}_p}{\omega L_m}[\cos \omega t - \cos \omega t_1] \qquad t_2 < t < t_3 \tag{8-5}$$

Since the inverter current drops to zero at t_3, the time t_2 can be expressed in terms of t_1 and t_3:

$$t_2 = t_1 + \frac{\hat{V}_p}{\omega V_d}[\cos \omega t_1 - \cos \omega t_3] \tag{8-6}$$

To ensure discontinuous current mode operation, t_3 has to be less than T/2. The maximum value of t_2 is thus:

$$t_{2,\max} = t_1 + \frac{\hat{V}_p}{\omega V_d}[\cos \omega t_1 + 1] \tag{8-7}$$

8-3.2 WAVEFORM OF THE INVERTER CURRENT

For a general analysis of the waveform of the inverter current, the resonant tank voltage is normalized with respect to the dc voltage as:

InductEV, Inc.
Exhibit 1008
Page 243

$$V_{pn} = \frac{\hat{V}_p}{V_d} \tag{8-8}$$

Time is normalized with respect to the period as:

$$t_n = \frac{t}{T} = \frac{\omega T}{2\pi} \tag{8-9}$$

The inverter current expressed in terms of these normalized parameters is then:

$$i_i(t_n) = \left(\frac{V_d}{\omega L_m}\right)\begin{cases} 0, & 0 < t_n < t_{1n} \\ 2\pi(t_n - t_{1n}) + V_{pn}[\cos(2\pi t_n) - \cos(2\pi t_{1n})], & t_{1n} < t_n < t_{2n} \\ 2\pi(t_{2n} - t_{1n}) + V_{pn}[\cos(2\pi t_n) - \cos(2\pi t_{1n})], & t_{2n} < t_n < t_{3n} \\ 0, & t_{3n} < t_n < 0.5 \end{cases} \tag{8-10}$$

where t_{2n} is derived from (8-6) as:

$$t_{2n} = t_{1n} + \frac{V_{pn}}{2\pi}[\cos(2\pi t_{1n}) - \cos(2\pi t_{3n})] \tag{8-11}$$

In the following analysis throughout this chapter, it is assumed that t_{2n} is controlled according to (8-11) using selections of t_{1n} and t_{3n}, and measurements of $\hat{V}_p$, V_d and ω.

The inverter current waveform is shown in Fig. 8-5 for selected V_{pn} assuming the switching instants are controlled to achieve maximum pulse width (here, t_{1n}=0, t_{3n}=0.5). In this figure and following similar figures, the maximum V_{pn} (defined as $V_{pn,max}$) is determined using (8-11) at the condition that t_{2n} equals t_{3n}. Discontinuous current operation is impossible with higher V_{pn}.

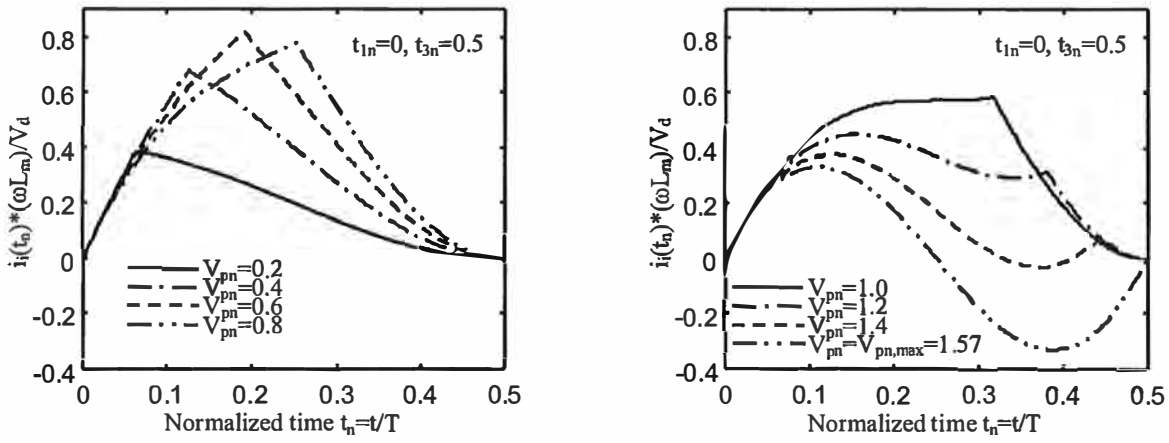


Fig. 8-5. Influences of varying V_{pn} on the inverter current waveform assuming maximum pulse width by setting t_{1n}=0, t_{3n}=0.5.

The waveform of the inverter current is a strong function of the resonant tank voltage. To ensure maximum power delivery, it is desirable to maximize the average current while minimizing peak current. This can be achieved when V_{pn} is close to unity. At this operating condition, the inverter

InductEV, Inc.
Exhibit 1008
Page 244

current waveform is close to a trapezoid.

The effect of increasing t_{1n} on the inverter current waveform is shown in Fig. 8-6 assuming maximum t_{3n} of 0.5. The average inverter current decreases as t_{1n} is increased, and becomes negative with high resonant tank voltage resulting in negative power flow that while possible theoretically is in practice not possible with an ICPT system as the pickups always consume power.

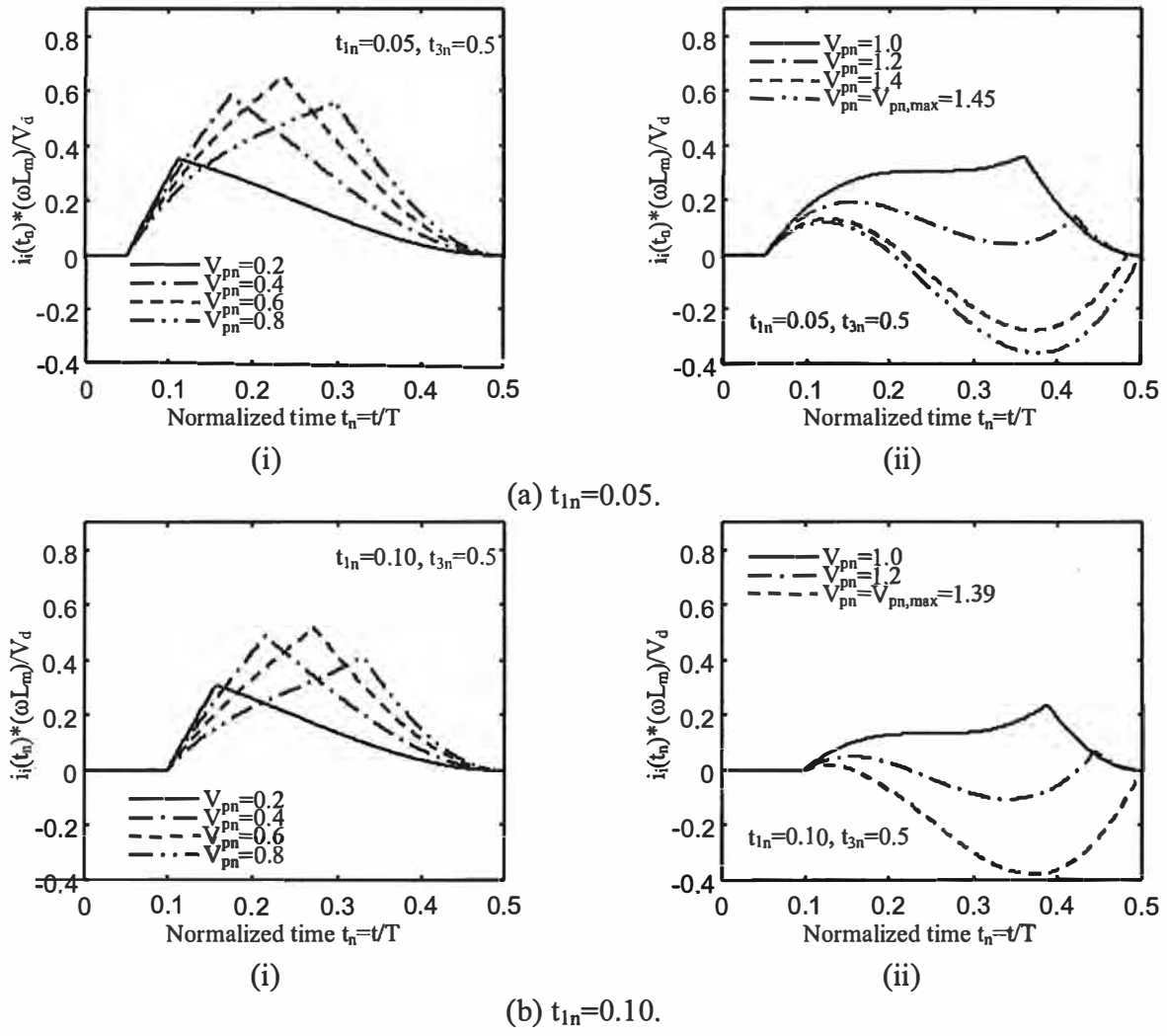


Fig. 8-6. Influences of V_{pn} and t_{1n} on the inverter current waveform (t_{3n} = 0.5).

The effect of decreasing t_{3n} on the inverter current waveform is shown in Fig. 8-7 assuming minimum t_{1n} of zero. The average inverter current reduces with decreasing t_{3n}. However, the sensitivity of the average current to decreases in t_{3n} is much lower than that seen with increases in t_{1n} (as seen in Fig. 8-6). Moreover, the average inverter current is positive across the whole range of possible resonant tank voltages ensuring positive power flow.

InductEV, Inc.
Exhibit 1008
Page 245

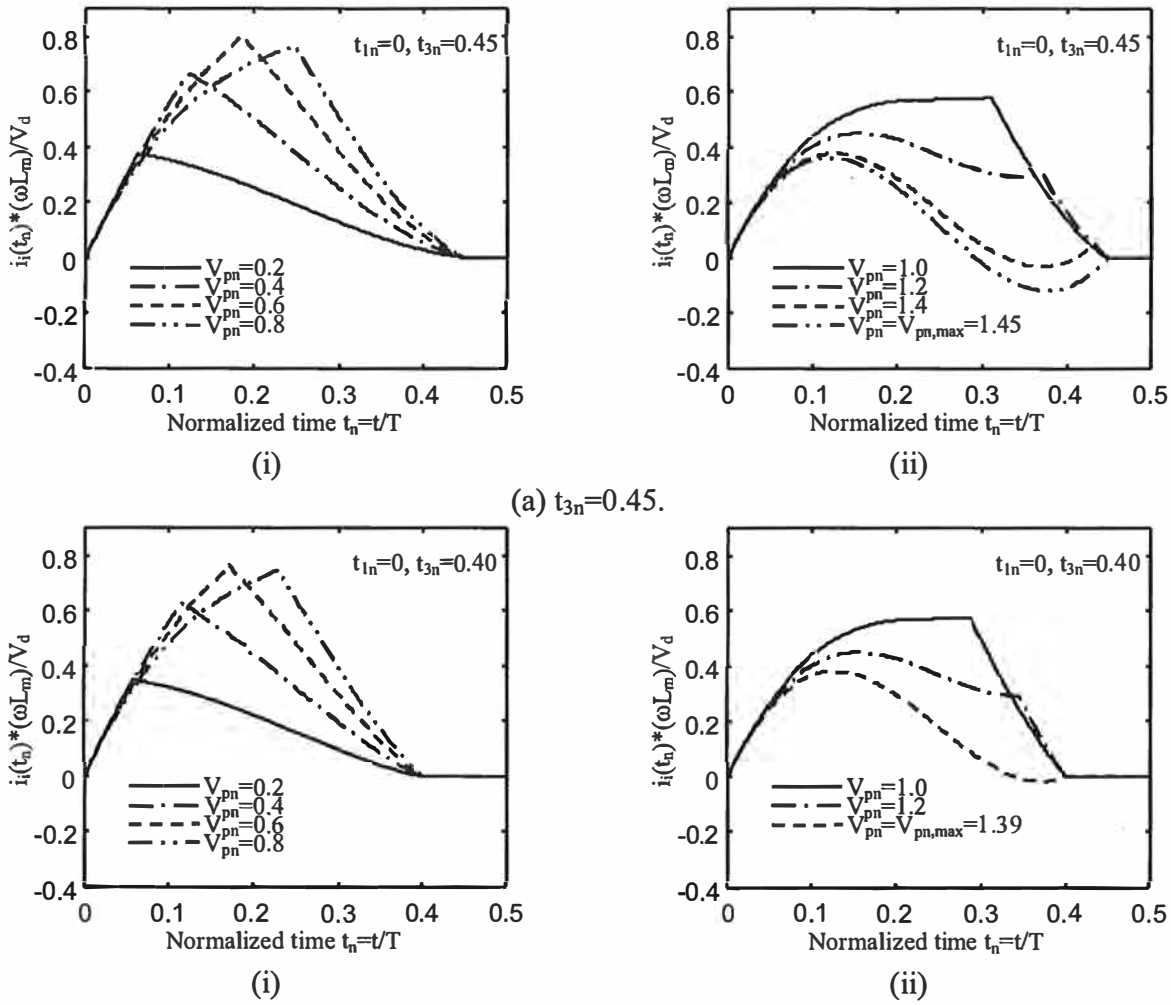


Fig. 8-7. Influences of V_{pn} and t_{3n} on the inverter current waveform (t_{1n} = zero).

8-3.3 INVERTER POWER DELIVERY CAPABILITY

The average power supplied by the inverter is equal to:

$$P_i = \frac{2}{T}\int_0^{T/2} v_i(t) i_i(t) dt \tag{8-12}$$

Before t_1 and after t_3, the inverter current is zero and the inverter supplies no power. During the freewheeling period from t_2 to t_3, the inverter voltage is zero, and again the inverter supplies no power. Power is only supplied by the inverter from t_1 to t_2, when the inverter voltage is equal to the dc bus voltage V_d. Equation (8-12) can thus be rewritten as:

$$P_i = \frac{2V_d}{T}\int_{t_1}^{t_2} i_i(t) dt \tag{8-13}$$

Substituting (8-4) into (8-13) results in:

$$P_i = \frac{V_d}{2\pi\omega L_m}\left\{V_d(\omega t_2 - \omega t_1)^2 + 2\hat{V}_p\left[\sin\omega t_2 - \sin\omega t_1 - (\omega t_2 - \omega t_1)\cos\omega t_1\right]\right\} \tag{8-14}$$

This equation shows that the inverter power can be controlled by varying t_1 and t_2.

InductEV, Inc.
Exhibit 1008
Page 246

In terms of the normalized primary resonant tank voltage given in (8-8) and the normalized time given in (8-9), the inverter power delivery capability given in (8-14) can be expressed as:

$$P_i = \left(\frac{V_d^2}{\pi\omega L_m}\right)\left\{2\pi^2(t_{2n}-t_{1n})^2 + V_{pn}\left[\sin(2\pi t_{2n}) - \sin(2\pi t_{1n}) - 2\pi(t_{2n}-t_{1n})\cos(2\pi t_{1n})\right]\right\} \quad (8\text{-}15)$$

where t_{2n} is a function of V_{pn}, t_{1n} and t_{3n} as given by (8-11).

8-3.4 FUNDAMENTAL COMPONENT OF THE INVERTER CURRENT

In this section, the fundamental inverter current is calculated to determine the phase relationship between the inverter current and the resonant tank voltage. Using Fourier analysis, the inverter current can be expressed as the sum of its Fourier components:

$$i_i(t) = \sum_{h=odd}\{A_h\cos(h\omega t) + B_h\sin(h\omega t)\} \quad (8\text{-}16)$$

where

$$A_h = \frac{4}{T}\int_0^{T/2} i_i(t)\cos(h\omega t)dt$$

$$B_h = \frac{4}{T}\int_0^{T/2} i_i(t)\sin(h\omega t)dt$$

Substituting (8-4) and (8-5) into (8-16), the fundamental component of the inverter current is:

$$i_{i1}(t) = A_1\cos\omega t + B_1\sin\omega t = C_1\sin(\omega t + \Phi_1) \quad (8\text{-}17)$$

where

$$A_1 = \frac{2}{\pi\omega L_m}\left\{\begin{bmatrix} V_d\left[(\omega t_2 - \omega t_1)\sin(\omega t_3) + \cos(\omega t_2) - \cos(\omega t_1)\right] \\ +\hat{V}_p\left[\cos(\omega t_1)\sin(\omega t_1) - \cos(\omega t_1)\sin(\omega t_3)\right] \end{bmatrix} + \hat{V}_p\left[+\frac{\omega t_3 - \omega t_1}{2} + \frac{\sin(2\omega t_3) - \sin(2\omega t_1)}{4}\right]\right\}$$

$$B_1 = \frac{2}{\pi\omega L_m}\left\{\begin{bmatrix} V_d\left[(\omega t_1 - \omega t_2)\cos(\omega t_3) + \sin(\omega t_2) - \sin(\omega t_1)\right] \\ +\hat{V}_p\left[\cos(\omega t_1)\cos(\omega t_3) - \cos^2(\omega t_1)\right] \end{bmatrix} + \hat{V}_p\left[+\frac{\sin^2(\omega t_3) - \sin^2(\omega t_1)}{2}\right]\right\}$$

$$C_1 = \sqrt{A_1^2 + B_1^2}$$

$$\Phi_1 = \tan^{-1}(A_1/B_1)$$

The phase angle Φ_1 is the angle between the resonant tank voltage and the fundamental of the inverter current, and gives a good indication of how well the inverter matches the resonant tank.

InductEV, Inc.
Exhibit 1008
Page 247

In terms of the normalized resonant tank voltage given in (8-8) and the normalized time given in (8-9), the phase angle of the fundamental inverter current derived in (8-17) can be expressed as:

$$\Phi_1 = \tan^{-1}\frac{\begin{bmatrix}\cos(2\pi t_{2n})-\cos(2\pi t_{1n})\\+2\pi(t_{2n}-t_{1n})\sin(2\pi t_{3n})\end{bmatrix}+V_{pn}\begin{bmatrix}\cos(2\pi t_{1n})\sin(2\pi t_{1n})-\cos(2\pi t_{1n})\sin(2\pi t_{3n})\\+\pi(t_{3n}-t_{1n})+\dfrac{\sin(4\pi t_{3n})-\sin(4\pi t_{1n})}{4}\end{bmatrix}}{\begin{bmatrix}\sin(2\pi t_{2n})-\sin(2\pi t_{1n})\\-2\pi(t_{2n}-t_{1n})\cos(2\pi t_{3n})\end{bmatrix}+V_{pn}\begin{bmatrix}\cos(2\pi t_{1n})\cos(2\pi t_{3n})-\cos^2(2\pi t_{1n})\\+\dfrac{\sin^2(2\pi t_{3n})-\sin^2(2\pi t_{1n})}{2}\end{bmatrix}} \quad (8\text{-}18)$$

where t_{2n} is a function of V_{pn}, t_{1n} and t_{3n} as given by (8-11).

The phase angle Φ_1 is a function t_{1n}, t_{3n} and V_{pn}. Importantly, it is independent of the frequency and will be used later to determine the steady state operating frequency.

The effect of increasing t_{1n} on the phase angle Φ_1 is shown in Fig. 8-8 assuming maximum t_{3n} of 0.5. In each case, there exists a maximum V_{pn} where the phase angle is either 90° or –90°. Here, the fundamental inverter current is zero and no power is transferred into the resonant tank. Further increases in V_{pn} would theoretically result in negative power flow. This is practically impossible with ICPT systems and therefore is not considered.

With t_{1n} controlled at zero, the minimum phase angle is about 10° when V_{pn} is slightly above unity. As noted in section 8-3.2, maximum inverter power is achieved when V_{pn} is near unity. It is thus desirable to make the phase angle in this range close to zero to ensure a suitable matching between the inverter and the resonant tank, which is designed to transfer maximum power with zero phase angle of the resonant tank impedance (as noted in Chapter 5). This can be achieved by increasing t_{1n} to around 0.04.

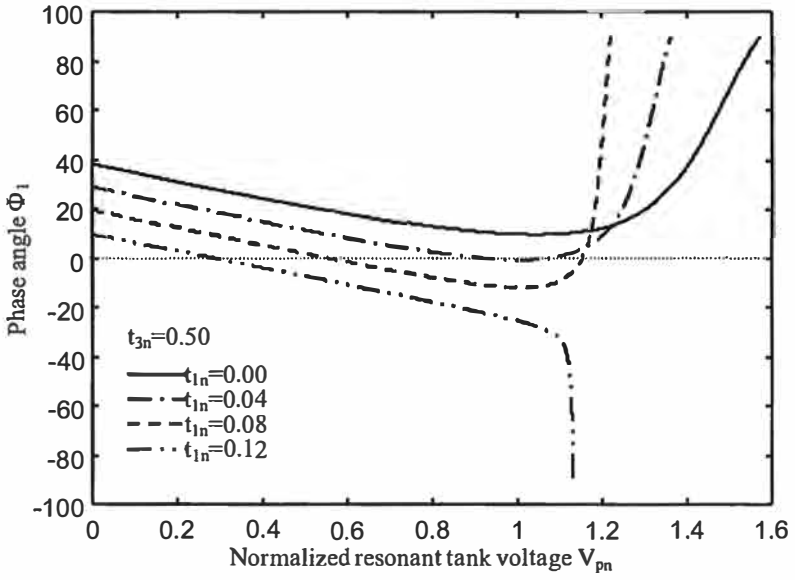


Fig. 8-8. Influences of increasing t_{1n} on the inverter current phase relationship assuming maximum t_{3n} of 0.5.

InductEV, Inc.
Exhibit 1008
Page 248

The effect of decreasing t_{3n} on the phase angle Φ_1 is shown in Fig. 8-9 assuming minimum t_{1n} of zero. Decreasing t_{3n} results in an increasing phase angle between the inverter current and the resonant tank voltage. Consequently, in the rest of this chapter it is assumed that t_{2n} is controlled using (8-11) to force t_{3n} to be 0.5.

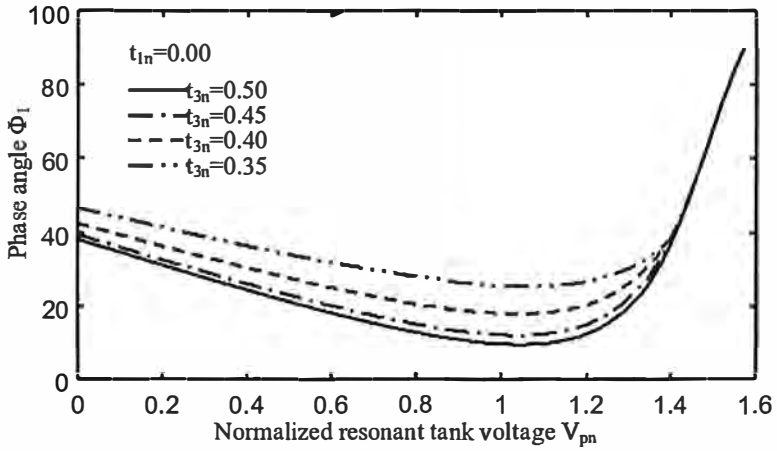


Fig. 8-9. Influences of decreasing t_{3n} on the inverter current phase relationship assuming minimum t_{1n} of zero.

8-4 CAPABILITY OF THE RESONANT TANK

The electromagnetic structure, the primary and secondary compensations as well as the load are now considered in more detail using the contact-less electric vehicle battery charger (described in section 3-11 and investigated in sections 4-6 and 5-6). This example is designed using the design methodology proposed in chapter 4 and the tuning scheme suggested in Chapter 5. It is assumed in this design that the primary current is controlled constant, the secondary pickup is tuned to resonate at the nominal frequency, and the primary is tuned to have unity DPF at rated load. However, when matching the inverter into the resonant tank, these ideal operating conditions may be not available due to non-linear behaviour of the inverter. This is investigated in this section to determine influences of the inverter switching control on the capability of the resonant tank.

8-4.1 THE RESONANT TANK MODEL

The total impedance (Z_t) of the resonant tank circuit can now be calculated using the load model developed in section 3-10.1. For PP topology, it is more convenient to express this in terms of an admittance as:

InductEV, Inc.
Exhibit 1008
Page 249

$$Y_t = j\omega C_p + \cfrac{1}{j\omega L_p + \cfrac{\omega^2 M^2}{j\omega L_s + \cfrac{1}{j\omega C_s + \cfrac{1}{R}}}} \tag{8-19}$$

The phase angle of the resonant tank admittance is determined as:

$$\angle Y_t = \tan^{-1}\left(\frac{\mathrm{Im}\, Y_t}{\mathrm{Re}\, Y_t}\right) \tag{8-20}$$

where the 'Re Y_t' and 'Im Y_t' represents the real and imaginary components of the resonant tank admittance.

With given electromagnetic structure (L_p, L_s, M), primary and secondary compensations (C_p, C_s) as well as load (R), the resonant tank admittance and its phase angle are functions of the operating frequency.

8-4.2 OPERATING FREQUENCY

The phase angle of the resonant tank admittance at rated load is shown in Fig. 8-10 as a function of the normalized frequency u (ω/ω_0). As expected, the phase angle is zero at u of unity.

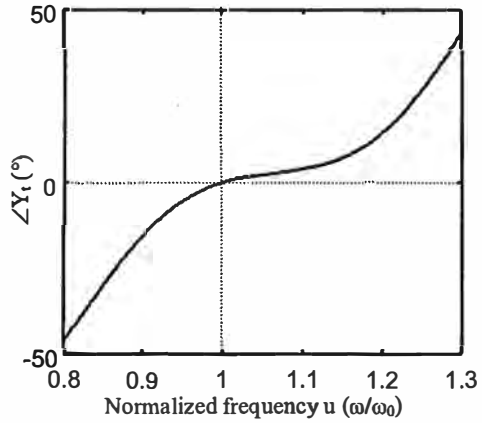


Fig. 8-10. Phase angle of the resonant tank admittance at rated load.

As noted in section 8-3.4, the phase angle of the fundamental inverter current is independent of the operating frequency. This enables the steady state operating frequency to be determined by matching the inverter model to the resonant tank model. At steady state, the phase angle of the primary resonant tank admittance must equal the phase angle of the fundamental inverter current. With the phase angle calculated based on selections of t_{1n}, t_{3n} and known V_{pn} using the inverter model, the operating frequency can be determined using the resonant tank model as a function of these same parameters. Influences of increasing t_{1n} on the operating frequency are shown in Fig. 8-11 assuming maximum t_{3n} of 0.5. For selected t_{1n} and t_{3n}, the phase angle of the fundamental inverter current is calculated as a

InductEV, Inc.
Exhibit 1008
Page 250

function of V_{pn} (Fig. 8-8). The operating frequency is then determined using the calculated phase angle (The dependence between the phase angle and the operating frequency is shown in Fig. 8-10).

With maximum inverter pulse width (t_{1n}=0,t_{3n}=0.5), the operating frequency is significantly above ω_0 across the whole range of resonant tank voltages. Here, the operating frequency is detuned from the designed value (ω_0) by at least 18%.

With t_{1n} controlled near 0.04, the operating frequency is close to ω_0 when V_{pn} is near unity. This region arises when the phase angle is close to zero as noted in section 8-3.4, and is desirable as this minimizes pickup detuning effect. Here, the inverter is well matched to the resonant tank.

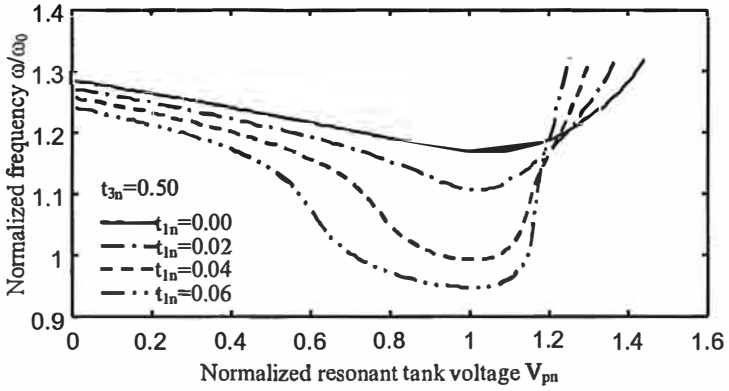


Fig. 8-11. Influences of increasing t_{1n} on the operating frequency assuming maximum t_{3n} of 0.5 at rated load.

8-4.3 POWER ABSORPTION CAPABILITY

At steady state, the power delivered by the inverter is completely absorbed by the resonant tank. The power transferred into the resonant tank can be calculated as:

$$P_t = (\mathrm{Re}\, Y_t)\frac{\hat{V}_p^2}{2} \tag{8-21}$$

It can be expressed in terms of the normalized resonant tank voltage as:

$$P_t = (\mathrm{Re}\, Y_t)\frac{V_d^2 V_{pn}^2}{2} \tag{8-22}$$

The power absorption capability of the resonant tank is thus proportional to the real component of the resonant tank admittance (the resonant tank conductance). The resonant tank conductance at rated load is shown in Fig. 8-12 as a function of the normalized operating frequency. It reaches a maximum at a frequency slightly higher than the secondary resonant frequency. Assuming a constant resonant tank voltage, maximum power can be achieved at this operating point, where the resonant tank runs at a small leading phase angle.

As noted in section 8-4.2, the operating frequency is dependent on selections of t_{1n} and t_{3n}, and the

InductEV, Inc.
Exhibit 1008
Page 251

resonant tank voltage (V_{pn}). Since the resonant tank conductance (Re Y_t) is a function of the frequency, both the resonant tank conductance and power absorption capability are dependent on these parameters. Influences of increasing t_{1n} on the resonant tank conductance and power absorption capability are shown in Fig. 8-13 and 8-14 for rated load (R=6Ω) assuming maximum t_{3n} of 0.5. For selected t_{1n} and t_{3n}, the operating frequency can be calculated as a function of V_{pn} (Fig. 8-11). The resonant tank conductance is then determined using the calculated operating frequency (The dependence between these two parameters is shown in Fig. 8-12). Using the determined resonant tank conductance, the power absorption capability of the resonant tank is then calculated by (8-22). It is divided by the square of the dc voltage to ensure the analysis remains independent of the choice of dc voltage. Once again, a t_{1n} of about 0.04 is most desirable because here the resonant tank power absorption capability is maximized.

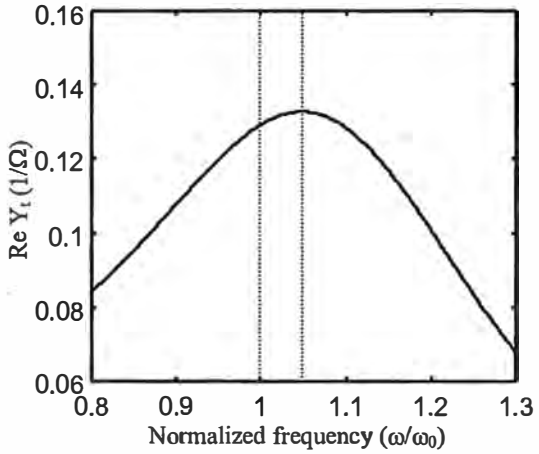


Fig. 8-12. Resonant tank conductance at rated load.

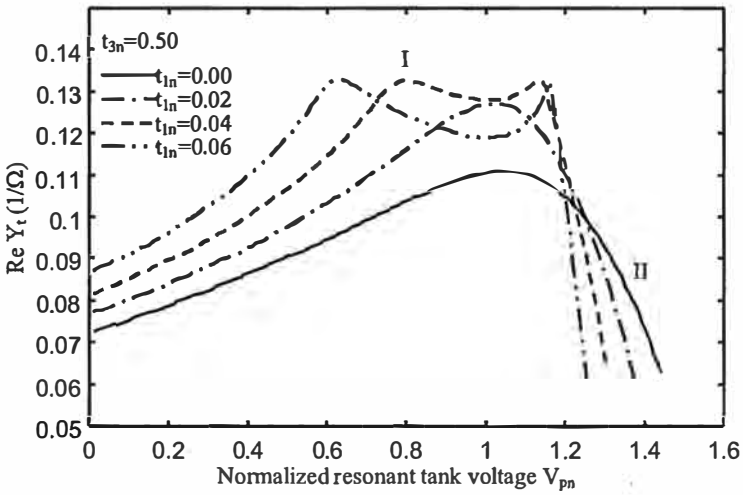


Fig. 8-13. Effects of t_{1n} on the resonant tank conductance at rated load.

InductEV, Inc.
Exhibit 1008
Page 252

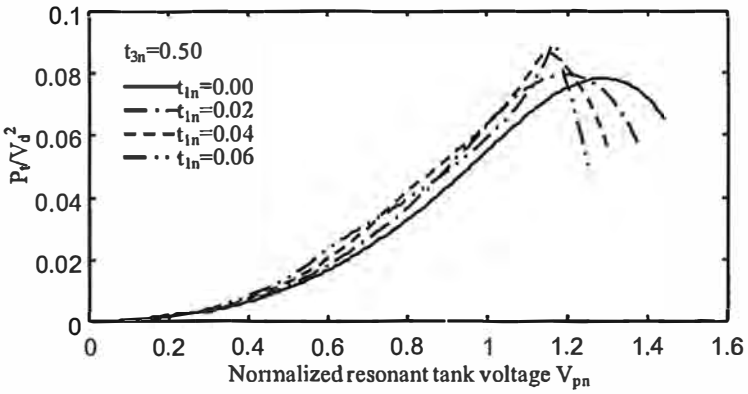


Fig. 8-14. Influences of t_{1n} on resonant tank power absorption capability at rated load.

8-5 STEADY STATE POWER FLOW ANALYSIS

The balance in power flow between the inverter and resonant tank is used in this section to develop an analytical procedure to determine suitable switching instant (t_{1n}) and series inductance (L_m) for maximum power transfer at rated load using the example discussed in section 8-4 for contact-less electric vehicle battery charging. The resulting design is then investigated under light load.

8-5.1 AN ANALYTICAL PROCEDURE FOR STEADY STATE ANALYSIS

The analytical procedure proposed for the determination of the steady state operation is shown in Fig. 8-15. This procedure is iterated in the next section for different values of t_{1n} and L_m in order to determine suitable designs for maximum power transfer.

Under steady state conditions it is assumed that the controller keeps the parameters t_{1n} and t_{3n} fixed. The steady state analysis thus starts by specifying selections of t_{1n} and t_{3n}, with t_{2n} calculated using (8-11). The phase angle then becomes a function of V_{pn} alone (as noted in section 8-3.4). The operating frequency, determined by matching the phase of the inverter current to the phase of the impedance of the resonant tank, is only a function of V_{pn} (as noted in section 8-4.2). Consequently, both the power delivery capability of the inverter (as noted in section 8-3.3) and the power absorption capability of the resonant tank (as noted in section 8-4.3) also become functions of V_{pn} allowing V_{pn} to be determined using the power flow balance between the inverter and the resonant tank. This enables the steady state operation to be identified.

8-5.2 THE SWITCHING INSTANTS AND THE SERIES INDUCTANCE

The power delivery characteristics of the inverter are very different to the power absorption characteristics of the resonant tank, and the inverter needs to be matched to the resonant tank for

InductEV, Inc.
Exhibit 1008
Page 253

efficient power transfer. This can be done by a correct choice of the series inductor L_m and a proper control of the switching instant t_{1n} assuming maximum t_{3n} of 0.5.

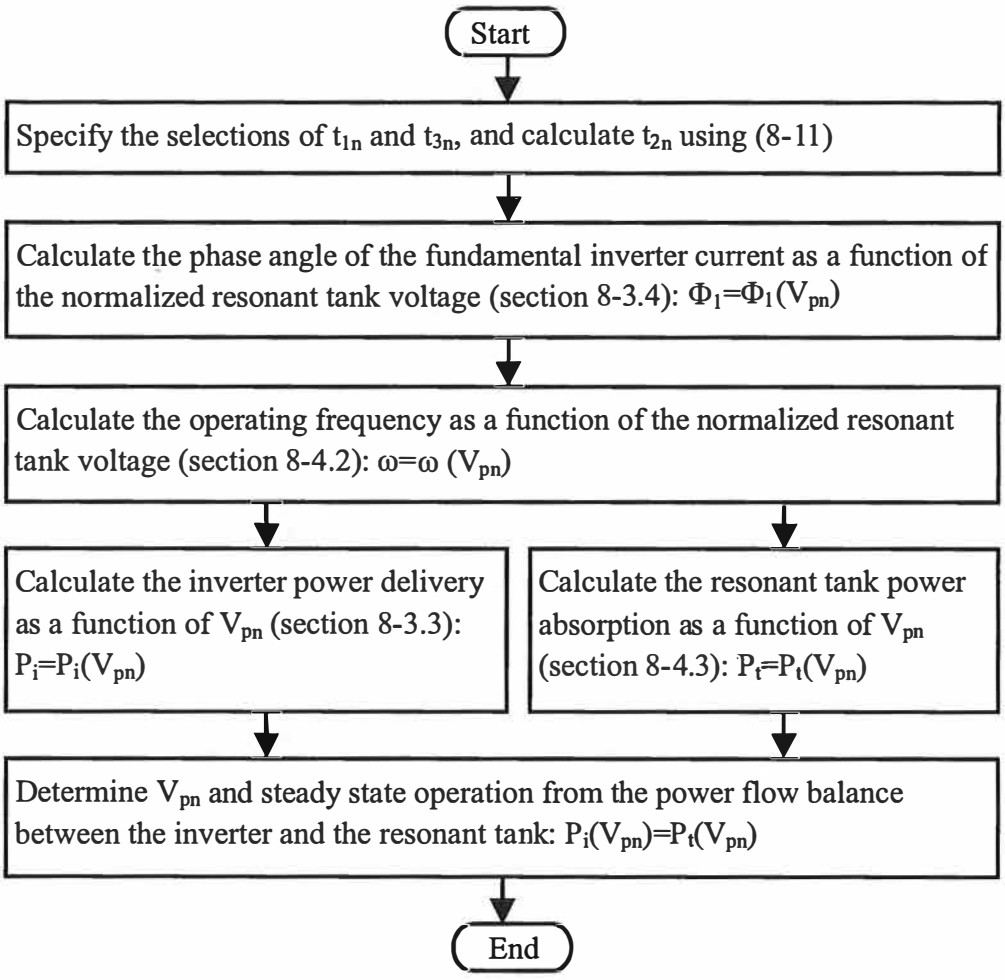


Fig. 8-15. An analytical procedure for the determination of steady state operation.

By plotting the inverter power for different values of L_m against the resonant tank power, a good choice of L_m can be made. This is shown in Fig. 8-16 (a) and (b) with t_{1n} chosen as 0.00 and 0.04 respectively. In this figure, both the inverter and resonant tank power are divided by the square of the dc voltage (V_d) enabling an analysis independent of V_d.

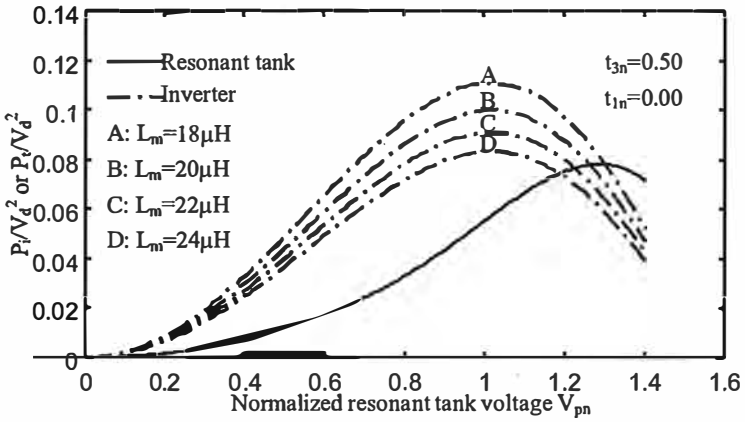
It can be seen that for large resonant tank voltages the inverter limits the power transfer, while for low resonant tank voltages the resonant tank limits the power transfer. A good choice for L_m is where the crossover point is at the maximum power absorption capability of the resonant tank. The effect of the series inductor L_m can be seen clearly, with the inverter power delivery increasing as L_m is made smaller. The price paid for using a smaller series inductor, however, is an increase in the inverter current, which directly increases the required VA rating of the inverter. From an inverter perspective, the largest possible value of L_m is desirable. From Fig. 8-16 it can be seen that both the inverter power delivery and the resonant tank power absorption depend on the choice of t_{1n}. Consequently, the

InductEV, Inc.
Exhibit 1008
Page 254

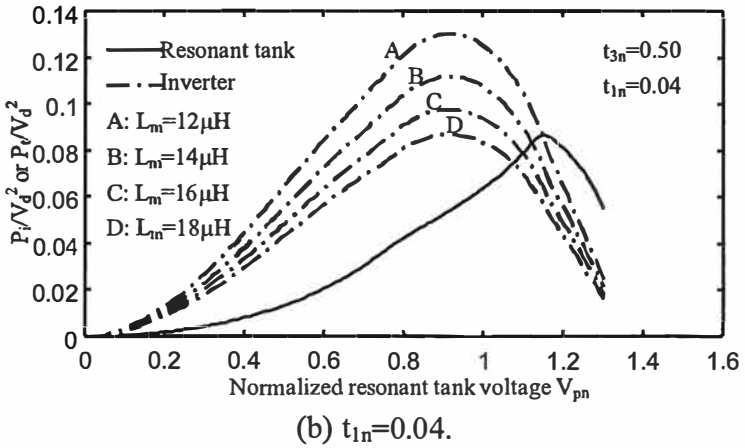
optimum value of L_m is also dependent on t_{1n}. With t_{1n} equal to 0.00, the optimum L_m is about 19μH. The optimum L_m decreases to about 12μH when t_{1n} is increased to 0.04.

Various maximum power points for different values of t_{1n} are compared in Table 8-1 along with the optimum series inductance L_m. In this table the dc bus voltage V_d is set at 130V in order to compare the results experimentally as discussed in section 8-6.

As t_{1n} is increased, the maximum power initially increases and the primary current reduces as the operating frequency moves closer to the secondary resonant frequency. However, the required series inductance L_m also becomes smaller as t_{1n} is increased, causing the peak inverter current i_i to increase. As t_{1n} is increased further to 0.06, very little power gain is achieved, but the inverter current increases by more than 20%. A further increase in t_{1n} results in a reduced power transfer capability but a much larger inverter current. For this application t_{1n} should be controlled close to 0.04 in order to maximize the power and minimize the primary current, while still keeping an acceptable peak inverter current level. At this condition, the optimal series inductance is 12μH.



(a) t_{1n}=0.00.



(b) t_{1n}=0.04.

Fig. 8-16. Inverter and resonant tank power flow balance at rated load.

InductEV, Inc.
Exhibit 1008
Page 255

TABLE 8-1
STEADY STATE OPERATIONS FOR MAXIMUM POWER WITH SELECTIONS OF t_{1n}

V_d	130V				
R	6Ω				
t_{3n}	0.5				
t_{1n}	0.00	0.02	0.04	0.06	0.08
L_m	19μH	16μH	12μH	6.5μH	3.2μH
$\hat{V}_p$	166.4V	154.8V	149.1V	151.3V	150.7V
P	1323W	1342W	1467W	1518W	1507W
I_p	38.5A	36.2A	34.1A	34.8A	33.9A
Peak i_i	18.8A	18.9A	21.1A	25.9A	38.5A
f	24.0kHz	23.0kHz	21.1kHz	20.9kHz	20.5kHz
Φ_1	17.7°	9.1°	3.1°	1.8°	2.1°

8-5.3 BEHAVIOUR AT LIGHT LOAD

The above analysis and design assumed operation at rated load. An identical approach can be used to investigate the behaviour of the system at other loading conditions. In this section, various steady state operations under light load are compared against rated load in Table 8-2 assuming t_{1n} and t_{3n} are controlled at the optimum values determined under rated load. The variation of the primary current at reduced load is notably small, which is a desirable characteristic for ICPT systems.

TABLE 8-2
SYSTEM BEHAVIOUR AT LIGHT LOAD

V_d	130V			
t_{1n}	0.04			
t_{3n}	0.5			
L_m	12μH			
R	6Ω	4Ω	2Ω	0Ω
$\hat{V}_p$	149.1V	158.5V	167.7V	177.1V
P	1467W	1006W	541W	0W
I_p	34.1A	34.9A	34.9A	39.5A
f	21.1kHz	22.5kHz	23.2kHz	21.7kHz

Inverter current waveforms are compared for different loading conditions in Fig. 8-17. As the load reduces, the current that needs to be turned off decreases. At loads of about 3Ω or less, zero turn-off losses can be achieved by turning off the switches while the current is flowing through the freewheeling diodes.

With decreasing load, the secondary harmonic gradually dominates the waveform of the inverter current. In order to reduce conduction losses under light load, the secondary harmonic can be minimized by reducing the duty cycle of the inverter (increasing t_{1n} and reducing t_{3n}).

InductEV, Inc.
Exhibit 1008
Page 256

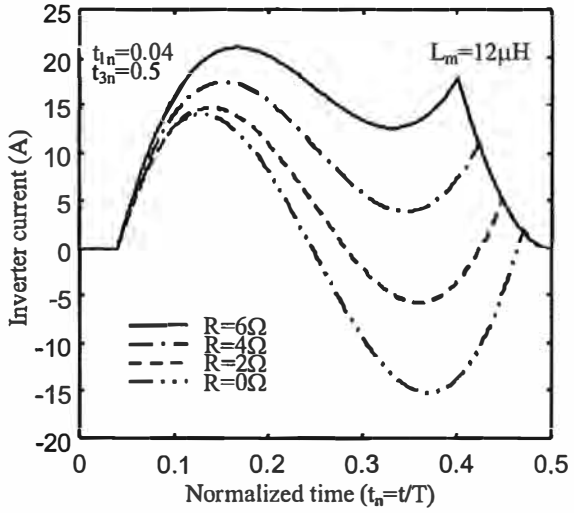


Fig. 8-17. Inverter current waveforms at light loads.

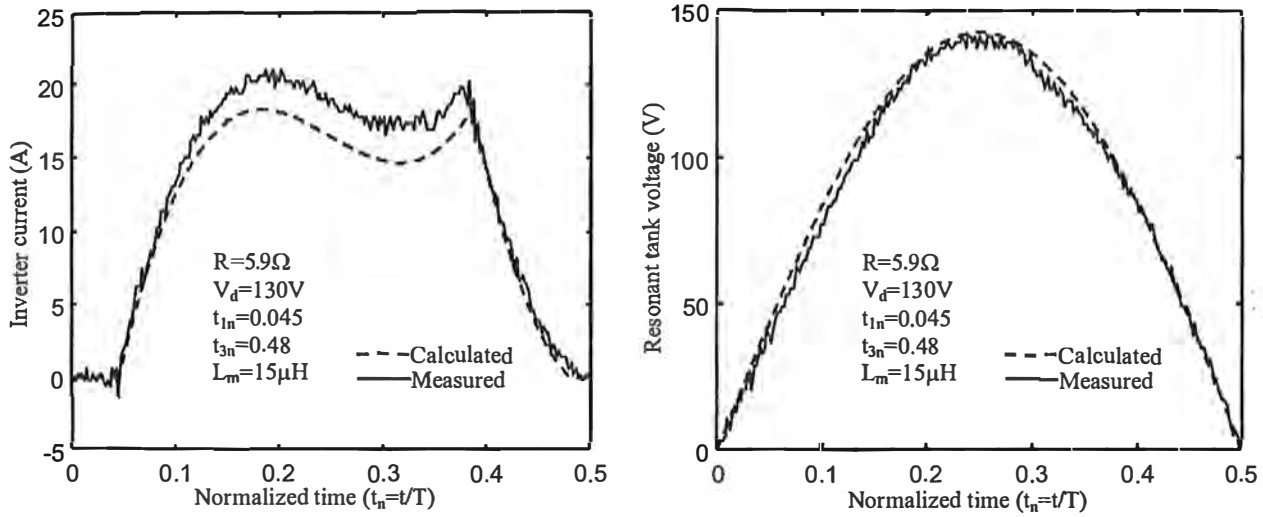
8-6 VERIFICATION

The developed theory was compared with experimental results taken on a system with the dc bus voltage V_d set at 130V. At this voltage the primary current is much lower than the rated current of 150A, and the power levels need to be scaled down correspondingly. SEMIKRON IGBT modules SKM150GB125D driven by SEMIKRON IGBT drivers SKHI22B are used in the test system. This IGBT module has low turn-off losses but high conduction losses, for the chosen example conduction losses are higher than turn-off losses. By choosing an IGBT with a lower on-state voltage, on-state losses can be traded off against switching losses.

The calculated and measured waveforms of the inverter current and the resonant tank voltage at steady state are shown in Fig. 8-18. The inverter is switched so that t_{1n} is equal to 0.04 and t_{3n} slightly less than 0.5. This ensures that the inverter current drops back to zero before the start of the next negative half cycle. The series inductor of 15μH is slightly larger than the optimal theoretical value of 12μH.

As shown, the form of the measured waveforms is well predicted. The magnitude of the measured resonant tank voltage is slightly smaller but close to the theoretical value, while the magnitude of the measured inverter current is a little bit larger. The difference is mainly due to the power losses within the system. The developed theory assumes the power drawn from the source is completely transferred to the load. Practically, the power drawn from the source must be higher than the power transferred to the load, mainly because of the conduction and switching losses of the inverter as well as the copper and core losses of the electromagnetic structure.

InductEV, Inc.
Exhibit 1008
Page 257



(a) Inverter current. (b) Resonant tank voltage.

Fig. 8-18. Calculated and measured steady state operation.

The measured operating frequency, primary current, and input and output powers are given in Table 8-3. These results compare well with the theoretical calculations in Table 8-1 despite the loss-less assumption of the analytical model.

TABLE 8-3
MEASURED FREQUENCY, PRIMARY CURRENT AND POWER

	Measurements	Calculations in Table 8-1
Frequency	20.9kHz	21.1kHz
Primary current	31.5A	34.1A
Input power to DC link	1485W	N/A
Output power	1275W	1467W
Efficiency	85.9%	N/A

8-7 CONCLUSIONS

In this chapter an LCL resonant inverter was investigated for ICPT applications using a variable-frequency controller operating in discontinuous current mode. This control philosophy reduces the required inverter VA rating, but results in a complex design. A feasible design approach is to derive the steady state operation using a power flow balance analysis between the inverter and the resonant tank.

The non-linear characteristics of the inverter were described using a differential equation model, while the resonant tank was modelled using the impedance model developed in Chapter 3. The theory

InductEV, Inc.
Exhibit 1008
Page 258

predicted the inverter operating point and enabled the optimum value of the series inductance and switching instants to be found. The system exhibits highly non-linear characteristics, requiring special care for controller design. The theoretical analysis and design considerations were confirmed using a contact-less electric vehicle battery charger.

REFERENCES

[1]. S. Dieckerhoff, M. J. Ruan, R. W. De Doncker, "Design of an IGBT-based LCL-resonant inverter for high-frequency induction heating," in Proc. *IEEE Industry Applications Society Annual Meeting*, vol. 3, 1999, pp. 2039-2045.

[2]. T. Bieler, M. Perrottet, V. Nguyen, and Y. Perriard, "Contactless power and information transmission," in Proc. *Industry Applications Society Annual Meeting, 2001,* vol. 1, pp. 83-88.

[3]. R. Laouamer, M. Brunello, J. P. Ferrieux, O. Normand, N. Buchheit, "A multi-resonant converter for non-contact charging with electromagnetic coupling," in Proc. *International Conference on Industrial Electronics, Control and Instrumentation*, vol. 2, 1997, pp. 792-797.

[4]. H. Abe, H. Sakamoto, and K. Harada, "A noncontact charger using a resonant converter with parallel capacitor of the secondary coil." *IEEE Transactions on Industry Applications,* vol. 36, pp 444-451, Mar./Apr. 2000.

[5]. Gyu Bum Joun, B. H. Cho, "An energy transmission system for an artificial heart using leakage inductance compensation of transcutaneous transformer," *IEEE Transactions on Power Electronics,* vol. 13, pp. 1013-1022, Nov. 1998.

[6]. J. T. Boys, G. A. Covic, A. W. Green, "Stability and control of inductively coupled power transfer systems," *IEE Proceedings-Electric Power Applications*, vol. 147, pp. 37-43, Jan. 2000.

[7]. J. G. Hayes, M. G. Egan, J. M. D. Murphy, S. E. Schulz, J. T. Hall, "Wide-load-range resonant converter supplying the SAE J-1773 electric vehicle inductive charging interface," *IEEE Transactions on Industry Applications*, vol. 35, pp. 884-895, July-Aug. 1999.

[8]. A. P. Hu, *Selected resonant converters for IPT power supplies*, PhD thesis, The Electrical and Electronics Engineering Department, The University of Auckland, Auckland, New Zealand, 2001, pp. 151-167.

InductEV, Inc.
Exhibit 1008
Page 259

InductEV, Inc.
Exhibit 1008
Page 260

CHAPTER 9

CONCLUSIONS AND FUTURE WORK

9-1 Conclusions
9-2 Future work

9-1 CONCLUSIONS

This thesis investigated the interactions between the primary power supply and the secondary pickups of ICPT systems. The influences of these interactions on the power transfer capability, the DPF, and the operating frequency were quantified for both variable and fixed frequency systems in terms of four fundamental design parameters: the normalized frequency ($u=\omega/\omega_0$), the primary and secondary quality factors (Q_p and Q_s), and the magnetic coupling coefficient (k).

The effect of the secondary loading on the primary was shown to increase with increasing k or Q_s, and is also highly sensitive to u. Notably, k, Q_p and Q_s were shown to be inter-related. Q_p decreases with increases in k or Q_s. When $Q_p>>Q_s$, the loading effects of the secondary on the primary are negligible, and the primary and secondary resonant designs can be considered independently. When Q_p is close to Q_s, the secondary loading significantly affects the primary resonance, and needs to be considered carefully to ensure power transfer capability and system stability.

Several new primary tuning schemes were proposed to improve the DPF of the power supply and the power transfer capability of the pickup by considering the interactions between the primary and secondary. These schemes enable the design of ICPT systems with smaller size, less weight, lower cost, greater power and better efficiency. The theory was verified using a contact-less electric vehicle battery charging system driven from an LCL resonant inverter operating under discontinuous current mode.

9-1.1 VARIABLE-FREQUENCY SYSTEMS

As discussed in Chapter 4 and 5, variable-frequency systems allow the operating frequency to vary so that the power supply operates with unity DPF. The amount of frequency variation depends on the loading effect of the secondary on the primary. Frequency variation is negligible in loosely coupled systems as the secondary loading effects are small. Here, with the primary and secondary resonant

InductEV, Inc.
Exhibit 1008
Page 261

circuits designed independently, the pickup can operate close to the designed frequency ensuring maximum power transfer. In well-coupled systems, where the secondary loading effects are more significant, it was found that this design approach also works well, providing that both the primary and secondary are series-compensated (the SS topology). However, when either the primary or the secondary is parallel compensated (the SP, PP and PS topologies), the operating frequency shifts significantly away from the pickup tuned frequency due to secondary loading effects. As a result, the pickup power transfer capability is substantially reduced.

In Chapter 5, a modified primary tuning scheme was proposed to minimize pickup frequency detuning effects for variable frequency systems in order to improve their power transfer capability. The primary compensation capacitance (C_p) is selected to compensate not only the primary self-inductance but also the reflected impedance (the loading effect) of the pickup. The necessary C_p was shown to depend on the choice of the compensation topology. With a parallel-compensated primary (the PP and PS topologies), the necessary change in C_p depends on Q_s. Consequently, here C_p was chosen for rated power, and while pickup frequency detuning effects under light load are unavoidable, rated power delivery is not affected.

Design criteria were also developed to ensure bifurcation could be avoided. These bifurcation criteria were found to be topology dependent, and can either be expressed in terms of Q_p and Q_s, or k and Q_s. With a high Q_s, the bifurcation criteria of all four topologies can be simply stated as $Q_p > Q_s$. When considered in terms of k, the maximum allowable Q_s before bifurcation decreases as k increases. For loosely coupled systems with a k of 0.1, the maximum allowable Q_s is about 10 in all four topologies. For well-coupled systems with a k of 0.6, the maximum allowable Q_s varies slightly between the topologies but is typically less than 2.

In Chapter 7, the sensitivity of the power transfer capability and the operating frequency to variations in the resonant parameters (C_p, C_s, L_p, L_s and M) were compared for both loosely coupled and well-coupled systems designed using both the original and modified tuning schemes. It was found that the original and modified tunings have similar sensitivities.

In Chapter 8, an LCL resonant inverter under discontinuous current mode was investigated. The modified tuning scheme proposed in chapter 5 was used in the system design. The selected control philosophy was shown to reduce the required VA rating of the power supply as well as turn-on losses, but required a complex design procedure. A feasible design methodology was prescribed by deriving the steady state operation of the inverter and ICPT system using a power flow balance analysis between the inverter and the resonant tank. An impedance model was used to analyse the resonant tank, while the inverter was modelled using differential equations. This approach was verified using a contact-less electric vehicle battery charging systems.

InductEV, Inc.
Exhibit 1008
Page 262

9-1.2 FIXED-FREQUENCY SYSTEMS

If a fixed-frequency controller is used in the primary, power transfer capability of the pickup can be assured providing the primary current is controlled constant. However, the DPF of the power supply is affected by the loading effects of the secondary on the primary.

In Chapter 6, a modified tuning scheme is proposed for fixed-frequency systems that aim to achieve load independent unity DPF. With series-compensated primary systems (the SS and SP topologies), load independent unity DPF is achieved when operating at ω_0. This in turn ensures maximum power transfer capability at the pickup.

In parallel-tuned primary systems (the PP and PS topologies), unity DPF is achievable only at rated load when operating at ω_0. At light load, the DPF can be very low. Load independent unity DPF is desirable, but can only be achieved if the operating frequency is deliberately raised above ω_0. This affects the power transfer capability and the required secondary VA rating of the pickup. It was found that rated power can be achieved with this modified tuning scheme for the majority of ICPT systems, which are either loosely coupled systems with reasonable Q_s or well-coupled systems with low Q_s. Furthermore, when delivering rated power, the required secondary VA rating for the PP topology increases slightly, but for the PS topology will be smaller. This arises from the fact that a series tuned pickup transfers maximum power at a frequency above ω_0, while a parallel tuned pickup transfers maximum power at ω_0.

In Chapter 7, the sensitivity of the DPF and the power transfer capability to variations in the resonant parameters (C_p, C_s, L_p, L_s and M) were compared for both loosely coupled and well coupled systems designed using either the original tuning scheme or the modified tuning scheme detailed in Chapter 6. Overall, the original and modified tunings have comparable sensitivities. The one exception arises in the tuning scheme for load independent unity DPF. Here, the DPF at light load is less sensitive to variations in all parameters considered, but the power transfer capability is more sensitive to variations in C_s. As shown here, C_s must be chosen to have good thermal and lifetime stability.

9-2 FUTURE WORK

The work of this thesis focused on single pickup applications and assumed the load to be linear and resistive. The thesis work may be extended to analyse and design multiple pickup systems, and also to investigate non-linear phenomena.

InductEV, Inc.
Exhibit 1008
Page 263

Multiple pickup applications: In many practical ICPT systems a common power supply transfers power to more than one secondary pickup. Optimal design of such systems needs to consider the loading effects of all pickups together.

Assuming all pickups have identical design and load, the secondary load impedance (Z_s) developed in section 3-4 is the same for each pickup, and the total reflected impedance from all pickups can be derived using (3-17) as:

$$Z_r = \sum_{i=1}^{n} Z_{ri} = n\frac{\omega^2 M^2}{Z_s} \tag{9-1}$$

where n is the number of pickups.

This is equivalent to the reflected impedance of a single identical pickup with an equivalent mutual inductance of:

$$M_n = \sqrt{n}M \tag{9-2}$$

The equivalent coupling coefficient is then:

$$k_n = \sqrt{n}k \tag{9-3}$$

With the above definition of 'equivalent mutual inductance' and 'equivalent coupling coefficient', the analyses and design considerations presented in this thesis for single pickup applications are also applicable for multiple pickup systems.

In practice, the design of each pickup can be different, and the loading condition on each pickup is almost always different. In this case, the equivalent magnetic coupling model could be extended to include a stochastic model to represent the secondary loads on the primary.

Non-linear phenomena: An ICPT system essentially consists of multiple power converters (the primary power supply and various pickup regulators) with mutual interactions via electromagnetic coupling. These power converters employ both semiconductor switches and reactive components. The switches control the power flow around the circuit, while the reactive components store energy. The circuits are non-linear, time varying dynamic systems. Practical switches and reactive components also have unwanted non-linear characteristics. The control circuits often have non-linear components. ICPT systems are therefore difficult to analyse, and full of unusual phenomena.

Fundamental circuit analysis of a power converter typically results in a non-linear time-varying model in terms of state-space variables. They are generally awkward to work with, and a simplified model is often required. A conventional approach is to take an average over a switching cycle such as that applied using state-space averaging. The aim is to replace the non-linear time-varying dynamic model by a linear time-invariant one. This is easy to understand and straightforward to implement. However, all information within a cycle is lost.

InductEV, Inc.
Exhibit 1008
Page 264

Considerable effort has gone into extending the basic state-space averaging process. One such extension is generalized state-space averaging. Here, the state-space variables are described within a sliding window moving with time. The order of the model can be arbitrarily determined according to system characteristics and the required accuracy. This approach has been used to model selected ICPT power converters successfully [1][2].

An alternative approach is to use discrete non-linear modelling such as a sampled-data model [3]. Here, the state-space variables are observed discretely at specific instants of time. With this model, the non-linear phenomena can be observed using conventional non-linear dynamic theory developed by mathematicians and physicists.

Advancement in the research of the non-linear phenomenon is useful in identifying the transient behaviour of ICPT systems, and could enable a variable-frequency system to operate in the bifurcation region, and as such significantly increase the power transfer capability.

REFERENCES

[1]. A. W. Green, "Modelling a push-pull parallel resonant convertor using generalised state-space averaging," *IEE Proc. Electric Power Applications*, vol. 140, pp. 350-356, Nov. 1993.

[2]. A. P. Hu, *Selected resonant converters for IPT power supplies*, PhD thesis, The Electrical and Electronics Engineering Department, The University of Auckland, Auckland, New Zealand, 2001, pp. 151-167.

[3]. S. Banerjee, G. C. Verghese, *Nonlinear phenomenon in power electronics – bifurcation, chaos, control and applications*, IEEE Press, NJ, 2001.

InductEV, Inc.
Exhibit 1008
Page 265

InductEV, Inc.
Exhibit 1008
Page 266

APPENDICES

A. Primary voltage and current gains
B. Reactive and real powers of the pickup coil
C. Quantified secondary current
D. Normalized reflected impedance of compensated pickup
E. Quantified impedance of the primary coil
F. Normalized reactance of the primary capacitance for systems with compensated pickup
G. Normalized impedance functions for systems with uncompensated pickup
H. Primary tuning for unity DPF at ω_0
I. Primary tuning for load independent unity DPF
J. Maximum allowable alternating voltage and current in capacitors

A. PRIMARY VOLTAGE AND CURRENT GAINS

In this section, the primary voltage and current gains are quantified in terms of the primary and secondary quality factors for series and parallel-compensated primary systems.

Series-compensated primary: When the primary is series compensated, the primary current (I_p) flows through the primary capacitor (C_p) and the primary winding (L_p).

The voltage across the primary winding is:

$$V_p = Z_p I_p = (j\omega L_p + Z_r) I_p = \left(j\omega L_p + \frac{\omega^2 M^2}{Z_s} \right) I_p \qquad \text{(A-1)}$$

where Z_s is given by (3-7) for series and parallel compensated secondary systems.

Substituting (2-1) into (A-1) results in:

$$V_p = j\omega L_p I_p \left(1 - \frac{jk^2 \omega L_s}{Z_s} \right) \qquad \text{(A-2)}$$

At ω_0, L_s is in resonance with C_s (i.e. $\omega_0 L_s = 1/(\omega_0 C_s)$) so that:

$$\frac{\omega_0 L_s}{Z_s} = \begin{cases} \dfrac{\omega_0 L_s}{j\omega_0 L_s + \dfrac{1}{j\omega_0 C_s} + R} = Q_{s0} & \text{series secondary} \\ \dfrac{\omega_0 L_s}{j\omega_0 L_s + \dfrac{1}{j\omega_0 C_s + \dfrac{1}{R}}} = -j + Q_{s0} & \text{parallel secondary} \end{cases} \qquad \text{(A-3)}$$

InductEV, Inc.
Exhibit 1008
Page 267

where Q_{s0} is the secondary quality factor at ω_0 as given by (2-23).

Substituting (A-3) into (A-2), the result is:

$$V_{p0} = \begin{cases} j\omega_0 L_p I_p \left(1 - jk^2 Q_{s0}\right) & \text{series secondary} \\ j\omega_0 L_p I_p \left(1 - k^2 - jk^2 Q_{s0}\right) & \text{parallel secondary} \end{cases} \tag{A-4}$$

Substituting the primary quality factor (Q_{p0}) at ω_0 as given in (2-29) into (A-4) results in:

$$V_{p0} = \begin{cases} j\omega_0 L_p I_p \left(\dfrac{Q_{p0} - j}{Q_{p0}}\right) & \text{series secondary} \\ j\omega_0 L_p I_p \left(\dfrac{Q_{p0}Q_{s0} - jQ_{s0}}{1 + Q_{p0}Q_{s0}}\right) & \text{parallel secondary} \end{cases} \tag{A-5}$$

The inverter output voltage can be calculated as:

$$V_i = \left(\frac{1}{j\omega C_p}\right) I_p + V_p \tag{A-6}$$

At ω_0, L_p is in resonance with C_p so that:

$$V_{i0} = \left(\frac{1}{j\omega_0 C_p}\right) I_p + V_{p0} = -j\omega_0 L_p I_p + V_{p0} \tag{A-7}$$

Substituting (A-5) into (A-7) results in:

$$V_{i0} = \begin{cases} j\omega_0 L_p I_p \left(\dfrac{-j}{Q_{p0}}\right) & \text{series secondary} \\ j\omega_0 L_p I_p \left(\dfrac{-1 - jQ_{s0}}{1 + Q_{p0}Q_{s0}}\right) & \text{parallel secondary} \end{cases} \tag{A-8}$$

The voltage gain (ratio of the voltage across the primary coil to the inverter output voltage) at ω_0 derived from (A-5) and (A-8) is:

$$V_{GAIN} = \begin{cases} \sqrt{1 + Q_{p0}^2} & \text{series secondary} \\ \sqrt{\dfrac{Q_{s0}^2\left(1 + Q_{p0}^2\right)}{1 + Q_{s0}^2}} & \text{parallel secondary} \end{cases} \tag{A-9}$$

Parallel-compensated primary: When the primary is parallel compensated, the inverter output voltage (V_i) is identical to the primary voltage (V_p).

The inverter output current can be calculated as:

$$I_i = j\omega C_p V_p + I_p \tag{A-10}$$

At ω_0, L_p is in resonance with C_p so that:

InductEV, Inc.
Exhibit 1008
Page 268

$$I_{i0} = j\omega_0 C_p V_{p0} + I_p = \frac{jV_{p0}}{\omega_0 L_p} + I_p \tag{A-11}$$

Substituting (A-5) into (A-11) results in:

$$I_{i0} = \begin{cases} I_p\left(\dfrac{j}{Q_{p0}}\right) & \text{series secondary} \\ I_p\left(\dfrac{1+jQ_{s0}}{1+Q_{p0}Q_{s0}}\right) & \text{parallel secondary} \end{cases} \tag{A-12}$$

The current gain (ratio of the current flowing through the primary coil to the inverter output current) at ω_0 derived from (A-12) is:

$$I_{GAIN} = \begin{cases} Q_{p0} & \text{series secondary} \\ \sqrt{\dfrac{(1+Q_{p0}Q_{s0})^2}{1+Q_{s0}^2}} & \text{parallel secondary} \end{cases} \tag{A-13}$$

B. REACTIVE AND REAL POWERS OF THE PICKUP COIL

The reactive and real powers associated with the pickup coil are calculated in this section for series and parallel-compensated secondary systems.

The apparent power (complex power) of the pickup coil can be calculated using the secondary voltage and current as:

$$S_s = I_s V_s \tag{B-1}$$

Series-compensated secondary: In a series-compensated pickup, the secondary voltage can be determined as:

$$V_s = I_s\left(\frac{1}{j\omega C_s} + R\right) \tag{B-2}$$

Substituting (B-2) into (B-1), the result is:

$$S_s = I_s^2\left(\frac{1}{j\omega C_s} + R\right) = I_s^2 R + \frac{I_s^2}{j\omega C_s} \tag{B-3}$$

As shown, the reactive power of the pickup coil equals the reactive power of the secondary compensation capacitor (C_s), while the real power transferred by the pickup coil equals the power going to the load (R).

Parallel-compensated secondary: In a parallel-compensated pickup, the secondary current can be

InductEV, Inc.
Exhibit 1008
Page 269

determined as:

$$I_s = V_s\left(j\omega C_s + \frac{1}{R}\right) \tag{B-4}$$

Substituting (B-4) into (B-1), the result is:

$$S_s = V_s^2\left(j\omega C_s + \frac{1}{R}\right) = \frac{V_s^2}{R} + V_s^2\left(j\omega C_s\right) \tag{B-5}$$

The reactive power of the pickup coil again equals the reactive power of the secondary compensation capacitor, while the real power transferred by the pickup coil equals the power going to the load.

C. QUANTIFIED SECONDARY CURRENT

The secondary current is quantified in this section in terms of the short circuit current (I_{sc}), the normalized frequency ($u=\omega/\omega_0$), and the secondary quality factor (Q_{s0}) at ω_0.

Substituting (3-7) into (3-31) results in:

$$\frac{I_s}{I_{sc}} = \frac{j\omega L_s}{Z_s} = \begin{cases} \dfrac{j\omega L_s}{j\omega L_s + \dfrac{1}{j\omega C_s} + R} & \text{series secondary} \\ \dfrac{j\omega L_s}{j\omega L_s + \dfrac{1}{j\omega C_s + \dfrac{1}{R}}} & \text{parallel secondary} \end{cases} \tag{C-1}$$

Substituting the normalized frequency defined by (3-29) into (C-1) results in:

$$\frac{I_s}{I_{sc}} = \begin{cases} \dfrac{ju\omega_0 L_s}{ju\omega_0 L_s + \dfrac{1}{ju\omega_0 C_s} + R} & \text{series secondary} \\ \dfrac{ju\omega_0 L_s}{ju\omega_0 L_s + \dfrac{1}{ju\omega_0 C_s + \dfrac{1}{R}}} & \text{parallel secondary} \end{cases} \tag{C-2}$$

Substituting (2-23) into (C-2) results in:

$$\frac{I_s}{I_{sc}} = \begin{cases} \dfrac{Q_{s0}^2 u^2\left(u^2-1\right) + jQ_{s0}u^3}{u^2 + Q_{s0}^2\left(u^2-1\right)^2} & \text{series secondary} \\ \dfrac{Q_{s0}^2 u^2\left(u^2-1\right) + u^2 + jQ_{s0}u}{u^2 + Q_{s0}^2\left(u^2-1\right)^2} & \text{parallel secondary} \end{cases} \tag{C-3}$$

The ratio of the secondary current to the short circuit current derived from (C-3) is:

InductEV, Inc.
Exhibit 1008
Page 270

$$\left|\frac{I_s}{I_{sc}}\right| = \begin{cases} \dfrac{\sqrt{Q_{s0}^4 u^4 \left(u^2-1\right)^2 + Q_{s0}^2 u^6}}{u^2 + Q_{s0}^2\left(u^2-1\right)^2} & \text{series secondary} \\ \dfrac{\sqrt{\left[Q_{s0}^2 u^2\left(u^2-1\right)+u^2\right]^2 + Q_{s0}^2 u^2}}{u^2 + Q_{s0}^2\left(u^2-1\right)^2} & \text{parallel secondary} \end{cases} \tag{C-4}$$

D. NORMALIZED REFLECTED IMPEDANCE OF COMPENSATED PICKUP

Dividing (3-18)&(3-19) by (3-26) results in:

$$\mathrm{Re}Z_{rn} = \frac{\mathrm{Re}Z_r}{\mathrm{Re}Z_{r0}} = \begin{cases} \dfrac{\omega^4 C_s^2 R^2}{\omega_0^2\left(\omega^2 C_s L_s - 1\right)^2 + \omega^2\omega_0^2 C_s^2 R^2} & \text{series secondary} \\ \dfrac{\omega^2 L_s^2}{R^2\left(\omega^2 C_s L_s - 1\right)^2 + \omega^2 L_s^2} & \text{parallel secondary} \end{cases} \tag{D-1}$$

and

$$\mathrm{Im}Z_{rn} = \frac{\mathrm{Im}Z_r}{\mathrm{Re}Z_{r0}} = \begin{cases} \dfrac{-\omega^3 C_s\left(\omega^2 C_s L_s - 1\right)R}{\omega_0^2\left(\omega^2 C_s L_s - 1\right)^2 + \omega^2\omega_0^2 C_s^2 R^2} & \text{series secondary} \\ \dfrac{-\omega^3\left[C_s R^2\left(\omega^2 C_s L_s - 1\right) + L_s\right]L_s^2}{R^3\left(\omega^2 C_s L_s - 1\right)^2 + \omega^2 L_s^2 R} & \text{parallel secondary} \end{cases} \tag{D-2}$$

Substituting (3-29) into (D-1)&(D-2) results in:

$$\mathrm{Re}Z_{rn} = \frac{\mathrm{Re}Z_r}{\mathrm{Re}Z_{r0}} = \begin{cases} \dfrac{u^4}{\left(\dfrac{u^2\omega_0 L_s}{R} - \dfrac{1}{\omega_0 C_s R}\right)^2 + u^2} & \text{series secondary} \\ \dfrac{u^2}{\left(u^2\omega_0 C_s R - \dfrac{R}{\omega_0 L_s}\right)^2 + u^2} & \text{parallel secondary} \end{cases} \tag{D-3}$$

and

$$\mathrm{Im}Z_{rn} = \frac{\mathrm{Im}Z_r}{\mathrm{Re}Z_{r0}} = \begin{cases} \dfrac{-u^3\left(\dfrac{u^2\omega_0 L_s}{R} - \dfrac{1}{\omega_0 C_s R}\right)}{\left(\dfrac{u^2\omega_0 L_s}{R} - \dfrac{1}{\omega_0 C_s R}\right)^2 + u^2} & \text{series secondary} \\ \dfrac{-u^3\left[u^2\left(\omega_0 C_s R\right)^2\left(\dfrac{\omega_0 L_s}{R}\right) - \omega_0 C_s R + \dfrac{\omega_0 L_s}{R}\right]}{\left(u^2\omega_0 C_s R - \dfrac{R}{\omega_0 L_s}\right)^2 + u^2} & \text{parallel secondary} \end{cases} \tag{D-4}$$

The normalized reflected resistance and reactance given in (D-3) and (D-4) can be represented as

InductEV, Inc.
Exhibit 1008
Page 271

functions of Q_{s0} and u by:

$$\mathrm{Re}Z_{rn} = \frac{\mathrm{Re}Z_r}{\mathrm{Re}Z_{r0}} = \begin{cases} \dfrac{u^4}{\left(u^2-1\right)^2 Q_{s0}^2 + u^2} & \text{series secondary} \\ \dfrac{u^2}{\left(u^2-1\right)^2 Q_{s0}^2 + u^2} & \text{parallel secondary} \end{cases} \tag{D-5}$$

and

$$\mathrm{Im}Z_{rn} = \frac{\mathrm{Im}Z_r}{\mathrm{Re}Z_{r0}} = \begin{cases} \dfrac{-u^3\left(u^2-1\right)Q_{s0}}{\left(u^2-1\right)^2 Q_{s0}^2 + u^2} & \text{series secondary} \\ \dfrac{-u^3\left[\left(u^2-1\right)Q_{s0} + \dfrac{1}{Q_{s0}}\right]}{\left(u^2-1\right)^2 Q_{s0}^2 + u^2} & \text{parallel secondary} \end{cases} \tag{D-6}$$

E. QUANTIFIED IMPEDANCE OF THE PRIMARY COIL

Substituting (C-3) into (3-41) results in:

$$\frac{Z_p}{j\omega_0 L_p} = \begin{cases} \dfrac{u\left\{u^2 + Q_s^2\left(u^2-1\right)\left[u^2\left(1-k^2\right)-1\right]\right\} - jk^2 Q_s u^4}{u^2 + Q_s^2\left(u^2-1\right)^2} & \text{series secondary} \\ \dfrac{u\left\{u^2\left(1-k^2\right) + Q_s^2\left(u^2-1\right)\left[u^2\left(1-k^2\right)-1\right]\right\} - jk^2 Q_s u^2}{u^2 + Q_s^2\left(u^2-1\right)^2} & \text{parallel secondary} \end{cases} \tag{E-1}$$

The impedance of the primary coil thus can be quantified in terms of the primary self-inductance ($\omega_0 L_p$) at ω_0 as well as u and Q_{s0} as:

$$\left|\frac{Z_p}{j\omega_0 L_p}\right| = \begin{cases} \dfrac{\sqrt{k^4 Q_s^2 u^8 + u^2\left\{u^2 + Q_s^2\left(u^2-1\right)\left[u^2\left(1-k^2\right)-1\right]\right\}^2}}{u^2 + Q_s^2\left(u^2-1\right)^2} & \text{series secondary} \\ \dfrac{\sqrt{k^4 Q_s^2 u^4 + u^2\left\{u^2\left(1-k^2\right) + Q_s^2\left(u^2-1\right)\left[u^2\left(1-k^2\right)-1\right]\right\}^2}}{u^2 + Q_s^2\left(u^2-1\right)^2} & \text{parallel secondary} \end{cases} \tag{E-2}$$

F. NORMALIZED REACTANCE OF THE PRIMARY CAPACITANCE FOR SYSTEMS WITH COMPENSATED PICKUP

The normalized reactance of the primary compensation capacitance (C_p) can be calculated using (3-26) as:

$$\frac{1}{\omega C_p\left(\mathrm{Re}Z_{r0}\right)} = \begin{cases} \dfrac{R}{\omega C_p \omega_0^2 M^2} & \text{series secondary} \\ \dfrac{L_s^2}{\omega C_p M^2 R} & \text{parallel secondary} \end{cases} \tag{F-1}$$

InductEV, Inc.
Exhibit 1008
Page 272

Substituting (3-29) into (F-1) results in:

$$\frac{1}{\omega C_p(\mathrm{Re}\,Z_{r0})}=\begin{cases}\dfrac{R}{uC_p\omega_0^3M^2} & \text{series secondary}\\[2ex] \dfrac{L_s^2}{u\omega_0C_pM^2R} & \text{parallel secondary}\end{cases} \tag{F-2}$$

Substituting (2-1) into (F-2) results in:

$$\frac{1}{\omega C_p(\mathrm{Re}\,Z_{r0})}=\begin{cases}\dfrac{R}{uk^2C_p\omega_0^3L_pL_s} & \text{series secondary}\\[2ex] \dfrac{L_s}{u\omega_0k^2C_pL_pR} & \text{parallel secondary}\end{cases} \tag{F-3}$$

Substituting (2-28) into (F-3) results in:

$$\frac{1}{\omega C_p(\mathrm{Re}\,Z_{r0})}=\begin{cases}\dfrac{R}{uk^2\omega_0L_s} & \text{series secondary}\\[2ex] \dfrac{\omega_0L_s}{uk^2R} & \text{parallel secondary}\end{cases} \tag{F-4}$$

In terms of Q_{s0}, (F-4) can represented as:

$$\frac{1}{\omega C_p(\mathrm{Re}\,Z_{r0})}=\frac{1}{uk^2Q_{s0}} \tag{F-5}$$

As shown, the normalized reactance of the primary capacitance is a function of u, Q_{s0}, and k.

Substituting (2-29) into (F-5), the normalized reactance of the primary compensation capacitance becomes a function of u, Q_{p0} and Q_{s0} given by:

$$\frac{1}{\omega C_p(\mathrm{Re}\,Z_{r0})}=\begin{cases}\dfrac{Q_{p0}}{u} & \text{series secondary}\\[2ex] \left(\dfrac{1}{u}\right)\left(Q_{p0}+\dfrac{1}{Q_{s0}}\right) & \text{parallel secondary}\end{cases} \tag{F-6}$$

G. NORMALIZED IMPEDANCE FUNCTIONS FOR SYSTEMS WITH UNCOMPENSATED PICKUP

At the condition that ω_0L_s and R are equal, the secondary impedance Z_s can be expressed as:

$$Z_s=j\omega L_s+R=j\omega L_s+\omega_0L_s=L_s(\omega_0+j\omega) \tag{G-1}$$

Substituting (G-1) into (3-17), the reflected resistance and reactance can be derived as:

$$\mathrm{Re}\,Z_r=\frac{\omega_0\omega^2M^2}{(\omega_0^2+\omega^2)L_s} \tag{G-2}$$

and

InductEV, Inc.
Exhibit 1008
Page 273

$$\mathrm{Im}Z_r = \frac{-\omega^3 M^2}{\left(\omega_0^2 + \omega^2\right)L_s} \tag{G-3}$$

The reflected resistance and reactance at ω_0 are then:

$$\mathrm{Re}Z_{r0} = \frac{\omega_0 M^2}{2L_s} \tag{G-4}$$

and

$$\mathrm{Im}Z_{r0} = \frac{-\omega_0 M^2}{2L_s} \tag{G-5}$$

The normalized reflected resistance and reactance defined in (3-33) are then:

$$\mathrm{Re}Z_{rn} = \frac{\mathrm{Re}Z_r}{\mathrm{Re}Z_{r0}} = \frac{2u^2}{1+u^2} \tag{G-6}$$

and

$$\mathrm{Im}Z_{rn} = \frac{\mathrm{Im}Z_r}{\mathrm{Re}Z_{r0}} = \frac{-2u^3}{1+u^2} \tag{G-7}$$

The normalized reactance of the self-inductance (L_p) of the primary coil can be calculated as:

$$\frac{\omega L_p}{\mathrm{Re}Z_{r0}} = \frac{2\omega L_p L_s}{\omega_0 M^2} \tag{G-8}$$

Substituting (2-1)&(3-29) into (G-8), the result is:

$$\frac{\omega L_p}{\mathrm{Re}Z_{r0}} = \frac{2u}{k^2} \tag{G-9}$$

The normalized reactance of the primary compensation capacitance (C_p) can be calculated as:

$$\frac{1}{\omega C_p\left(\mathrm{Re}Z_{r0}\right)} = \frac{2L_s}{\omega\omega_0 C_p M^2} \tag{G-10}$$

Substituting (2-28) into (G-10) results in:

$$\frac{1}{\omega C_p\left(\mathrm{Re}Z_{r0}\right)} = \frac{2\omega_0 L_p L_s}{\omega M^2} \tag{G-11}$$

Substituting (2-1)&(3-29) into (G-11), the result is:

$$\frac{1}{\omega C_p\left(\mathrm{Re}Z_{r0}\right)} = \frac{2}{uk^2} \tag{G-12}$$

H. PRIMARY TUNING FOR UNITY DPF AT ω_0

In this section, the required C_p is calculated for each topology to achieve unity DPF when operating

InductEV, Inc.
Exhibit 1008
Page 274

at ω_0.

SS topology: Substituting (3-52) into (5-1) results in:

$$\omega_0 L_p - \frac{1}{\omega_0 C_p} + \mathrm{Im}\, Z_{r0} = 0 \tag{H-1}$$

Substituting (3-27) into (H-1) results in:

$$\omega_0 L_p - \frac{1}{\omega_0 C_p} = 0 \tag{H-2}$$

The required C_p determined from (H-2) is:

$$C_p = \frac{1}{\omega_0^2 L_p} \tag{H-3}$$

Substituting (2-22) into (H-3) results in:

$$C_p = \frac{C_s L_s}{L_p} \tag{H-4}$$

SP topology: Equation (H-1) is also valid for the SP topology. Substituting (3-27) into (H-1) results in:

$$\omega_0 L_p - \frac{1}{\omega_0 C_p} - \frac{\omega_0 M^2}{L_s} = 0 \tag{H-5}$$

The required C_p determined from (H-5) is:

$$C_p = \frac{1}{\omega_0^2 \left(L_p - \dfrac{M^2}{L_s} \right)} \tag{H-6}$$

Substituting (2-22) into (H-6) results in:

$$C_p = \frac{C_s L_s}{L_p - \dfrac{M^2}{L_s}} \tag{H-7}$$

Substituting (2-1) into (H-7) results in:

$$C_p = \left(\frac{C_s L_s}{L_p} \right) \left(\frac{1}{1 - k^2} \right) \tag{H-8}$$

PP topology: Substituting (3-52) into (5-1) results in:

$$\omega_0 C_p - \frac{\omega_0 L_p + \mathrm{Im}\, Z_{r0}}{\left(\mathrm{Re}\, Z_{r0}\right)^2 + \left(\omega_0 L_p + \mathrm{Im}\, Z_{r0}\right)^2} = 0 \tag{H-9}$$

InductEV, Inc.
Exhibit 1008
Page 275

Substituting (3-26)&(3-27) into (H-9) results in:

$$\omega_0 C_p - \frac{\omega_0 L_p - \frac{\omega_0 M^2}{L_s}}{\left(\frac{M^2 R}{L_s^2}\right)^2 + \left(\omega_0 L_p - \frac{\omega_0 M^2}{L_s}\right)^2} = 0 \tag{H-10}$$

The required C_p determined from (H-10) is:

$$C_p = \frac{L_p - \frac{M^2}{L_s}}{\left(\frac{M^2 R}{L_s^2}\right)^2 + \omega_0^2 \left(L_p - \frac{M^2}{L_s}\right)^2} \tag{H-11}$$

Substituting (2-22) into (H-11) results in:

$$C_p = \frac{L_p - \frac{M^2}{L_s}}{\left(\frac{M^2 R}{L_s^2}\right)^2 + \left(\frac{1}{C_s L_s}\right)\left(L_p - \frac{M^2}{L_s}\right)^2} \tag{H-12}$$

Substituting (2-1)&(2-23) into (H-12) results in:

$$C_p = \left(\frac{C_s L_s}{L_p}\right)\left(\frac{1-k^2}{Q_{s0}^2 k^4 + \left(1-k^2\right)^2}\right) \tag{H-13}$$

PS topology: Equation (H-9) is also valid for the PS topology. Substituting (3-26)&(3-27) into (H-9) results in:

$$\omega_0 C_p - \frac{\omega_0 L_p}{\left(\frac{\omega_0^2 M^2}{R}\right)^2 + \left(\omega_0 L_p\right)^2} = 0 \tag{H-14}$$

The required C_p determined from (H-14) is:

$$C_p = \frac{L_p}{\left(\frac{\omega_0^2 M^2}{R}\right)^2 + \omega_0^2 L_p^2} \tag{H-15}$$

Substituting (2-22) into (H-15) results in:

$$C_p = \frac{L_p}{\left(\frac{M^2}{C_s L_s R}\right)^2 + \frac{L_p^2}{C_s L_s}} \tag{H-16}$$

Substituting (2-1)&(2-23) into (H-16) results in:

InductEV, Inc.
Exhibit 1008
Page 276

$$C_p = \left(\frac{C_s L_s}{L_p}\right)\left(\frac{1}{Q_{s0}^2 k^4 + 1}\right) \tag{H-17}$$

As a summary of the above analysis, the necessary primary compensation capacitance for each topology is:

$$C_p = \begin{cases} \dfrac{C_s L_s}{L_p} & \text{SS topology} \\ \dfrac{C_s L_s}{L_p}\left(\dfrac{1}{1-k^2}\right) & \text{SP topology} \\ \dfrac{C_s L_s}{L_p}\left(\dfrac{1-k^2}{Q_{s0}^2 k^4 + (1-k^2)^2}\right) & \text{PP topology} \\ \dfrac{C_s L_s}{L_p}\left(\dfrac{1}{Q_{s0}^2 k^4 + 1}\right) & \text{PS topology} \end{cases} \tag{H-18}$$

Substituting (H-18) into (F-3) results in:

$$\frac{1}{\omega C_p (\mathrm{Re}\, Z_{r0})} = \begin{cases} \dfrac{R}{uk^2 \omega_0 L_s} & \text{SS topology} \\ \left(\dfrac{\omega_0 L_s}{uk^2 R}\right)(1-k^2) & \text{SP topology} \\ \left(\dfrac{\omega_0 L_s}{uk^2 R}\right)\left(\dfrac{Q_{s0}^2 k^4 + (1-k^2)^2}{1-k^2}\right) & \text{PP topology} \\ \left(\dfrac{R}{uk^2 \omega_0 L_s}\right)(Q_{s0}^2 k^4 + 1) & \text{PS topology} \end{cases} \tag{H-19}$$

Substituting (2-23) into (H-19) results in:

$$\frac{1}{\omega C_p (\mathrm{Re}\, Z_{r0})} = \begin{cases} \dfrac{1}{uk^2 Q_{s0}} & \text{SS topology} \\ \left(\dfrac{1}{uk^2 Q_{s0}}\right)(1-k^2) & \text{SP topology} \\ \left(\dfrac{1}{uk^2 Q_{s0}}\right)\left(\dfrac{Q_{s0}^2 k^4 + (1-k^2)^2}{1-k^2}\right) & \text{PP topology} \\ \left(\dfrac{1}{uk^2 Q_{s0}}\right)(Q_{s0}^2 k^4 + 1) & \text{PS topology} \end{cases} \tag{H-20}$$

Substituting (2-29) into (H-20), the normalized reactance of the primary compensation capacitance is found to be a function of u, and Q_{p0} given by:

InductEV, Inc.
Exhibit 1008
Page 277

$$\frac{1}{\omega C_p\left(\mathrm{Re}\,Z_{r0}\right)}=\begin{cases}\dfrac{Q_{p0}}{u} & \text{series primary (SS\&SP topologies)}\\ \dfrac{1+Q_{p0}^2}{uQ_{p0}} & \text{parallel primary (PP\&PS topologies)}\end{cases} \tag{H-21}$$

I. PRIMARY TUNING FOR LOAD INDEPENDENT UNITY DPF

In this section, the required C_p and operating frequency are calculated for each topology to achieve unity DPF for all loading conditions.

SS Topology: As C_p determined in (H-4) is independent of Q_{s0}, this choice enables the SS topology to achieve unity DPF for all loading conditions by operating at ω_0.

SP Topology: Since C_p determined in (H-8) is also independent of Q_{s0}, this choice similarly enables the SP topology to achieve load independent unity DPF by operating at ω_0.

PP topology: With a parallel-compensated secondary, the impedance of the primary coil given by (3-39) can be expressed in the form of admittance as:

$$\frac{1}{Z_p}=\frac{R\left(1-\omega^2C_sL_s\right)+j\omega L_s}{-\omega^2\left(L_pL_s-M^2\right)+jR\omega\left[L_p-\omega^2C_s\left(L_pL_s-M^2\right)\right]} \tag{I-1}$$

If the operating frequency is:

$$\omega=\frac{\omega_0}{\sqrt{1-k^2}} \tag{I-2}$$

it can be shown using (2-1) and (2-22) that the following equation is true:

$$L_p-\omega^2C_s\left(L_pL_s-M^2\right)=0 \tag{I-3}$$

The equation (I-3) can be rearranged to:

$$\omega^2C_s=\frac{L_p}{L_pL_s-M^2} \tag{I-4}$$

Substituting (I-3) and (I-4) into (I-1), the result is:

$$\frac{1}{Z_p}=\frac{1}{j\omega\left(L_p-\dfrac{M^2}{L_s}\right)}+\frac{M^2R}{\omega^2\left(L_pL_s-M^2\right)^2} \tag{I-5}$$

Substituting (I-5) into (3-52) results in:

InductEV, Inc.
Exhibit 1008
Page 278

$$Y_t = \frac{1}{Z_t} = j\omega C_p + \frac{1}{Z_p} = j\omega C_p + \frac{1}{j\omega\left(L_p - \frac{M^2}{L_s}\right)} + \frac{M^2 R}{\omega^2\left(L_p L_s - M^2\right)^2} \tag{I-6}$$

If C_p is selected to be:

$$C_p = \frac{1}{\omega^2\left(L_p - \frac{M^2}{L_s}\right)} \tag{I-7}$$

the equation (I-6) can be simplified to:

$$Y_t = \frac{M^2 R}{\omega^2\left(L_p L_s - M^2\right)^2} \tag{I-8}$$

As shown the load admittance is a conductance for all loading conditions, and as such assures load independent unity DPF.

Substituting (I-2), (2-1) and (2-22) into (I-7), the required C_p can be calculated as:

$$C_p = \frac{C_s L_s}{L_p} \tag{I-9}$$

PS Topology: With a series-compensated secondary, the impedance of the primary coil given by (3-39) can be expressed in the form of admittance as:

$$\frac{1}{Z_p} = \frac{1 - \omega^2 C_s L_s + j\omega C_s R}{-R\omega^2 L_p C_s + j\omega\left[L_p - \omega^2 C_s\left(L_p L_s - M^2\right)\right]} \tag{I-10}$$

At the operating frequency given in (I-2), (I-3) and (I-4) are valid. Substituting (I-3) and (I-4) into (I-10) results in:

$$\frac{1}{Z_p} = \frac{1}{j\omega L_p} + \frac{M^2}{L_p^2 R} \tag{I-11}$$

Substituting (I-11) into (3-52), the load admittance is calculated as:

$$Y_t = \frac{1}{Z_t} = j\omega C_p + \frac{1}{Z_p} = j\omega C_p + \frac{1}{j\omega L_p} + \frac{M^2}{L_p^2 R} \tag{I-12}$$

If C_p is selected to be:

$$C_p = \frac{1}{\omega^2 L_p} \tag{I-13}$$

the equation (I-12) can be simplified to:

$$Y_t = \frac{M^2}{L_p^2 R} \tag{I-14}$$

The load admittance again is a conductance for all loading conditions and as such assures load

InductEV, Inc.
Exhibit 1008
Page 279

independent unity DPF.

Substituting (I-2), (2-1) and (2-22) into (I-13), the required C_p can be calculated as:

$$C_p = \left(\frac{C_s L_s}{L_p}\right)\left(1-k^2\right) \tag{I-15}$$

As a summary of the above analysis, the necessary operating frequency and C_p to achieve load independent unity DPF for each topology are:

$$\omega = \begin{cases} \omega_0 & \text{series primary (SS\&SP topologies)} \\ \dfrac{\omega_0}{\sqrt{1-k^2}} & \text{parallel primary (PP\&PS topologies)} \end{cases} \tag{I-16}$$

and

$$C_p = \begin{cases} \dfrac{C_s L_s}{L_p} & \text{SS topology} \\ \dfrac{C_s L_s}{L_p}\left(\dfrac{1}{1-k^2}\right) & \text{SP topology} \\ \dfrac{C_s L_s}{L_p} & \text{PP topology} \\ \dfrac{C_s L_s}{L_p}\left(1-k^2\right) & \text{PS topology} \end{cases} \tag{I-17}$$

J. MAXIMUM ALLOWABLE ALTERNATING VOLTAGE AND CURRENT IN CAPACITORS

In this section, the maximum allowable alternating voltage and current of a capacitor characterised in Fig. 7-1 into three regions labelled as 'I', 'II' and 'III' are discussed in detail.

Region I: Below f_1, the applied alternating voltage should not exceed the rated ac voltage $V_{ac,rated}$ of the capacitor and the maximum allowable alternating current is given by:

$$I_{ac,\max} = \omega C V_{ac,\max} = 2\pi f C V_{ac,rated} \tag{J-1}$$

where C is the capacitance of the capacitor.

Region II: Between f_1 and f_2, the power loss of the capacitor should not exceed its thermal power transfer capability. The power loss in the capacitor is the product of the apparent power and the dissipation factor (tan δ), and is given by:

InductEV, Inc.
Exhibit 1008
Page 280

$$P_{loss} = V_{ac}^2 \omega C \tan\delta = V_{ac}^2 2\pi f C \tan\delta \quad \text{(J-2)}$$

The thermal power transfer of the capacitor is:

$$P_{thermal} = \alpha A \Delta T \quad \text{(J-3)}$$

where 'α' is the heat transfer coefficient, 'A' is the surface area, and 'ΔT' is the temperature gradient from the surface to the ambient.

The maximum permissible alternating voltage and current can be determined by equating (J-2) and (J-3). The results are:

$$V_{ac,\max} = \sqrt{\frac{\alpha A \Delta T_{\max}}{2\pi f C \tan\delta}} \quad \text{(J-4)}$$

and

$$I_{ac,\max} = \omega C V_{ac,\max} = \sqrt{\frac{2\pi f C \alpha A \Delta T_{\max}}{\tan\delta}} \quad \text{(J-5)}$$

In this frequency range, the dissipation factor (tan δ) typically increases at a rate less than the frequency. As a result, the maximum allowable alternating voltage decreases with increasing frequency, while the maximum allowable alternating current increases.

At f_1, the maximum permissible alternating voltage ($V_{ac,\max}$) calculated using (J-4) equals the rated ac voltage $V_{ac,rated}$. The frequency f_1 thus can be determined as:

$$f_1 = \frac{\alpha A \Delta T_{\max}}{V_{ac,rated}^2 2\pi C \tan\delta} \quad \text{(J-6)}$$

Region III: Above f_2, the applied alternating current should not exceed the rated ac current $I_{ac,rated}$ of the capacitor, and the maximum permissible alternating voltage is given by:

$$V_{ac,\max} = \frac{I_{ac,rated}}{\omega C} = \frac{I_{ac,rated}}{2\pi f C} \quad \text{(J-7)}$$

At f_2, the maximum permissible alternating current ($I_{ac,max}$) calculated using (J-5) equals the rated ac current $I_{ac,rated}$. The frequency f_2 thus can be determined as:

$$f_2 = \frac{I_{ac,rated}^2 \tan\delta}{2\pi C \alpha A \Delta T_{\max}} \quad \text{(J-8)}$$

InductEV, Inc.
Exhibit 1008
Page 281